8-2015

Investigating into the Dynamics of Mammalian Cell Growth: Using In Vitro to Help Improve Therapies

Arthur Nathan Brodsky
Clemson University

INVESTIGATIONS INTO THE DYNAMICS OF MAMMALIAN CELL GROWTH: USING IN VITRO INSIGHTS TO HELP IMPROVE THERAPIES

A Dissertation
Presented to
the Graduate School of
Clemson University

In Partial Fulfillment
of the Requirements for the Degree
Doctor of Philosophy
Bioengineering

---

by
Arthur Nathan Brodsky
August 2015

Accepted by:
Dr. Sarah Harcum, Committee Chair
Dr. Susan Chapman
Dr. Robert Latour
Dr. Dan Simionescu

ABSTRACT

In the past several decades, advances in our understanding of cells that comprise our bodies have been remarkable. This is due in large part to the development of mammalian cell culture practices that allow researchers to mimic conditions in the body. Cell culture techniques have allowed researchers to study the behavior of cells under various circumstances that would be impossible to study in humans. While there are some drawbacks to the reductionism inherent in studying cells in a dish, many medical treatments have resulted from cell culture experiments. Additionally, many new therapeutics are only possible due to these improved cell culture techniques.

To that end, this research has encompassed the full spectrum of cell culture techniques and applications. For example, DNA microarrays can be used to study glycosylation gene expression in mammalian cells, where glycosylation is an important quality attribute of recombinant human therapeutic proteins. Specifically, a method is described to conduct glycosylation experiments. Next, research is described where DNA microarrays were used to investigate the response to elevated ammonium levels for a mammalian cell line often used to produce human therapeutics, because it has been show that elevated ammonium decreases product quality for these recombinant therapeutics. So, understanding if gene expression controlled the response was important. It was determined, through DNA microarray and PCR analysis, that glycosylation genes in these cells are unaffected by the elevated ammonium levels commonly experienced in end-stage cultures. Therefore, it was concluded that the effects of ammonium on protein quality appear to be due to translational or substrate-level effects.

This research transitioned from analyzing the behavior of NS0 cell cultures to analyzing the behavior of stem cell cultures. For NS0 cells, the recombinant proteins are the product of interest. For stem cells, the products are the actual cells, which are anticipated to serve as starting material for future cell-based regenerative therapies. For NS0 cells, the goal is to produce high quality protein products. For stem cells, the goal is to produce robust multipotent stem cells. To that end, we developed a novel method for buffering the pH of mesenchymal stem cell (MSCs) cultures, such that it might be easier to culture the MSCs in large volumes without requiring carbon dioxide sparging. Through the use of PCR and histological staining, it was demonstrated that MSCs were capable of growth in the absence of an elevated CO_2 environment and differentiation into adipogenic, chondrogenic, and osteogenic lineages. These results provide a route for simplifying bioreactor control and paving the way for efficient, large-scale generation of high-quality multipotent stem cells.

Just as elevated ammonium affects the protein quality for NS0 cells and pH governs the behavior of stem cells, metabolites within tumors affect the behavior of cancer cells. One such metabolite – lactate – accumulates in tumors and adversely affects patient outcomes. Interestingly, lactate accumulation is also a major challenge in therapeutic protein production and cell-based therapy cell production. Thus, gaining a better understanding of elevated extracellular lactate's effects on the metabolic behavior of breast cancer cells was examined. Three breast cancer cell lines were used. A comprehensive technique called ^{13}C-metabolic flux analysis (MFA) was used to estimate

intracellular fluxes. All three cell lines has decreased glucose consumption and decreased lactate production under the elevated lactate compared to the control condition. Under the elevated lactate conditions, all three cell lines also consumed lactate, an effect seen in stage late cultures of cells used for recombinant protein production, which might represent a general cellular mechanism used by a variety of cell lines to deal with extracellular lactate accumulation. At the same time, all three cell lines increased reductive carboxylation in the TCA cycle under elevated lactate compared to control, and this effect has also been observed in cells – both normal and cancerous - under hypoxia. These results suggest a previously unreported link between hypoxia and lactate, which demands further investigation.

DEDICATION

This work is dedicated first and foremost to my parents – Sidney and Eileen. Their love and support – not to mention careers in medicine – crucially impacted my life and the direction it has taken, and I would not have had the passion nor the ability to complete this dissertation without them. I would also like to thank my brother, David Matthew, as well as all of my aunts and uncles, for always being there for me. My friends have also been very influential in my life: I have been lucky to have friends that both enjoy discussing philosophy and science as well as possess the patience to put up with me and all of my faults, obsessions, and idiosyncrasies. Finally, I would like to thank all of the scientists and authors out there who stoked my curiosity and desire to learn about our world. In the words of Isaac Newton, none of my work would have been possible without the view afforded me from the shoulders of these many giants.

ACKNOWLEDGMENTS

My advisor Dr. Sarah Harcum has been amazing to me these last 5 years and I am extremely grateful for the opportunity to pursue this degree under her watch. I owe her many thanks, but above all I have valued her ability to let my creative intellect flourish while at the same time knowing when to reign me in when it gets the best of me. Her guidance and support have been indispensible to me, and it has been a pleasure to work on these research projects with her. I would also like to thank my committee members, Dr. Susan Chapman, Dr. Robert Latour, and Dr. Dan Simionescu, for investing their time and energy in guiding me through these projects and providing their productive feedback along the way. My labmates – Yogi Gowtham and Daniel Odenwelder – also deserve many thanks. Yogi was one of my first great friends at grad school here, and it has been very rewarding to work alongside him as we have tackled these challenges, while Dan played an important role in my most recent research project on cancer, and will proudly continue to carry the torch in our lab moving forward. Dr. Neil Burton contributed many positive and influential impacts on me as well. Through many long and insightful conversations with him I have developed a much more refined sense of myself as well as my place in this world, and the impacts that I hope to make in the future will be largely due to his guidance. Finally, I would also like to thank the Centers of Biomedical Research Excellence (COBRE) and the National Institutes of Health (NIH) for providing the funding that enabled me to conduct the research in this dissertation.

TABLE OF CONTENTS

Page

Table of Contents (continued) Page

Table of Contents (continued) Page

LIST OF TABLES

LIST OF FIGURES

CHAPTER 1: INTRODUCTION

1.1 Motivation

Cell culture technology provides an indispensible tool for advancements in the biomedical and bioengineering fields. Performing studies on cells outside of the complex environment in the human body allows researchers to derive insights into cell biology and disease progression that might otherwise be hard to uncover. Additionally, we can harness the unique attributes of mammalian cells to create complex therapeutics and hopefully improved cell-based therapies. Ultimately, cell culture experiments allow researchers to simplify the situation, so that links between environmental factors and cell behavior can be more clearly discerned. As the scientific and medical communities gather more knowledge about the causes and effects of phenomena surrounding us, this knowledge can be used to develop solutions to the problems that we face. Above all, the motivation for all of my projects – from NS0 cells to stem cells to cancer – stemmed from the basic desire to contribute to this enterprise: to expand scientific knowledge in order to improve patients' lives.

1.2 Organization

This dissertation contains six chapters. Chapter 1 outlines and explains the motivation for this research. Chapter 2 is a published methods paper that describes DNA microarray technology and its application in studying mammalian cell gene expression. My co-authors were Mary Caldwell and Dr. Sarah W. Harcum (Brodsky et al., 2012). Chapter 3 is a published research paper, which follows thematically from the methods paper and describes the application of this method to NS0 cells and how elevated ammonium levels affects the expression of key glycosylation genes. My co-authors were Mary Caldwell, Sooneon Bae, and Dr. Sarah W. Harcum (Brodsky et al., 2014). Chapter 4 is a published research paper that describes a novel method to expand mesenchymal stem cells (MSCs) in atmospheric carbon dioxide. My co-authors were Dr. Jing Zhang, Dr. Richard P. Visconti, and Dr. Sarah W. Harcum (Brodsky et al., 2013). Chapter 5 describes ongoing research that examines the effects of high extracellular lactate on the metabolism of three different breast cancer cell lines using ^{13}C-metabolic flux analysis (MFA). My co-investigators are Daniel Odenwelder and Dr. Sarah W. Harcum. Chapter 6 describes future work, mostly related to the ^{13}C-MFA studies.

1.3 References

Brodsky AN, Caldwell M, Harcum SW. Glycosylation and post-translational modification gene expression analysis by DNA microarrays for cultured mammalian cells. Methods. 2012;56:408-417.

Brodsky AN, Caldwell M, Bae S, Harcum SW. Glycosylation-related genes in NS0 cells are insensitive to moderately elevated ammonium concentrations. J Biotech. 2014;187:78-86.

Brodsky AN, Zhang J, Visconti RP, Harcum SW. Expansion of mesenchymal stem cells under atmospheric carbon dioxide. Biotech Prog. 2013;29:1298-1306.

CHAPTER TWO: GLYCOSYLATION AND POST-TRANSLATIONAL MODIFICATION GENE EXPRESSION ANALYSIS BY DNA MICROARRAYS FOR CULTURED MAMMALIAN CELLS

2.1 Abstract

DNA microarray analysis of gene expression has become a valuable tool for bioprocessing research aimed at improving therapeutic protein yields. The highly parallel nature of DNA microarray technology allows researchers to assess hundreds of gene simultaneously, essentially enabling genome-wide snapshots. The quality and amount of therapeutic proteins produced by cultured mammalian cells rely heavily on the culture environment. In order to implement beneficial changes to the culture environment, a better understanding of the relationship between the product quality and culture environment must be developed. By analyzing gene expression levels under various environmental conditions, light can be shed on the underlying mechanisms. This paper describes a method for evaluating gene expression changes for cultured NS0 cells, a mouse-derived myeloma cell line, under culture environment conditions, such as ammonia buildup, known to affect product quality. These procedures can be easily adapted to other environmental conditions and any mammalian cell lines cultured in suspension, so long as a sufficient number of gene sequences are publicly available.

2.2 Introduction

Production of therapeutic proteins in cultured mammalian cells has advanced significantly over the last few decades. Yields during this time have increased from less than ten milligrams per liter to over five grams per liter of product mainly due to improved cell numbers (Hacker et al., 2009). However, there has not been the same level of improvement in protein quality, specifically with respect to glycosylation and other post-translational modifications that directly impact a therapeutic protein's efficacy (Jenkins et al., 2008; Lim et al., 2010). Much research has examined how culture variants – including substrate and precursor- feeding, oxygen and carbon dioxide levels, amino acid additions, and osmolarity – influence protein quality (Ozturk et al., 1990; Patel et al., 1992; Maiorella et al, 1993; Hayter et al., 1993; Chotigeat et al., 1994; Gawlitzek et al., 1995; Castro et al., 1995; Gu et al., 1997; Chuppa et al, 1997; Etchevarry et al., 1998; Kunkel et al., 1998; Hooker et al., 1999; Valley et al., 1999; Kaufmann et al., 1999; deZengotita et al., 2002; Chung et al., 2001; Baker et al., 2001; Yang and Butler, 2002; Sung and Lee, 2005), but currently no robust, reliable means to positively influence protein quality are known (Jenkins et al., 2009).

Many studies have investigated gene expression in mammalian cell culture under bioreactor conditions designed to improve protein productivity. Earlier work used real-time quantitative reverse transcription polymerase chain reaction (real-time qRT-PCR) to assess the expression levels of a few particular genes in response to induced culture variants (Kim et al., 2005; Yoon et al., 2003; Clark et al., 2005; Clark et al., 2004; Chen and Harcum, 2006; Chen and Harcum, 2007; Wong et al., 2010a; Wong et al., 2010b).

However, these narrow depictions of gene expression did not provide the global analysis necessary to formulate comprehensive models of glycosylation and other post-translational modifications, whereas DNA microarray analysis is beginning to provide adequate levels of detail (Jaluria et al., 2007).

DNA microarray technology, with its ability to take genome-wide snapshots, provides a comprehensive tool for gene expression analysis (Jaluria et al., 2007) that when combined with proteomic and metabolic data will finally provide the inputs needed to design predictive models for control of post-translational modification, especially glycosylation (Jenkins et al., 2009; Jaluria et al., 2007; Redestig and Costa, 2011). However, DNA microarrays are still most effective for genetically sequenced species, such as mouse cell lines. Thus, the lack of a complete genome prior to July 2011 (Xu et al., 2011) has limited Chinese hamster ovary (CHO) cell applications, though analysis using private DNA microarrays has yielded insightful results (Korke et al., 2004; Wlaschin et al., 2006; Nissom et al., 2006; Gatti et al., 2007; Kumar at al., 2007; Yee et al., 2009; Kantardjieff et al., 2010; Shen et al., 2010; Qian et al., 2011; Clarke et al., 2011). Studies have revealed that genes for vesicle trafficking, endocytosis and cytoskeletal elements critically influenced antibody production (Yee et al., 2009) and that death receptor- and mitochondria-mediated pathways, not endoplasmic reticulum-mediated pathways, signaled apoptosis (Nissom et al., 2006). Studies with sodium butyrate have linked its positive effect on protein productivity and improved glycosylation to histone modifications, chaperones, lipid metabolism, and protein processing (Gatti et al., 2007). When sodium butyrate was combined with lower culture

temperatures, genes associated with the Golgi apparatus, cytoskeleton, and signal transduction contributed to the improved protein quality, despite diminished growth rates Kantardjieff et al., 2010). Additionally, hyperosmolarity has been investigated in hybridoma cells (a mouse-derived cell line) using DNA microarrays and it has been observed that differential expression of genes associated with catabolism, cell-cycle regulation, apoptosis, regulation of transcription and translation, and transport and signaling pathways play a significant part in cell survival. Surprisingly, hyperosmolarity affected few genes involved in stress response (Shen et al., 2010). The positive affects of copper sulfate on protein productivity and aggregation have been examined via DNA microarrays. The down-regulation of the transferrin receptor and lactate dehydrogenase genes, and the up-regulation of cytochrome P450 family genes were determined to mediate the positive metabolic responses (Qian et al., 2011). A weighted gene expression network analysis has been used to identify patterns in gene expression due to relevant bioprocess conditions from 295 DNA microarrays. As expected, genes associated with cell cycle, nucleic acid metabolism, and DNA replication were enriched in the clusters that had positive effects on cell growth and protein production. These clusters may prove useful in identifying biomarkers indicative of high producing CHO cell lines (Clarke et al., 2011). As these previous results demonstrate, the parallel, high throughput capabilities of DNA microarray technology makes it an ideal tool for evaluating a larger scope of transcriptomic responses to design strategies for improving protein yields and quality.

This article covers step-by-step protocols for mimicking the elevated ammonium

stress associated with late-stage bioreactor cultures (Gawlitzek et al., 2000) and using DNA microarrays to analyze the effect of these culture conditions on glycosylation gene expression. While the analysis will focus on NS0 cells (a mouse myeloma cell line used commonly for monoclonal antibody production), these procedures are, in principle, easily adaptable to CHO cells and other relevant suspension cell lines. Additionally, the glycosylation and housekeeping gene sequences that are publicly available could be used with any DNA microarray platform and could be extended to include other post-translational modification genes.

2.3 Materials

Cell Lines

1. NS0 cells (ECACC#85110503) from the European Collection of Cell Culture (a mouse myeloma cell line with lymphoblast morphology, non-secreting clone, and cholesterol auxotroph).

2. (Alternative) Chinese hamster ovary (CHO) cells from the American Tissue Culture Collection (ATCC).

Cell Culture Media

1. ADCF-MAb™ media without L-glutamine (HyClone) plus Lglutamine (200 mM) with LS-250 or LS-1000 lipid supplement (HyClone), or (Alternative) SyntheChol™ cholesterol supplement (Sigma) and fatty acid supplement (Sigma).

2. (Alternative) EX-CELL® NS0 Serum-Free Medium (Sigma) plus L-glutamine (200 mM).

3. (Alternative) CDM4NS0® Medium (Hyclone).

Cell culture reagents, plasticware, and glassware

1. T-75 (75 cm^2) Flasks (e.g. Nunc).

2. One or two 250 mL spinner flask (Kontes Cytostir or similar).

3. Four or five 1 L spinner flasks (Kontes Cytostir or similar).

4. Orbital Shaker Platform/Multiple Purpose Rotator (e.g. Barnstead Lab-Line).

5. Stir Plate with at least 4 places for 1L spinner flasks

6. 5 M NH_4Cl stock (in Milli-Q water) (e.g. Sigma).

7. 5 M NaCl stock (in Milli-Q water) (e.g. Sigma).

8. 5 M Proline stock (in Milli-Q water) (e.g. Sigma).

9. (Alternative/Additional) Computer-controlled fermenter system (e.g. Sartorius BiostatB Plus).

Cell counting

1. Scepter™ 2.0 Handheld Automated Cell Counter (Millipore).

2. (Alternative) Trypan Blue (e.g. Invitrogen), Microscope (e.g. Olympia), and Hemocytometer.

3. (Alternative) Coulter counter (e.g. Beckman).

Glucose analysis

1. HemoCue® B-Glucose Analyzer (HemoCue).

2. (Alternative) YSI 2300 STAT Plus™ Glucose & Lactate Analyzer (Yellow Springs Instruments).

3. (Alternative) NOVA BioProfile® Basic analyzer (NOVA Biomedical).

RNA stabilization

1. Ice bath to quickly cool cells.

2. (Optional) RNAlater® (Ambion).

3. (Optional) RNAProtect® (Qiagen).

RNA isolation and purification

1. RNAqueous-Midi®kits (Ambion).

2. (Alternative) PureYield™ RNA Midiprep System (Promega).

3. (Alternative) RNeasy® Midi Kit (Qiagen).

RNA clean-up (optional)

1. RNeasy® Mini Kit (Qiagen).

2. RiboPure™ Kit (Ambion).

3. (Optional) RNase-Free DNase Set (Qiagen).

RNA quantification

1. Agilent 2100 Bioanalyzer (Agilent Technologies).

2. (Alternative) Ribogreen® RNA Quantification kit (e.g. Molecular Probes).

3. (Alternative) Spectrophotometer with 280 and 260 nm filters (e.g. TECAN).

4. (Alternative) Gel electrophoresis apparatus (e.g. Nunc).

DNA microarray

1. GLYCOv4 GeneChip® (Affymetrix), not available for commercial use.

2. (Alternative) Custom Nimblegen DNA microarray.

3. (Altenative) Custom spotted DNA microarray.

Gene expression analysis

1. GeneSpring® (Agilent).

2. (Alternative) ArrayStar® (DNASTAR).

3. (Alternative) ORIOGEN v3, not for commercial use

.(http://www.niehs.nih.gov/research/resources/software/oriogen/index.cfm),

Real-time qRT-PCR validation

1. Access RT-PCR kit (Promega, WI).

2. SYBR®Green I dye chemistry (Molecular Probes, Eugene, OR).

3. Primer Express® (Applied Biosystems, Foster City, CA).

4. Smart Cycler® (Cepheid, Sunnyvale, CA).

2.4 Methods

Overview

This article will cover the key elements of the procedures needed to assess gene expression changes under bioreactor conditions with particular focus on protein glycosylation and other posttranslational modification genes. The factors that should be considered when planning such experiments will be discussed. Although DNA microarrays are central to assessing gene expression levels, much of the experimental procedures described here – including experimental setup and sampling procedures – are independent of the selected DNA microarray platform. Additionally, most DNA microarray scanning software can generate multiple types of specialized files (such as CEL for Affymetrix) as well as tab-delimited text files, and gene expression software programs can read a variety of file types. Due to this flexibility, the experimental procedures mentioned here can be performed fairly independent of the DNA microarray platform to be used. A flow diagram outlining the basic procedure can be found in Figure 2.1. The details of the experimental design and set up will be discussed in more detail and the reader will be informed of potential options.

Experimental design and set-up

As a means to demonstrate how to set up and run an experiment focused on quantifying expression changes in genes associated with glycosylation and post-

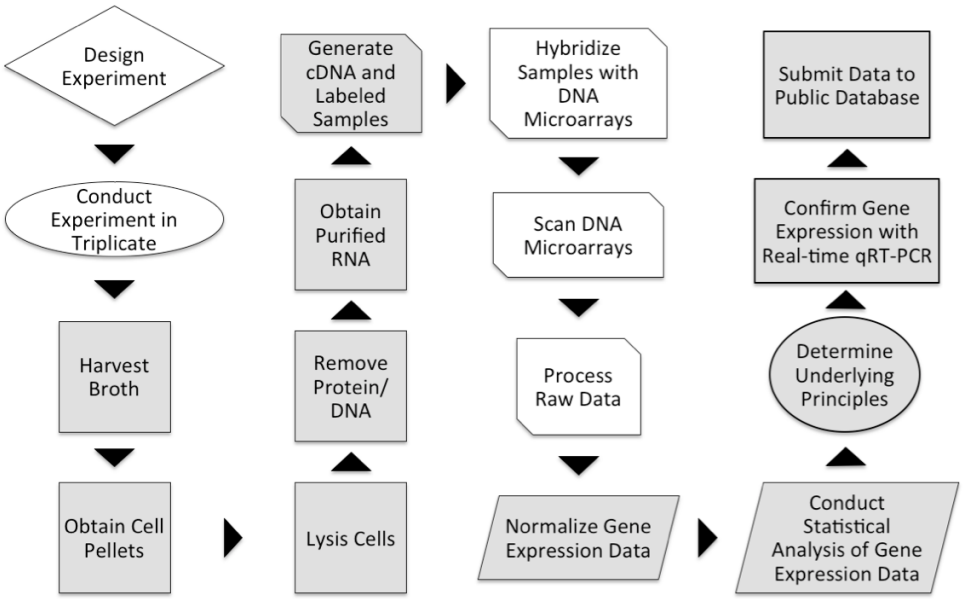

Figure 2.1 Flow diagram for the collection and analysis of gene expression data. The process begins with the experimental design. Next, the experiments are conducted in triplicate for each condition. From each condition, the samples are harvested and the cells obtained. In order to analyze gene expression, the total RNA is separated from the cells and purified. Depending on the DNA microarray platform, the researcher will convert the mRNA to cDNA, or send the total RNA to the DNA microarray contract facility for processing. The cDNA is then hybridized with DNA microarray, the DNA microarray is scanned and the data is processed. At this point the process data will be returned to the researcher for analysis. The processed data is usually imported into a DNA microarray analysis software tool, where the data is normalized. Once the data is normalized, statistical analysis is conducted to identify genes with differential expression between the replicates. A variety of tools can be used to determine underlying gene regulation principles. In order to publish the research results, the data is then submitted to a public database.

translation modification, a step-by-step procedure will be described for a model system. The model system will be NS0 cells exposed to conditions known to affect protein glycosylation, including elevated ammonium (Valley et al., 1999; Gawlitzek et al., 2000; Gawlitzek et al., 1998) as well as three other conditions. Specifically, the experimental procedure to set up ammonium-stressed, salt-stressed, ammonium-stressed with proline, and control cultures will be described. The salt-stressed will provide a control for osmolarity. The ammonium-stressed with proline will examine the ability of proline to mitigate the negative effects of ammonium (Chen and Harcum, 2006). Additionally, a control will normalize volumes, nutrients, and osmolarity. Biological triplicates for each condition will be needed, thus requiring 12 individual culture vessels.

Since the anticipated gene expression changes are likely to be small, relative to the large magnitude changes observed due to a heat-shock, it is important to synchronize the control and ‘‘stressed’’ cultures as much as possible to reduce the growth-associated differences. The use of a common inoculum for the control and stressed conditions synchronizes the culture behavior, which should reduce the noise-to-signal ratio. In Figure 2.2, a scale-up plan is shown for using a common inoculum to seed four 1 L spinner flasks. These four spinner flasks represent only one-third of the experiment and one complete set of the conditions. This process would need to be repeated two more times to generate the biological triplicates (12 experimental vessels total). Since most CO_2 incubators can only hold one multi-place stirrer with four 1 L spinner positions, the procedure outlined in this article runs biological triplicates from three separate inocula, sequentially. It is possible to reduce the overall time by staggering the T-75 flasks and

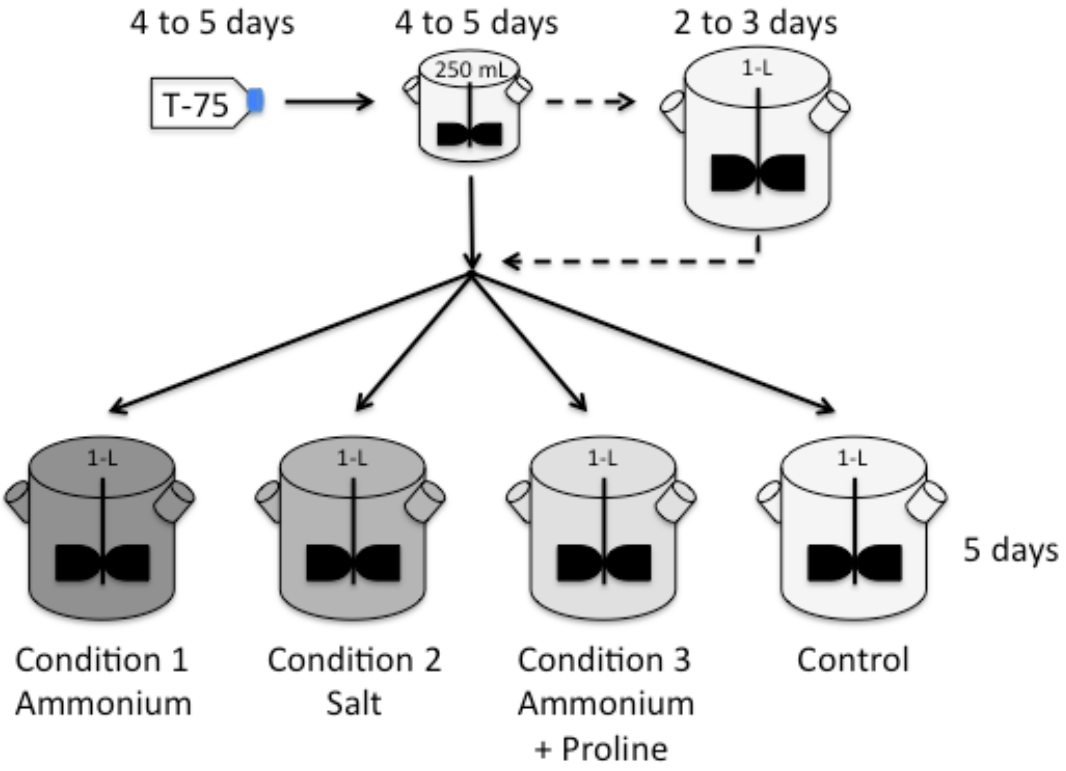

Figure 2.2 Expansion timeline for NS0 cells to be used in parallel 1 L spinner flasks. NS0 cells are inoculated into a T-75 flask and allowed to expand to 1.5 x 10^5 cells/mL, which takes 4 to 5 days. The T-75 flask cells (25 mL) are used to inoculate one 250 mL spinner flask with 225 mL fresh media added. If the desired volume in the four 1 L spinners is only 500 mL each, the cells from one 250 mL spinner flask can be used to inoculate all four 1 L spinners. However, if a higher volume is required in the 1 L spinners, an additional 1 L spinner can be used. Inoculate the extra 1 L spinner with the entire contents of the 250 mL spinner flask and add up to 750 mL fresh media. Inoculate the Control and Condition spinner flasks with the same volume of cells from either the 250 mL spinner or the extra 1 L spinner flasks (50 mL to 250 mL depending on desired timeframe).

recycling the 250 mL spinner with a one-day delay. This would stagger the four experimental 1 L spinner flasks by one day, allowing sufficient time to harvest, wash, and sterilize the spinner flasks.

For stresses sufficiently mild as to not alter the growth significantly, inoculating the cells directly into the vessels containing the control and ‘‘stressed’’ media allows for synchronization. An example set of growth profiles are shown in Figure 2.3A where the stresses were mild, as indicated by the parallel growth profiles. An alternative approach is required if the stresses to be investigated cause significant growth rate changes. In this case, it is best to inoculate all the vessels with cells in control media. This will allow the cells to grow sufficiently to obtain a baseline growth rate and confirm that cultures are not different, and then the stresses can be applied. An example set of growth profiles are shown in Figure 2.3B that highlights this approach, where the stresses were added at 40-h. The growth profiles were similar prior to the stress at 40-h, and divergent after 40-h.

The sampling frequency and types needed for analysis will directly determine the minimum volumes needed in the experimental vessels. In the model system, 500 mL media was used in 1 L spinner flasks to assure sufficient material throughout the entire experiment. The volume reduction due to sampling should not significantly alter the culture characteristics, such as the mixing dynamics. For the model case, samples would be taken for cell density, cell viability, glucose, lactate, osmolarity, and total RNA. If the cell line of interest expressed a therapeutic recombinant protein, samples analyzing the product quality should be taken periodically. The cell density, cell viability, glucose, and lactate samples would be taken approximately every 12-h (see Figure 2.3A). For

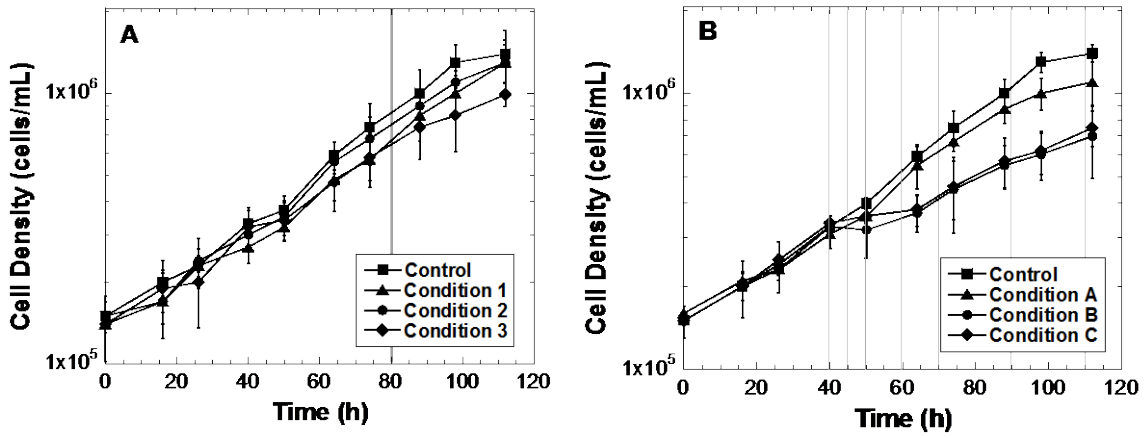

Figure 2.3 Example growth profiles for biological triplicate conditions. A) The conditions being examined did not significantly affect the growth rate; however, the final cell densities were significantly different. In this case, obtaining gene expression analysis data from one time point, late in culture (around 90 hours) would not have high noise in the data due to a growth effect. B) The conditions being examined significantly affect the growth rate. In this case, the stress was applied at 40 hours. Sampling throughout the culture's growth (before and after the stress) would be desirable, such that gene expression changes due to growth effect could be identified.

mammalian cells, the sampling frequency can vary from 10 to 16-h without missing the culture dynamics; however, it is important that the time intervals used be the same for all replicates such that error bars in time are not needed. In the model case, the sample interval was initially 16-h, and then alternated between 10 and 14-h to accommodate more user-friendly work hours (see Figure 2.3). The volumes withdrawn for these samples should be 5 mL per time point with 10 time points (50 mL total). The frequency of these sample types would be the same for the growth inhibitory stress conditions (see Figure 2.3B).

For DNA microarrays, a minimum of 10 μg total RNA is usually required. Thus, it is critical that the cell pellet samples for total RNA to be sufficiently large enough to assure sufficient material is obtained. Cultured cells typically have much lower total RNA levels than tissue sample, consequently 1 x 10^7 cells are a minimum target of cells to assure that 10 μg total RNA is obtained at the necessary concentration (1 μg/μL). For beginning cultures with cell densities in the 2 x 10^5 cell/mL range, harvesting 50 mL culture media per sample is sufficient. Once the cell densities are greater than 3 x 10^5 cell/mL, the harvest volumes can be decreased to 15 mL. The recommended RNA isolation kits can handle up to 100 μg total RNA and associated cell debris, so it is unlikely that a kit will be saturated with cell debris. For the non-growth altering stresses, a single, late-stage exponential-phase total RNA sample from each condition would be sufficient to capture gene expression changes due to the stress, which was indicated by the vertical line in Figure 2.3A. Taken together with the other sample volumes (50 mL), the total anticipated volume change in the vessel is only approximately 65 mL out of 500

mL. For the growth altering stresses, multiple total RNA samples from each condition would be needed to capture gene expression changes due to the stress. For the model experiment shown in Figure 2.3B as vertical lines, total RNA samples should be taken at 40, 45, 50, 60, 70, 90, and 110-h to fully capture the potential culture gene expression dynamics. Taken together with the other sample volumes (50 mL), the total anticipated volume change in the vessel would be 155 mL. The similarity of mixing dynamics can be assessed using culture media and tracer dyes at the various anticipated volumes to confirm minimal effects. So, depending on the placement of the stirring paddles, the initial culture volume for the growth altering stressed cultures may need to be increased to between 750 and 1000 mL.

Culturing NS0 cells

Standard cell culture techniques should be used to thaw and expand the NS0 cells.

Standard media preparation

The ADCF-MAb media requires a cholesterol supplement, since NS0 cells are cholesterol auxotrophs. ADCF-MAb media was designed to be used with the LS 250 lipid supplement (4 mL per liter media; Hyclone) or LS 1000 (1 mL per liter media; HyClone). Alternatively, the cholesterol supplement SyntheChol™ (2 mL per liter, Sigma) and the fatty acid supplement (0.5 mL per liter, Sigma) can be used as well. As needed, add L-glutamine (25 mL of 200 mM L-glutamine stock per liter) to the ADCF-MAb media. If other cell lines or media are used, prepare media appropriately.

The NS0 cells will be inoculated into fresh media at approximately 2 x 10^5 cells/mL and allowed to reach 1.5 x 10^6 cells/mL prior to subsequent inoculation. Preparation of the first spinner flask requires a cell density in the T-75 flask greater than 1.0 x 10^6 cells/mL. For example, 25 mL of 1.0 x 10^6 cells/mL added to 225 mL of fresh media will result in an initial cell density of 1 x 10^5 cells/mL in the 250 mL spinner flask. The 250 mL spinner flask will reach approximately 1.0 x 10^6 cells/mL in about 3–4 days. Since the complete ADCF-MAb media supports cell densities of approximately 2 x 10^6 cells/mL, the cells should be transferred to fresh media in the exponential phase (<1.5 x 10^6 cells/mL) to reduce the potential of a growth lag. For NS0 cells, a lead-time of 8–12 days is needed for each replicate set. These lead-times can be shortened if the cell line to be examined has faster doubling times than NS0 cells. For example, the higher growth rate of CHO cells compared to NS0 cells results in less time required to expand the cells.

If the phenomenon to be investigated requires high cell density cultures, computer-controlled fermenters operated in a fed-batch manner will be required. The description of fed-batch operation of mammalian cell cultures will not be described; however, there are several research papers that describe fed-batch operation (Zhou et al., 1997; Lee et al., 2003; Wong et al., 2005). The inoculum for the fermenters will be generated in spinner flasks, as described above. Depending on the number of fermenters available, the conditions to be examined may need to be run sequentially. If sequential operation is required, it is very important to have standardized expansion trains.

Media preparation

For the model case, three stressed conditions were compared to the control, representing cells cultured in the standard media. In order to minimize osmolarity and nutrient concentration differences, the final volumes in the experimental spinner flasks were kept constant by water additions to the control and other stressed conditions as required (see Table 2.1). For example, for the ammonium- stressed condition (Condition 1), 2 mL of the 5 M NH_4Cl stock was added to the media and 4 mL of Milli-Q water. For the salt-stressed condition (Condition 2), 2 mL of the 5 M NaCl stock was added and 4 mL of Milli-Q water. For the ammonium-stressed plus proline condition (Condition 3), 2 mL of the 5 M NH_4Cl stock was added and 4 mL of the 5 M proline stock. For the control culture (Control), 6 mL of Milli-Q water was added. To reduce any potential osmolarity shocks, the salts, proline, ammonia, and water should be added to the medias prior to the addition of cells. If the stresses significantly affect growth after the stress is added, the control culture should have a water addition of equal volume to any chemical addition.

Initial sampling

Once the vessels are inoculated, the initial cell density should be determined. A Scepter™ 2.0 Handheld Automated Cell Counter or a similar device can be used to obtain the initial cell densities and if cell viability is desired, the Trypan Blue exclusion method can be used. Additionally, samples should be taken for glucose and lactate analysis using a NOVA BioProfile® Basic analyzer or the YSI 2300 STAT Plus™

Table 2.1. Experimental media formulations. Media additions to induce the stressful condition, while normalizing the nutrient concentrations and osmolality. Amounts listed are per liter of the final media.

Additions	Control	Condition 1 (10 mM Ammonium)	Condition 2 (10 mM Salt)	Condition 3 (10 mM Ammonium + 20 mM Proline)
5 M NH_4Cl	0	2 mL	0	2 mL
5 M NaCl	0	0	2 mL	0
5 M Proline	0	0	0	4 mL
Milli-Q Water	6 mL	4 mL	4 mL	0

Glucose & Lactate Analyzer. Procedures for the NOVA BioProfile Basic® analyzer or the YSI 2300 STAT Plus™ Glucose & Lactate Analyzer can be found from the manufacturers.

Sampling

The cultures should be monitored periodically for 110 h with sampling every 10–14 h. Samples for every time point should minimally include cell density and glucose concentrations. Cell viability and lactate may provide additionally information on cell health. The cell pellets for total RNA samples should be taken as per the experimental design. Protein quality assessment samples should also be taken for systems that express a therapeutic recombinant protein.

RNA isolation and purification

Sampling for total RNA isolation requires some type of stabilization. One method simply rapidly cools the cell broth on ice water (4°C), then centrifuges at 4°C. The cell pellet is then stored at -80° C. Alternatively, a stabilization agent can be added directly to the cell broth for storage. Usually an equal volume of the stabilization agent is needed. Commercially available stabilization agents include RNAlater® Stabilization Solution (Ambion) and RNAprotect® cell reagent (Qiagen). The stabilized cell broth is then either stored at -20 or -80°C depending on the manufacturer

Although the RNA extraction kits are designed to inactivate RNAses and other degradative compounds, it is essential that proper sterile practices be used, and that no

part of the kits be touched with bare hands, as RNAses are especially abundant on human skin, and could affect reagents and samples. Also, all water and pipette tips used in conjunction with these kits must be nuclease-free. It is best to process all the RNA from all samples together.

RNA isolation

The RNAqueous® Midi Kit can be used to extract and isolate the total RNA, although many other kits, such as RNeasy® Mini Kits, are also effective. These procedures can be found at http://www.ambion.com and http://www.qiagen.com. Also, the phenol–chloroform extraction method can be utilized. It is sold under the name TRI Reagent (Sigma) and TRIzol® (Invitrogen). Essentially, these procedures all have steps to lyse the cells, remove cellular debris including lipids, proteins and DNA, followed by binding and eluting the total RNA in nuclease-free water.

RNA purification

Many DNA microarray contract facilities require an additional RNA purification. The RNeasy® Mini Kits can be used for all RNA purifications procedures. Other companies, such as Norgen Biotek offer alternatives; however, one should confirm the compatibility with the DNA microarray contract facility beforehand. Normally, RNA purification kits efficiently remove the majority of DNA without DNAse treatment; however, if any of the mRNA transcripts of interest are in low abundance, an additional DNAse digestion step should be performed. An RNase-Free DNAse Set should be used.

The procedure for Qiagen's DNAse digestion can be found at www.qiagen.com/hb/rnasefreednaseset. In the model case, the DNAse digestion step was not needed; however, the additional Qiagen RNA clean-up was required by the Consortium for Function Genomics DNA microarray facility.

RNA quantification

The Ribogreen® RNA Quantification Kit (Molecular Probes) was used to quantify the concentration of all RNA samples, although other alternatives include the Agilent 2100 Bioanalyzer, UV/VIS spectrophotometer, or gel electrophoresis apparatus. The Ribogreen® Quantification Kit procedure can be found at http://hcgs.unh.edu/protocol/realtime/RiboGreen.pdf.

DNA microarray

There are several existing DNA microarray technologies; however, for this article, the descriptions will focus on the usage of a high-density oligonucleotide DNA microarray synthesized in situ using photolithography, a method developed by Affymetrix. Other DNA microarray platforms that could be used with the glycosylation and post-translational modification genes include pin-based fluid transfer systems, piezo-based inkjet dispenser systems, and electronic-based addressing systems (Heller et al., 2002). Selection of a DNA microarray platform depends on the experimental design, gene sequences available, processing facility availability, and cost. Muyal et al. provides a good review of the different platform technologies (Muyal et al., 2008). Further, Larkin

et al. demonstrated that results obtained obtain from Affymetrix and two-color DNA microarray platforms agreed, as long as reliable and consistent methods of identifying genes were used. This makes sense when one considers that the biological and procedural variation exerts a greater effect than platform variation (Larkin et al., 2005).

The specific DNA microarray that will be described is the GLYCOv4 GeneChip® DNA microarrays. The GLYCOv4 GeneChips® are Affymetrix-manufactured DNA microarrays that contain the known glycosylation-related genes for human and mouse. The GLYCOv4 DNA microarrays were constructed for the Consortium for Functional Glycomics with funding from the National Institutes of Health (NIH). The GLYCOv4 GeneChips® are only available through a proposal process to academic researchers from the Consortium for Function Genomics. Alternatively, a researcher could have a custom DNA microarray manufactured containing these glycosylation genes using any platform technology, as all the gene sequences are publicly available.

The GLYCOv4 GeneChip® DNA microarray contains 25 perfect match and mismatch (PM-MM) probes for each of the 1127 mouse glycosylation-related genes and the 119 housekeeping genes. The list of all the included genes and probe sequences can be found at http://www.functionalglycomics.org/static/consortium/resources/resourcecoree.shtml. The gene types include:

- Glycosyltransferases
- Glycan degradation proteins
- Intercellular protein transport proteins

- Nucleotide sugar synthesis and transporter proteins
- N-glycan biosynthesis-related proteins
- Interleukins and receptors
- Growth factors and receptors
- Cytokines

Affymetrix DNA microarrays also include numerous control probes on the array. Details of the Affymetrix Eukaryotic Hybridization Controls can be found at http://www.affymetrix.com. Briefly, the GeneChip_ Eukaryotic Hybridization Controls contains a mixture of four biotin-labeled cRNA controls with staggered concentrations. The controls provides alignment signals used by the scanning software to provide calibrated intensities that determine ‘‘present’’ and ‘‘absent’’ calls for a gene as well as confirm hybridization and chip integrity.

RNA sample preparation for DNA microarray

The total RNA samples need to be very concentrated (1 μg/μL) for DNA microarray analysis. Therefore, it may be necessary to precipitate the total RNA after the purification step. For the model case, a vacuum concentrator was used to dry the 10 μg samples, which then were re-suspended in 10 μL. Theses samples were sent to the Consortium for Function Genomics. As typical of contract DNA microarray facilities, the total RNA quality and concentration were determined upon arrival with an Agilent 2100 Bioanalyzer. This quality assurance step, allows the contractor to avoid expense of labeling total RNA that has degraded in transit. Alternatively, some contract DNA

microarray facilities require the researcher to reverse transcribe the RNA to cDNA, as shipping the more stable cDNA is less problematic. If required to reverse transcribe the RNA on-site, make sure to budget the cost of the reserve transcriptase (~$100 per sample).

At the contract DNA microarray facilities, the RNA will be reverse transcribed in the presence of the fluorescently-labeled dNTP analogues to obtain biotinylated cRNA. The labeled RNA will be hybridized to a DNA microarray, such as the GLYCOv4 GeneChip®, including Affymetrix's GeneChip® Eukaryotic Hybridization Controls. The GLYCOv4 GeneChips® will be scanned using the Hewlett– Packard GeneArray Scanner G2500A and a processed image file with calculated signal intensities assigned to each oligonucleotide spot on the GLYCOv4 GeneChip® will be created. The data will be reviewed for quality control at the contract DNA microarray facilities. The data files are processed and returned as CEL files (for Affymetrix) to the researcher. Additionally, data regarding the probes is provided. An example of the probe data provide in shown in Table 2.2 for a GLYCOv4 GeneChip®. Only data for the first 10 probes is shown in Table 2.2 for brevity. Muyal et al. provides a good overview description of the DNA microarray process from RNA sample preparation to data acquisition (imaging) (Muyal et al., 2008). Additionally, the GeneChip® Expression Analysis Technical Manual provides details of the RNA preparation through imaging steps for Affymetrix DNA microarrays.

Statistical analysis of gene expression data

Table 2.2 Example probe set data information for the GLYCOv4 GeneChip. Information for only the first 10 genes is listed. The GLYCOv4 GeneChip contains 25 probes per accession number. The accession numbers are sufficient information to create a custom DNA microarray.

Probeset ID	Category	Sub-category	Common name	Accession Number	Probe Set Score
NM_013630.2_psr1	CBP: C-Type Lectin	10-Polycystin	Pkd1 [Polycystin]	NM_013630	10.6
NM_029686.2_psr1	CBP: C-Type Lectin	10-Polycystin	Pkd1l2 [Polycystin 1-like protein 2]	NM_029686	12.6
NM_181415.3_psr1	CBP: C-Type Lectin	11-Attractin	Atrnl1 [Attractin homolog]	NM_181415	10.5
NM_009730.2_psr1	CBP: C-Type Lectin	11-Attractin	Attractin	NM_009730	10.8
NM_008920.4_psr1	CBP: C-Type Lectin	12-CTLD + acidic neck	Prg2 [proteoglycan 2 bone marrow]	NM_008920	12.3
NM_016914.2_psr1	CBP: C-Type Lectin	12-CTLD + acidic neck	Prg3 [proteoglycan 3; Eosinophil major basic protein homolog]	NM_016914	12.1
NM_010048.3_psr1	CBP: C-Type Lectin	12-CTLD + acidic neck	DGCR2 DiGeorge syndrome protein C	NM_010048	11.1
NM_054042.2_psr1	CBP: C-Type Lectin	13-IDD	Cd248 [CD248 antigen endosialin]	NM_054042	11.7
NM_010740.3_psr1_s	CBP: C-Type Lectin	14-Endosialin	CD93 [C1q receptor; Cd93 antigen]	NM_010740	10.5
NM_009378.2_psr1	CBP: C-Type Lectin	14-Endosialin	Thbd [Thrombomodulin]	NM_009378	11.6

In order to interpret the DNA microarray data, the raw DNA microarray data files must be imported into a statistical analysis software program. Microsoft Excel is the simplest program that could be used, but has limited function. In the model case, GeneSpring® was used; however, there are many commercial programs (e.g. ArrayStar®) and one public domain program (ORIOGEN) available. These programs provide multiple statistical and post hoc tests, visualization and clustering tools, and often pathway mapping. GeneSpring® can directly import the CEL data generated by the Affymetrix compatible scanner. Many gene expression analysis software tools can also import gene expression data from tab-delimited text files. A portion of a tab-delimited text file from the GLYCOv4 GeneChip® is shown in Table 2.3. In this case, the data from three biological replicates were combined into a single file.

The first step once the data has been imported into the software package is to normalize the raw data between the DNA microarrays. Normalization adjusts for the effects that are due to DNA microarray processing (Wit and McClure, 2004). For example, with two-color DNA microarrays, imbalances in the red and green dyes can occur due to labeling efficiency differences (Smyth and Speed, 2003). In GeneSpring®, the researcher needs to select a normalized protocol for the data. GeneSpring® also performs a quality check on the Affymetrix Hybridization Controls, which check for minimum detection levels and titration of concentrations. The default normalization is quartile and it is commonly normalized to the total intensity of the chip, which is often set to the arbitrary value of 500. This method assumes that on average the total RNA level in a cell is constant. Alternatively, one can normalize to the median chip intensity or

Table 2.3 Example gene expression data outputs for one condition. The gene expression signal, call, and p-values for 10 Probesets are shown for only the first 10 genes. Genes that are assigned as present (P) have $p \leq 0.04$, whereas the genes assigned as absent (A) have $p \geq 0.06$ and low signals. Genes with p-values in-between are assigned marginal (M) calls.

Probeset ID	Replicate 1			Replicate 2			Replicate 3		
	Signal	Call	P-value	Signal	Call	P-value	Signal	Call	P-value
NM_013630.2_psr1	64	P	0.00148	73.6	P	0.001049	100.4	P	0.000451
NM_029686.2_psr1	37.5	A	0.160942	16.4	M	0.056885	25.1	A	0.122135
NM_181415.3_psr1	7.8	A	0.493067	1.7	A	0.629375	14.9	A	0.227444
NM_009730.2_psr1	566.8	P	0.00003	428.9	P	0.00003	404.8	P	0.00003
NM_008920.4_psr1	32.8	A	0.129317	30.9	P	0.009484	31.9	P	0.007135
NM_016914.2_psr1	6.2	A	0.728492	3	A	0.728492	6.9	A	0.58937
NM_010048.3_psr1	9.5	A	0.424197	10.3	A	0.090421	1.6	A	0.655316
NM_054042.2_psr1	316.8	P	0.00003	304.5	P	0.00003	308.4	P	0.00003
NM_010740.3_psr1_s	3.3	A	0.990516	1.5	A	0.870683	11	A	0.197229
NM_009378.2_psr1	5.4	A	0.728492	2	A	0.79298	3.7	A	0.772556

a particular set of housekeeping genes. Bahr et al. identified over 100 potential housekeeping genes for CHO cells after reviewing multiple DNA microarray studies (Bahr et al., 2009). Normalization methods also include linear models, global normalization, LOESS normalization, and subset quantile normalization (Khoo et al., 2007; Wu and Aryee, 2010; Yang et al., 2002). For Affymetrix CEL files, the steps used are summarization, log transformation, and baseline transformation as described in the Gene-Spring® GX Manual.

After data normalization, differentially expressed genes can be identified from the replicates and between the conditions of interest. In the model case, there are three biological replicates for the four conditions, thus data from 12 DNA microarrays was analyzed. Experiment groupings are used to identify sample parameters and the replicates. For example, in the model case ammonium would be a parameter, as well as proline and salt. Also, a principle component analysis is used by GeneSpring® to check data quality per DNA microarray. DNA microarray data that is of low quality can be discarded if necessary at this step; however, then all the quality control checks are repeated on the new experimental groupings (GeneSpring® GX Manual).

An ANOVA analysis is used to detect differential expression. The Welch ANOVA test using a Benjamini and Hochberg false discovery rate correction is a fairly robust tool for multiple comparisons ($p \leq 0.05$) (Benjamini and Hochberg, 1995). Many software packages can also conduct numerous types of post hoc tests on the data (pairwise comparisons). A Tukey Honestly Significant Difference (HSD) post hoc test is one example that can identify genes that are significantly different between a pair of

conditions (GeneSpring® GX Manual). Table 2.4 shows an example Tukey post hoc for an experiment with four conditions. Analyzing these differentially expressed genes for biological relevant comparisons is crucial. For example, in the model case, a direct comparison of the salt-stressed cultures to the ammonium with proline-stressed cultures may not provide any meaningful biological information. However, the other pairwise comparisons are more likely to result in biologically meaningful information. Specifically, comparing the control and ammonium-stressed cultures would provide information on the effects of ammonium on glycosylation genes. Comparing the control and salt-stressed cultures would identify glycosylation genes sensitive to a low salt addition (a mild osmolarity change). Comparing the ammonium-stressed and ammonium-stressed with proline cultures would identify genes sensitive to the proline addition.

Identifying differentially expressed genes and establishing links between these changes and altered biological activity in response to stressful conditions is crucial. Functional annotation can be used to assist with identifying underlying principles. Several databases can be accessed to provide functional annotation such as the Gene Ontology Consortium (GO), Metacyc, and the Kyoto Encyclopedia of Genes and Genomes (KEGG). The Gene Ontology Consortium maintains a database of controlled vocabularies for the description of molecular functions, biological processes and cellular components of gene products, which can be accessed directly from Gene-Spring_. Metacyc is a database of non-redundant, experimentally elucidated metabolic pathways. The Metacyc Pathway Tools Omics Viewers allows for gene expression data to be overlaid onto the metabolic pathway. KEGG is collection of manually drawn pathway

Table 2.4 Example pairwise comparison of the culture conditions (Tukey post-hoc) – hypothetical data. The ANOVA analysis ($p \leq 0.05$) identified 310 of the 952-glycosylation genes as regulated across the four conditions. The diagonal represents self-comparisons. Values above the diagonal represent the genes that have significantly different expression levels between the two conditions. Values below the diagonal represent the genes that are not significantly different between the two conditions.

Conditions	**Control**	**Condition 1**	**Condition 2**	**Condition 3**
Control	X	230	180	110
Condition 1	722	X	150	165
Condition 2	772	787	X	155
Condition 3	842	802	797	X

maps representing the current knowledge of molecular interaction networks, including glycan biosynthesis and metabolism. Additionally, tools like the MAPPFinder software have been used to identify gene ontology with a higher-than-expected proportion in the differentially expressed data (Kantardjieff et al., 2010).

Many different approaches can be taken to identify the biological significance for an observed set of gene expression changes. Cluster analysis, principle component analysis, heat-maps, k-means clustering, and self-organizing maps (SOM) are all common tools (Wit and McClure, 2004; Landgrebe at al., 2002; Kantardjieff et al., 2009). Hierarchical clustering was used to identify cell-cycle genes that were differentially expressed due to hyperosmolarity (Shen et al., 2010) and principal components analysis was used to condense the dimensionality for butyrate-treated culture gene expression data (Kantardjieff et al., 2010). Wit and McClure reviewed these various tools and provides examples of how each compares (Wit and McClure, 2004).

DNA microarray gene expression data is customarily validated using an orthogonal method, with real-time qRT-PCR being the most commonly employed tool. In the recent cell culture DNA microarray literature, the number of gene expression changes that have been validated by real-time qRT-PCR varies from none to six genes (Gatti et al., 2007; Kantardjieff et al., 2010; Shen et al., 2010; Khoo et al., 2007; Wlaschin and Hu, 2007). Work by Canales et al. demonstrated excellent concordance between real-time qRT-PCR and DNA microarray fold change results using the three common real-time qRT-PCR chemistries; calling into question the need for this validation step (Canales et al., 2006). However, real-time RT-qPCR does provide lower thresholds of detection and

larger assay ranges, which can be used to complement DNAmicroarray analysis for both highly and rarely expressed mRNA species (Canales et al., 2006).

Real-time qRT-PCR uses primers to hybridize the mRNA species and amplify a portion of the mRNA, in which either the DNA product or probes fluoresce proportionally to the amount of mRNA in the sample. Gasparic et al. recently reviewed nine real-time qRTPCR technologies and provides a description of the mechanism of each (Gasparic et al., 2010). As with DNA microarrays, it is necessary to normalize the gene expression data. For real-time qRT-PCR, housekeeping genes are used to provide this normalization. Often actin, glyceraldehyde-3-phospahte dehydrogenase (GAPDH), and 18S rRNA are used as normalizers for mammalian mRNA (Canales et al., 2006; Gasparic et al., 2010). Using many DNA microarray data sets, Bahr et al. identified over 100 housekeeping gene targets for CHO cells due to consistent expression among a variety of culture stresses (Bahr et al., 2009).

To validate DNA microarray gene expression results by real-time qRT-PCR, one must select a real-time qRT-PCR chemistry, design primers to the target mRNA and housekeeping genes, run the reactions, process the data, then compare to the DNA microarray data. Schefe et al. provide a comprehensive guide to real-time qRT-PCR methods and data analysis (Schefe et al., 2006). Canales et al. provides details for comparing DNA microarray and real-time qRT-PCR results (Canales et al., 2006).

In the model case, gene expression levels were quantified using SYBR® Green I dye chemistry (Molecular Probes, Eugene, OR) (Richards et al., 2004; Hein et al., 2001). Primers for each of the mRNA targets were designed using Primer Express (Applied

Biosystems, Foster City, CA). Conventional reverse transcription polymerase chain reactions (RT-PCR) and 2.0% agarose gels were used to confirm primer design, after which visible products on the gels were sequenced to confirm primer specificity. A one step RT-PCR kit (Promega, WI) was used for both conventional RT-PCR and real-time qRT-PCR. The conventional RTPCR should be performed, as per kit instructions. The real-time qRT-PCR can be performed using a Smart Cycler (Cepheid, Sunnyvale, CA). For the model case, CT values were calculated using the Gene Expression's CT Difference (GED) method (Schefe et al., 2006). Alternatively, a second derivative analysis CT method (Luu-The et al., 2005) outlined by Schwarz et al. and Peters et al. (Schwarz et al., 2004; Peters et al., 2003) and normalized as per Pfaffl (Pfaffl et al., 2001) can be used. The normalized gene expression levels for the control, ammonium-stressed, salt-stressed, and ammonium-stressed with proline cultures were assessed using Statistical Analysis Software (SAS). An ANOVA analysis ($p \leq 0.05$) was used to identify gene expression differences.

Data dissemination

Researchers are often required by journals to submit gene expression data to public databases. Gene Expression Omnibus (GEO) at the National Institutes of Health (NIH) in the United States and ArrayExpress at the European Bioinformatics Institute (EBI) part of the European Molecular Biology Laboratory (EMBL) in the United Kingdom, are two well-recognized public gene expression repositories. These public databases offer great opportunities to compare data to other experimental results as well

as learn from results of other experiments. Both GEO and ArrayExpress use the Minimum Information About a Microarray Experiment (MIAME) guidelines that specify the minimum information that should be included when describing a microarray experiment. For GEO submission, the types of data input are categorized – including metadata, raw data files, matrix tables, and the platform. The metadata comprises the descriptive information and protocols used. The raw data files are the original, software-generated quantitative results files. For Affymetrix DNA microarray data, the raw data is contained in the CEL files. The matrix table is a spreadsheet that contains the normalized data. The platform is a description of the DNA microarray architecture and probe sequences. Many commercial platforms have already been submitted to GEO; however, if a new platform has been used, the researcher will have to provide this information. As more data becomes available and accessible through these databases, existing models can be updated and improved. The procedure for GEO submission using MIAME can be found online at http://www.ncbi.nlm.nih.gov/geo/info/MIAME.html (Barrett et al., 2011).

2.5 Conclusion

DNA microarray technologies are extremely useful tools for evaluating how cells respond at the gene expression level to stresses in their culture environment. It is known that the culture environment can greatly impact protein quality, but so far, there has been limited research devoted to evaluating the gene expression levels in response to these culture conditions. While the lack of sequenced genomes hindered previous research, as more genomes continue to be sequenced, the potential for gene expressional analysis using DNA microarrays continues to grow. With DNA microarrays' ability to look at many different genes at once, researchers can now evaluate a larger scope of cellular responses to specific stresses. This allows for the discovery of more comprehensive patterns, involving not only the genes responsible for the enzymes in the glycosylation pathway but also genes associated with other cellular functions that indirectly influence the protein quality. Additionally, data collections from gene expression studies are now publicly available online, providing researchers with even more data with which to formulate models. With these deeper insights, more effective strategies can be designed to take advantage of various culture parameters known to positively affect glycosylation and other post-translational modifications in an effort to develop methods to improve both the quality and quantity of therapeutic protein yields.

2.6 Acknowledgements

This material is based upon work supported by CSREES/USDA, under Project number SC-SC-1700287. Any opinions, findings, conclusions or recommendations expressed in this publication are those of the author(s) and do not necessarily reflect the view of the USDA. The DNA microarrays and services were provided by Consortium for Functional Glycomics' Gene Microarray Core Facility funded by NIH NIGMS Grant# GM62116. Additional funded was provided by Clemson University via a URGC Project Completion Grants and the South Carolina COBRE Center of Biomaterials for Tissue Regeneration sponsored by NIH Grant# P20RR021949.

2.7 References

Androulakis IP, Yang E, Almon RR. Analysis of Time-Series Gene Expression Data: Methods, Challenges, and Opportunities. Annu Rev Biomed Eng. 2007;9:205–228.

Bahr SM, Borgschulte T, Kayser KJ, Lin N. Using microarray technology to select housekeeping genes in Chinese hamster ovary cells. Biotechnol Bioeng. 2009;104:1041–1046.

Baker KN, Rendall MH, Hills AE, Hoare M, Freedman RB, James DC. Metabolic control of recombinant protein N-glycan processing in NS0 and CHO cells. Biotechnol Bioeng. 2001;73:188–202.

Barrett T, Troup DB, Wilhite SE, Ledoux P, Evangelista C, Kim IF, Tomashevsky M, Marshall KA, Phillippy KH, Sherman PM, Muertter RN, Holko M, Ayanbule O, Yefanov A, Soboleva A. NCBI GEO: archive for functional genomics data sets—10 years on. Nucleic Acids Res. 2011;39:D1005–D1010.

Benjamini Y, Hochberg Y. Controlling the False Discovery Rate: A Practical and Powerful Approach to Multiple Testing. J R Statist Soc. B. 1995;57 :289–300.

Canales RD, Luo YL, Willey JC, Austermiller B, Barbacioru CC, Boysen C, Hunkapiller K, Jensen RV, Knight CR, Lee KY, Ma YQ, Maqsodi B, Papallo A, Peters EH, Poulter K, Ruppel PL, Samaha RR, Shi LM, Yang W, Zhang L, Goodsaid FM. Evaluation of DNA microarray results with quantitative gene expression platforms. Nat Biotechnol. 2006;24:1115–1122.

Castro PML, Ison AP, Hayter PM, Bull AT. The macroheterogeneity of recombinant human interferon-r produced by Chinese hamster ovary cells is affected by the protein and lipid content of the culture medium. Biotechnol Appl Biochem. 1995;25:87–100.

Chotigeat W, Watanapokasin Y, Mahler S, Gray PP. Role of environmental conditions on the expression levels, glycoform pattern and levels of sialyltransferase for hFSH produced by recombinant CHO cells. Cytotechnology 1994;15:217–221.

Chen PF, Harcum SW. Effects of elevated ammonium on glycosylation gene expression in CHO cells. Metab Eng. 2006;8:123–132.

Chen PF, Harcum SW. Differential display identifies genes in Chinese hamster ovary cells sensitive to elevated ammonium. Appl Biochem Biotechnol. 2007;141:349–359.

Chung BS, Jeong YT, Chang KH, Kim JS, Kim JH. Effect of Sodium Butyrate on glycosylation of recombinant Erythropoietin. J Microbiol Biotechnol. 2001;11:1087–

1092.

Chuppa S, Tsai YS, Yoon S, Shackleford S, Rozales C, Bhat R, Tsay G, Matanguihan C, Konstantinov K, Naveh D. Fermentor temperature as a tool for control of high-density perfusion cultures of mammalian cells. Biotechnol Bioeng. 1997;55:328–338.

Clark KJR, Chaplin FWR, Harcum SW. Temperature Effects on Product-Quality-Related Enzymes in Batch CHO Cell Cultures Producing Recombinant tPA. Biotechnol Prog. 2004;20:1888–1892.

Clark KJR, Griffiths J, Bailey KM, Harcum SW. Gene-expression profiles for five key glycosylation genes for galactose-fed CHO cells expressing recombinant IL-4/13 cytokine trap. Biotechnol Bioeng. 2005;90:568–577.

Clarke C, Doolan P, Barron N, Meleady P, O'Sullivan F, Gammell P, Melville M, Leonard M, Clynes M. Predicting cell-specific productivity from CHO gene expression. J Biotechnol. 2011;151:159–165.

deZengotita VM, Abston LR, Schmelzer AE, Shaw S, Miller WM. Selected amino acids protect hybridoma and CHO cells from elevated carbon dioxide and osmolality. Biotechnol. Bioeng. 2002;78:741–752.

Etchevarry T, Ryll T, Genentech, Inc. Mammalian cell culture process. 1998; US Patent 5705:364.

Gasparic MB, Tengs T, La Paz JL, Holst-Jensen A, Pla M, Esteve T, Zel J, Gruden K. Comparison of nine different real-time PCR chemistries for qualitative and quantitative applications in GMO detection. Anal Bioanal Chem. 2010;396:2023–2029.

Gatti MD, Wlaschin KF, Nissom PM, Yap M, Hu WS. Comparative transcriptional analysis of mouse hybridoma and recombinant Chinese hamster ovary cells undergoing butyrate treatment. J Biosci Bioeng. 2007;103:82–91.

Gawlitzek M, Conradt HS, Wagner R. Effect of different cell culture conditions on the polypeptide integrity and N-glycosylation of a recombinant model glycoprotein. Biotechnol Bioeng. 1995;46:536–544.

Gawlitzek M, Valley U, Wagner R. Ammonium ion and glucosamine dependent increases of oligosaccharide complexity in recombinant glycoproteins secreted from cultivated BHK-21 cells. Biotechnol Bioeng. 1998;57:518–528.

Gawlitzek M, Ryll T, Lofgren J, Sliwkowski MB. Ammonium alters N-glycan structures of recombinant TNFR-IgG: Degradative versus biosynthetic mechanisms. Biotechnol Bioeng. 2000;68:637–646.

Gu XJ, Xie LZ, Harmon BJ, Wang DIC. Influence of Primatone RL supplementation on sialylation of recombinant human interferon-gamma produced by Chinese hamster ovary cell culture using serum-free media. Biotechnol Bioeng. 1997;56:353–360.

Hacker DL, De Jesus M, Wurm FM. 25 years of recombinant proteins from reactor-grown cells - where do we go from here? Biotechnol Adv. 2009;27:1023–1027.

Hayter PM, Curling EMA, Gould ML, Baines AJ, Jenkins N, Salmon I, Strange PG, Bull AT. The effect of the dilution rate on CHO cell physiology and recombinant interferon-g production in glucoselimited chemostat culture. Biotechnol Bioeng. 1993;42:1007–1085.

Hein J, Schellenberg U, Bein G, Hackstein H. Quantification of Murine IFN-γ mRNA and Protein Expression: Impact of Real-Time Kinetic RT–PCR Using SYBR Green I Dye. Scand J Immunol. 2001;54:285–291.

Heller MJ. DNA microarray technology: devices, systems, and applications. Annu Rev Biomed Eng. 2002;4:129–153.

Hooker AD, Green NH, Baines AJ, Bull AT, Jenkins N, Strange PG, James DC. Constraints on the transport and glycosylation of recombinant IFN-γ in Chinese hamster ovary and insect cells. Biotechnol Bioeng. 1999;63:559–572.

Jaluria P, Konstantopoulos K, Betenbaugh M, Shiloach J. A perspective on microarrays: current applications, pitfalls, and potential uses. Microb Cell Factor. 2007;6.

Jenkins N, Murphy L, Tyther R. Post-translational modifications of recombinant proteins: Significance for biopharmaceuticals. Mol Biotechnol. 2008;39:113–118.

Jenkins N, Meleady P, Tyther R, Murphy L. Strategies for analysing and improving the expression and quality of recombinant proteins made in mammalian cells. Biotechnol Appl Biochem. 2009;53:73–83.

Kantardjieff A, Nissom PM, Chuah SH, Yusufi F, Jacob NM, Mulukutla BC, Yap M, Hu WS. Developing genomic platforms for Chinese hamster ovary cells. Biotechnol Adv. 2009;27:1028–1035.

Kantardjieff A, Jacob NM, Yee JC, Epstein E, Kok YJ, Philp R, Betenbaugh M, Hu WS. Transcriptome and proteome analysis of Chinese hamster ovary cells under low temperature and butyrate treatment. J Biotechnol. 2010;145:143–159.

Kaufmann H, Mazur X, Fussenegger M, Bailey JE. Influence of low temperature on productivity, proteome and protein phosphorylation of CHO cells. Biotechnol Bioeng. 1999;63:573–582.

Khoo SHG, Falciani F, Al-Rubeai M. A genome-wide transcriptional analysis of producer and non-producer NS0 myeloma cell lines. Biotechnol Appl Biochem. 2007;47:85–95.

Kim NY, Kim JH, Kim HJ. Effect of low adapted temperature and medium composition on growth and erythropoietin (EPO) production by Chinese hamster ovary cells. Arch Pharmacal Res. 2005;28:220–226.

Korke R, Gatti MD, Lau ALY, Lim JWE, Seow TK, Chung MCM, Hu WS. Large scale gene expression profiling of metabolic shift of mammalian cells in culture. J Biotechnol. 2004;107:1–17.

Kumar N, Gammell P, Clynes M. Proliferation control strategies to improve productivity and survival during CHO based production culture. Cytotechnology 2007;53:33–46.

Kunkel JP, Jan DCH, Jamieson JC, Butler M. Dissolved oxygen concentration in serum-free continuous culture affects N-linked glycosylation ofs a monoclonal antibody. J Biotechnol. 1998;62:55–71.

Landgrebe J, Wurst W, Welzl G. Permutation-validated principal components analysis of microarray data. Genome Biol. 2002;3.

Larkin JE, Frank BC, Gavras H, Sultana R, Quackenbush J. Independence and reproducibility across microarray platforms. Nat Methods 2005;2:337–343.

Lee YY, Yap MGS, Hu WS, Wong KTK. Low-Glutamine Fed-Batch Cultures of 293-HEK Serum-Free Suspension Cells for Adenovirus Production. Biotechnol Prog. 2003;19:501–509.

Lim Y, Wong NSC, Lee YY, Ku SCY, Wong DCF, Yap MGS. Engineering mammalian cells in bioprocessing – current achievements and future perspectives. Biotechnol Appl Biochem. 2010;55:175–189.

Luu-The V, Paquet N, Calvo E, Cumps J. Improved real-time RT-PCR method for high-throughput measurements using second derivative calculation and double correction. BioTechniques 2005;38:287–293.

Maiorella BL, Winkelhake J, Young J, Moyer B, Bauer R, Hora M, Andya J, Thomson J, Patel T, Parekh R. Effect of culture conditions on IgM antibody structure, pharmacokinetics and activity. Biotechnology 1993;11:387–392.

Muyal JP, Singh SK, Fehrenbach H. DNA-Microarray Technology: Comparison of Methodological Factors of Recent Technique Towards Gene Expression Profiling. Crit Rev Biotechnol. 2008;28:239–251.

Nissom PM, Sanny A, Kok YJ, Hiang YT, Chuah SH, Shing TK, Lee TT, Wong KTK, Hu WS, Sim MYG, Philp R. Transcriptome and proteome profiling to understanding the biology of high productivity CHO cells. Mol Biotechnol. 2006;34:125–140.

Ozturk SS, Palsson BO. Effects of dissolved oxygen on hybridoma cell growth, metabolism, and antibody production kinetics in continuous culture. Biotechnol Prog. 1990;6:437–446.

Patel TP, Parekh RG, Poellering BJ, Prior CP. Different culture methods lead to differences in glycosylation of a murine IgG monoclonal antibody. Biochem J. 1992;285:839–845.

Peters IR, Helps CR, Batt RM, Day MJ, Hall EJ. Quantitative real-time RT-PCR measurement of mRNA encoding alpha-chain, pIgR and J-chain from canine duodenal mucosa. J Immunol Methods. 2003;275:213–222.

Pfaffl MW. A new mathematical model for relative quantification in real-time RT-PCR. Nucleic Acids Res. 2001;29:e45.

Redestig H, Costa IG. Detection and interpretation of metabolite–transcript coresponses using combined profiling data. Bioinformatics 2011;27:I357–I365.

Richards GP, Watson MA, Kingsley DH. A SYBR green, real-time RT-PCR method to detect and quantitate Norwalk virus in stools. J Virol Methods. 2004;116:63–70.

Schefe JH, Lehmann KE, Buschmann IR, Unger T, Funke-Kaiser H. Quantitative real-time RT-PCR data analysis: current concepts and the novel "gene expression's CT difference" formula. J Mol Med Jmm. 2006;84:901–910.

Schwarz G, Baumler S, Block A, Felsenstein FG, Wenzel G. Determination of detection and quantification limits for SNP allele frequency estimation in DNA pools using real time PCR. Nucleic Acids Res. 2004;32:e24.

Shen DA, Kiehl TR, Khattak SF, Li ZJ, He AQ, Kayne PS, Patel V, Neuhaus IM, Sharfstein ST. ranscriptomic responses to sodium chloride-induced osmotic stress: a study of industrial fed-batch CHO cell cultures. Biotechnol Prog. 2010;26:1104–1115.

Smyth GK, Speed T. Normalization of cDNA microarray data. Methods. 2003;31:265–273.

Sung YH, Lee GM. Enhanced Human Thrombopoietin Production by Sodium Butyrate Addition to Serum-Free Suspension Culture of Bcl-2-Overexpressing CHO Cells. Biotechnol Prog. 2005;21:50–57.

Qian YM, Khattak SF, Xing ZZ, He AQ, Kayne PS, Qian NX, Pan SH, Li ZJ. Cell culture and gene transcription effects of copper sulfate on Chinese hamster ovary cells. Biotechnol Prog. 2011;27:1190–1194.

Valley U, Nimtz M, Conradt HS, Wagner R. Incorporation of ammonium into intracellular UDP-activated N-acetylhexosamines and into carbohydrate structures in glycoproteins. Biotechnol Bioeng. 1999;64:401–417.

Wit E, McClure J. Statistics for Microarrays: Design, Analysis, and Inference. John Wiley and Sons, West Sussex, 2004.

Wlaschin KF, Seth G, Hu WS. Toward genomic cell culture engineering. Cytotechnology 2006;50:121–140.

Wlaschin KF, Hu WS. Engineering cell metabolism for high-density cell culture via manipulation of sugar transport. J Biotechnol. 2007;131:168–176.

Wong DCF, Wong KTK, Goh LT, Heng CK, Yap MGS. Impact of dynamic online fed-

batch strategies on metabolism, productivity and N-gycosylation quality in CHO cell cultures. Biotechnol Bioeng. 2005;89:164–177.

Wong DCF, Wong NSC, Goh JSY, May LM, Yap MGS. Profiling of N-glycosylation gene expression in CHO cell fed-batch cultures. Biotechnol Bioeng. 2010;107:516–528.

Wong NSC, Wati L, Nissom PM, Feng HT, Lee MM, Yap MGS. An investigation of intracellular glycosylation activities in CHO cells: Effects of nucleotide sugar precursor feeding. Biotechnol Bioeng. 2010;107:321–336.

Wu ZJ, Aryee MJ. Subset quantile normalization using negative control features. J Comput Biol. 2010;17:1385–1395.

Xu X, Nagarajan H, Lewis NE, Pan S, Cai Z, Liu X, Chen W, Xie M, Wang W, Hammond S, Andersen MR, Neff N, Passarelli B, Koh W, Fan HC, Wang J, Gui Y, Lee KH, Betenbaugh MJ, Quake SR, Famili I, Palsson BO, Wang J. The genomic sequence of the Chinese hamster ovary (CHO)-K1 cell line. Nat Biotechnol. 2011;29:735–741.

Yang M, Butler M. Effects of Ammonia and Glucosamine on the Heterogeneity of Erythropoietin Glycoforms. Biotechnol Prog. 2002;18:129–138.

Yang YH, Dudoit S, Luu P, Lin DM, Peng V, Ngai J, Speed TP. Normalization for cDNA microarray data: a robust composite method addressing single and multiple slide systematic variation. Nucleic Acids Res. 2002;30:e15.

Yee JC, Gerdtzen ZP, Hu WS. Comparative transcriptome analysis to unveil genes affecting recombinant protein productivity in mammalian cells. Biotechnol Bioeng. 2009;102:246–263.

Yoon SK, Kim SH, Lee GM. Effect of low culture temperature on specific productivity and transcription level of anti-4-1BB antibody in recombinant Chinese hamster overy cells. Biotechnol Prog. 2003;19:1383–1386.

Zhou WC, Chen CC, Buckland B, Aunins J. Fed-batch culture of recombinant NS0 myeloma cells with high monoclonal antibody production. Biotechnol Bioeng. 1997;55:783–792.

CHAPTER THREE: GLYCOSYLATION-RELATED GENES IN NS0 CELLS ARE INSENSITIVE TO MODERATELY ELEVATED AMMONIUM CONCENTRATIONS

3.1 Abstract

NS0 and Chinese hamster ovary (CHO) cell lines are used to produce recombinant proteins for human therapeutics; however, ammonium accumulation hinders cell growth, recombinant protein production, and protein glycosylation. To improve product quality and decrease costs, the link between ammonium and protein glycosylation must be resolved. While ammonium is known to disrupt glycosylation-related gene expression in CHO cells, NS0 studies have not been performed. This study examined if NS0 cells were ammonium-sensitive at the gene expression level. The effects of various culture conditions – ammonium, salt, and ammonium with proline - on gene expression were assessed by DNA microarrays with mouse glycosylation-related and housekeeping genes. Surprisingly, no significant differences in gene expression levels were observed between the control and these conditions. Further, the elevated ammonium condition was analyzed using real-time quantitative reverse transcriptase PCR (qRT-PCR) for key glycosylation genes, and the qRT-PCR results corroborated the microarray results, showing NS0 cells to be ammonium-insensitive at the gene expression level. Thus, this study suggests that for NS0 cells, the observed ammonium-induced effects on protein glycosylation and sugar nucleotide pools are due to translational or enzymatic changes rather than transcriptional changes.

3.2 Introduction

Mammalian cells are increasingly being used to produce glycoproteins for human clinical therapies. The extent of glycosylation – or the addition of sugar groups to proteins – plays an important role in the effectiveness of treatments, which makes protein glycosylation quality a top priority (Butler, 2006; Butler and Meneses-Acosta, 2012; Hudak and Bertozzi; Jenkins et al., 1996; Lingg et al., 2012; Ozturk, 1992). The culture environment, in which ammonia and ammonium ions accumulate, plays a significant role in determining cell growth rates, recombinant protein production, and protein glycosylation quality (Berlec and Strukelj, 2013; Butler, 2006; Chen and Harcum, 2005; deZengotita et al., 2002; Gawlitzek et al., 1999; Hansen and Emborg, 1994; Jenkins, 1996; Jenkins et al., 1996; Miller et al., 1988; Quek et al., 2010; Reuveny et al., 1986; Schneider et al., 1997; Yang and Butler, 2000a). Specifically, elevated ammonium levels reduce protein glycosylation quality, by decreasing terminal sialylation levels as well as both the tetraantennary and tetrasialylated oligosaccharide structures, while increasing molecular heterogeneity (Baker et al., 2001; Chen and Harcum, 2005; Yang and Butler, 2000b, 2002). All of these factors lower the efficacy of a therapeutic glycoprotein and having to remove these isoforms increases costs (Jenkins et al., 1996).

Interestingly, elevated ammonium has been shown to lead to higher intracellular nucleotide sugar pools, which serve as precursors for many glycosylation reactions, in NS0 cells (Ryll, 1994; Valley et al., 1999). Additionally, when cells are supplemented with glycosylation precursors, such as N-acetylmannosamine and galactose, glycosylation was not significantly increased, despite increased nucleotide sugar pools

(Baker et al., 2001; Clark et al., 2005; Gu and Wang, 1998). Furthermore, cloning additional copies of two genes encoding important glycosylation enzymes – sialyltransferase and galactosyltransferase – produced only modest improvements in protein glycosylation (Weikert et al., 1999).

In this research, we sought to expand our limited understanding of protein glycosylation control, by investigating how elevated ammonium levels influence glycosylation at the gene expression level. To this end, an Affymetrix-platform DNA microarray was employed, that contains the known mouse glycosylation-related nucleotide sequences and numerous housekeeping genes for mouse, the host organism of the NS0 cell line. Elevated ammonium is known to significantly decrease protein sialylation in NS0 cells (Baker et al., 2001), and the sialyltransferase gene has been observed to be ammonium-sensitive in Chinese hamster ovary (CHO) cells (Chen and Harcum, 2006), altered gene expression was expected in NS0 cells, as well. Additionally, both CHO and NS0 cell lines are used to manufacture recombinant glycoproteins for clinical therapies and can be cultured in defined media in suspension cultures (Gatti et al., 2007). Initially, four culture conditions were compared – control, elevated ammonium, elevated salt as an osmolarity control, and elevated ammonium with a proline addition, as proline had been observed to reduce the negative effects of ammonium on product quality for CHO cells. Additionally, the orthogonal gene expression quantification method real-time qRT-PCR was used to confirm the results observed for the elevated ammonium culture condition using a newer media formulation.

3.3 Materials and Methods

The NS0 cells (ECACC 85110503) for the DNA microarray studies were donated to Clemson University by Merck, Inc, and originally from the European Collection of Cell Cultures. The NS0 cells for the real-time qRT-PCR studies were purchased from Sigma (catalog no. 03061601— ECACC 85110503), where Sigma is the official US distributor ECACC. NS0 cells are a mouse myeloma cell line with lymphoblast morphology, non-secreting clone, and cholesterol auxotroph (Whitford, 2003). The NS0 cell lines used in these studies do not express a recombinant protein and represent the host strain or the fusion partner for generation of hybridomas. For the DNA microarray studies, an animal-derived protein-free media, HyQ ADCF-Mab (Hyclone) (first-generation media), was used and supplemented with 5 mM glutamine (Hyclone) and LS-250 cholesterol supplement (4 mL per L media; Hyclone) in 1000 mL spinner flasks with 100 rpm agitation. For the cultures analyzed by real-time qRT-PCR, a second-generation ADCF-Mab media (Thermo Hyclone) was used with a LS-1000 cholesterol supplement (1 mL per L media; Hyclone) in 250 mL spinner flasks with 60 rpm agitation. Both studies cultured the cells in humidified incubators at 37°C and 5% CO_2. A common seed culture was used to inoculate the control and treatment cultures, which were then cultured in parallel. Biological triplicates were used for each condition examined. The ammonium, salt, and proline stock solutions (all 5000 mM) were prepared in Milli-Q water and added to the fresh media prior to the addition of cells. Milli-Q water was added to the control and treatment cultures to normalize culture volumes and media concentrations (1 to 6 mL per L). For initial growth studies, the culture conditions were basal media (control), and

basal media supplemented with either 10 mM NH_4Cl (ammonium), 10 mM NaCl (salt), or 10 mM NH_4Cl and 20 mM proline (proline). For the DNA microarray studies, the culture conditions were basal media (control), and basal media supplemented with either 5 mM NH_4Cl (ammonium), 5 mM NaCl (salt), or 5 mM NH_4Cl and 10 mM proline (proline). Osmolality of the media was measured using the freezing point method (Schmelzer et al., 2000). The 5 mM additions increased osmolality by approximately 30 mOsm/kg, or only approximately 10%. Cell concentrations and viabilities were determined by the Trypan blue exclusion method. Glucose was measured using a Blood Glucose Analyzer (Hemacue). For the real-time qRT-PCR studies, the control and elevated ammonium (5 mM) conditions were investigated. Cell concentrations were quantified using the Scepter 2.0 Handheld Automated Cell Counter (Millipore). Glucose and lactate were quantified using a Yellow Springs Instruments (Yellow Springs, OH) 2900 Biochemistry Analyzer.

RNA isolation

Cells were harvested by centrifugation at 3000 g for 5 min at 4°C in order to obtain total RNA. The supernatant and pellets were saved at –20°C and –80°C, respectively. Total RNA was isolated from the pellet using the RNAqueous-MidiTM kits (Ambion), except the DNase treatment was increased to 2 µl of DNase and 1 hour. The total RNA was further purified using the RNeasy Qaigen kit. RNA concentrations were determined using a Ribogreen RNA quantification kit (Molecular Probes).

DNA microarray analysis

Ten micrograms of total RNA (1 μg/μl) per sample was sent to the Consortium for Functional Genomics for gene expression analysis on the GLYCOv3 Chip. The Affymetrix-platform and data discussed in this publication have been deposited in NCBI's Gene Expression Omnibus (Barrett et al., 2013) and are accessible through GEO Platform accession GPL11096: http://www.ncbi.nlm.nih.gov/geo/query/acc.cgi?acc=GPL11096. The GLYCOv3 Chip Mouse Gene List can also be found at http://www.functionalglycomics.org/static/consortium/resources/resourcecoree.shtml (accessed April 10, 2014). These Glyco-Gene Chips are available to academic researchers through a proposal process. The GLYCOv3 Chip contains 952 mouse glycosylation-related probes, including probes for the sialyltransferase, galactosyltransferase, sialidase, and fucosyltransferase genes. All 14 of the genes (including the two housekeeping genes), previously investigated in CHO cells under elevated ammonium by qRT-PCR, were on GLYCOv3 Chip (Aebi et al., 2000). Biological triplicates for each condition were analyzed for a total of 12 DNA microarrays.

Briefly, upon arrival of the total RNA, the Consortium for Functional Genomics staff assessed the RNA quality using a Bioanalyzer (Agilent). Then, the RNA was reverse transcribed in the presence of the fluorescently-labeled dNTP analogues. The labeled RNA was then hybridized to the GLYCOv3 Chip, including the GeneChip Eukaryotic Hybridization Controls, Bacteriophage Controls, and GC Controls (Affymetrix). The GeneChip Eukaryotic Hybridization Controls contains a mixture of four biotin-labeled

cRNA controls with staggered concentrations. The Bacteriophage Controls contains four bacteriophage P1 oligonucleotides, and the GC Control contains 44 random and specific GC oligonucleotides that provide titrated fluorescent signals. These controls provide calibrated intensities that are used to confirm hybridization and chip integrity. These controls are used to determine the "Present" and "Absent" calls for a gene. Additionally, there are 104 housekeeping mouse gene controls on the chip as probes. The GLYCOv3 Chips were scanned with a confocal scanner, which calculated the signal intensities associated with each oligonucleotide on the GLYCOv3 chip into image files viewable by researchers. The data was reviewed for quality control at the Consortium for Functional Genomics, where the data files were processed and returned as .CEL files. GeneSpring® imported the .CEL data, and each gene was then normalized to the total intensity of the chip. The data discussed in this publication have been deposited in NCBI's Gene Expression Omnibus (Barrett et al., 2013) and are accessible through GEO Series accession number GSE28920 (http://www.ncbi.nlm.nih.gov/geo/query/acc.cgi?acc=GSE28920).

Real-time qRT-PCR analysis

The cDNA was synthesized using 1 μg of total RNA from each sample as template using Retroscript Kit (Life Technologies). Real-time RT-PCR was performed with Quantitect SYBR® Green PCR Kit (Qiagen) using primers designed for five glycosylation-related genes: solute carrier family 35 (CMP-sialic acid transporter) [Slc35a1], ST3 β-galactoside α-2,3-sialyltransferase 3 [St3gal3], ST3 β-galactoside α-

2,3-sialyltransferase 4 [St3gal4], ST3 β-galactoside α-2,3-sialyltransferase 6 [St3gal6], β(1,4)-galactosyltransferase [B4galt1], and two endogenous control genes: Actin, beta (Actb) and glyceraldehyde-3-phosphate dehydrogenase (Gapdh) in a Rotor-Gene 3000 Real-Time Thermal Cycler (Qiagen). Primer sequences are listed in Table 3.1. Relative gene expression levels were calculated using the $2^{-\Delta\Delta C_T}$ method with Gapdh as an internal standard (Livak and Schmittgen, 2001).

Statistical analysis

For the DNA microarray data, a Welch ANOVA test using a Benjamini and Hochberg false discovery rate correction was used for the multiple comparisons ($p \leq 0.05$, $p \leq 0.10$, and $p \leq 0.99$) with Tukey Post-Hoc tests. ANOVA analysis was used to analyze the effect of ammonium on cell densities and growth rates ($p \leq 0.05$). For real time qRT-PCR, a student's two-tailed t-test was employed to determine the significant differences between groups, with $p \leq 0.05$ being considered as statistically different.

Table 3.1 PCR primer sequences for analysis of NS0 cells. *M. musculus* primer sequences used for qRT-PCR analysis of elevated ammonium for NS0 cultures.

Gene	Forward Primer Sequence	Reverse Primer Sequence
Actb	5'- GGT GTG ATG GTG GGA ATG G -3'	5'- TCT CCA TGT CGT CCC AGT TG -3'
B4galt1	5' TGT CTC TCC TCA CAA GGT GG 3	5' TGG TGT CTC CAG CCT GAT TG 3'
Gapdh	5'- GCA AAT TCA ACG GCA CAG TC -3'	5'- ATA CTC AGC ACC GGC CTC AC -3'
Slc35a1	5'- TCT ACA CGT CAG TGG TGG TG -3'	5'- AGC TCC CAG TGC AAA TGA AAG -3'
St3gal3	5' CTG TGA TGA AGT GGC AGT CG 3'	5' CTC TCG CTG GAT GTT GTG TG 3'
St3gal4	5'- GAG TGA TAA GAA GCG GGT GC -3'	5'- GCT TGT CTG CTG CAA TCT CC -3'
St3gal6	5' CCC AAA CAC CCT ACA ACA GG 3'	5' ACA TGG TGG CAT TCC CGT AG 3'

3.4 Results

To study the impact of elevated ammonium on gene expression using a DNA microarray, NS0 cells were cultured under four conditions: normal (control), elevated ammonium, elevated salt, and elevated ammonium with proline. The elevated salt treatment provided an osmolality control, while the proline-addition cultures were included because previous elevated ammonium studies in CHO cells showed that a proline-addition could reduce ammonium-induced growth inhibition and restore some protein glycosylation (Chen and Harcum, 2005). Initially, NS0 were cultured under 10 mM ammonium, 10 mM salt, 10 mM ammonium with 20 mM proline; however, the growth rates of the ammonium-stressed cultures (with and without proline) were only approximately one-fifth of the control culture, while the salt-stressed culture growth rate was only approximately one-third of the control culture (data not shown). These very different growth rates were unquestionably too great to allow for meaningful gene expression comparisons, as samples would have to be taken at different culture ages to obtain similar cell densities, and the cells would be in very different growth phases. Interpretation of data from cultures with multiple growth rate and cell densities differences would have required significantly more samples than were available due to the high cost of DNA microarrays. Thus, cell growth rates were examined at 5 mM ammonium, 5 mM salt, and 5 mM ammonium with 10 mM proline. Previous studies have shown that ammonium levels as low as 2 mM can negatively impact glycosylation, thus a 5 mM ammonium treatment was deemed to have the characteristics representative of elevated ammonium (Andersen et al., 1994; Andersen and Goochee, 1995). The growth

profiles for NS0 cells cultured under 5 mM ammonium, 5 mM salt, and 5 mM ammonium with 10 mM proline are shown in Figure 3.1 for the control and treated cultures shown as the average of triplicates with 95% confidence intervals. The ANOVA analysis of the growth rates and final cell densities indicated that the culture treatment was a significant factor. Further post hoc testing using paired t-tests showed no differences for growth rates between the control and treated cultures ($p > 0.05$); however, the paired t-tests did indicate that the final cell densities were different ($p \leq 0.05$). The final cell densities for the control, 5 mM ammonium, and 5 mM ammonium/10 mM proline cultures were all different from each other; however, the final cell densities for salt cultures were not different from the control cultures ($p > 0.05$), and were not different from 5 mM ammonium cultures ($p > 0.05$). The final cell densities for salt cultures were also different from the 5 mM ammonium/10 mM proline cultures ($p \leq 0.05$). These profiles and statistical analysis indicate that the culture conditions were very similar, such that growth rate differences would not be a contributing factor in any gene expression differences that might be identified and the final cell densities would only be a minor factor.

For the DNA microarray experiments, the 90-h time point (indicated by a vertical line in Figure 3.1) was selected for RNA isolation and DNA microarray analysis to identify genes sensitive to ammonium in the exponentially growing cultures. The gene expression analysis was performed at the 90 h time point to balance several experimental constraints. The cultures needed to be in the same growth phase and at similar cell densities, where mid-exponential growth was desired. The cell density needed to be

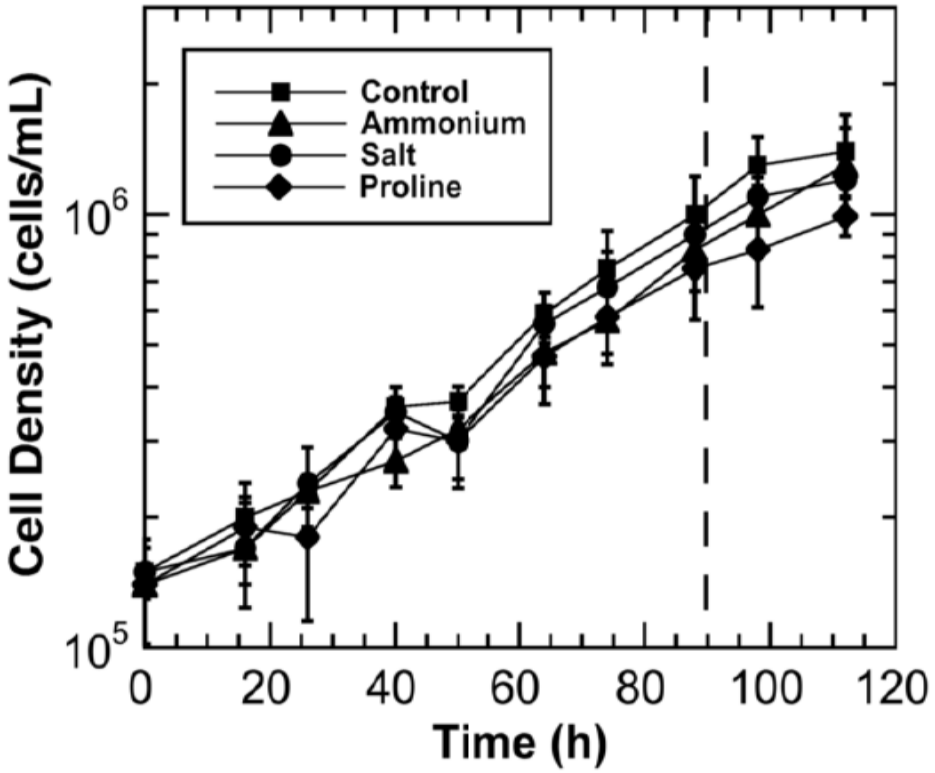

Figure 3.1. Growth profiles for NS0 cells. NS0 cells were cultured under control, elevated ammonium, elevated salt, and elevated ammonium with proline conditions in a first-generation HyQ ADCF-Mab media with LS-250 cholesterol. RNA samples were taken at 90-h for gene expression analysis by DNA microarrays as shown by the vertical line. Error bars represent 95% confidence intervals.

sufficiently high to obtain enough total RNA from a single sample (50 mL). And, exponential growth after sampling needed to verifiable after sampling, at least another 12 hours of growth possible in the media. Additionally, due the cost of DNA microarrays, only 12 DNA microarrays were available to the project from the Scripps Institute. Thus, for four culture conditions to be sampled in triplicate, the experiment was limited to one time point. As shown in Figure 3.1, all cultures continued to grow exponentially for at least another 12 hours. GeneSpring® was used to analyze the gene expression levels using a Welch ANOVA test with a Benjamini and Hochberg false discovery rate correction for the four conditions, where each chip was normalized to total intensity. Initially, the p-value cut-off was set to $p \leq 0.05$; however, at this level no genes were determined to be significantly different. Due to the high levels of noise commonly observed in biological systems, the p-value cut-off was increased to $p \leq 0.10$ and the data re-examined; however, even at this level no genes were identified as being significantly different between the conditions. In order to better understand why the ANOVA analysis was not identifying any significant genes, the p-value was increased to $p \leq 0.99$, and all genes passed, as expected. The gene with the lowest p-value had a p-value of $p = 0.964$, which indicates no significant difference in gene expression levels between the four conditions examined, when gene intensities were normalized to the total chip intensity. This means that none of the glycosylation genes had different gene expression levels between any of the four conditions.

Further analysis of the DNA microarray data demonstrated that the Affymetrix titrated controls had the expected dynamic range, indicating the gene chips were

responsive to sample-level changes. It was also determined that noise was not the reason for the high p-values as shown in Figure 3.2 by the high-level of reproducibility of the biological replicates and low noise to signal ratio. Figure 3.2 only shows the gene expression levels for the twelve glycosylation and two housekeeping genes previously examined for CHO cells, as a graph of all 952 unchanged genes would be unreadable (Chen and Harcum, 2006). Table 3.2 includes these selected genes with official Mus musculus gene names, abbreviations, and Genbank accession number on the GLYCOv3 DNA microarray and the CHO cell (*Cricetulus griseus*) homolog, common name, and GenBank accession number. The gene expression levels for the NS0 cell culture conditions are connected between the conditions only to improve visualization. The standard error bars for each condition and gene are shown (and are barely visible for some genes). These very small standard error bars support that there are "no significant difference" due to the underlying behaviour of the biological system, and not due to a high signal-to-noise ratio in the data. Note: the Fut4 and Neu2 genes were identified as "Absent", not expressed, under these conditions in NS0 cells. These two genes are only shown to highlight the range of magnitude for gene expression and because these are the homologs of the CHO genes previously reported to be sensitive to ammonium. At the other extreme are the housekeeping genes, which are commonly among the mostly highly expressed genes within an organism. These gene expression data for these glycosylation and housekeeping genes demonstrate the well-distributed dynamic range of gene expression levels within the study and detected by the DNA microarrays. Thus, as further shown in Figure 3.2, no glycosylation-related genes had significantly different gene

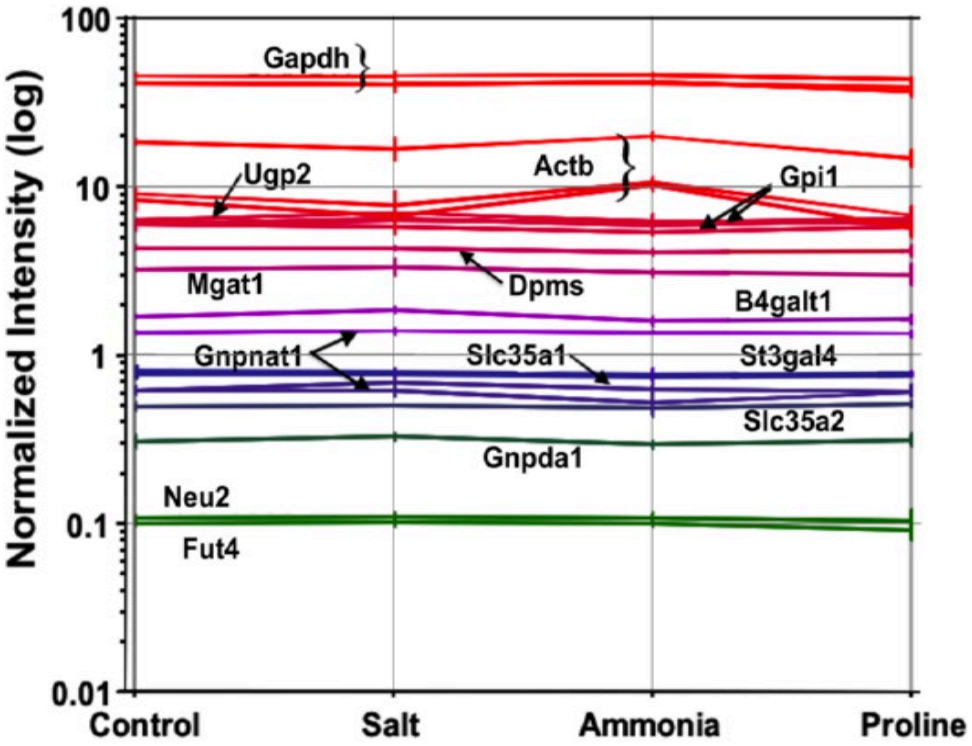

Figure 3.2. Gene expression levels for 12 key glycosylation genes and two housekeeping genes in NS0 cells. The NS0 cells were cultured under control, elevated ammonium, elevated salt, and elevated ammonium with proline conditions in a first-generation HyQ ADCF-Mab media with LS-250 cholesterol. Data points between the culture conditions are connected to assist with visualization only. The Fut4 and Neu2 genes were "Absent", i.e., not expressed, under these conditions. Abbreviations are listed in Table 3.2. Standard error bars are shown.

Table 3.2 Selected *M. musculus* and *Cricetulus griseus* glycosylation and housekeeping genes.

Abbreviation	Official Name	GenBank Accession # (GLYCOv3)	Gene Name (From Chen and Harcum, 2006)	GenBank Accession #
Actb	Actin, beta	M12481	Actin	U20114.1
B4galt1	UDP-Gal:betaGlcNAc beta 1,4-galactosyl transferase, polypeptide 1	NM_022305.2	β(1,4)-Galactosyltransferase (β(1,4)-GT)	AF318896.1
Dpm1	dolichol-phosphate (beta-D) mannosyltransferase 1	NM_010072.2	Dolicholphosphate mannose synthase (DPMS)	AF121895.1
Fut4[a]	fucosyltransferase 4	NM_010242	α(1,3)-Fucosyltransferase (α(1,3)-FT)	AF090449
Gapdh	glyceraldehyde-3-phosphate dehydrogenase	M32599	Glyceraldehyde-3-phosphate dehydrogenase (GAPDH)	X52123.1
Gnpda1	glucosamine-6-phosphate deaminase 1	NM_011937	Glucosamine-6-phosphate isomerase Mesocricetus auratus (G6PI)	X94699.1
Gnpnat1	glucosamine-phosphate Nacetyltransferase 1	NM_019425	UDP-GlcNAc:UDP N-acetyl-Dglucosamine-1-phosphate transferase (UDP-NAG)	U09453.1
Gp1	glucose phosphate isomerase 1	NM_008155	Glucose phosphate isomerase (GPI)	Z37977.1
Mgat1	mannosideacetylglucosaminyltransferase 1	NM_010794.2	N-acetylglucos-aminyltransferase (NAGAT)	U65791
Neu2 [a]	neuraminidase 2	NM_015750	Sialidase	U06143.1
Slc35a1	solute carrier family 35 (CMP sialic acid transporter), member 1	NM_011895	CMP-sialic acid transporter (CMPSiaT)	Y12074.1
Slc35a2	solute carrier family 35 (UDPgalactose transporter), member A2	AB027147	UDP-galactose transporter (UDPGalT)	AF299335.1
St3gal3[b]	ST3 beta-galactoside alpha-2,3-sialyltransferase 3	NM_009176.2	NA	NA
St3gal4	ST3 beta-galactoside alpha-2,3-sialyltransferase 4	NM_009178.2	Gal(β -1,3/4)-GlcNAc-α(2,3)-sialyltransferase IV (α(2,3)-ST)	AY266675.1
St3gal6 [a,b]	ST3 beta-galactoside alpha-2,3-sialyltransferase 6	NM_018784	NA	NA
Ugp2	UDP-glucose pyrophosphorylase 2	AF424698	UDP-glucosepyrophosphorylase (UDP-GPP)	AF004368.1

Table 3.2 (Continued): Selected *M. musculus* and *Cricetulus griseus* glycosylation and housekeeping genes. Also listed are gene abbreviations, official names, and Genbank accession numbers.

a Fut4 , Neu2, and St3gal6 were "Absent", i.e., not expressed as assessed by DNA microarray under the condition studied.

b St3gal3 and St3gal6 are only shown quantitatively by real time qRT-PCR

NA – Not Applicable: Gene was not examined in Chen and Harcum, 2006.

expression levels between the four conditions examined using the DNA microarray for the NS0 cultures.

As DNA microarrays are not sensitive to small gene expression changes, and to confirm these surprising gene expression results, the control and elevated ammonium conditions of the experiment were repeated and the gene expression changes were analyzed using real-time qRTPCR, an orthogonal and more sensitive gene expression quantification method (Canales et al., 2006; Provenano and Mocellin, 2007; Schefe et al., 2006; Wurmbach, 2009). For the real-time qRT-PCR experimental repeats, several minor changes were necessary. Specifically, the protein-free, animal-free media originally used for the microarray experiments was no longer available, so the next generation of that media was used. The LS-1000 cholesterol supplement was used instead, since the previous LS-250 supplement was unavailable. The culture volume was decreased from 1000 mL to 250 mL, since less total RNA is needed to perform real-time qRT-PCR analysis. New NS0 cells were purchased from the European Collection of Cell Cultures via Sigma. The second-generation media and LS-1000 supplement resulted in higher growth rates and higher final cell concentration for both the control and elevated ammonium cultures. Figure 3.3 shows the cell growth profiles for the control and elevated ammonium cultures as the average of triplicates with 95% confidence intervals. As with the DNA microarray experiment, the control NS0 cultures achieved higher final cell concentration than the ammonium-stressed cultures. Three different time points during the exponential growth phase were selected for RNA harvesting: 63-h, 66-h, and 72-h. These time points were chosen to obtain similar cell densities as the NS0 cultures

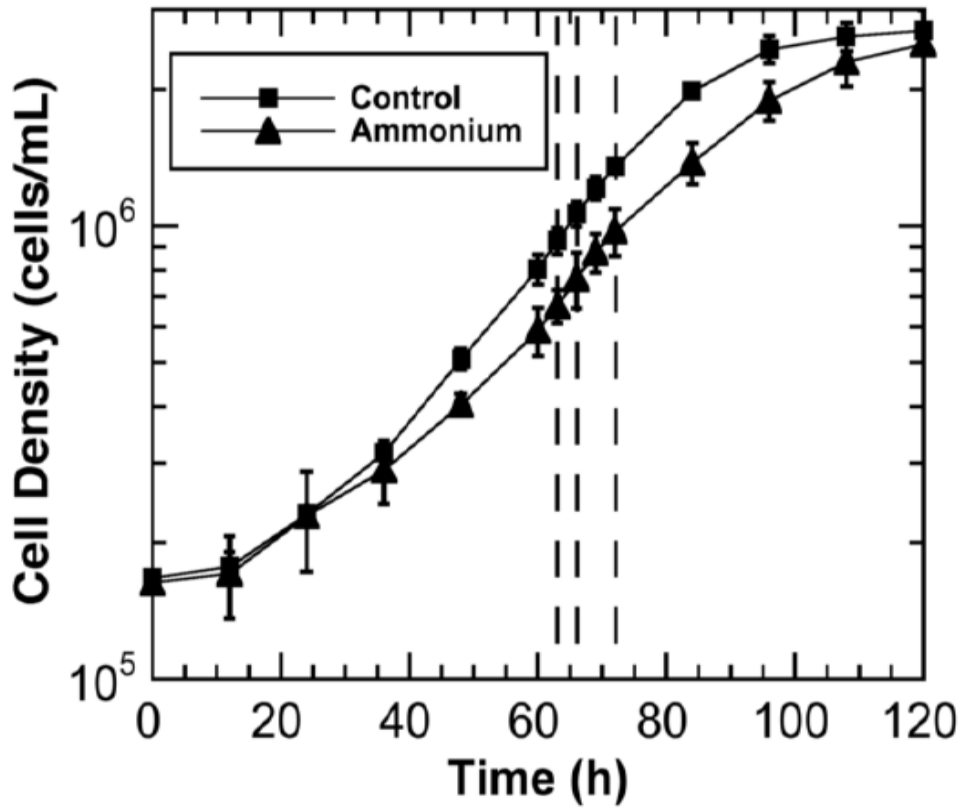

Figure 3.3 Growth profiles for NS0 cells cultured under control and elevated ammonium conditions. NS0 cells were grown in a second-generation ADCF-MAb Media with LS-1000 cholesterol. RNA samples for real-time qRT-PCR were taken at 63-h, 66-h, and 72-h for gene expression analysis as shown by the vertical lines. Error bars represent 95% confidence intervals.

harvested for the DNA microarray study to allow for more appropriate comparisons. The real-time qRT-PCR analysis examined five glycosylation and two housekeeping genes: Slc35a1, B4galt1, St3gal3, St3gal4, and St3gal6, where Actb and Gapdh served as housekeeping genes for quantification. These five glycosylation genes were selected because these genes represent key control reactions that significantly impact a biopharmaceuticals efficacy (Damiani et al., 2009; Zhang et al., 1998). Additionally, St3gal4 and B4galt1 gene expression was sensitive to ammonium for CHO cells (Chen and Harcum, 2006), thus these two genes were thought to be more likely to have detectable changes in NS0 than genes that were insensitive to ammonium in CHO cells. The Slc35a1 gene product is a membrane protein responsible for nucleotide sugar transport into the Golgi (Bill et al., 1998). The B4galt1 gene product catalyses the linkage of a galactose onto N-acetylglucosamine on a glycoprotein (Kotani et al., 2001). The product of the St3gal3, St3gal4, and St3gal6 genes catalyse the addition of a sialic acid on the terminal galactose of a glycoprotein, which increases the efficacy of many therapeutic glycoproteins (Bill et al., 1998; Butler and Meneses-Acosta, 2012). The M. musculus primer sequences for these seven genes can be found in Table 3.1.

The normalized gene expression levels for Slc35a1, B4galt1, St3gal3, St3gal4, and St3gal6 are shown in Figure 3.4 normalized to Gapdh of the time 63-h control cultures. Both Gapdh and Actb did not changed throughout the study (ANOVA, $p > 0.05$), as expected. Additionally, there was no statistical difference between the control and ammonium cultures at any time point for the five-glycosylation genes, and these gene expression levels did not change across the nine hours examined ($p > 0.05$). To highlight

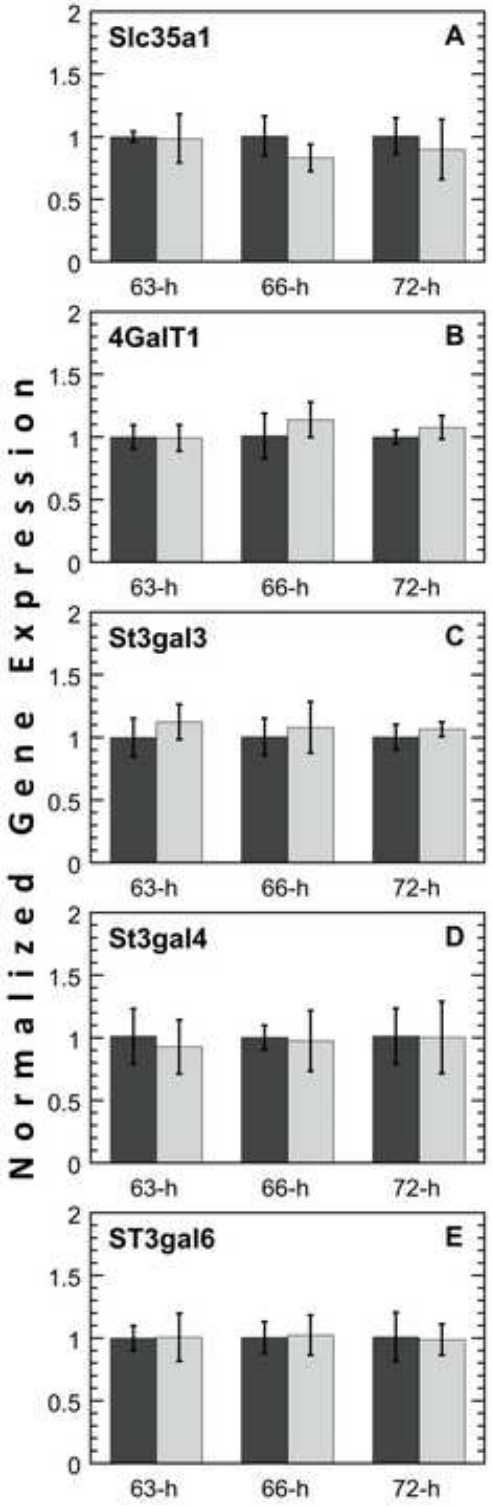

Figure 3.4 Gene expression for Slc35a1, B4galt1, St3gal3, St3gal4, and St3gal6.

Figure 3.4 (Continued). Gene expression for Slc35a1, B4galt1, St3gal3, St3gal4, and St3gal6. NS0 cells were cultured under control and elevated ammonium conditions in a second generation ADCF-MAb Media with LS-1000 cholesterol. The normalized gene expression levels for the glycosylation genes A) Slc35a1, B) B4galt1, C) St3gal3, D) St3gal4, and E) St3gal6 assessed by real-time qRT-PCR. Gene expression levels were analyzed at 63-h, 66-h, and 72-h, and were normalized to the 63-h time point and Gapdh. Error bars represent 95% confidence intervals. The dark gray bars represent control cultures, while the white bars represent the elevated ammonium cultures.

Table 3.3 Statistics on gene expression levels. The t-tests between the control and ammonium-treated cultures for the five genes determined that the gene expression levels were not different ($p > 0.05$). The p-values are listed for each pairs for the three time points examined, which correspond to the error bars shown in Figure 3.4.

Gene	Significance level (p-value)		
	63-h	**66-h**	**72-h**
B4galt1	0.89	0.33	0.26
Slc35a1	0.89	0.16	0.51
St3gal3	0.33	0.60	0.37
St3gal4	0.62	0.85	0.96
St3gal6	0.97	0.85	0.87

that these gene expression levels were not different, Table 3.3 lists the p-values for the paired t-test p-valves for each time point. Additionally, the relative expression levels of the St3gal3, St3gal4, and St3gal6 genes real-time qRT-PCR was consist with the relative levels observed by DNA microarrays, where the expression levels were St3gal4 > St3gal3 >> St3gal6. Thus, real-time qRT-PCR analysis demonstrates that NS0 cells are not sensitive to 5 mM ammonium with respect to these five glycosylation-related genes. And, the real-time qRT-PCR results confirm the DNA microarray results as accurate, where the DNA microarray analysis demonstrated that none of the known glycosylation-related genes were sensitive in NS0 cells at 5 mM ammonium.

3.5 Discussion

Gene expression studies have been conducted on both NS0 and hybridoma cells lines under hyperosmotic pressure (Gao et al., 2004; Shen and Sharfstein, 2006). Wu et al. (2004) examined antibody production in NS0 cells, while Shen and Sharfstein (2006) investigated gene expression changes in OKT3 cells, a hybridoma line, due to hyperosmolality (Shen and Sharfstein, 2006; Wu et al., 2004). Wu et al. (2004) focused their analysis on the cell physiology, thus providing few specific gene details; however, they did report that three carbohydrate genes were upregulated while one carbohydrate gene was down-regulated. Shen and Sharfstein (2006) used the Affymetrix Gene Chip MOE430A, which contains over 14,000 genes and 4000 EST probe sets. The GLYCOv3 and MOE430A Chips have 482 genes in common. Of these, only two of the incommon genes were identified as sensitive to hyperosmolality in OKT3 cells (glucosamine-6-phosphate deaminase, and hexokinase 1, GenBank accession nos. NM_011937 and NM_010438, respectively). If the responses were proportional to the stress introduced, then the much lower osmotic level used in this NS0 cell study was unlikely to cause changes in gene expression that were significant enough to detect, as these genes only changed 2-fold under the hyperosmotic stress.

The NS0 cells used in this study did not produce a recombinant protein. A study that compared non-producing (parental) and producing (monoclonal antibody) strains of NS0 cells using DNA microarrays identified 104 genes with differential gene expression (Khoo et al., 2007). The functional annotation of these genes determined that the differentially expressed genes were involved in protein synthesis, lipid metabolism, and

cell cycle regulation; however, none of these affected genes were glycosylation-related. The absence of glycosylation-related genes sensitive to ammonium in the current study cannot be entirely attributed to the non-producing status of the strain; however, it is recognized that any genetic modifications could influence the cells' response to elevated ammonium. Consequently, the current study provides a baseline for future quantification of the effects of elevated ammonium on recombinant NS0 cells. Sodium butyrate is cell culture media additive than increases productivity, yet has been observed to have variable effects on protein glycosylation where most studies have been conducted only with CHO cells (Chen et al., 2011; Chung et al., 2001; Cost et al., 2010; Crowell et al., 2008; Etchevarry and Ryll, 1998; Hong et al., 2011; Hossler et al., 2009; Lee et al., 2014; Liu et al., 2014; Mohan and Lee, 2009; Sung and Lee, 2005; Sunley and Butler, 2010; Yee et al., 2008a; Yee et al., 2008b). The effects of sodium butyrate on gene expression have been examined in both CHO and NS0 cell using two CHO cell and mouse DNA microarrays developed in-house (Gatti et al., 2007). Both CHO and NS0 cells were studied with cross-species DNA microarray hybridization, in addition to the species-specific DNA microarray hybridization. These studies were conducted to corroborate physiology and gene expression observations (Gatti et al., 2007). Both in-house DNA microarrays contained glycosylation-related genes (Korke et al., 2004; Wlaschin et al., 2005); however, which is unknown. Interestingly, their gene expression analysis did not identify any glycosylation-related genes with significant expression changes due to sodium butyrate in the CHO and NS0 cell lines (Gatti et al., 2007). More recently, 52 glycosylation-related gene expression levels have been quantified in recombinant CHO

cells under sodium butyrate (Lee et al., 2014). Despite several biosynthetic genes having slightly higher levels under sodium butyrate, the glycoprotein most likely had poorer quality due to increased sialidase (Neu1) gene expression levels and lower b4galt2 and st3gal3 levels, both critical sialic acid biosynthesis genes (Lee et al., 2014). These differences in gene expression responses might be attributable to the nature of these cells. NS0 cells are a cancer cell line, while CHO cells, despite being immortal are not a cancerous cell line (Wlaschin et al., 2006).

The detrimental effects of ammonium on cell growth, protein productivity, and protein glycosylation has results in studies to reduce the major source of ammonium, the glutamine. Early studies that controlled glutamine with fed-batch techniques, reported decreased protein glycosylation quality (Wong et al., 2005). These early results selected the target glucose and glutamine levels arbitrary, where is possible, their early targets in the ground breaking approach were just too low, but their approach was correct (Young, 2013). Other research groups have replaced the glutamine with alternative sources concurrent with reducing the levels in CHO cell cultures with improved results or adapted cells to growth in glutamine-free media (Kim et al., 2013; Taschwer et al., 2012). And more recently, three different TCA cycle intermediates, α-ketoglutarate, citric acid, and succinic acid, were examined for recombinant CHO cells to reduced ammonia accumulation in culture medium (Ha and Lee, 2014). The α-ketoglutarate replacement decreased the growth rate, but also increased sialylation and decrease ammonium accumulation. The observed sialylation increase was correlated with increased ST3gal and decreased Neu enzyme activity (Ha and Lee, 2014). Interestingly, the relative

abundance of the Neu1, Neu2, and Neu3 genes shown in Kim et al., 2013 are significantly different than the relevant abundance of the Neu1, Neu2, and Neu3 proteins shown in Ha and Lee, 2014 for the control cultures, albeit the studies are from the same laboratory with different CHO cell host cell lines. These results demonstrate that gene expression and protein levels are not always proportional. Taken together, the gene expression results for NS0 cells and the glutamine substitution outcomes for CHO cells suggest that enzyme or substrate-level control is likely a very significant factor with respect to ammonium affects on protein glycosylation in NS0 cells.

3.6 Conclusion

Sialyltransferase gene expression was anticipated to be significantly different between the control and elevated ammonium cultures for the NS0 cells (Chen and Harcum, 2006), since previous NS0 cell culture experiments observed elevated intracellular nucleotide sugar pools in NS0 cells compared to CHO cells (Baker et al., 2001). Also, it was anticipated that other glycosylation genes would be identified as ammonium-sensitive by the NS0 cell experiments, since ammonium adversely affects protein glycosylation. However, the results of this work indicate that the ammonium-sensitivity in NS0 cells for protein glycosylation is not at the gene expression level. Thus, the further studies should focus on translational and substrate-level control as the mechanism by which elevated ammonium impacts protein glycosylation changes in NS0 cells.

3.7 Acknowledgements

This research was supported by funds provided by Institutional Development Award (IDeA) from the National Institute of General Medical Sciences of the National Institutes of Health (P20GM103444). The DNA microarrays and services were provided by Consortium for Functional Glycomics' Gene Microarray Facility funded by the National Institute of General Medical Sciences of the National Institutes of Health (GM62116). Additionally, this material is based upon work supported by CSREES/USDA, under project number SC-SC-1700287. Any opinions, findings, conclusions or recommendations expressed in this publication are those of the author(s) and do not necessarily reflect the view of the USDA.

3.8 References

Aebi M, Helenius A, Schenk B, Barone R, Fiumara A, Berger EG, Hennet T, Imbach T, Stutz A, Bjursell C, Uller A, Wahlstrom JG, Briones P, Cardo E, Clayton P, Winchester B, CormierDaire V, deLonlay P, Cuer M, Dupre T, Seta N, deKoning T, Dorland L, deLoos F, Kupers L, Fabritz L, Hasilik M, Marquardt T, Niehues R, Freeze H, Grunewald S, Heykants L, Jaeken J, Matthijs G, Schollen E, Keir G, Kjaergaard S, Schwartz M, Skovby F, Klein A, Roussel P, Korner C, Lubke T, Thiel C, vonFigura K, Koscielak J, Krasnewich D, Lehle L, Peters V, Raab M, Saether O, Schachter H, Van Schaftingen E, Verbert A, Vilaseca A, Wevers R, Yamashita K. Carbohydrate-deficient glycoprotein syndromes become congenital disorders of glycosylation: an updated nomenclature for CDG. Glycobiology. 2000;10:R3-R5.

Andersen DC, Goochee CF. The Effect of Ammonia on the O-Linked Glycosylation of Granulocyte-Colony-Stimulating Factor Produced by Chinese-Hamster Ovary Cells. Biotechnol Bioeng. 1995;47:96-105.

Andersen, DC, Goochee, CF, Cooper, G, Weitzhandler, M. Monosaccharide and oligosaccharide analysis of isoelectric focusing-separated and blotted granulocyte colony-stimulating factor glycoforms using high-pH anion exchange chromatography with pulsed amperometric detection. Glycobiology. 1994;4:459-467.

Baker KN, Rendall MH, Hills AE, Hoare M, Freedman RB, James DC. Metabolic control of recombinant protein N-glycan processing in NS0 and CHO cells. Biotechnol Bioeng. 2001;73:188–202.

Barrett T, Wilhite SE, Ledoux P, Evangelista C, Kim IF, Tomashevsky M, Marshall KA, Phillippy KH, Sherman PM, Holko M, Yefanov A, Lee H, Zhang N, Robertson CL, Serova N, Davis S, Soboleva A. NCBI GEO: archive for functional genomics data sets—update. Nucleic Acids Res. 2013;41:D991-D995.

Berlec A, Strukelj B. Current state and recent advances in biopharmaceutical production in Escherichia coli, yeasts and mammalian cells. J Industr Microbio Biotech. 2013;40:257-274.

Bill RM, Revers L, Wilson IBH. Protein Glycosylation. Kluwer Academic Publishers, Boston. 1998.

Burleigh SC, van de Laar T, Stroop CJM, van Grunsven WMJ, O'Donoghue N, Rudd PM, Davey GP. Synergizing metabolic flux analysis and nucleotide sugar metabolism to understand the control of glycosylation of recombinant protein in CHO cells. BMC Biotechnol. 2011;11.

Butler M. Optimisation of the cellular metabolism of glycosylation for recombinant

proteins produced by mammalian cell systems. Cytotechnology. 2006;50:57-76.

Butler M, Meneses-Acosta A. Recent advances in technology supporting biopharmaceutical production from mammalian cells. Appl Microbiol Biotechnol. 2012;96:885-894.

Canales RD, Luo YL, Willey JC, Austermiller B, Barbacioru CC, Boysen C, Hunkapiller K, Jensen RV, Knight CR, Lee KY, Ma YQ, Maqsodi B, Papallo A, Peters EH, Poulter K, Ruppel PL, Samaha RR, Shi LM, Yang W, Zhang L, Goodsaid FM. Evaluation of DNA microarray results with quantitative gene expression platforms. Nat Biotechnol. 2006;24:1115-1122.

Chen F, Kou TC, Fan L, Zhou Y, Ye ZY, Zhao L, Tan WS. The combined effect of sodium butyrate and low culture temperature on the production, sialylation, and biological activity of an antibody produced in CHO cells. Biotech Bioprocess Eng. 2011;16:1157-1165.

Chen PF, Harcum SW. Effects of amino acid additions on ammonium stressed CHO Cells. J Biotechnol. 2005;117:277-286.

Chen PF, Harcum SW. Effects of elevated ammonium on glycosylation gene expression in CHO cells. Metab Eng. 2006;8:123–132.

Chung BS, Jeong YT, Chang KH, Kim JS, Kim JH. Effect of Sodium Butyrate on glycosylation of recombinant Erythropoietin. J Microbiol Biotechnol. 2001;11:1087–1092.

Clark KJR, Griffiths J, Bailey KM, Harcum SW. Gene-expression profiles for five key glycosylation genes for galactose-fed CHO cells expressing recombinant IL-4/13 cytokine trap. Biotechnol Bioeng. 2005;90:568–577.

Cost GJ, Freyvert Y, Vafiadis A, Santiago Y, Miller JC, Rebar E, Collingwood TN, Snowden A, Gregory PD. BAK and BAX Deletion Using Zinc-Finger Nucleases Yields Apoptosis-Resistant CHO Cells. Biotechnol Bioeng. 2010;105:330-340.

Crowell CK, Qin Q, Grampp GE, Radcliffe RA, Rogers GN, Scheinman RI. Sodium butyrate alters erythropoietin glycosylation via multiple mechanisms. Biotechnol Bioeng. 2008;99:201-213.

Damiani R, Oliveira JE, Vorauer-Uhl K, Peroni CN, Vianna EG, Bartolini P, Ribela M. Stable expression of a human-like sialylated recombinant thyrotropin in a Chinese hamster ovary cell line expressing alpha 2,6-sialyltransferase. Prot Express Purif. 2009;67:7-14.

deZengotita VM, Schmelzer AE, Miller WM. Characterization of hybridoma cell responses to elevated pCO_2 and osmolality: Intracellular pH, cell size, apoptosis, and metabolism. Biotechnol Bioeng. 2002;77:369-380.

Etchevarry T, Ryll T, Genentech, Inc. Mammalian cell culture process. 1998; US Patent 5705:364.

Gao HC, Wang Y, Liu XD, Yan TF, Wu LY, Alm E, Arkin A, Thompson DK, Zhou JZ. Global transcriptome analysis of the heat shock response of Shewanella Oneidensis. J Bacteriol. 2004;186:7796-7803.

Gatti MD, Wlaschin KF, Nissom PM, Yap M, Hu WS. Comparative transcriptional analysis of mouse hybridoma and recombinant Chinese hamster ovary cells undergoing butyrate treatment. J Biosci Bioeng. 2007;103:82–91.

Gawlitzek M, Papac DI, Sliwkowski MB, Ryll T. Incorporation of $N\text{-}^{15}$ from ammonium into the N-linked oligosaccharides of an immunoadhesin glycoprotein expressed in Chinese hamster ovary cells. Glycobiology 1999;9:125-131.

Genzel Y, Ritter JB, Konig S, Alt R, Reichl U. Substitution of glutamine by pyruvate to reduce ammonia formation and growth inhibition of mammalian cells. Biotechnol Prog. 2005;21:58-69.

Gu XJ, Wang DIC. Improvement of interferon-gamma sialylation in Chinese hamster ovary cell culture by feeding of N-acetylmannosamine. Biotechnol Bioeng. 1998;58:642-648.

Ha TK, Lee GM. Effect of glutamine substitution by TCA cycle intermediates on the production and sialylation of Fc-fusion protein in Chinese hamster ovary cell culture. J Biotechnol. 2014;180:23-29.

Hansen HA, Emborg C. Influence of Ammonium on Growth, Metabolism, and Productivity of a Continuous Suspension Chinese-Hamster Ovary Cell-Culture. Biotechnol Prog. 1994;10:121-124.

Hong JK, Cho SM, Yoon SK. Substitution of glutamine by glutamate enhances production and galactosylation of recombinant IgG in Chinese hamster ovary cells. Appl Microbiol Biotechnol. 2010;88:869-876.

Hong JK, Lee GM, Yoon SK. Growth factor withdrawal in combination with sodium butyrate addition extends culture longevity and enhances antibody production in CHO cells. J Biotechnol. 2001;155:225-231.

Hossler P, Khattak SF, Li ZJ. Optimal and consistent protein glycosylation in mammalian

cell culture. Glycobiology. 2009;19:936-949.

Hudak JE, Bertozzi CR. Glycotherapy: New Advances Inspire a Reemergence of Glycans in Medicine. Chem Biol. 2014;21:16-37.

Jenkins N. Role of physiology in the determination of protein heterogeneity. Curr Opin Biotechnol. 1996; 7:205-209.

Jenkins N, Parekh RB, James DC. Getting the glycosylation right: Implications for the biotechnology industry. Nat Biotechnol. 1996; 14:975-981.

Khoo SHG, Falciani F, Al-Rubeai M. A genome-wide transcriptional analysis of producer and non-producer NS0 myeloma cell lines. Biotechnol Appl Biochem. 2007;47:85-95.

Kim DY, Chaudhry MA, Kennard ML, Jardon MA, Braasch K, Dionne B, Butler M, Piret JM. Fed-batch CHO cell t-PA production and feed glutamine replacement to reduce ammonia production. Biotechnol Prog. 2013;29:165-175.

Korke R, Gatti MD, Lau ALY, Lim JWE, Seow TK, Chung MCM, Hu WS. Large scale gene expression profiling of metabolic shift of mammalian cells in culture. J Biotechnol. 2004;107: 1-17.

Kotani N, Asano M, Iwakura Y, Takasaki S. Knockout of mouse b1,4 galactosyltransferase-1 gene results in a dramatic shift of outer chain moieties of N-glycans from Type 2 to Type 1 chains in hepatic membrane and plasma glycoproteins. Biochem J. 2001;357:827-834.

Lee JS, Ha TK, Lee SJ, Lee GM. Current state and perspectives on erythropoietin production. Appl Microbiol Biotechnol. 2012;95:1405-1416.

Lee SM, Kim YG, Lee EG, Lee GM. Digital mRNA profiling of N-glycosylation gene expression in recombinant Chinese hamster ovary cells treated with sodium butyrate. J Biotechnol. 2014;171:56-60.

Lingg N, Zhang PQ, Song ZW, Bardor M. The sweet tooth of biopharmaceuticals: Importance of recombinant protein glycosylation analysis. Biotechnol J. 2012;7:1462-1472.

Liu YW, Zhou XS, Song ZW, Zhang YX. Sodium butyrate enhances the acidic isoform content of recombinant human erythropoietin produced by Chinese hamster ovary cells. Biotechnol Lett. 2014;36:907-911.

Livak KJ, Schmittgen TD. Analysis of relative gene expression data using real-time

quantitative PCR and the 2^(-ΔΔC$_T$) method. Methods. 2001;25:402-408.

Miller WM, Wilke CR, Blanch HW. Transient Responses of Hybridoma Cells to Lactate and Ammonia Pulse and Step Changes in Continuous Culture. Bioprocess Eng. 1988;3:113-122.

Mohan C, Lee GM. Calnexin overexpression sensitizes recombinant CHO cells to apoptosis induced by sodium butyrate treatment. Cell Stress Chaperones. 2009;14:49-60.

Onitsuka M, Kim WD, Ozaki H, Kawaguchi A, Honda K, Kajiura H, Fujiyama K, Asano R, Kumagai I, Ohtake H, Omasa T. Enhancement of sialylation on humanized IgG-like bispecific antibody by overexpression of alpha 2,6-sialyltransferase derived from Chinese hamster ovary cells. Appl Microbiol Biotechnol. 2012; 94:69-80.

Ozturk SS, Riley MR, Palsson BO. Effects of ammonia and lactate on hybridoma growth, metabolism, and serum concentration. Biotechnol Prog. 1992;6:121-128.

Provenzano M, Mocellin S. Complementary techniques: Validation of gene expression data by quantitative real time PCR. Adv Exp Med Biol. 2007;593:66-73.

Quek LE, Dietmair S, Kromer JO, Nielsen LK. Metabolic flux analysis in mammalian cell culture. Metab Eng. 2010;12:161-171.

Reuveny S, Velez D, Macmillan JD, Miller L. Factors affecting cell growth and monoclonal antibody production in stirred reactors. J Immunol Methods. 1986;86:53-59.

Ryll T, Valley U, Wagner R. Biochemistry of growth inhibition by ammonium ions in mammalian cells. Biotechnol Bioeng. 1994;44:184-193.

Schefe JH, Lehmann KE, Buschmann IR, Unger T, Funke-Kaiser H. Quantitative real-time RT-PCR data analysis: current concepts and the novel "gene expression's C(T) difference" formula. J Mol Med. 2006;84:901-910.

Schmelzer AE, deZengotita VM, Miller WM. Considerations for osmolality measurement under elevated pCO_2:Comparison of vapor pressure and freezing point osmometry. Biotechnol Bioeng. 2000;67:189-196.

Schneider M, El Alaoui M, von Stockar U, Marison IW. Batch cultures of a hybridoma cell line performed with in situ ammonia removal. Enzyme Microb Technol. 1997;20:268-276.

Seo JS, Min BS, Kim YJ, Cho JM, Baek E, Cho MS, Lee GM. Effect of glucose feeding on the glycosylation quality of antibody produced by a human cell line, F2N78, in fed-batch culture. Appl Microbiol Biotechnol. 2014;98:3509-3515.

Shen D, Sharfstein ST. Genome-wide analysis of the transcriptional response of murine hybridomas to osmotic shock. Biotechnol Bioeng. 2006;93:132-145.

Sung YH, Lee GM. Enhanced human thrombopoietin production by sodium butyrate addition to serum-free suspension culture of Bcl-2-overexpressing CHO cells. Biotechnol Prog. 2005;21: 50-57.

Sunley K, Butler M. Strategies for the enhancement of recombinant protein production from mammalian cells by growth arrest. Biotechnol Adv. 2010;28:385-394.

Taschwer M, Hackl M, Bort JAH, Leitner C, Kumar N, Puc U, Grass J, Papst M, Kunert R, Altmann F, Borth N. Growth, productivity and protein glycosylation in a CHO EpoFc producer cell line adapted to glutamine-free growth. J Biotechnol. 2012;157:295-303.

Valley U, Nimtz M, Conradt HS, Wagner R. Incorporation of ammonium into intracellular UDP-activated N-acetylhexosamines and into carbohydrate structures in glycoproteins. Biotechnol Bioeng. 1999;64:401-417.

Wahrheit J, Nicolae A, Heinzle E. Dynamics of growth and metabolism controlled by glutamine availability in Chinese hamster ovary cells. Appl Microbiol Biotechnol. 2014;98:1771-1783.

Weikert S, Papac D, Briggs J, Cowfer D, Tom S, Gawlitzek M, Lofgren J, Mehta S, Chisholm V, Modi N, Eppler S, Carroll K, Chamow S, Peers D, Berman P, Krummen L. Engineering Chinese hamster ovary cells to maximize sialic acid content of recombinant glycoproteins. Nat Biotechnol. 1999;17:1116-1121.

Werner A, Horstkorte R, Glanz D, Biskup K, Blanchard V, Berger M, Bork K. Glycoengineering the N-acyl side chain of sialic acid of human erythropoietin affects its resistance to sialidase. Biol Chem. 2012;393:777-783

Whitford W. NS0 serum-free culture and applications. BioProc Inter. 2003;36-47.

Wlaschin KF, Nissom PM, Gatti MD, Ong PF, Arleen S, Tan KS, Rink A, Cham B, Wong K, Yap M, Hu WS. EST sequencing for gene discovery in Chinese hamster ovary cells. Biotechnol Bioeng. 2005;91:592-606.

Wlaschin KF, Seth G, Hu WS. Toward genomic cell culture engineering. Cytotechnology. 2006;50:121-140.

Wong DCF, Wong KTK, Goh LT, Heng CK, Yap MGS. Impact of dynamic online fed-batch strategies on metabolism, productivity and N-glycosylation quality in CHO cell cultures. Biotechnol Bioeng. 2005;89:164-177.

Wong NSC, Wati L, Nissom PM, Feng HT, Lee MM, Yap MGS. An Investigation of Intracellular Glycosylation Activities in CHO Cells: Effects of Nucleotide Sugar Precursor Feeding. Biotechnol Bioeng. 2010;107:321-336.

Wu MH, Dirnopoulos G, Mantalaris A, Varley J. The effect of hyperosmotic pressure on antibody production and gene expression in the GS-NS0 cell line. Biotechnol Appl Biochem. 2004;40:41-46

Wurmbach E. Validation of Array Data. Real-Time PCR: Current Technology and Applications. 2009; pp 137-148.

Yang M, Butler M. Effect of Ammonia on CHO Cell Growth, Erythropoietin Production and Glycosylation. Biotechnol Bioeng. 2000a;68:370-380.

Yang M, Butler M. Effect of ammonia on the glycosylation of human recombinant erythropoietin in culture. Biotechnol Prog. 2000b;16:751-759.

Yang M, Butler M. Effects of ammonia and glucosamine on the heterogeneity of erythropoietin glycoforms. Biotechnol Prog. 2002;18:129-138.

Yao K, Yin YL, Li XL, Xi PB, Wang JJ, Lei J, Hou YQ, Wu GY. Alphaketoglutarate

inhibits glutamine degradation and enhances protein synthesis in intestinal porcine epithelial cells. Amino Acids. 2012;42:2491-2500.

Yee JC, Gatti MD, Philp RJ, Yap M, Hu WS. Genomic and proteomic exploration of CHO and hybridoma cells under sodium butyrate treatment. Biotechnol Bioeng. 2008a;99:1186-1204.

Yee JC, Wlaschin KF, Chuah SH, Nissom PM, Hu WS. Quality Assessment of Cross-Species Hybridization of CHO Transcriptome on a Mouse DNA Oligo Microarray. Biotechnol Bioeng. 2008b;101:1359-1365.

Young JD. Metabolic flux rewiring in mammalian cell cultures. Curr Opin Biotechnol. 2013;24:1108-1115.

Zhang XQ, Lok SHL, Kon OL. Stable expression of human a-2,6-sialyltransferase in Chinese hamster ovary cells: functional consequences for human erythropoietin expression and bioactivity. Biochimica Et Biophysica Acta-General Subjects. 1998;1425:441-452.

CHAPTER FOUR: EXPANSION OF MESENCHYMAL STEM CELLS UNDER ATMOSPHERIC CARBON DIOXIDE

4.1 Abstract

Stem cells are needed for an increasing number of scientific applications, including both fundamental research and clinical disease treatment. To meet this rising demand, improved expansion methods to generate high quantities of high quality stem cells must be developed. Unfortunately, the bicarbonate buffering system – which relies upon an elevated CO_2 environment – typically used to maintain pH in stem cell cultures introduces several unnecessary limitations in bioreactor systems. In addition to artificially high dissolved CO_2 levels negatively affecting cell growth, but more importantly, the need to sparge CO_2 into the system complicates the ability to control culture parameters. This control is especially important for stem cells, whose behavior and phenotype is highly sensitive to changes in culture conditions such as dissolved oxygen and pH. As a first step, this study developed a buffer to support expansion of mesenchymal stem cells (MSC) under an atmospheric CO_2 environment in static cultures. MSC expanded under atmospheric CO_2 with this buffer achieved equivalent growth rates without adaptation compared to those grown in standard conditions and also maintained a stem cell phenotype, self-renewal properties, and the ability to differentiate into multiple lineages after expansion.

4.2 Introduction

Stem cells offer much potential for scientific applications. In addition to enabling insights into developmental biology, pathology, and toxicology, stem cells also show promise in treating human ailments such as spinal cord injuries, myocardial infarction, Parkinson's, type I diabetes, and sickle cell anemia (Berry et al., 2006; Hanna et al., 2007; Ashton et al., 2011; Fernandes Platzgummer et al., 2011; Kinney et al., 2011; Olmer et al., 2012; Serra et al., 2012; Alfred et al., 2011; Rodrigues et al., 2011). Many treatments require large quantities of stem cells, but currently there are no readily available sources that can meet these high demands (Fernandes Platzgummer et al., 2011; Kinney et al., 2011; Zweigerdt, 2009; Shafa et al., 2011; Ratcliffe et al., 2012). Consequently, in vitro expansion methods must be developed to generate high numbers of stem cells (Kinney et al., 2011; Serra et al., 2012; Alfred et al., 2011; Shafa et al., 2011; Yeatts et al., 2013; King and Miller 2007; Grolms et al., 2011). In addition to high quantities, maintaining high quality in stem cell yields is equally important to maximize treatment responses (Serra et al., 2012; King and Miller, 2007). The stem cell niche — consisting of factors such as oxygen tension, pH, and mechanical forces — influences the behavior of stem cells and dictates whether the stem cells will proliferate, differentiate, or undergo apoptosis (Ashton et al., 2011; Serra et al., 2012; Yeatts et al., 2013; Grolms et al., 2011; Papoutsakis, 2009; Wuertz et al., 2009; Frith et al., 2009; dos Santos et al., 2010). Learning how these various factors regulate stem cell fate in vivo, and then constructing systems that can replicate the desired conditions in vitro will be crucial (Ashton et al., 2011; Yeatts et al., 2013). Through development of cost-efficient methods

that allow maintenance of optimal culture parameters during in vitro expansion, it may be possible to more effectively direct stem cell yields and enhance the clinical success of stem cell-based therapies (Rodrigues et al., 2011; Shafa et al., 2011; Yeatts et al., 2013).

Stirred systems—in particular fed-batch, computer-controlled bioreactors—are capably equipped to deliver high quantities of high quality mammalian cells due to operational flexibility (Fernandes Platzgummer et al., 2011; Olmer et al., 2012; Ratcliffe et al., 2012; Yeatts et al., 2013; King and Miller 2007; Grolms et al., 2011; Schroeder et al., 2005). Bioreactors, where CO_2 sparging is used for pH control, support the expansion of mammalian cells in suspension (Fernandes Platzgummer et al., 2011; Rodrigues et al., 2009). Expansion of anchorage-dependent cells, such as mesenchymal stem cells (MSC), can also be achieved with the use of microcarriers in stirred bioreactors (Serra et al., 2012; Alfred et al., 2011; Rodrigues et al., 2011; Sart et al., 2011). Through dynamic monitoring and online control of parameters, stirred bioreactors can enable culture conditions to be maintained within a desired range (Fernandes Platzgummer et al., 2011; Olmer et al., 2012; Rodrigues et al., 2011; Ratcliffe et al., 2012; Grolms et al., 2011; Schroeder et al., 2005). Additionally, bioreactors allow for scalability that is simply not possible with other culture formats, potentially paving the way for delivery of the large numbers of stem cells required for widespread clinical use (Olmer et al., 2012; Ratcliffe et al., 2012; Grolms et al., 2009). However, the bicarbonate buffering system used to regulate pH appears to be limiting the potential of stem cell expansion as it can hinder the ability of stirred bioreactors to provide a highly consistent culture pH environment (Rodrigues et al., 2011; Rodrigues et al., 2009; Goudar et al., 2006). The bicarbonate

buffering system relies on the equilibrium between the CO_2 gas sparged into the bioreactor and the dissolved CO_2 (dCO_2) in the medium, which is maintained well above physiological levels and can negatively affect cell growth and behavior (Rodrigues et al., 2009; Goudar et al., 2006; Pattison et al., 2000; Zhang et al., 2010). This situation is compounded by the production of CO_2 by metabolically active cells (Goudar et al., 2006). Previous efforts have been undertaken to remove excess dCO_2 from the bioreactor by adjusting the sparging profile; however, the coupling of the CO_2 supply to the oxygen supply complicates both dissolved oxygen and pH control (Goudar et al., 2006; Hu et al., 2011). This mutual dependency leads to recurring cyclic fluctuations of both dissolved oxygen and pH in bioreactors as efforts to regulate one inadvertently affects the other (Olmer et al., 2012; Rodrigues et al., 2011; Grolms et al., 2009; Rodrigues et al., 2009; Zhang et al., 2010; Yang et al., 2007; Osman et al., 2001). Other approaches to remove dCO_2 have modified the size of sparged bubbles, but this can compromise oxygen transfer (Hu et al., 2011). Thus, methods to independently control dissolved oxygen and pH may enable bioreactor systems to improve stem cell expansion as stem cells are extremely sensitive to fluctuations in both dissolved oxygen and pH (Ashton et al., 2011; Rodrigues et al., 2011; Grolms et al., 2009; Wuertz et al., 2009; dos Santos et al., 2010). One simple method to reduce the dependence between dissolved oxygen and pH control in mammalian cell culture is to decrease or eliminate the bicarbonate buffer's role in pH buffering. This would allow atmospheric CO_2 levels to be used in the air/oxygen sparging supplies. Several groups have developed media to support mammalian cell lines under an atmospheric CO_2 environment. Leibovitz (1963) developed the L-15 medium, which uses

an amino acid buffer in addition to substituting galactose for glucose, for use in mammalian cell culture (Leibovitz, 1963). Battista and Weiss (1991) developed a medium for Chinese hamster ovary cells and baby hamster kidney (BHK) cells; however, it is not appropriate for undifferentiated stem cell expansion, due to the presence of β-glycerophosphate, which induces osteogenesis (Battista and Weiss, 1991; Fiorentini et al., 2011). Goudar et al. (2006) developed a 3-(N-morpholino) propanesulfonic acid (MOPS)-histidine buffer for BHK cells; however, the low pH of 6.8 makes it too acidic for stem cells (Goudar et al., 2006). Swain and Pool (2009) investigated the use of various nonbicarbonate buffers in Tyrode's solution, composed of salt and glucose, for potential use with in vitro fertilization, although they did not culture cells in their proposed buffer (Swain and Pool, 2009). To our knowledge, attempts to expand stem cells under an atmospheric CO_2 environment have not been conducted.

The overall aim of this study was to develop a buffer system for a stem cell medium that de-emphasized CO_2-dependent pH buffering and to ensure that MSC expanded in this medium under atmospheric CO_2 behaved similarly to those expanded under standard conditions. These initial studies were conducted in static cultures; however, by eliminating the need for elevated CO_2 sparging, large-scale stem cell expansion could potentially be improved by preventing excessive dCO_2 levels, as well as enabling simpler controls to increase batch-to-batch reproducibility. The first goal of this study was to determine whether MSC could be effectively expanded under atmospheric CO_2 levels as this has not yet been investigated. L-15 medium and various combinations of MOPS-4-(2-hydroxyethyl)-1-piperazineethanesulfonic acid (HEPES) buffered media

were examined to select a medium buffer that maintained growth rates and final cell densities comparable to the standard buffer conditions without any prior adaptation period. One MOPS-HEPES buffered medium was selected to address the subsequent goals, where the second goal was to determine whether MSC maintained an undifferentiated state and self-renewal ability when cultured in the MOPS-HEPES buffered medium under atmospheric CO_2 without prior adaptation. Histological staining and stem cell-associated gene expression markers were compared for the undifferentiated MSC cultured under the standard conditions and the MOPS-HEPES buffered medium under atmospheric CO_2. The third goal of the study was to assess the differentiation potential of the MSC expanded under atmospheric CO_2. Histological staining and multiple lineage gene expression markers were compared for differentiated MSC that were previously expanded under the standard conditions or in the MOPS-HEPES buffered medium under atmospheric CO_2. Finally, the fourth goal was to determine whether MSC growth rates and stemness were maintained through multiple passages in the MOPS-HEPES buffer under atmospheric CO_2.

4.3 Materials and Methods

MSC Expansion

Undifferentiated mouse MSC (Gibco) were maintained as anchorage-dependent monolayers in T-75 flasks (Nunc) under 5% CO_2 at 37°C in minimal essential medium-a (MEM-α) (Gibco), which was supplemented with 10% fetal bovine serum (FBS) (Gibco). For our custom compositions developed for atmospheric CO_2 conditions, MOPS and HEPES were added as buffering components, while sodium hydroxide was used to adjust the initial pH. Leibovitz L-15 medium was also supplemented with 10% FBS. For growth rate comparisons, undifferentiated MSC were initially seeded into 6-well plates (Nunc) at 3.8×10^4 cells/well, corresponding to 4.0×10^3 cells/cm^2. Warmed medium was added to the wells (1.5×10^3 cells/mL). Plates were incubated under 5% CO_2 or atmospheric CO_2 at 37°C. Cell growth in all three media was measured at five time points over 57 h. Five parallel sets of cultures were grown for each condition. One set of cultures was harvested at each time point. Each data point represents distinct independent cultures in triplicate. Cell densities were quantified using the Scepter 2.0 Handheld Automated Cell Counter (Millipore).

MSC Differentiation

For the differentiation experiments, undifferentiated MSC were grown for 48 h in T-75 flasks at 37°C. The undifferentiated MSC were seeded at 4.0×10^3 cells/cm^2 in either the standard medium or MOPS-HEPES buffered medium. The standard medium cultures were incubated under 5% CO_2, while the MOPS-HEPES buffered medium

cultures were incubated under atmospheric CO_2. The undifferentiated MSC were harvested and used to examine differentiation along the adipogenic, osteogenic, and chondrogenic lineages. The StemPro Differentiation kits (Gibco) were used following the manufacturer protocols. All differentiation cultures were incubated under 5% CO_2 and harvested at 16 days for analysis by histological staining and gene expression. The MSC differentiation cultures were conducted in four triplicate sets, one set for each of the histological staining and qRT-PCR analysis.

Extended MSC Expansion

Undifferentiated MSC were seeded at 4.0 x 10^3 cells/cm^2 in either the standard growth medium under 5% CO_2 or the MOPS-HEPES buffered growth medium under atmospheric CO_2. One T-75 flask was used to seed 3 six-well plates in parallel for end-point cell density analysis and a single T-75 flask for subsequent passages. MSC were passaged every 60 h for five passages, which corresponds to approximately 75% confluent and a 6.25-fold expansion at the end of each passage.

Histological Staining

Osteogenic activity was measured using the Alkaline Phosphatase Detection Kit (Milipore). HCS LipidTox Green neutral lipid stain (Molecular Probes) was used to detect the presence of lipids in the adipogenic cultures. The adipocyte samples were mounted in SlowFade Gold Antifade reagent with DAPI (Molecular Probes), and imaged using an Eclipse Ti Confocal microscope. Alcian Blue (Poly Scientific) was used to stain

glycosaminoglycans in the chondrogenic cultures. Chondrogenic and osteogenic samples were mounted using Permount (Fisher Scientific) and imaged using the Nikon AZ 100 Multizoom microscope.

Real time qRT-PCR

Total RNA was extracted from triplicate undifferentiated T-75 flask cultures or triplicate differentiated T-25 flask cultures. The RNeasy Mini Kit (Qiagen) was used following manufacturer's protocol. cDNA was synthesized by Super-Script III First-Strand Synthesis System for RT-PCR (Invitrogen) with 200 ng total RNA. RT^2 SYBR® Green qPCR Mastermix (SABiosciences) was used for qPCR analysis with MyiQ Optical System Software Version 1.0 (Bio-Rad). Further data analysis was conducted using Real-time PCR Miner software (UC Berkeley). Normalized gene expression values were obtained using the method previously outlined (Chen and Harcum, 2006). The primer sequences are listed in Table 4.1.

Statistical Analysis

Statistical analysis of the growth rates, final cell densities, and gene expression data was performed with SAS 9.3 using the general linear model procedure for the final cell densities and gene expression levels ($p \leq 0.05$) and the regression procedure for the growth rate data ($p \leq 0.05$).

Table 4.1 PCR primer sequences for analysis of MSC.

Gene	Forward Primer Sequence	Reverse Primer Sequence
Oct4	5′-GAA GCC GAC AAC AAT GAG AAC	3′-ACA GAA CCA TAC TCG AAC CAC A
Lipoprotein lipase	5′-AGC CAC CAG GCA GAT AGA GA	3′-CCT TGT TGG AGG AGG TGT GT
PPAR γ	5′-ACA GCC ACA TGA ATG GTG AA	3′-TTA ACT GCC CAG CGC TAG AT
C/EBPα	5′-CTC CCA GAG GAC CAA TGA AA	3′-AAG TCT TAG CCG GAG GAA GC
Collagen I	5′-AGG TGT GTG TCA AGG GGA AG	3′-CTC TCT TCC TGC ACC CAA AG
Osteonectin	5′-TCT GTT GTG TTG GGG ACG TA	3′-GCT TGA GCC ATC ACA CTT GA
CBFα	5′-AAA CTC ACA GCC TCG AAG GA	3′-TGT GGC TCA TTG TTC TCT GC
Collagen II	5′-GAA GGT GCT CAA GGT TCT CG	3′-TTT GTG ACA AGG CCA CAC AT
Aggrecan	5′-CGA GCT ACA GAG GGA ACC TG	3′-CCA GAC TTG GAA CCT GTG GT
Sox9	5′-CCC CAA AAG CAC ACA TTC TT	3′-ACC CGC AGG TAC ACA CTA GG

4.4 Results and Discussion

Formulation of a CO_2-independent medium

Initially, the growth rate of undifferentiated MSC was evaluated in MEM-α buffered with various concentrations of MOPS and HEPES under atmospheric CO_2 by endpoint assessment of cell densities. The range of MOPS and HEPES investigated were 12 to 18 mM. The cell densities using MOPS and HEPES were compared to the cell densities obtained from the standard conditions using a common seed culture. Many of the MOPS and HEPES combinations could achieve cell densities equal to that attained in the standard medium under 5% CO_2 (data not shown). The MOPS-HEPES buffered medium selected to be examined further contained 12 mM MOPS, 12 mM HEPES, and 5 mM sodium bicarbonate ($NaHCO_3$). This formulation was selected to minimize the potential cytotoxic effects associated with HEPES buffer (Zigler et al., 1985). A low level (5 mM) of $NaHCO_3$ was added to the MOPS-HEPES buffered medium, because bicarbonate is reported to be an essential cell nutrient for mammalian cells (Swim and Parker, 1958).

There are several considerations when formulating a buffer for MSC expansion under atmospheric CO_2. Due to the multipotency of MSC, it is crucial that none of the buffering components interfere with the normal behavior of undifferentiated MSC during expansion. For instance, the β-glycerophosphate in Invitrogen's CO_2 independent-medium can induce osteogenesis, and therefore does not promote maintenance of an undifferentiated MSC phenotype (Battista and Weiss, 1991; Fiorentini et al., 2011). At the same time, the behavior of MSC is highly pH-dependent, so the buffering

components must have sufficient buffering capacity within the desired pH range (Wuertz et al., 2009). As Swain and Pool (2009) pointed out, pH buffering must also be accomplished with buffer concentrations that are low enough to avoid cytotoxicity (Swain and Pool, 2009). Their work demonstrated that buffers used in combination allow for lower concentrations without compromising buffering capacity, a principle that was used in our work. In short, the buffering components to be substituted for bicarbonate must maintain pH effectively within a precise range while not altering the health or phenotype of the MSC.

Undifferentiated MSC can be effectively expanded under an atmospheric CO_2 environment while retaining stem cell characteristics

To evaluate the growth rates and final cell densities, undifferentiated MSC were first expanded in standard MEM-α medium under 5% CO_2 and this common stock was used to seed subsequent cultures. The undifferentiated MSC were then grown in the standard MEM-α medium and the MOPS-HEPES buffered MEM-α medium under both 5% and atmospheric CO_2 environments without prior adaptation. Additionally, the undifferentiated MSC were grown under atmospheric CO_2 in Leibovitz L-15 medium. The L-15 medium was designed to support CO_2-independent growth of mammalian cells, but is now mainly used to grow specific cancer cell lines and buffer solutions while performing analysis of cells under atmospheric conditions (Leibovitz, 1963; Maffia et al., 2007; Mantegazza et al., 2008). To date, Leibovitz L-15 medium has not been investigated for stem cell expansion. As expected, the cultures grown in the standard

MEM-α medium under 5% CO_2 had exponential growth without a lag phase, and the cultures grown in the MEM-a standard medium under atmospheric CO_2 failed to grow (Figure 4.1A). In contrast, cultures grown in Leibovitz L-15 medium under atmospheric CO_2 had observable growth, albeit at a lower rate. The lower growth rate in the L-15 medium was most likely due to the medium's buffering system and carbon energy source. The L-15 medium relied on high amino acid concentrations to provide buffering capacity. Elevated amino acids are not always problematic, but it has been observed that some amino acids in elevated concentrations reduce growth rates in mammalian cells (Chen and Harcum, 2005; Xing et al., 2011). Specifically, the L-15 medium contained 225 mM alanine compared to 25 mM in the standard MEM-a medium (Leibovitz, 1963). The L-15 medium also substitutes galactose for glucose. Galactose has been implicated in shifting cell metabolism from a predominantly glycolytic state to one relying more on oxidative phosphorylation in several cell lines (Higuera et al., 2011; Aguer et al., 2011). Actively growing cells appear to rely more heavily on glycolysis than oxidative phosphorylation for energy production (Kinney et al., 2011; dos Santos et al., 2010; Pattappa et al., 2011), which means galactose may not be a suitable primary carbon source for maintaining high growth rates. Thus, the lower growth rates associated with MSC in the L-15 medium is hypothesized to be due to the presence of high amino acid levels and the use of galactose instead of glucose.

The undifferentiated MSC cultures grown in the MOPS-HEPES buffered medium under 5% CO_2 grew better than in Leibovitz L-15 medium ($p \leq 0.05$), but still at a suboptimal rate. The decreased growth rate in the MOPS-HEPES buffered medium under

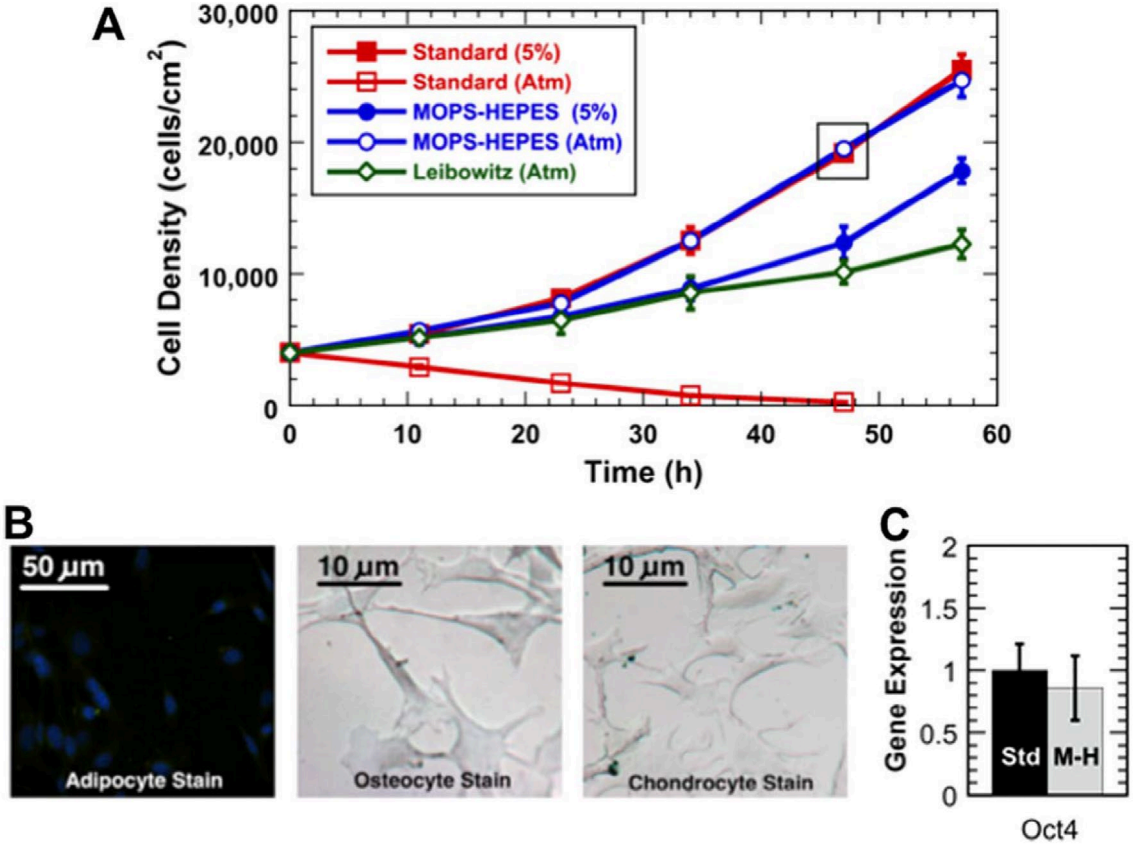

Figure 4.1 Proliferation of MSC. A: Growth profiles for MSC cultured in a standard medium, a MOPS-HEPES buffered medium under both 5% and atmospheric CO_2 conditions as well as the Leibovitz L-15 medium under atmospheric CO_2. B: Negative control staining for lineage-specific markers in undifferentiated MSCs cultured in MOPS-HEPES buffered medium for 48-h. C: Oct4 normalized gene expression levels for undifferentiated MSCs cultured in the standard medium in 5% CO_2 (Std) and the MOPS-HEPES buffered medium in atmospheric CO_2 (M-H) for 48-h as indicated in panel A. Error bars represent 95% confidence intervals.

5% CO_2 can be attributed to the low culture pH. More importantly, the undifferentiated MSC cultures grown in the MOPS-HEPES buffered medium under atmospheric CO_2 had exponential growth without a lag phase. The observed growth rates for the undifferentiated MSC in standard medium under 5% CO_2 and the MOPS-HEPES buffered MEM-α medium under atmospheric CO_2 were not significantly different ($p > 0.05$) with observed growth rates of 0.033 h^{-1}; which corresponds to a doubling time of 21-h. These results indicate that undifferentiated MSC can be expanded in MOPS-HEPES buffered MEM-α medium under atmospheric CO_2 at an equivalent rate to undifferentiated MSC in standard MEM-α medium under a 5% CO_2 environment, and also achieve final cell densities that are not significantly different.

While growth rates were equivalent for the undifferentiated MSC cultured in the standard MEM-α medium under 5% CO_2 and the MOPS-HEPES buffered MEM-α medium under atmospheric CO_2, equally important is that the MSC maintained an undifferentiated state and self-renewal abilities. The phenotype and multipotency of undifferentiated MSC were assessed for MSC expanded for 48 h in the standard MEM-α medium under 5% CO_2 and the MOPS-HEPES buffered MEM-α medium under atmospheric CO_2. First, undifferentiated MSC were stained for markers of adipogenic, osteogenic, and chondrogenic differentiation after expansion as negative controls. The histological staining of the undifferentiated MSC showed absence of lineage markers (Figure 4.1B), as expected, suggesting no gross signs of differentiation for both conditions. Only the MSC cultured in the MOPS-HEPES buffered MEM-α medium under atmospheric CO_2 negative control stainings are shown (Figure 4.1B), as the MSC

cultured in the standard MEM-a medium under 5% CO_2 were not significantly different from negative control the images provided in the standard staining protocol. The negative control stainings for the undifferentiated MSC cultured in the MOPS-HEPES buffered MEM-a medium under atmospheric CO_2 can be compared with the positive control stainings shown in Figure 4.2A, 4.3A, and 4.4A. Second, the MSC were analyzed for a gene marker indicative of an undifferentiated stem cell state after expansion. Gene expression levels for Oct4 ($p = 0.75$) (Figure 4.1C) were not significantly different between undifferentiated MSC cultured in either the standard MEM-α medium under 5% CO_2 and the MOPS-HEPES buffered MEM-a medium under atmospheric CO_2, representing a similar extent of stemness.

These results indicate that undifferentiated MSC can be expanded under atmospheric CO_2 without compromising growth rates or the stem cell phenotype as determined by gene expression markers, and supported by the undifferentiated appear under histological staining. This is important because many MSC-based treatments rely on undifferentiated MSC. Even in applications where the differentiated progeny of MSC are desired, differentiation is typically induced after initial expansion generates a sufficient quantity of undifferentiated MSC (Sart et al., 2011). These results indicate that MSC can be effectively expanded without prior adaptation to the MOPS-HEPES buffer and atmospheric CO_2 conditions. The lack of an adaptation phase would allow for easier translation to clinical applications.

MSC retain multilineage differentiation potential after prior expansion under atmospheric CO_2

In order to characterize the differentiation potential of MSC cultured under atmospheric CO_2, cells were obtained from T-75 flasks that had been cultured for 48 h in either the standard MEM-α medium under 5% CO_2 or the MOPS-HEPES buffered MEM-a medium under atmospheric CO_2. These MSC were then differentiated along the adipogenic, osteogenic, and chondrogenic lineages under 5% CO_2 to assess multipotency. As shown in Figure 4.2A, staining for lipid vesicle formation indicated a similar extent of adipogenic differentiation between the two conditions. Also, adipogenic gene expression levels for lipoprotein lipase ($p = 0.095$), PPARγ2 ($p = 0.86$), and C/EBPα ($p = 0.47$) were not significantly different between the two conditions (Figure 4.2B). As shown in Figure 4.3A, staining for alkaline phosphatase activity indicated a similar extent of osteogenic differentiation between the two conditions. Also, osteogenic gene expression levels for collagen I ($p = 0.89$), osteonectin ($p = 0.088$), and CBFα1 ($p = 0.99$) were not significantly different between the two conditions (Figure 4.3B). As shown in Figure 4.4A, staining for glycosaminoglycan production indicated a similar extent of chondrogenic differentiation between the two conditions. Also, chondrogenic gene expression levels for collagen II ($p = 0.22$), aggrecan ($p = 0.55$), and Sox9 ($p = 0.94$) were not significantly different between the two conditions (Figure 4.4B). These results demonstrate that the tri-lineage differentiation potential of undifferentiated MSC along the adipogenic, osteogenic, and chondrogenic lineages were not impacted by prior expansion in the MOPS-HEPES buffered medium under atmospheric CO_2.

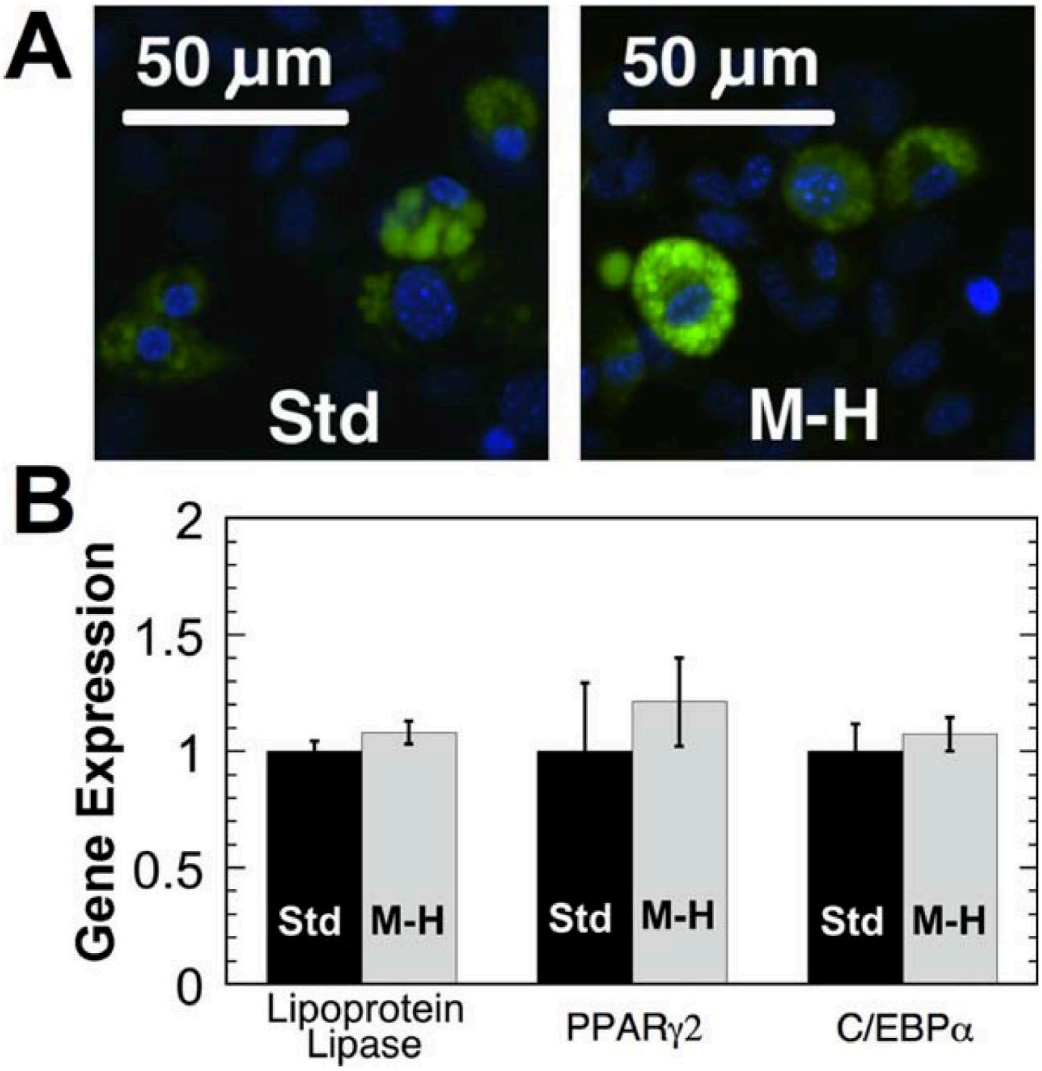

Figure 4.2. Adipogenic differentiation of MSC. A: Histological staining of MSC cultured in a standard medium under 5% CO_2 (Std) and in a MOPS-HEPES buffered medium under atmospheric CO_2 (M-H). The stain HCS LipidTox was used to visualize lipids (green) and DAPI was used to visualize the nuclei (blue). B: Lipoprotein lipase, PPARγ2, and C/EBPα normalized gene expression levels in adipogenically differentiated MSC. Error bars represent 95% confidence intervals.

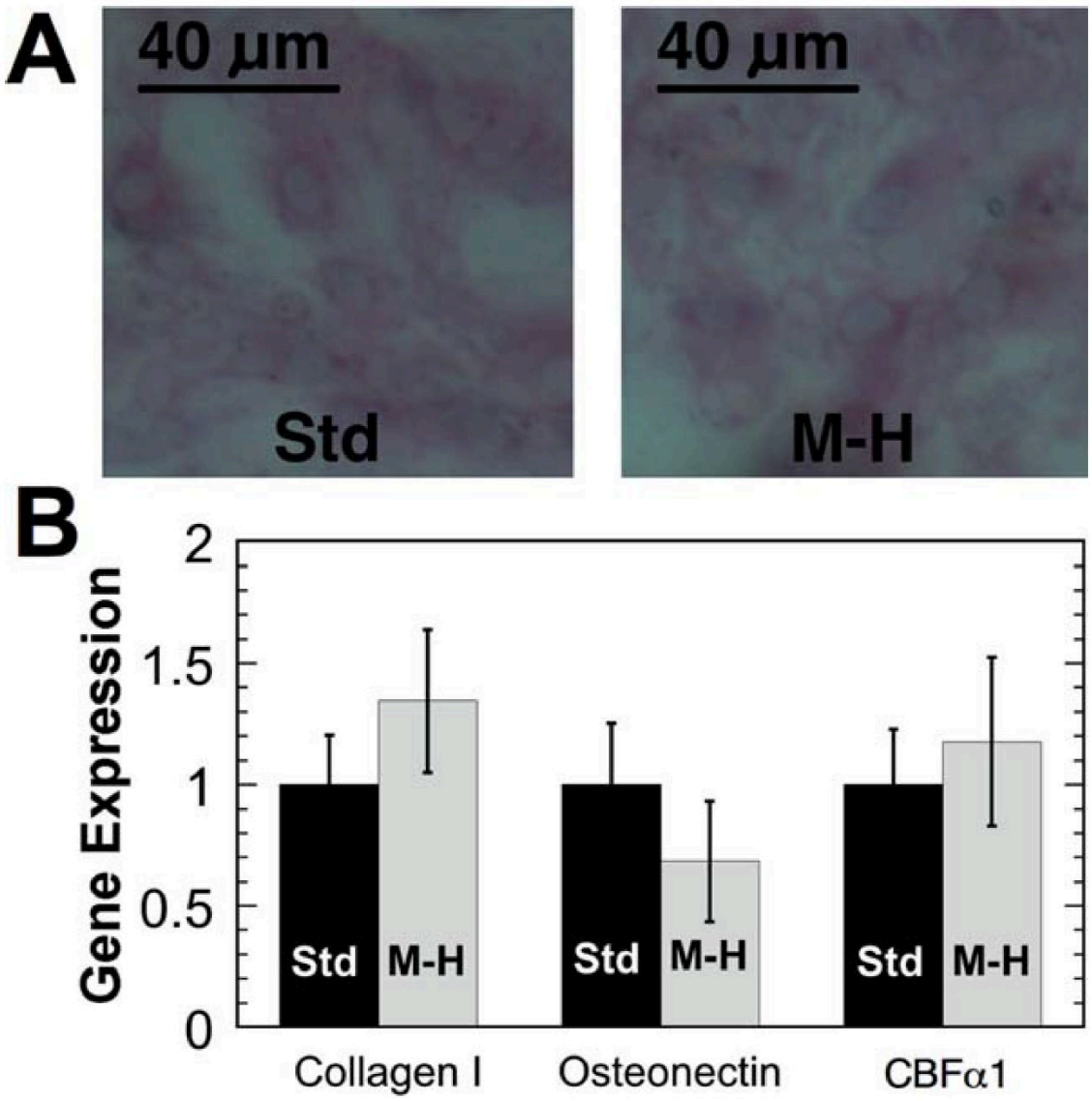

Figure 4.3 Osteogenic differentiation of MSC. A: Histological staining of MSC cultured in a standard medium under 5% CO_2 (Std) and in a MOPS-HEPES buffered medium under atmospheric CO_2 (M-H). The stains FRV and Napthol Phosphate were used to visualize alkaline phosphatase activity in pink. B: Collagen I, Osteonectin, and CBFα1 normalized gene expression levels in osteogenically differentiated MSC. Error bars represent 95% confidence.

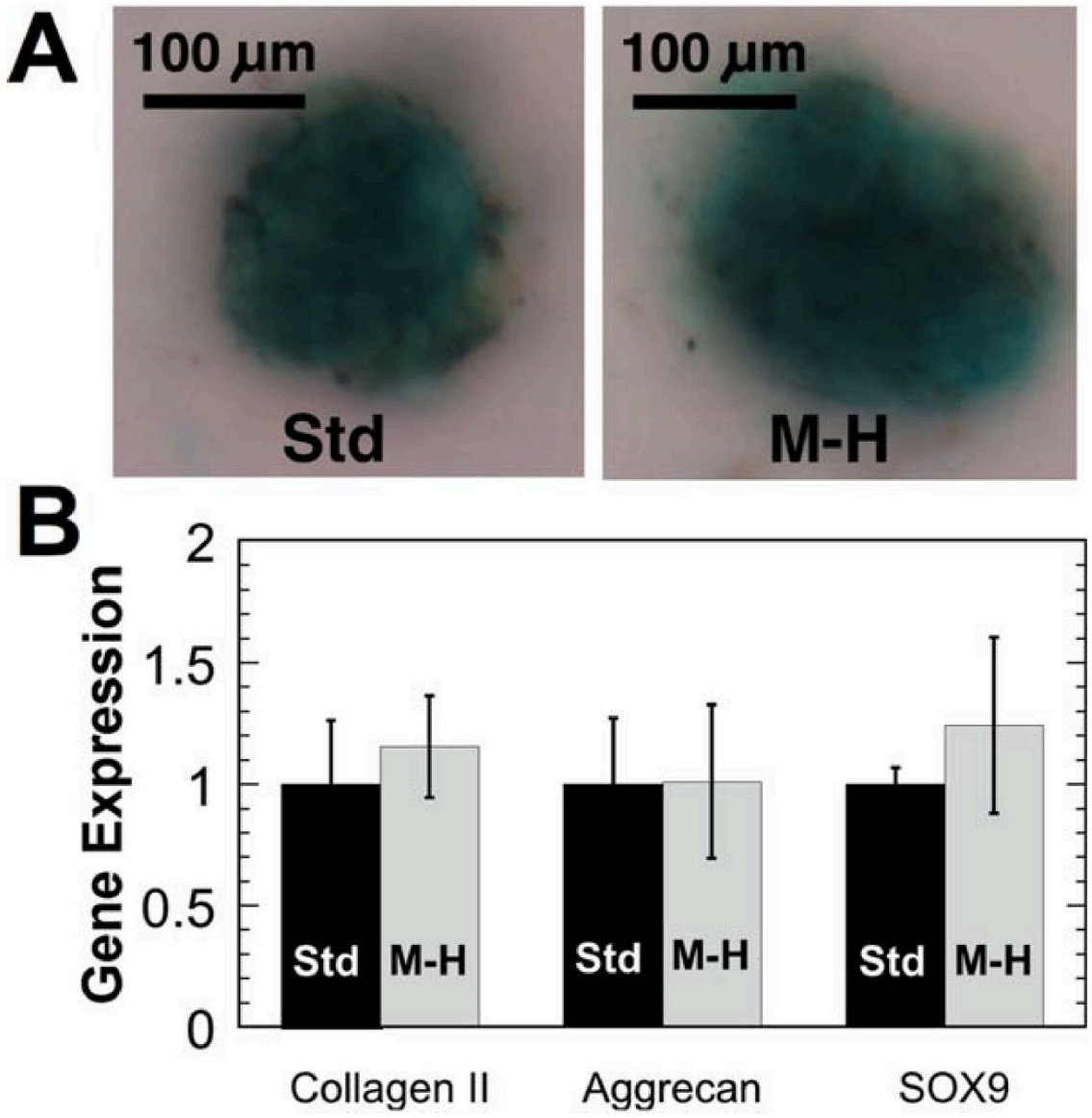

Figure 4.4 Chondrogenic differentiation of MSC. A: Histological staining of MSC cultured in a standard medium under 5% CO_2 (Std) and in a MOPS-HEPES buffered medium under atmospheric CO_2 (M-H). The stain Alcian Blue was used to visualize glycosaminoglycans in blue. B: Collagen II, Aggrecan, and SOX9 normalized gene expression levels in chondrogenically differentiated MSC. Error bars represent 95% confidenceintervals.

Undifferentiated MSC retain expansion potential and stem cell characteristics after multiple passages under atmospheric CO_2

While expanding MSC effectively without prior adaptation to the MOPS-HEPES buffer and atmospheric CO_2 enables easier translation to clinical applications, prolonged expansion may be required to generate larger quantities of undifferentiated stem cells. To this end, serial passages of undifferentiated MSC were conducted. Both the standard medium under 5% CO_2 and the MOPS-HEPES buffered medium under atmospheric CO_2 were examined for five passages. To ensure that growth rates were maintained in the exponential phase, the cultures were only expanded to approximately 75% confluent at the 60-h time point representing a potential fold-expansion in each passage of 6.25-fold. The final cell densities for all five passages were not significantly different between MSC expanded in the standard medium under 5% CO_2 and the MOPS-HEPES buffered medium under atmospheric CO_2 ($p > 0.05$) (Figure 4.5A). Additionally, the final cell densities were not different between the passages ($p > 0.05$). These end-point cell densities correspond to an overall growth rate of 0.031 h^{-1} over 60-h, which is not statistically different ($p > 0.05$) from the 57-h overall growth rates observed for the passage 1 MSC cultured in the standard medium under 5% CO_2 and the MOPS-HEPES buffered medium under atmospheric CO_2 (Figure 4.1A). Gene expression levels for Oct4 were not significantly different for the undifferentiated MSC expanded in the standard medium under 5% CO_2 and the MOPS-HEPES buffered medium under atmospheric CO_2 after passage five ($p > 0.05$) (Figure 4.5B). It has been previously shown that MSC growth rates change in vitro after only five passages (Wall et al., 2007), thus maintenance

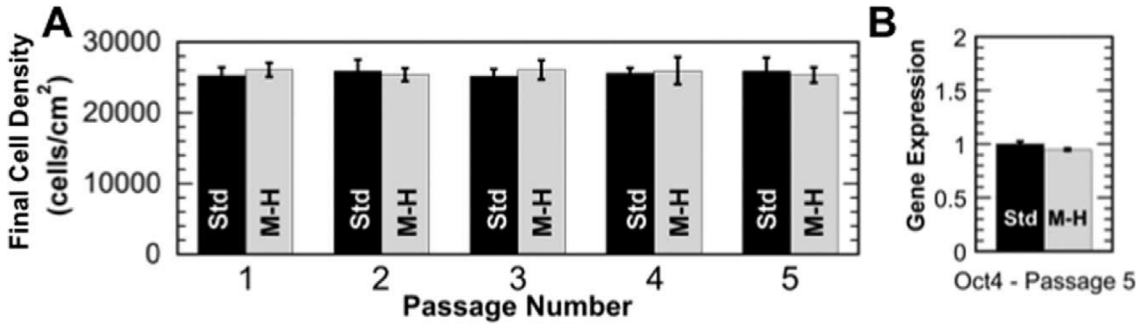

Figure 4.5 Extended MSC expansion. A: End-point cell density analysis for undifferentiated MSC through five passages cultured in a standard medium under 5% CO_2 (Std) and in a MOPS-HEPES buffered medium under atmospheric CO_2 (M-H). B: Oct4 normalized gene expression for undifferentiated MSC after passage 5. Error bars represent 95% confidence intervals.

of growth rate in the MOPS-HEPES buffer under atmospheric CO_2 for this duration would meet current expected outcomes. Additionally, in vitro MSC growth rates are a highly sensitive indicator of stemness and were shown to decrease prior to changes in differentiation markers (Wall et al., 2007). It has been previously shown that Oct4 gene expression levels are highly correlated with a more primitive stem cell-like state capable of extended proliferation, increased colony forming potential, and multilineage differentiation. For example, hypoxia increased MSC stemness as determined by the potential for proliferation, colony formation, and differentiation and coincided with the upregulation of Oct4 and Rex-1 gene expression (Grayson et al., 2006). In addition, overexpression of Oct4 and Nanog were shown to enhance stem cell properties in MSC as determined by proliferation and differentiation potential, while knockdown of Oct4 and Nanog decreased proliferation and differentiation potential (Tsai et al., 2012). Therefore, the similar Oct4 expression levels and similar growth patterns that were observed indicate similar levels of stemness between the MSC grown in 5% CO_2 and those MSC grown in atmospheric CO_2.

Potential impacts of CO_2 independence on large-scale stem cell expansion in stirred bioreactors

Stirred bioreactors—with unmatched scalability—represent a very promising culture format for delivering high yields of either suspension or anchorage-dependent stem cells with uniform properties (Fernandes Platzgummer et al., 2011; Serra et al.,

2012; King and Miller, 2007; Grolms et al., 2009). The online monitoring and control capabilities allow culture parameters to be adjusted throughout the duration of expansion, which can provide crucial batch-to-batch reproducibility (Shafa et al. 2011). The biopharmaceutical industry has long taken significant advantage of these systems, but stem cell expansion techniques have lagged behind and not yet transitioned into truly large-scale vessels (Olmer et al., 2012; Zweigerdt, 2009). Many stem cell-based treatments require large quantities of stem cells, and because native stem cells are relatively scarce in adult tissues, sufficient quantities of stem cells must be expanded in a timely manner in vitro for use in treatments. Additionally, adult stem cells decline in quantity and quality over time in a person, thus reducing the ability to harvest autologous supplies (dos Santos et al., 2010). These considerations have led some to suggest that establishing stem cell banks may be a more practical solution (Serra et al., 2012). Allogenic stem cell stocks would allow patients access to stem cells on demand, in much the same way that blood banks currently work. These stem cell banks would further necessitate large-scale cultivation at optimal growth rates to produce sufficient quantities of cells. The MSC cultured in the MOPS-HEPES buffer under atmospheric CO_2 were able to maintain high/optimal growth rates for five passages, which would allow for large-scale cultivation.

As stem cell expansion moves toward large-scale, issues similar to those currently encountered in other large-scale mammalian cell cultures will likely be encountered. Many of these problems result from the widespread use of the bicarbonate buffering system to regulate culture pH. In contrast to pH buffer redundancies in the body, the

bicarbonate buffering system essentially functions alone in typical mammalian cell culture. In cell culture media, elevated levels of $NaHCO_3$ are added, which necessitates the use of high CO_2 levels in the gas phase that are significantly higher than physiological levels (See Figure 4.6) (Goudar et al., 2006; Pattison et al., 2000). The indirect equilibrium between the CO_2 from the gas phase and the $NaHCO_3$ added to the medium maintains pH, via H^+ concentration. Due to the nonpolar nature of CO_2, it can freely diffuse across cell membranes. At high concentrations, it can lower intracellular pH. (Goudar et al., 2006; Pattison et al., 2000) In addition to affecting growth rates, these elevated dCO_2 levels can also alter the metabolism, productivity, and glycosylation profiles in other mammalian cell lines, although this has not yet been reported in stem cells (Goudar et al., 2006; Pattison et al., 2000; Hu et al., 2011). As cell densities increase in large-scale cultures, additional CO_2 is produced by the actively growing cells, which causes a buildup of dCO_2 and gas phase CO_2 levels (Goudar et al., 2006). This dCO_2 buildup can negatively impact cells grown in stirred bioreactors, and the effects increase with vessel size (Goudar et al., 2006; Hu et al., 2011). The use of a nonbicarbonate buffer would reduce dCO_2 buildup and potentially improve growth.

In stirred bioreactors, oxygen and CO_2 gases are sparged into the vessel as bubbles, to increase mass transfer between the gas and liquid phases (King and Miller, 2007). The breakup of these bubbles at the gas–liquid interface is responsible for the majority of cell death and damage during stirred bioreactor cultures (Rodrigues et al., 2011; Papoutsakis, 2009; Zhang et al., 2010). Interestingly, managing the size of these bubbles has been proposed as a solution to the problem of dCO_2 buildup (Pattison et al.,

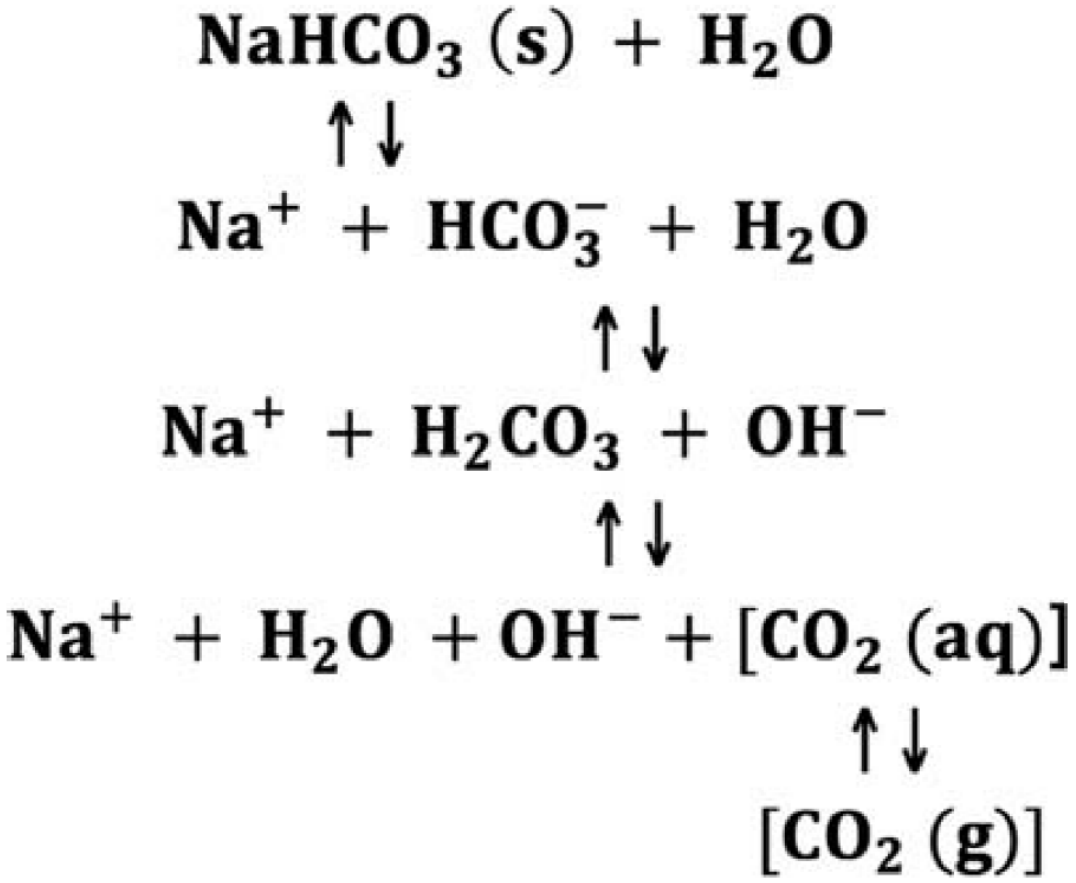

Figure 4.6 Bicarbonate buffer equilibrium. $NaHCO_3$ salt is commonly added to mammalian cell culture medium to provide buffering in concert with elevated gas phase CO_2, which will equilibrate with dCO_2.

2000; Zhang et al., 2010; Hu et al., 2011). Larger bubbles are more effective in stripping dCO_2, while smaller bubbles are more effective at delivering oxygen to the culture (Hu et al., 2011). With both oxygen and CO_2 being supplied via the same sparged gas phase, only one bubble size distribution can be supplied. As vessels are scaled-up, the dCO_2 buildup becomes problematic, such that sparger designs allow for larger bubbles to strip dCO_2 at the expense of adequate oxygen supply (Hu et al., 2011). Hu et al. (2011) proposed decoupling the oxygen and CO_2 supplies by supplying pure oxygen via microspargers into the bioreactor, and air via standard spargers; however, they were concerned about the added control complexity (Hu et al., 2011). A nonbicarbonate buffer would allow for a single gas supply (air/oxygen), thus decreasing controller complexity.

The coupling of the oxygen and CO_2 supplies complicates control of culture parameters and allows for pH and dissolved oxygen variability that is unacceptable, particularly for stem cells (Serra et al., 2012; Rodrigues et al., 2011; Yeatts et al., 2013; Wuertz et al., 2009; dos Santos et al., 2010). Several researchers have indicated that this $pH/CO_2/O_2$ interdependence complicates bioreactor control and have gone on to quantify the effects of pH, CO_2, or dissolved oxygen variability on growth or productivity (Rodrigues et al., 2009); however, few have suggested replacing the bicarbonate buffer system as a means to improve pH control (Goudar et al., 2006). Yet it would appear far simpler to use a nonbicarbonate buffer—such as the MOPS-HEPES combination used in this study—that does not rely on elevated dCO_2 levels for pH control. This work was the first to demonstrate that the bicarbonate buffering system and an elevated CO_2 environment are not required for effective expansion of undifferentiated MSC.

Elimination of the bicarbonate buffer should lead to improved control of culture conditions and enhanced stem cell expansion in bioreactors.

4.5 Conclusion

Stem cells will be used in increasing numbers of scientific applications in the future, ranging from basic research to clinical treatments. To provide stem cells for these applications, new large-scale stem cell expansion methods must be developed. Stirred bioreactors possess many advantages that allow for generation of large quantities of uniform stem cells in a reproducible manner. Unfortunately, the bicarbonate buffer used in mammalian cell culture, and the excessive CO_2 sparging required by that system hinder the ability to optimize process controls and generate stem cell yields of the highest quality. This work developed a MOPS-HEPES buffering system that de-emphasized the role of CO_2 in pH buffering. Undifferentiated MSC were expanded without prior adaptation under an atmospheric CO_2 environment in the presence of the MOPS-HEPES buffer at growth rates equal to those expanded under 5% CO_2 in the presence of the standard bicarbonate buffer. Additionally, the undifferentiated MSC expanded under an atmospheric CO_2 environment retained equivalent differentiation potential along the adipogenic, osteogenic, and chondrogenic lineages compared to undifferentiated MSC previously expanded under 5% CO_2, as determined by histological staining and gene expression markers. Furthermore, serial passaging of MSC in the MOPS-HEPES buffered medium under atmospheric CO_2 did not hinder MSC expansion or decrease stemness gene expression markers as compared to MSC serially passaged under standard conditions. Utilization of CO_2-independent buffers, such as the MOPS-HEPES buffer developed here, has the potential to improve stem cell bioreactor expansion by allowing for tighter control of pH and dissolved oxygen.

4.6 Acknowledgements

This research was supported by an Institutional Development Award (IDeA) from the National Institute of General Medical Sciences of the National Institutes of Health under grant number P20GM103444. Additionally, we would like to thank Dr. Terri Bruce of the Clemson Light Imaging Facility for assistance with microscopy and Wallace Campbell for assistance with statistical analysis.

4.7 References

Aguer C, Gambarotta D, Mailloux RJ, Moffat C, Dent R, McPherson R, Harper ME. Galactose enhances oxidative metabolism and reveals mitochondrial dysfunction in human primary muscle cells. PLoS One. 2011;6:e28536.

Alfred R, Radford J, Fan J, Boon K, Krawetz R, Rancourt D, Kallos M. Efficient suspension bioreactor expansion of murine embryonic stem cells on microcarriers in serum-free medium. Biotechnol Prog. 2011;27:811–823.

Ashton RS, Keung AJ, Peltier J, Schaffer DV. Progress and prospects for stem cell engineering. Annu Rev Chem Biomol. 2011;2:479–502.

Battista J, Weiss A. Development and application of a carbon dioxide independent medium. Focus. 1991;13:110–114.

Berry MF, Engler AJ, Woo YJ, Pirolli TJ, Bish LT, Jayasankar V, Morine KJ, Gardner TJ, Discher DE, Sweeney HL. Mesenchymal stem cell injection after myocardial infarction improves myocardial compliance. Am J Physiol-Heart C. 2006;290:H2196–H2203.

Chen P, Harcum SW. Effects of amino acid additions on ammonium stressed CHO cells.

J Biotechnol. 2005;117:277 286.

Chen P, Harcum SW. Effects of elevated ammonium on glycosylation gene expression in CHO cells. Metab Eng. 2006;8:123–132.

dos Santos F, Andrade PZ, Boura JS, Abecasis MM, da Silva CL, Cabral J. Ex vivo expansion of human mesenchymal stem cells: a more effective cell proliferation kinetics and metabolism under hypoxia. J Cell Physiol. 2010;223:27–35.

Fernandes Platzgummer A, Diogo MM, Baptista RP, Silva CL, Cabral J. Scale up of mouse embryonic stem cell expansion in stirred bioreactors. Biotechnol Prog. 2011;27:1421–1432.

Fiorentini E, Granchi D, Leonardi E, Baldini N, Ciapetti G. Effects of osteogenic differentiation inducers on in vitro expanded adult mesenchymal stromal cells. Int J Artif Organs. 2011;34:998–1011.

Frith JE, Thomson B, Genever PG. Dynamic three-dimensional culture methods enhance mesenchymal stem cell properties and increase therapeutic potential. Tissue Eng Part C: Methods. 2009;16:735–749.

Goudar CT, Matanguihan R, Long E, Cruz C, Zhang C, Piret JM, Konstantinov KB.

Decreased pCO2 accumulation by eliminating bicarbonate addition to high cell-density cultures. Biotechnol Bioeng. 2006;96:1107–1117.

Grayson WL, Zhao F, Izadpanah R, Bunnell B, Ma T. Effects of hypoxia on human mesenchymal stem cell expansion and plasticity in 3D constructs. J Cell Physiol. 2006;207:331– 339.

Grolms M, Olmer R, Martin U, Zweigerdt R. Facilitating scale up: Controlled stem cell cultivation in stirred suspension bioreactors. Stem Cells. 2011;2009:19.

Hanna J, Wernig M, Markoulaki S, Sun CW, Meissner A, Cassady JP, Beard C, Brambrink T, Wu, LC, Townes TM, Jaenisch R. Treatment of sickle cell anemia mouse model with iPS cells generated from autologous skin. Science. 2007;318:1920–1923.

Higuera GA, Schop D, Spitters TWGM, van Dijkhuizen-Radersma R, Bracke M, de Bruijn JD, Martens D, Karperien M, van Boxtel A, van Blitterwijk CA. Patterns of amino acid metabolism by proliferating human mesenchymal stem cells. Tissue Eng Part A. 2011;18:654–664.

Hu W, Berdugo C, Chalmers JJ. The potential of hydrodynamic damage to animal cells of industrial relevance: current understanding. Cytotechnology. 2011;63:445–460.

King JA, Miller WM. Bioreactor development for stem cell expansion and controlled differentiation. Curr Opin Chem Biol. 2007;11:394–398.

Kinney MA, Sargent CY, McDevitt TC. The multiparametric effects of hydrodynamic environments on stem cell culture. Tissue Eng Part B: Rev. 2011;17:249–262.

Leibovitz A. The growth and maintenance of tissue–cell cultures in free gas exchange with the atmosphere. Am J Epidemiol. 1963;78:173–180.

Maffia P, Zinselmeyer BH, Ialenti A, Kennedy S, Baker AH, McInnes IB, Brewer JM, Garside P. Multiphoton microscopy for 3-dimensional imaging of lymphocyte recruitment into apolipoprotein-E–deficient mouse carotid artery. Circulation. 2007; 115:e326–e328.

Mantegazza AR, Savina A, Vermeulen M, PO˜ rez L, Geffner J, Hermine O, Rosenzweig SD, Faure F, Amigorena S. NADPH oxidase controls phagosomal pH and antigen cross-presentation in human dendritic cells. Blood. 2008;112:4712–4722.

Olmer R, Lange A, Selzer S, Kasper C, Haverich A, Martin U, Zweigerdt R. Suspension culture of human pluripotent stem cells in controlled, stirred bioreactors. Tissue Engineering Part C: Methods. 2012;18:772–784.

Osman JJ, Birch J, Varley J. The response of GS-NS0 myeloma cells to pH shifts and pH perturbations. Biotechnol Bioeng. 2001;75:63–73.

Papoutsakis ET. From CHO-cell to stem-cell biotechnology, oxygenation, and mixing in animal-cell culture: bioreactors, bubbles, and cell injury. Biotechnol Bioeng. 2009;102: 977–979.

Pattappa G, Heywood HK, de Bruijn JD, Lee DA. The metabolism of human mesenchymal stem cells during proliferation and differentiation. J Cell Physiol. 2011;226:2562–2570.

Pattison RN, Swamy J, Mendenhall B, Hwang C, Frohlich BT. Measurement and control of dissolved carbon dioxide in mammalian cell culture processes using an in situ fiber optic chemical sensor. Biotechnol Prog. 2000;16:769–774.

Ratcliffe E, Glen KE, Workman VL, Stacey AJ, Thomas RJ. A novel automated bioreactor for scalable process optimisation of haematopoietic stem cell culture. J Biotechnol. 2012;161: 387–390.

Rodrigues CAV, Fernandes TG, Diogo MM, da Silva CL, Cabral J. Stem cell cultivation in bioreactors. Biotechnol Adv. 2011;29:815–829.

Rodrigues ME, Costa AR, Henriques M, Azeredo J, Oliveira R. Technological progresses in monoclonal antibody production systems. Biotechnol Prog. 2009;26:332–351.

Sart S, Errachid A, Schneider Y, Agathos SN. Controlled expansion and differentiation of mesenchymal stem cells in a microcarrier based stirred bioreactor. BMC Proc. 2011;5:P55.

Schroeder M, Niebruegge S, Werner A, Willbold E, Burg M, Ruediger M, Field LJ, Lehmann J, Zweigerdt R. Differentiation and lineage selection of mouse embryonic stem cells in a stirred bench scale bioreactor with automated process control. Biotechnol Bioeng. 2005;92:920–933.

Serra M, Brito C, Correia C, Alves PM. Process engineering of human pluripotent stem cells for clinical application. Trends Biotechnol. 2012;30(6):350–359.

Shafa M, Sjonnesen K, Yamashita A, Liu S, Michalak M, Kallos M, Rancourt DE. Expansion and longterm maintenance of induced pluripotent stem cells in stirred suspension bioreactors. J Tissue Eng Regen Med. 2011;6(6):462–472.

Swain JE, Pool TB. New pH-buffering system for media utilized during gamete and embryo manipulations for assisted reproduction. Reprod Biomed Online. 2009;18:799–810.

Swim H, Parker R. The role of carbon dioxide as an essential nutrient for six permanent strains of fibroblasts. J Biophys Biochem Cytol. 1958;4(5):525–528.

Tsai C, Su P, Huang Y, Yew T, Hung S. Oct4 and Nanog directly regulate Dnmt1 to maintain self-renewal and undifferentiated state in mesenchymal stem cells. Mol Cell. 2012;47: 169–182.

Wall ME, Bernacki SH, Loboa EG. Effects of serial passaging on the adipogenic and osteogenic differentiation potential of adipose-derived human mesenchymal stem cells. Tissue Eng. 2007;13:1291–1298.

Wuertz K, Godburn K, Iatridis JC. MSC response to pH levels found in degenerating intervertebral discs. Biochem Biophys Res Commun. 2009;379:824–829.

Xing Z, Kenty B, Koyrakh I, Borys M, Pan SH, Li ZJ. Optimizing amino acid composition of CHO cell culture media for a fusion protein production. Process Biochem. 2011;46:1423–1429.

Yang JD, Lu C, Stasny B, Henley J, Guinto W, Gonzalez C, Gleason J, Fung M, Collopy B, Benjamino M, Gangi J, Hanson M, Ille E. Fed-batch bioreactor process scale-up from 3-L to 2,500-L scale for monoclonal antibody production from cell culture. Biotechnol

Bioeng. 2007;98:141–154.

Yeatts AB, Choquette DT, Fisher JP. Bioreactors to influence stem cell fate: Augmentation of mesenchymal stem cell signaling pathways via dynamic culture systems. Biochim Biophys Acta. 2013;1830:2470–2480.

Zhang H, Wang W, Quan C, Fan S. Engineering considerations for process development in mammalian cell cultivation. Curr Pharm Biotechnol. 2010;11:103–112.

Zigler J, Lepe-Zuniga J, Vistica B, Gery I. Analysis of the cytotoxic effects of light-exposed HEPES-containing culture medium. In Vitro Cell Dev Biol. 1985;21:282–287.

Zweigerdt R. Large scale production of stem cells and their derivatives. Adv Biochem Eng Biotechnol. 2009;114:201–235.

CHAPTER 5: IMPACT OF HIGH EXTRACELLULAR LACTATE ON THE METABOLISM OF THREE BREAST CANCER CELL LINES: MCF10A, MCF7, AND MDA-MB-231

5.1 Abstract

Metabolism is a crucial component of cancer's malignant arsenal, and flexibility with respect to nutrient sources allow it to survive harsh conditions as well as efforts to treat it. Lactate, which accumulates in tumors and was long thought to be simply a waste product that results from the Warburg Effect, is now becoming appreciated for its ability to serve as a metabolic substrate for cancer cells to utilize. Additionally, lactate has also been shown to promote metastasis, gene expression patterns consistent with the "cancer stem cell" phenotype, and treatment resistance in tumors. Therefore, to better understand the impact of extracellular lactate on the metabolism of cancer, three breast cancer cell line – MCF-10A, MCF-7, and MDA-MB-231 - were analyzed using ^{13}C-metabolic flux analysis in response to being cultured in high-lactate conditions. Metabolic flux maps that quantify individual pathway activity were generated for each cell line and each condition, and compared between the control and high-lactate cultures, and between the cell lines.

5.1 Introduction

Cell metabolism plays a pivotal role in cancer. Metabolism governs the energy production, macromolecular synthesis, and intracellular redox balance necessary for cell replication and other vital processes, and therefore when normal metabolism becomes unbalanced it can enable malignant behaviors. The Warburg effect – defined as glucose to lactate conversion rates even in the presence of adequate oxygen – has been witnessed in many types of cancer since its discovery in the 1920s. Since then, additional metabolic mechanisms have been discovered and have been shown to play a significant role in cancer progressions and malignancy. One of these important alternative mechanisms centers around lactate. Lactate accumulation in tumors is associated with increased malignant activity and poor patient prognosis (Kennedy and Dewhirst, 2010). Secreted from glycolytic cancer cells and autophagic carcinoma-associated fibroblasts, lactate can be utilized metabolically by other cancer cell populations, a process known as the Reverse Warburg effect (Kennedy and Dewhirst, 2010; Kennedy et al., 2013; Martinez-Outschoorn et al., 2011; Pavlides et al., 2010; Sonveaux et al., 2008). For example, when lactate was injected into mice with xenografts of the human breast cancer cell line MDA-MB-231, metastasis increased ten-fold (Bonuccelli et al., 2010). Additionally, when the human breast cancer cell line MCF-7 was exposed to lactate *in vitro*, genes associated with "stemness" were upregulated and gene expression patterns consistent with the "cancer stem cell" phenotype were observed (Martinez-Outschoorn et al., 2011). In several other types of cancers, intratumoral lactate levels – which can sometimes rise to as high as 40 mM – correlate with treatment resistance as well as poor patient prognosis

(Kennedy and Dewhirst, 2010). It has been shown in xenotransplants and mouse cancer models that inhibiting the ability of cancer cells to utilize lactate can force cells to become glycolytic and retard tumor growth through glucose starvation, while rendering the remaining cells more susceptible to radiation treatments (Sonveaux et al., 2008). Since lactate accumulation and its subsequent utilization by surrounding cells appears to negatively affect cancer patient outcomes, deciphering the role of lactate at the metabolic level within central metabolism is crucial.

Metabolic flux analysis (MFA) is a tool that can be used to quantify metabolic fluxes through individual metabolic pathways, and thus can be used to compare changes in metabolic activity rates due to various factors. MFA uses extracellular uptake and secretion rates of nutrients and waste products, and a discrete metabolic network model of the relevant metabolic reactions (Hiller and Metallo, 2012). The use of stable isotopic tracers, typically ^{13}C-labeled nutrients, and the resulting mass isotopomer distribution (MID) data increases the resolution of individual fluxes within the defined metabolic reaction network. Several mammalian systems have been characterized including Chinese hamster ovary (CHO) cells at both stationary and exponential growth phases, MDA-MB-231 cells under various nutrient considerations, and several other cancer cell lines under hypoxia (Ahn and Antoniewicz, 2011; Ahn and Antoniewicz, 2013; Gaglio et al., 2011). Several software tools – all relying upon regression analysis to solve the system of linear equations specified by the metabolic network - exist to allow researchers to conduct MFA without having to develop programming code, including Metran, OpenFLUX, ^{13}CFlux^{2},

and FiatFlux (Ahn and ANtoniewicz 2011; Quek et al., 2009; Weitzel et al., 2013; Zamboni et al., 2009).

The aim of this study was to determine the role of extracellular lactate on the metabolism of proliferating breast cancer cells during exponential growth. Three human breast cell lines were examined that represent three different stages of breast cancer. MCF-10A cells are a non-tumorigenic breast cell line, MCF-7 cells are a tumorigenic, luminal breast cancer cell line, and MDA-MB-231 cells are metastatic, basal breast cancer cell line (Zancan et al., 2010). Each cell line was grown in both a control condition without a lactate addition, as well as a high-lactate condition for which lactate was added to the extracellular culture medium. The high-lactate concentration was selected for each cell line to allow equivalent growth rates between the control and high-lactate conditions. Three isotopic tracers were used individually, in parallel labeling studies: [1,2-^{13}C] glucose - as it has been shown to most accurately resolve fluxes in glycolysis and the pentose-phosphate pathway (PPP) (Metallo et al., 2009); [U-^{13}C] L-glutamine - as it has been shown to most accurately resolve fluxes in the mitochondrial TCA cycle (Metallo et al., 2009); and [U-^{13}C] sodium lactate - to elucidate lactate metabolism. For the control cultures, only [1,2-^{13}C] glucose and [U-^{13}C] L-glutamine tracers were used, since no extracellular lactate was added to these cultures. Metran was used to solve the metabolic fluxes using the glucose and glutamine data. The lactate tracer data for the high-lactate conditions was able to characterize the distribution of labeled carbon within the intracellular metabolites. Metabolic flux maps for each cell line

and each condition were generated, and compared between the control and high-lactate cultures, and between the cell lines.

5.2 Materials & Methods

Cell lines and media formulations

MCF-10A (ATCC® CRL-10317™) and MCF-7 (ATCC® HTB-22™) cells were purchased from ATCC, while MDA-MB-231 (ATCC® CRL-10317™) were kindly provided to us by Dr. Brian Booth of Clemson University. Dulbecco's modified Eagle medium (DMEM) without glucose, glutamine, sodium pyruvate, and phenol red (Life Technologies) was used as the growth media. The growth media was supplemented with 5 mM glucose (FIsher), 3 mM glutamine (Life Technologies), 10% dialyzed fetal bovine serum (dFBS, Life Technologies) and 1% penicillin-streptomycin solution (Life Technologies). High-lactate cultures were supplemented with 10 mM sodium L-lactate (Sigma) for the MCF-10A cultures and 20 mM for the MCF-7 and MDA-MB-231 cultures. The isotopic tracers used in this study were [1,2-^{13}C] glucose, [U-^{13}C] L-glutamine, and [U-^{13}C] sodium lactate. All isotopes were purchased from Sigma-Aldrich.

Cell growth and parallel labeling experiments

All cell lines were initially seeded at 2 x 10^4 cells/cm^2 in the control growth media. Cells were cultured at 37°C in a 5% CO_2 humidified incubator. At 24-h, the media for the MDA-MB-231 cultures was exchanged and the experimental conditions were introduced. For MCF-10A and MCF-7 the media was replenished at 24-h, and at 48-h the media was exchanged to introduce the experimental conditions. The later start point for the MCF-10A and MCF-7 cultures was due to a reproducible longer lag phase. For clarity, the full experimental setup is shown in Figure 5.1. Cell numbers and extracellular metabolite

concentrations were measured at two time points, 24-h and 48-h after the media exchange. Cell numbers and glucose and lactate concentrations were obtained from the six-well plates, while the amino acid concentrations were obtained from the T-25 flasks. The intracellular MIDs were obtained from the T-25s at 24-h after the media exchange. The control condition had parallel cultures for both glucose (95% molar enriched [1,2-^{13}C] glucose) and glutamine tracers (95% molar enriched [U-^{13}C] L-glutamine), whereas the high-lactate cultures also had parallel replicates for the lactate tracer (50% molar enriched [U-^{13}C] sodium L-lactate). Six-well plates (Nunc) were used to obtain cell numbers and glucose and lactate concentrations with six replicates for each time point. T-25 flasks were used to obtain extracellular amino acid concentrations and intracellular MID measurements in triplicate.

Cell numbers, and glucose and lactate concentrations

Cell numbers were obtained using the Scepter 2.0 Handheld Automated Cell Counter (Millipore). Glucose and lactate concentrations were measured using a YSI 2700 Bioanalyzer.

Preparation of samples for GC-MS analysis

The methods used here for the extraction and derivatization of intracellular and extracellular metabolites, as well as the specific metabolite fragments used for identification, were performed according to the protocol outlined by Ahn and Antoniewicz (2011), with a few minor alterations. Samples were incubated and allowed

to derivatize for 60 min, and the sample volumes were increased to 1 mL after derivatization. The injection volume used was 3 μL and samples were injected in splitless mode. Amino acid standards were used .to calculate amino acid concentrations in the [U–^{13}C] algal amino acid solution, which were then used to quantify the amino acid concentrations in the extracellular medium.

Extracellular amino acid concentrations and intracellular MID measurements

GC-MS analysis was performed using a Hewlett Packard 7683 GC equipped with an HP-5 (30 m x 0.32 mm i.d. x 0.25 μm; J&W Scientific) capillary column, interfaced with a Hewlett Packard 5973 MS operating under ionization by electron impact as 2000 eV and 200°C ion source temperature. The injection port and interface temperatures were both 250°C while helium flow was maintained at 1 mL/min. Mass spectra were recorded in full scan mode for amino acid quantification and in single ion mode (SIM) for MIDs as well as internal standards and standardization curves. MIDs were obtained by integration of single ion chromatograms, and corrected for natural isotope abundances using the Metran software (Fernandez et al., 1996; Yoo et al., 2008).

Determination of biomass specific consumption and production rates

Specific consumption and production rates for nutrients and waste metabolites in the extracellular medium were determined based on cell growth rate and nutrient time profiles using the previously described method of Meadows et al. (2008). Each sample was independent, so average values were used to calculate fluxes. Prior to the flux

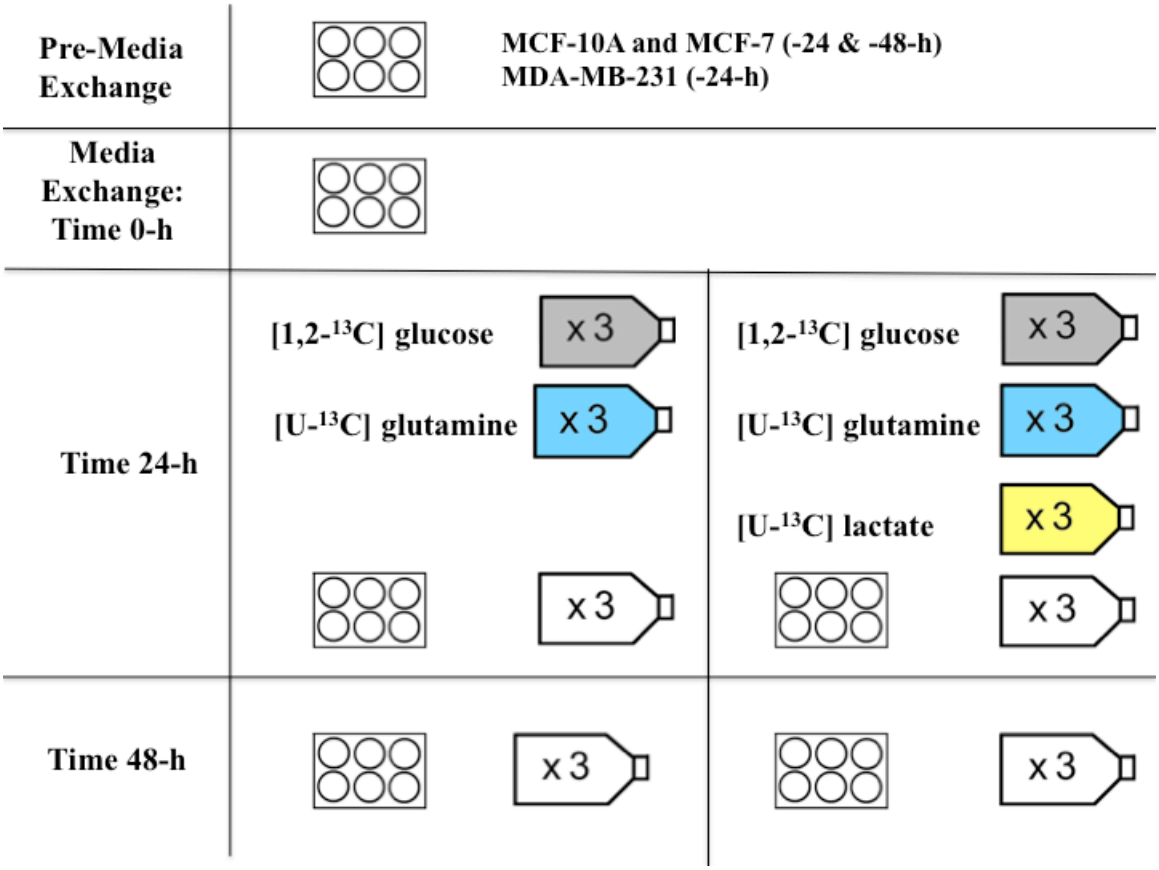

Figure 5.1. Experimental setup for parallel labeling experiment for each of the three breast cancer cell lines. Six-well plates and T-25 flasks were all seeded together. Times indicate when the plates or flasks were harvested for analysis relative to the media exchange. Isotopic labeling is graphically shown by shading. Clear for no isotope, gray for glucose, blue for glutamine, and yellow for lactate. None of the six-well plates contained isotopically-labeled media.

calculations, statistical analysis of the amino acid concentration data was conducted using jmp 10.0.0 (SAS Institute, Inc). The generalized linear model was used where cell line, condition, and time were examined as effectors of the amino acid concentration ($p \leq 0.05$). Amino acid concentrations were averaged if determined not to be statistically different with respect to the cell lines, condition, or time ($p \leq 0.05$). All amino acid concentrations were significantly affected by time ($p \leq 0.05$). Several amino acid concentrations were not significantly affected by cell line, condition, or both ($p \leq 0.05$). In those cases, the similar values were averaged to calculate fluxes. The spontaneous glutamine degradation rate was accounted for in the glutamine flux calculation. The lactate flux into the cells for the high-lactate cultures was estimated from the change in the extracellular M3 labeled lactate species concentration between 24 and 48-h after the media change.

Metabolic network model

To model central carbon metabolism for the three breast cancer cell lines, a general mammalian cell model was used. This generalized mammalian cell model was adapted from the previously developed framework by Ahn and Antoniewicz (2013). The major reactions for glycolysis, PPP, the TCA cycle, amino acid metabolism, lactate metabolism, and fatty acid metabolism were included in the mammalian cell model. Due to the varying lipid content reported across the breast cancer cell lines and breast cancer tissue (Abramczyk et al., 2015), a two-compartment biomass description was used, where the Main Biomass includes proteins, nucleotides, and carbohydrates (Ahn and

Antoniewicz, 2013). The protein amino acid composition appears to be relatively consistent between the three cell lines by Raman spectra (Talari et al., 2015). Lipid Biomass includes lipids and phospholipid (Bonarius et al., 1996). The two intracellular compartments were modeled; cytosolic and mitochondrial, as well as a pyruvate sink to account for reactions and pathways not explicitly included in the metabolic network model (Ahn and Antoniewicz, 2013; Metallo et al., 2009; Metallo et al., 2012). Cofactor balances, such as NADH and NADPH were not included in the model, as different isoenzymes have varying cofactor requirements and the inclusion of these assumptions can skew subsequent analysis (Ahn and Antoniewicz, 2011). Carbon dioxide was treated as an unbalanced metabolite, and was not measured. Oxygen uptake was excluded from the model and was also not measured. For the high-lactate cultures, an additional extracellular reaction was included to account for the uptake of the labeled lactate tracer. The control condition mammalian cell model has 73 reactions and the high-lactate condition mammalian cell model has 74 reactions. The full metabolic network model with atom transitions can be found in the Appendix A.

Metabolic flux analysis

^{13}C-Metabolic flux analysis was performed using the software package Metran (Yoo et al. 2008), which utilizes the elementary metabolite unit (EMU) framework (Antoniewicz et al., 2007b) Metabolic fluxes were estimated using experimentally measured-values for consumption and production rates and from mass isotopomer distributions for intracellular metabolites. In Metran, the metabolic fluxes were based on

the quantities that minimized the variance-weighted sum of squared residuals (SSRes) between the measured and simulated values. Metran can handle MID data from parallel labeling experiments to be used simultaneously to generate a single flux map, per condition and cell line, a capability that has been validated by MFA experiments for both *E. coli* and CHO cells (Leighty and Antoniewicz, 2012; Ahn and Antoniewicz, 2013). For this study, random initial fluxes were used and the MID error was 0.7 mol%. The MIDs for each tracer were: glucose [3-phosphoglycerate (3PG), phosphoenolpyruvate (PEP), dihydroxyacetone phosphate (DHAP), pyruvate, lactate, and alanine] and glutamine [succinate, malate, α-oxoglutarate (AKG), glutamate, citrate, glutamine, pyruvate, and lactate]. The MIDs from the lactate tracer for the high-lactate condition were not included in the Metran simulations; however, the lactate tracer flux was included. The fluxes for glucose, lactate, and glutamine were assigned 10% error, while the other amino acid fluxes were assigned 50% error, due to the low concentration values limiting precision. The main biomass and lipid biomass fluxes were assigned 25% error, due to the imprecision of previous estimates of cancer cell lipid content (Abramczyk et al., 2015). The lactate tracer flux was assigned 50% error, due to assumptions regarding how the value was calculated. Namely, the M3 isotope was only an approximation of total extracellular lactate, and the extracellular fluxes of M1 and M2 isotopes out of the cells were not accounted for. The simulations were determined to have converged when a global solution was achieved that satisfied the accepted SSRes criteria. This was determined from analyzing the simulated fit results via a chi-square statistical test to measure goodness-of-fit (Antoniewicz et al., 2006; Antoniewicz et al., 2007a). After

convergence, 95% confidence intervals were generated for all parameters based on the SSRes parameter (Antoniewicz et al., 2006).

5.3 Results and Discussion

Cell growth

To determine the effects of high extracellular lactate on breast cancer metabolism, three human breast cell lines, MCF-10A, MCF-7, and MDA-MB-231, were grown under both control and high-lactate conditions. For MCF-10A, the high-lactate culture media contained 10 mM lactate, while for MCF-7 and MDA-MB-231 the high-lactate culture media contained 20 mM lactate. In order to have more control over the nutrient conditions in the media and the isotopic labeling enrichment, the growth media used did not contain sodium pyruvate, and glucose and glutamine had to be added. The dialyzed FBS (dFBS) was also selected to minimize the carry over of glucose and other small molecules. The high-lactate concentration selected for the high-lactate condition was representative of lactate concentrations found within tumors that have been shown to elicit the malignant effects associated with lactate accumulation (Kennedy and Dewhirst, 2010; Martinez-Outschoorn et al., 2011), yet also allowed for equivalent growth rates between the control and high-lactate conditions. To characterize cell growth, cell counts were taken every 24-h for several days and the resulting growth profiles for the three cell lines are shown in Figure 5.2. All three cultures had significant lag phases; which were reproducible and predictable for each cell line (48-h for MCF-10A and MCF-7 and 24-h for MDA-MB-231). After the lag phase, the cultures were switched to the test conditions, as indicated by the arrow in Figure 5.2. For control condition cultures the media composition did not change, only isotopes were added; however, the cultures to be tested under the high-lactate condition, the media was switched to the high-lactate media. All

cultures exhibited exponential growth for 48-h after the media exchange, indicating that the high-lactate condition did not significantly affect the overall growth rates for each cell line ($p > 0.05$). The exponential growth rates were 0.017, 0.018, and 0.021 h^{-1}, respectively, for the MCF-10A, MCF-7, and MDA-MB-231 cell lines. In previous work with mammalian cell lines, it has been shown that isotopic steady-state is reached for glycolysis and the PPP metabolites with glucose labeling while TCA metabolites reach close to isotopic steady-state with glutamine labeling within this time frame (Ahn and Antoniewicz, 2013). Thus, samples for MID analysis were taken 24-h after the media change, indicated by the black arrow, while all cultures were in the mid-exponential phase (Figure 5.2).

Glucose, lactate, and amino acid metabolism

The glucose and lactate time profiles for each of the cell lines for each condition are shown in Figure 5.3. The calculated flux rates are listed in Table 5.1, while the concentrations for the 24-h and 48-h samples are listed in Appendix B. The three control cultures had high glycolytic efficiency, or conversion of glucose into lactate, where the theoretical maximum glycolytic efficiency is 2.0 mol lactate / mol glucose. Specifically, the control condition cultures had glycolytic efficiencies of 1.7, 1.5, and 1.8, respectively, for the MCF-10A, MCF-7, and MDA-MB-231 cell lines. The high-lactate condition cultures had glycolytic efficiencies of 1.4, 0.8 and 1.3, respectively, for MCF-10A, MCF-7, and MDA-MB-231 cell lines. The high extracellular lactate concentration caused all three cell lines to have decreased glycolytic efficiencies.

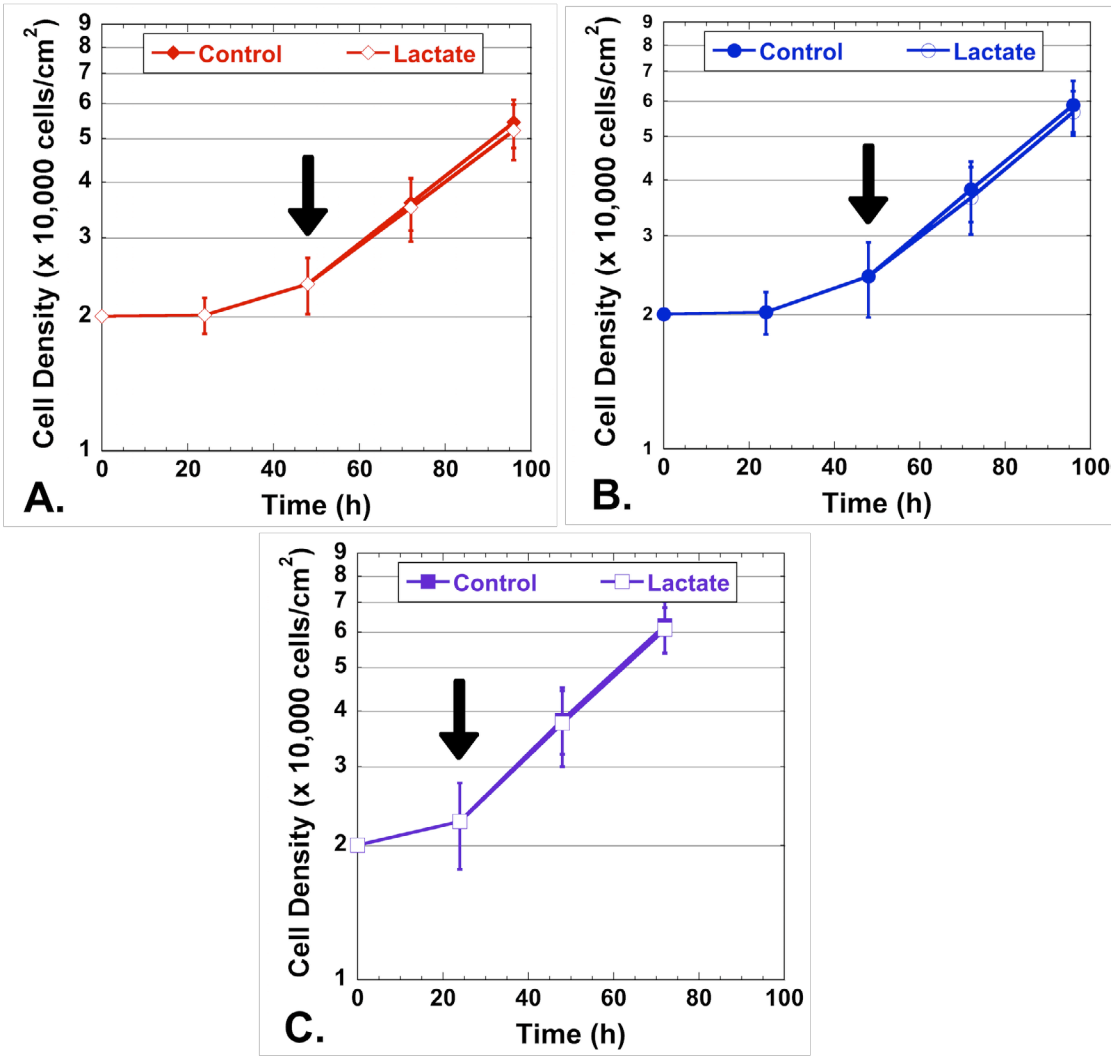

Figure 5.2. Growth profiles for the three breast cancer cell lines. A) The growth profiles of MCF-10A shown in red, B) The growth profiles of MCF-7 shown in blue, and C) The growth profiles of MDA-MB-231 shown in purple. The control cultures are represented by solid markers, while the high-lactate cultures represented by hollow markers. The media exchange occurred at the time point indiciated by the black arrow. Error bars represent 95% confidence intervals.

With respect to amino acid fluxes, the statistical analysis showed that several amino acid concentrations between cell lines or condition were not different ($p > 0.05$); however, they were different between 24-h and 48-h. Specifically, the glutamine, methionine, phenylalanine, and tyrosine concentrations were not significantly different ($p > 0.05$) between the cell lines or between conditions ($p > 0.05$). The concentrations of aspartate, glutamate, glycine, and threonine were significantly different between cell lines ($p \leq 0.05$), but within the same cell line were not significantly different between the control and high-lactate conditions ($p > 0.05$). Leucine concentrations were not significantly different between cell lines ($p > 0.05$), but were significantly different between the control and high-lactate conditions ($p \leq 0.05$). The amino acid flux rates are listed in Table 5.1, while the amino acid concentrations for the 24-h and 48-h samples are listed in Appendix B.

Lactate tracer uptake rate

To calculate the lactate tracer flux for the high-lactate condition, the amount of the M3 lactate isotope – corresponding to the [U-^{13}C] lactate tracer – that was taken up by the cells from the extracellular media was determined from the change in the M3 lactate isotope concentration (after it was corrected for natural isotope abundance) from 24-h to 48-h. Specifically, the lactate flux was assumed to be double this change, since only 50% of the initial extracellular lactate was labeled. It is possible that some of the M3 lactate was secreted into the extracellular media unaltered; however, it was assumed that this

was balanced by the M1/M2 lactate species secreted into the extracellular media. Table 5.1 lists the calculated lactate tracer uptake fluxes for the three cell lines.

To further understand the impact of the high extracellular lactate concentrations on metabolism, the distribution of labeled intracellular metabolites in central metabolism was examined. These MID values were obtained for intracellular metabolites cultured in the high-lactate condition where 50% of the extracellular lactate was [U-^{13}C] lactate. The intracellular metabolites that were labeled included pyruvate, lactate, alanine, citrate, AKG, glutamate, succinate, proline, aspartate, and malate. Though only intracellular metabolites were measured in this study, the labeling is in agreement with a previous labeling study where MCF-7 and MDA-MB-231 cells were incubated in a glucose-free media with 10 mM 3-^{13}C-lactate. In that glucose-free study, labeled alanine and glutamate were observed, which could only have been generated if alanine and glutamate were labeled intracellularly. In contrast, the labeling of the TCA metabolites and other amino acids had significantly lower labeling, with an average carbon labeling of only ~1%.

One notable characteristic of the intracellular labeling due to the lactate tracer, was the high fraction of M1 species relative to M2 species for both the intracellular pyruvate, alanine, and lactate, as well as TCA metabolites. Since the lactate tracer was [U-^{13}C] labeled, one might expect to observe mostly M3, then M2, followed by M1, if lactate were the sole carbon source and no lactate were being produced from the metabolism of glucose and glutamine. In a case where lactate was the sole carbon source

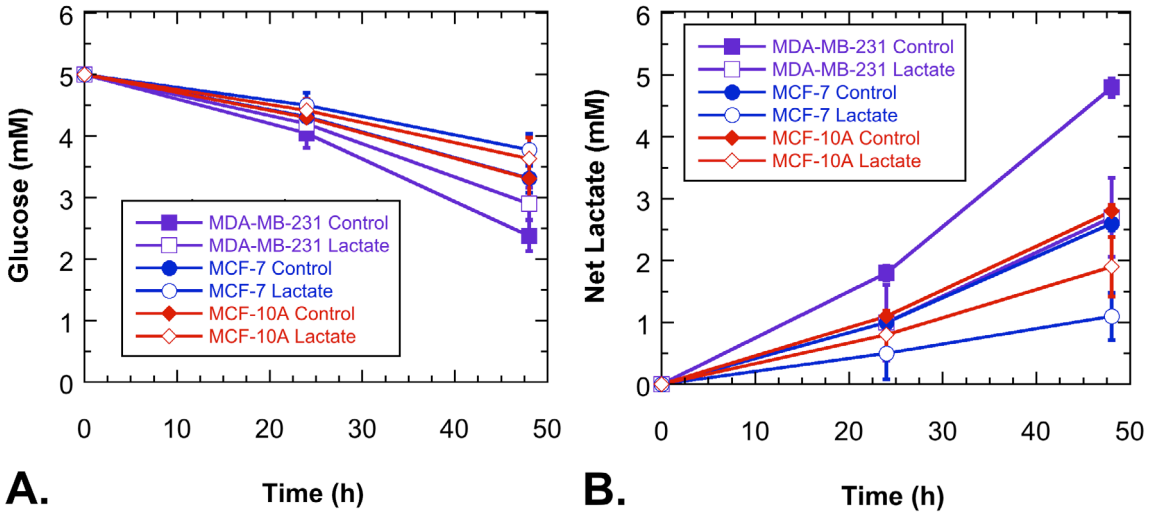

Figure 5.3 Glucose and lactate profiles for the three breast cancer cell lines. A) The left graph shows the glucose concentrations over time for the three breast cancer cell lines, while B) The right graph shows the net lactate concentrations over time adjusting for the initial extracellular lactate in the high-lactate cultures. MCF-10A is represented in red, MCF-7 in blue, and MDA-MB-231 in purple. The control cultures are represented by solid markers, while the high-lactate cultures are represented by hollow markers. All error bars represent 95% confidence intervals.

‘

Table 5.1. Glucose, lactate, and amino acid fluxes for the three breast cancer cell lines for the control and high-lactate conditions. Fluxes are given in nmol /10^6 cells/h, and correspond to the measured flux between the 24-h and 48-h time points.

Flux (nmol/10^6 cells/h)						
	MCF10-A		MCF-7		MDA-MB-231	
Metabolite	**Control**	**High-Lactate**	**Control**	**High-Lactate**	**Control**	**High-Lactate**
Glucose	-222	-181	-210	-159	-337	-268
Lactate	379	252	318	132	606	344
Alanine	10.6	10.7	13.7	11.7	10.2	8.2
Aspartate	4.9	3.7	6.6	5.4	3.5	4.5
Glutamate	12.1	10.2	11.5	11.6	8.6	10.4
Glutamine	-48	-55	-53	-64	-44	-55
Glycine	6.2	5.7	9.7	9.4	7.8	7
Isoleucine	-8.3	-8.4	-9.5	-9.2	-4.7	-8.4
Leucine	-6.7	-7.5	-8.3	-7.4	-4.7	-8.8
Methionine	-2.6	-1.5	-3.1	-2.2	-1.4	-2.2
Phenylalanine	-4.7	-4.5	-3.8	-3.8	-3.4	-4
Proline	1.5	1.3	2.8	2.3	0.83	1.3
Serine	-18.7	-20.3	-19.7	-22.5	-15.8	-19.8
Threonine	-1.9	-1.9	-1.2	-1.2	-1.2	-1.6
Tyrosine	-3.6	-3.7	-4	-3.8	-3.5	-3.8
Valine	-5.8	-6.3	-9.5	-10.4	-6.4	-9.1

and continuously consumed, labeled lactate would enter the cell and label pyruvate as M3 and the TCA metabolites as M2 after one turn of the TCA cycle, as shown in Figure 5.4A. If M3 lactate continued to enter the mitochondria as the primary source of acetyl-CoA, then the TCA metabolites would stay enriched with ^{13}C. However, since the labeled lactate flux into the cell and to pyruvate was relatively low compared to the unlabeled glucose flux to pyruvate, the majority of the pyruvate becoming acetyl-CoA in the mitochondria would be M0 labeled, as seen in Figure 5.4B. Therefore, when the M2-labeled oxaloacetate from the first TCA cycle run, indicated by the blue box in Figure 5.4A and 5.4B, goes through the TCA cycle again, the majority of the time it combine with an M0 acetyl-CoA, and will produce the M1-labeled the TCA metabolites from the lactate tracer, as was seen in this study.

The MID data from the high-lactate conditions demonstrated that the labeled lactate was consumed by the cells. Also, the presence of high extracellular lactate alters intracellular metabolism for all three breast cancer cell lines. Specifically, the high extracellular lactate concentration decreased glucose consumptions rates and decreased lipid production rates.

Intracellular labeling from [1,2-^{13}C] glucose

A [1,2-^{13}C] glucose isotope was used for this study because previous studies have shown it to be an optimal tracer for the glycolytic pathway for mammalian cells (Metallo et al., 2009). The composition of the tracer in the extracellular medium was 95% molar

enrichment, and 24-h has been shown to be sufficient to achieve isotopic steady-state for intermediate metabolites in the glycolytic pathway for CHO cells, another mammalian cell line with a similar growth rate (Ahn and Antoniewicz, 2013). The complete glucose-derived MID measurements for all cell lines and conditions can be found in Appendix C. All of the MID data was corrected for natural isotope abundances.

The average carbon labeling for PEP, 3PG, DHAP, pyruvate, alanine, and lactate was at least 20% for all three cell lines, and the labeling concentrations did not drastically change between the three cell lines, nor between the control and high-lactate conditions. This reflects the consistently high flux through glycolysis for each of the three cell lines, and makes sense considering that all three cell lines grew at an exponential rate for both the control and high-lactate conditions.

Intracellular labeling from [U-^{13}C] glutamine

The [U-^{13}C] glutamine isotope was used for this study because previous studies have shown it to be an optimal tracer for the TCA cycle pathway for mammalian cells (Metallo et al., 2009). The composition of the tracer in the extracellular medium was 95% molar enrichment, and the 24-h to be sufficient to nearly achieve isotopic steady-state for

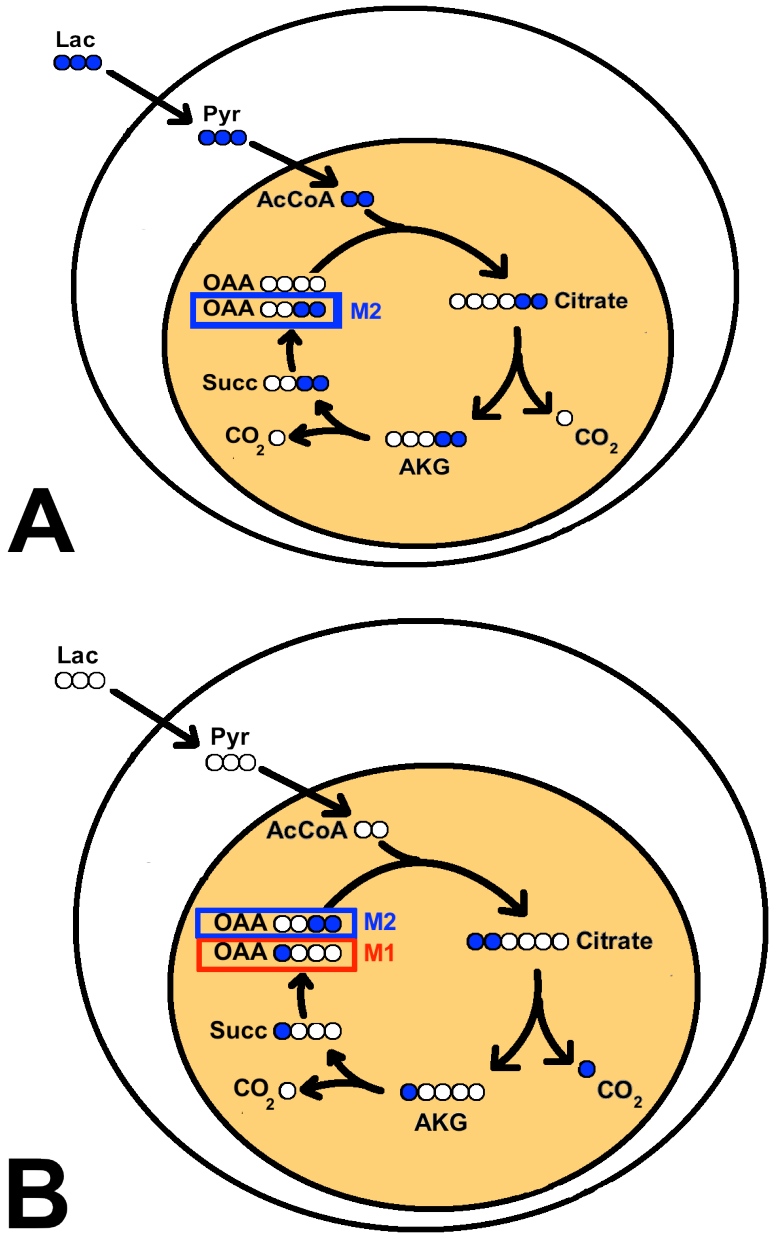

Figure 5.4 Generation of M1-labeled TCA metabolites from extracellular U-^{13}C lactate. A) Initial labeled lactate produces M2 TCA metabolites. B) M1 labeled metabolites will form on the second run, where the M2 oxaloacetate (OAA) will most likely encounter an M0 acetyl-CoA. For clarity, some reaction pathways were condensed.

intermediate metabolites in the TCA cycle for CHO cells (Ahn and Antoniewicz 2013). The complete glutamine-derived MID measurements for all cell lines and conditions can be found in Appendix C. All of the MID data was corrected for natural isotope abundances.

In all cell lines and conditions, glutamine, AKG, and glutamate were heavily enriched from the glutamine tracer. Pyruvate and lactate were minimally enriched from the glutamine isotope for all cell lines and conditions. In MCF-10A and MDA-MB-231, the high-lactate condition led to a higher average carbon labeling in pyruvate and lactate as compared to the control condition. In MCF-7, the trend seen in MCF-10A and MDA-MB-231 was reversed: decreased labeling in pyruvate and lactate was observed under the high-lactate condition compared to the control condition. The increased labeling of pyruvate and lactate from glutamine in MCF-10A and MDA-MB-231 under the high-lactate condition suggests that glutamine anaplerosis was enhanced to provide energy via oxidative phosphorylation, and then secreted as alanine and lactate, in response to decreased glucose consumption and decreased energy generation via glycolysis. While glucose consumption (and hence energy generation via glycolysis) decreased in MCF-7 cells under the high-lactate condition, the decreased labeling in pyruvate and lactate from glutamine suggests the glutamine-derived intermediates continued through the TCA cycle rather than being secreted as alanine and lactate.

The TCA metabolites succinate, malate, and citrate also showed significant labeling from the glutamine tracer. Succinate and malate had similar average carbon labeling in all three cell lines for both conditions, whereas citrate labeling was relatively

similar between the different cell lines, but had some notable differences between the control and high-lactate conditions. In response to the high-lactate conditions, all three breast cancer cell lines showed a much greater proportion of M5 citrate compared to the control condition, as can be seen in Figure 5.5. Increased M5 citrate was likely due to the TCA cycle running in "reverse" through the reductive carboxylation pathway, as seen in Figure 5.6. If correct, this labeling trend would be reflected – and it was - in the three cell lines having higher exchange fluxes from AKG to citrate for the high-lactate condition compared to the control. These results suggest that cancer cells continue to replenish TCA intermediates through glutamine anaplerosis, and use glutamine for citrate synthesis and fatty acid production via reductive carboxylation. Mammalian cells, including several cancer cell lines, have been observed to increase reductive carboxylation of glutamine under hypoxia (Metallo et al., 2012; Wise et al., 2011), but this is the first time it has been observed in response to high-lactate levels.

Metabolic flux analysis

To quantify the metabolic activity, Metran was used to simulate the metabolite flux rates, MIDs from parallel glucose and glutamine tracer labeling, and compare them to the measured results for the model. A flux map was generated for each cell line for each condition (Leighty and Antoniewicz, 2012; Ahn and Antoniewicz, 2013). Flux maps for all cell lines and conditions are shown in Figures 5.6-5.11, and listed in Appendix D.

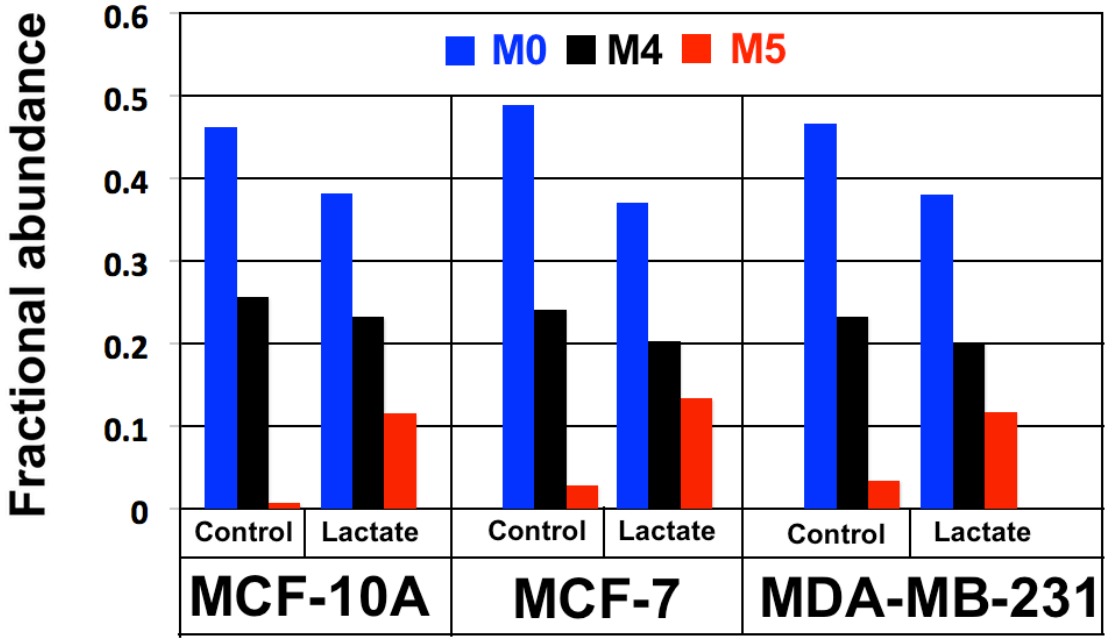

Figure 5.5 MID labeling of citrate from [U-^{13}C] glutamine. The fractional abundance of the M0, M4, and M5 labeled forms of citrate for MCF-10A, MCF-7, and MDA-MB-231 cultures for both control and high-lactate conditions.

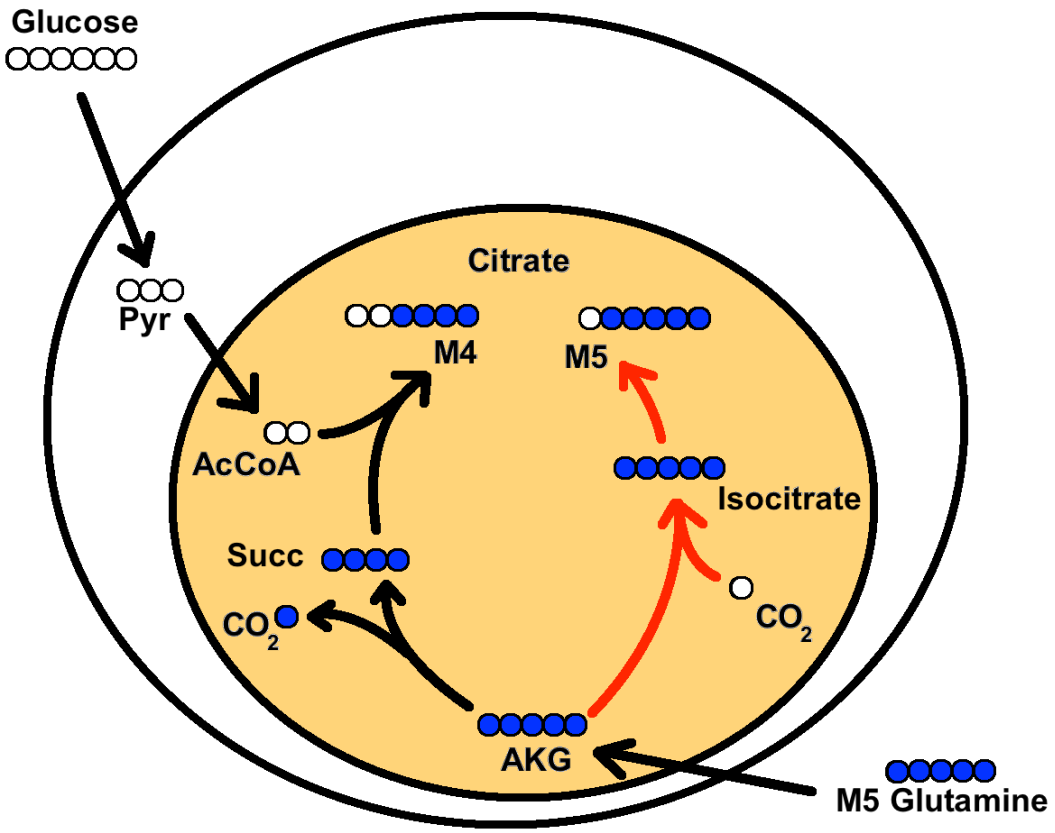

Figure 5.6 Reductive carboxylation of AKG to citrate. When AKG is oxidized through the normal TCA pathway shown by the black arrows, the resulting citrate will be M4. When AKG is carboxylated to isocitrate, the resulting citrate will be M5. For clarity, some reaction pathways were condensed.

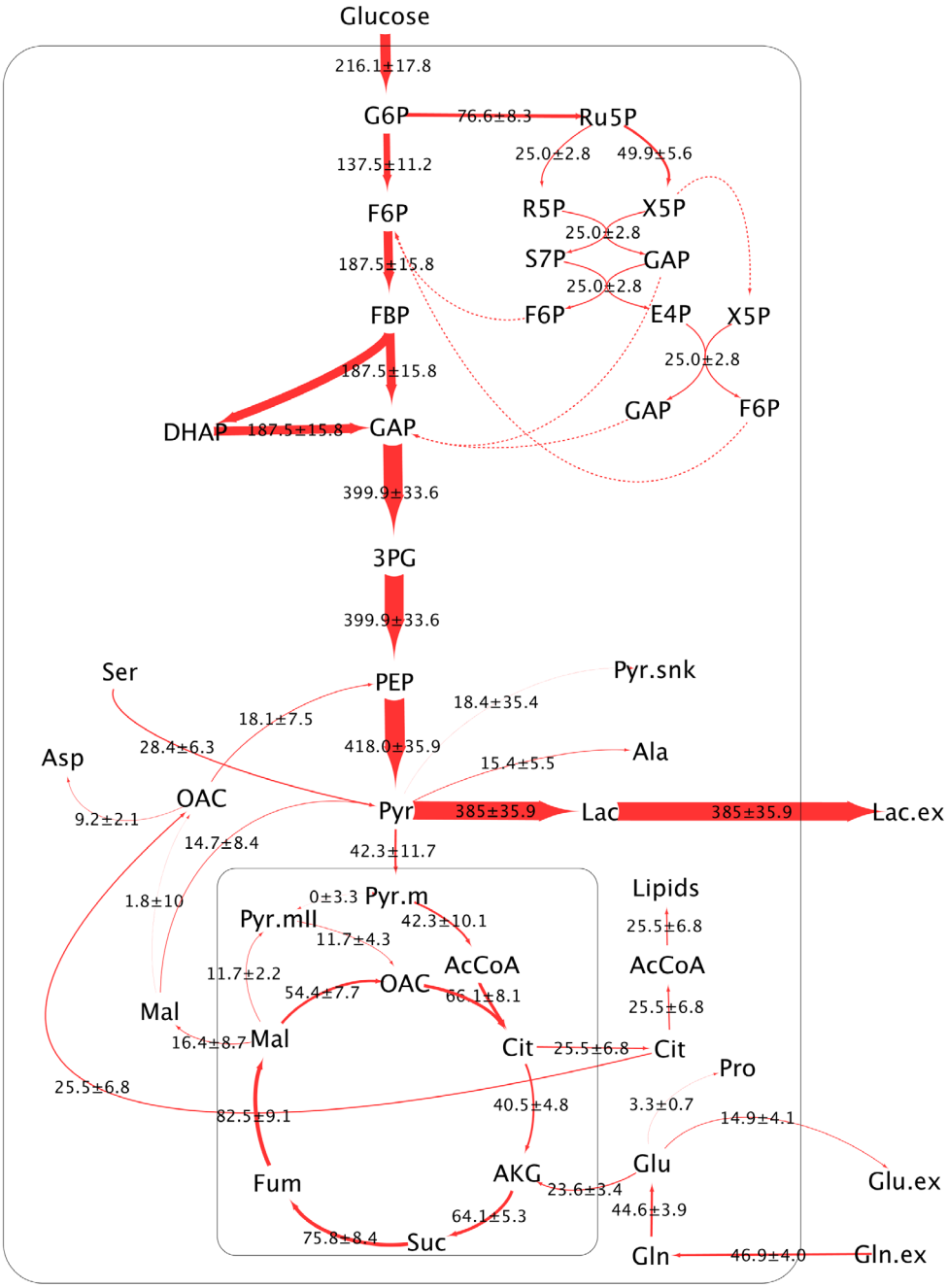

Figure 5.7A Metabolic flux map for MCF-10A cells for the control condition. Line thicknesses reflect relative flux values, which are in nmol/10^6 cells/h.

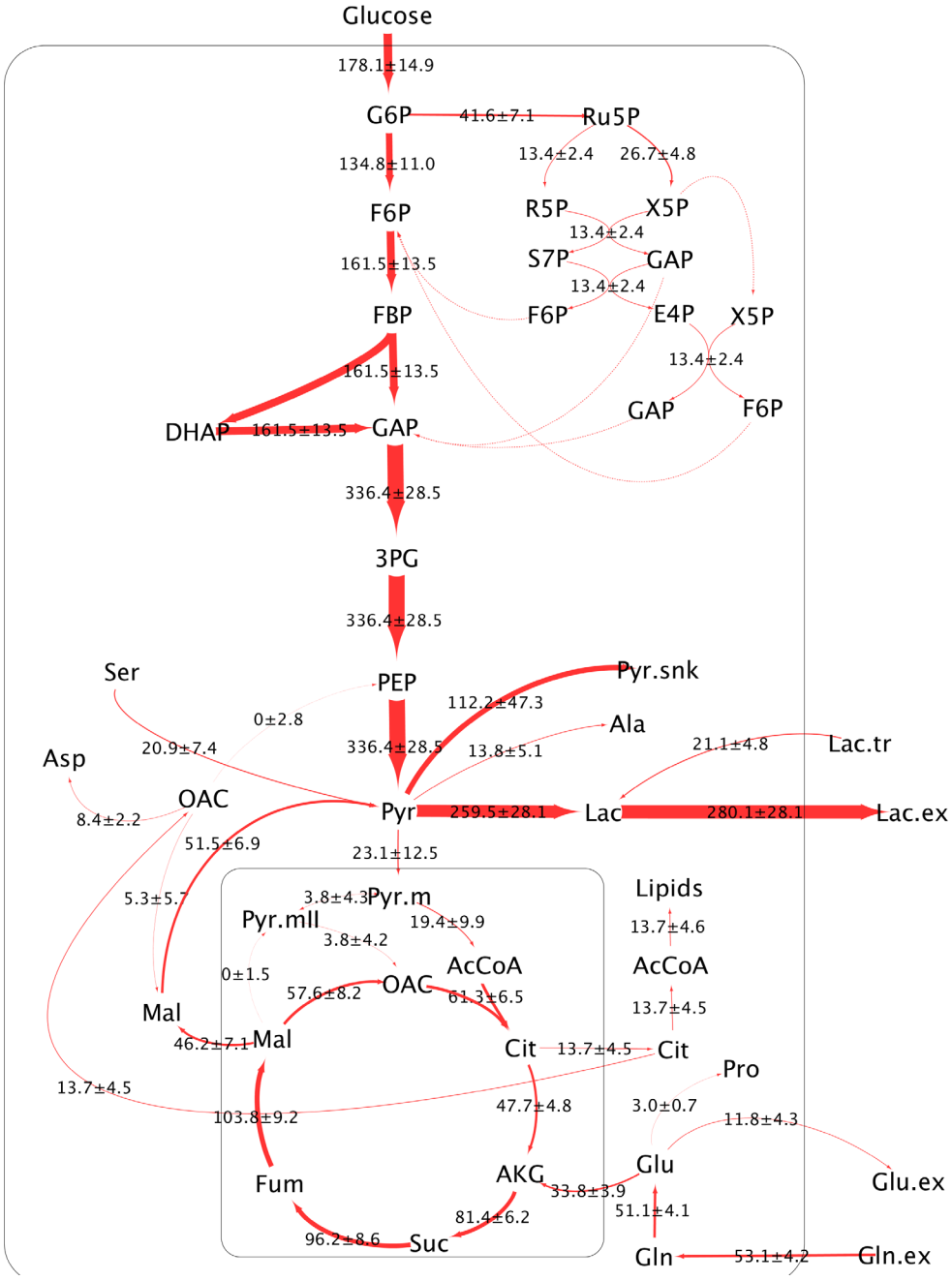

Figure 5.7B Metabolic flux map for MCF-10A cells for the high-lactate condition.

Line thicknesses reflect relative flux values, which are in nmol/10^6 cells/h.

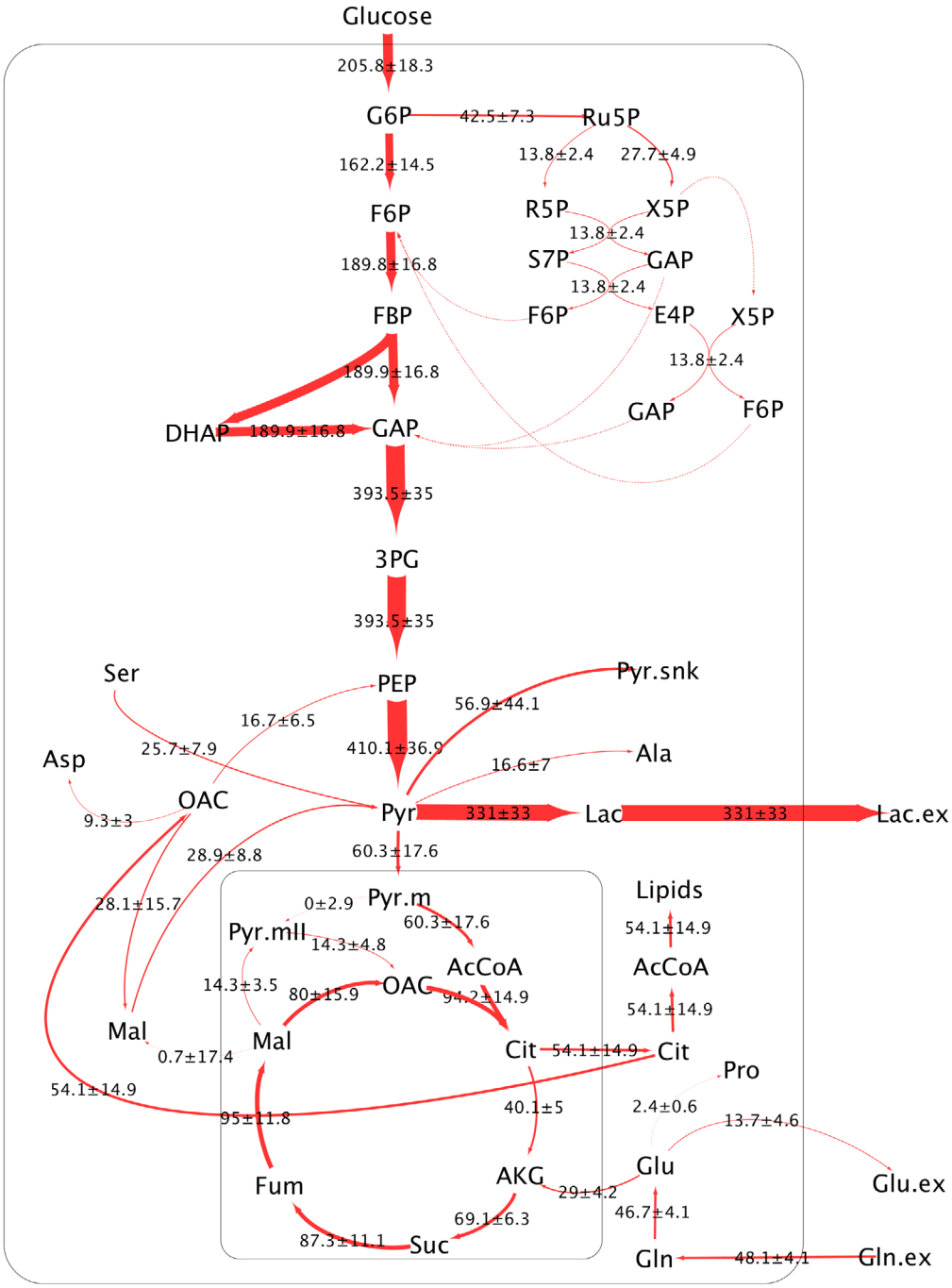

Figure 5.7C Metabolic flux map for MCF-7 cells for the control condition. Line thicknesses reflect relative flux values, which are in nmol/10^6 cells/h.

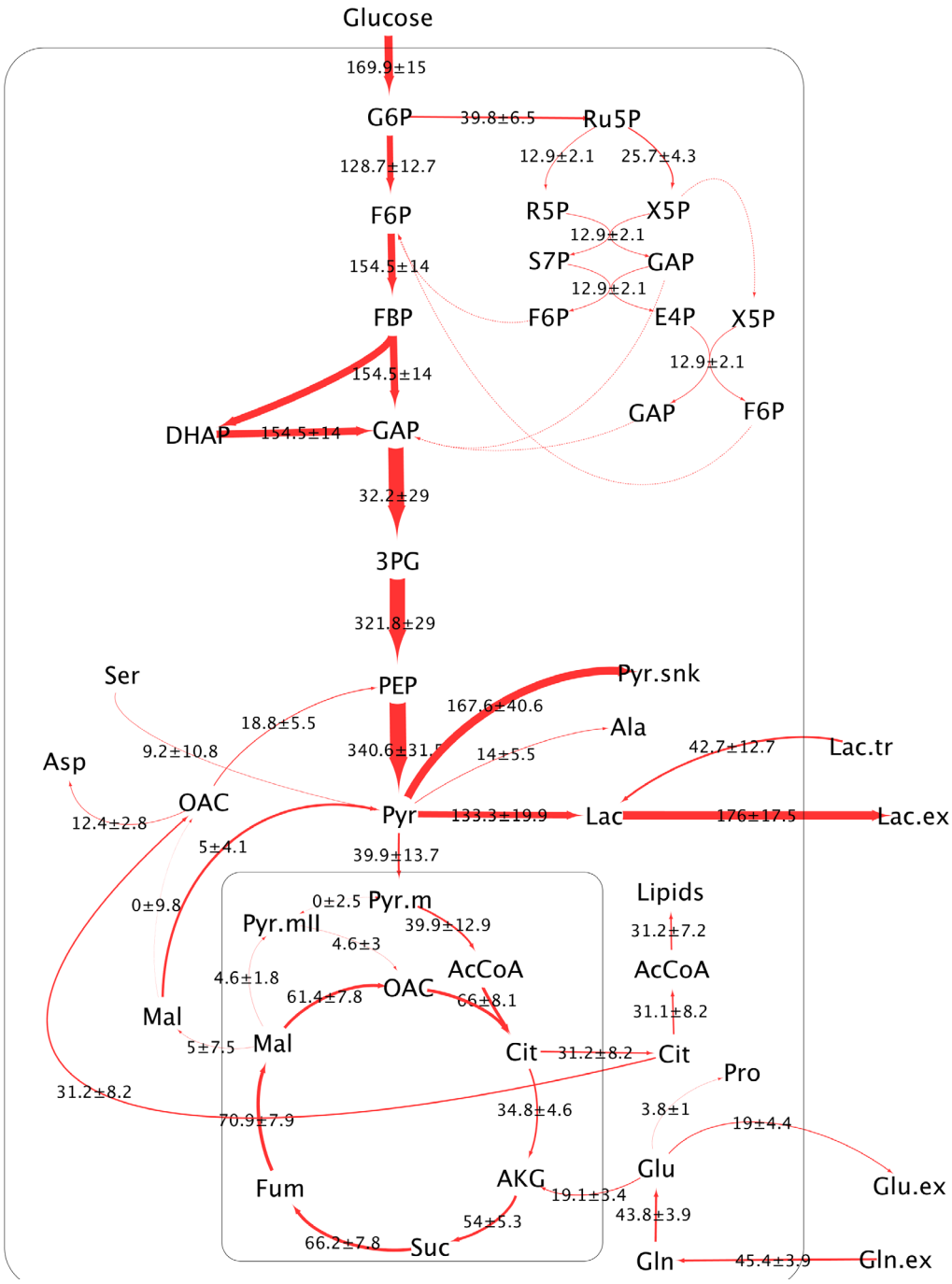

Figure 5.7D Metabolic flux map for MCF-7 cells for the high-lactate condition. Line thicknesses reflect relative flux values, which are in nmol/10^6 cells/h.

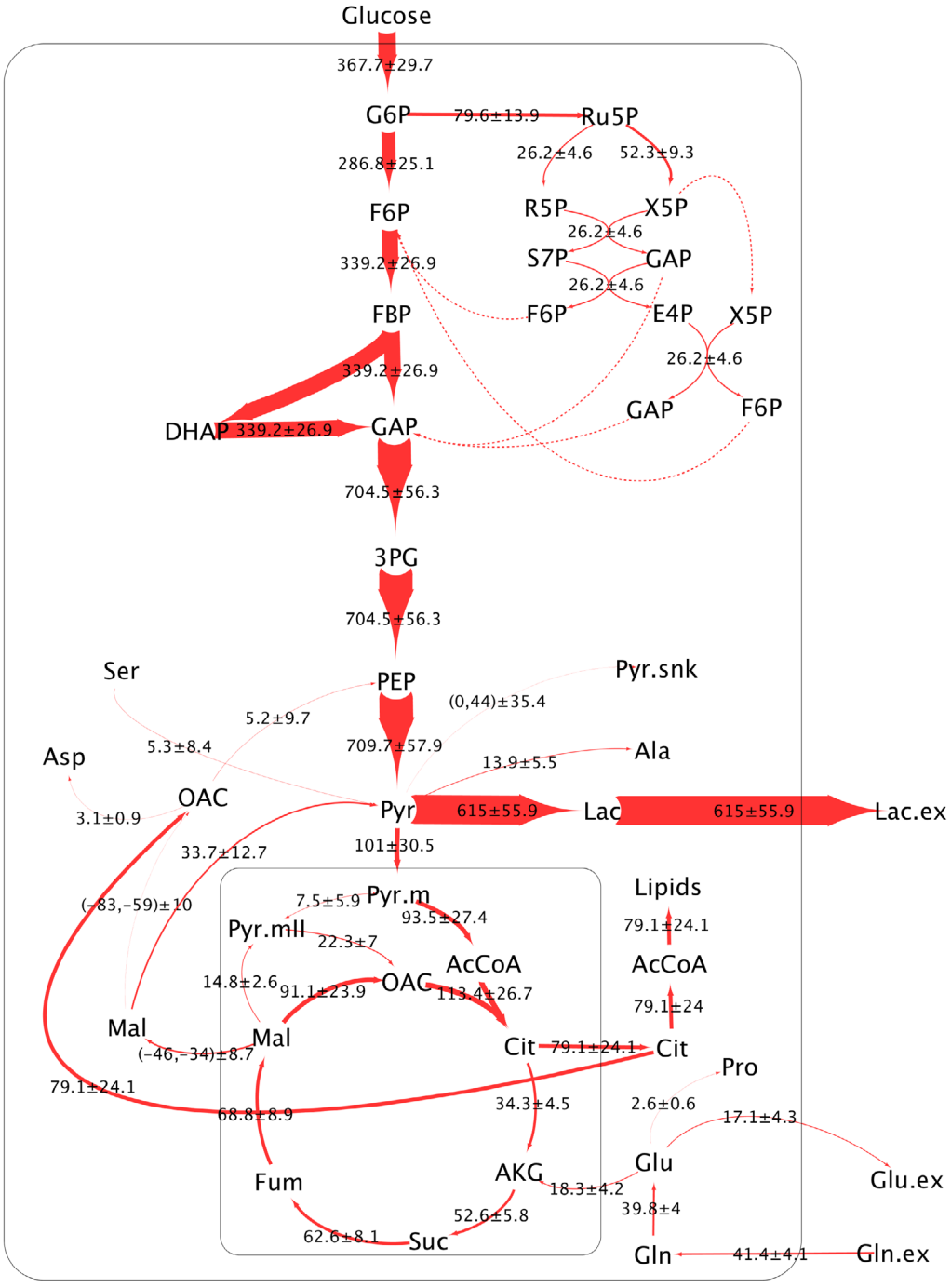

Figure 5.7E Metabolic flux map for MDA-MB-231 cells for the control condition.

Line thicknesses reflect relative flux values, which are in nmol/10^6 cells/h.

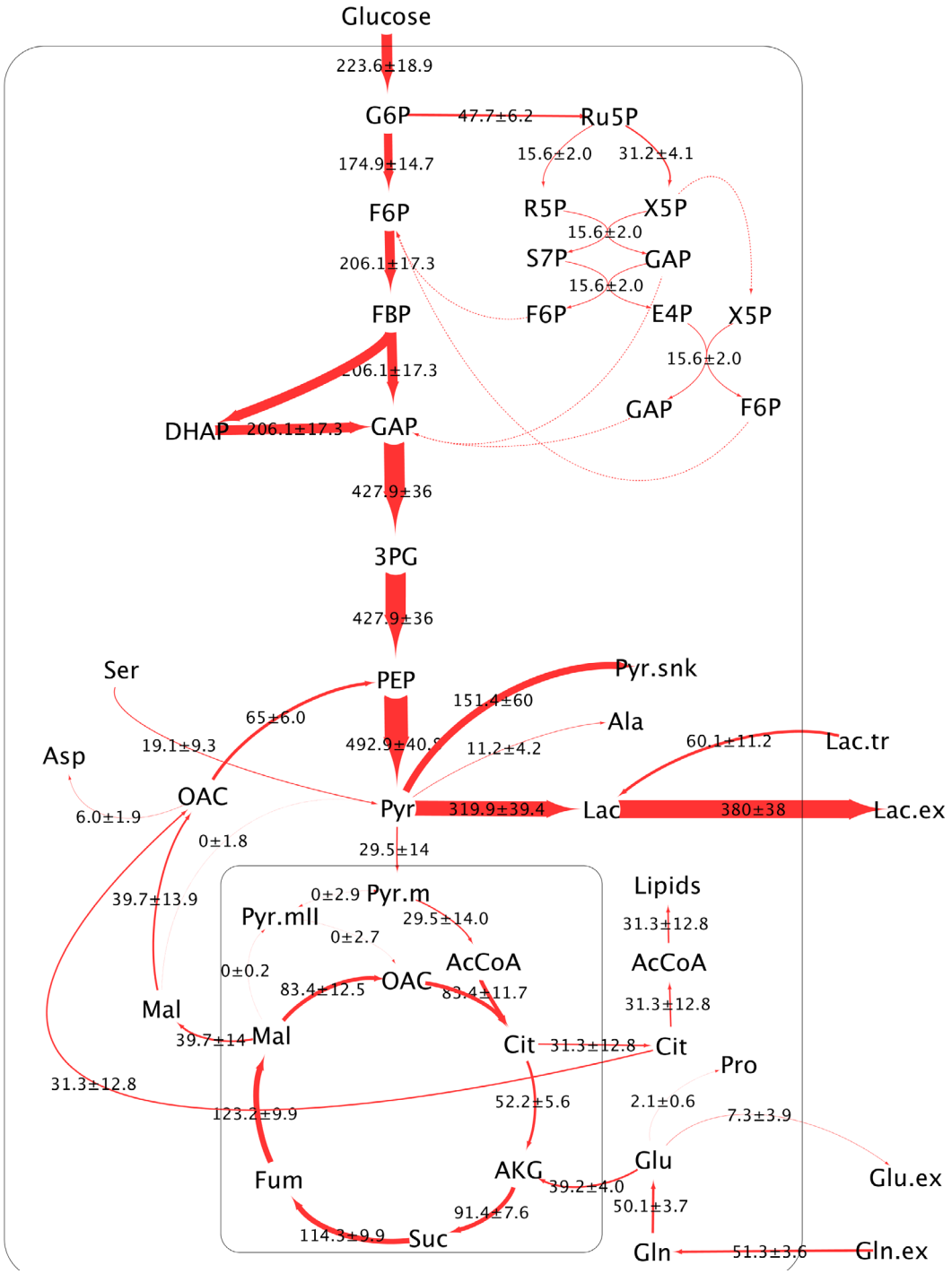

Figure 5.7F Metabolic flux map for MDA-MB-231 cells for the high-lactate condition. Line thicknesses reflect relative flux values, which are in nmol/10^6 cells/h.

For all three cell lines, the reactions in glycolysis had the highest fluxes in both the control and high-lactate conditions. Compared to the control condition, all three cell lines were characterized by decreased glucose consumption and decreased lactate production when cultured in the high-lactate conditions. This agrees with previous studies that showed lactate accumulation correlated with reduced entry of pyruvate into the TCA cycle in leukemia cells (Samudio, et al., 2009). In the mitochondria, the high-lactate condition resulted in decreased fluxes of acetyl-CoA into citrate for all three cell lines; however, production of citrate from AKG via reductive carboxylation (characterized by the exchange flux between AKG and citrate) increased for all three cell lines for the high-lactate condition and likely compensated for the lack of citrate produced from acetyl-CoA. This is consistent with the increased M5 citrate labeling for all three cell lines for the high-lactate condition shown in Figure 5.5, and in accordance with the behavior of several other cancer cell lines when exposed to hypoxia, suggesting a possible link between hypoxia and not only lactate accumulation but also consumption. The flux of citrate from the mitochondria to the cytosol – and subsequent conversion into acetyl-CoA for fatty acid synthesis – decreased for all three cell lines for the high-lactate condition compared the control condition. This is surprising, considering that the decreased flux of glucose into the mitochondria should make cells more dependent on glutamine-derived citrate for fatty acid synthesis. Previous studies demonstrated that MDA-MB-231 cells have a higher lipid content than MCF-7, which have a higher lipid content than MCF-10A (Abramczyk et al., 2015). These lipid biomass content values were obtained form

Raman spectra and staining. Without this data, the model would have assumed one lipid content for all three cell lines; however, the lipid concentrations were not precise enough to allow high confidence in the fatty acid lipid biomass fluxes.

Lactate's effects on cancer cell metabolism and behavior

In this study, the metabolic responses of three breast cancer cell lines, MCF-10A, MCF-7, and MDA-MB-231, to high lactate were examined using ^{13}C-MFA. MCF-10A represents normal, precancerous breast cells, MCF-7 represents early-stage breast cancer, and MDA-MB-231 represents a malignant and metastatic advanced breast cancer. Three isotope tracers were used to aid resolution of central carbon metabolism and the resulting fluxes and MID data sets were paired with a mammalian metabolic network model to develop intracellular metabolic activity maps for each cell line under the control condition, as well as the high-lactate condition. The three breast cancer cell lines cultured in high-lactate conditions continued to grow exponentially at equivalent rates ($p > 0.05$), despite having lower glucose consumption rates ($p \leq 0.05$). While lactate was consumed by MCF-10A, MCF-7, and MDA-MB-231 when exposed to high concentrations of extracellular lactate, the lactate consumption might have even been reduced in these conditions compared to *in vivo* conditions, due to the presence of glucose. MCF-7 and MDA-MB-231 have been shown to utilize lactate as the main carbon source in the absence of glucose (Kennedy et al., 2013). Most notably, all three cell lines exhibited increased reductive carboxylation, as determined by increased M5 citrate labeling, which can only occur if glutamine is metabolized through the reverse TCA cycle. Increased

reductive carboxylation has previously been observed in several types of cancer cells in response to hypoxia (Metallo et al., 2012; Wise et al., 2011). These results indicate that there may be a link between hypoxia and lactate metabolism in tumor cells, even when oxygen is sufficient, since oxygen was sufficient in the present experiments. Interestingly, both hypoxia and elevated lactate correlate with resistance to treatments that rely on induction of oxidative stress because lactate consumption allows cells to utilize its antioxidant capacity to reduce oxidative stress and hypoxia limits formation of reactive oxygen species (Groussard et al., 2000; Keith et al., 2007, Kennedy and Dewhirst, 2010). Additionally, both exposure to elevated lactate, and hypoxia seem to promote the "cancer stem cell" (CSC) phenotype independently (Heddleston et al., 2009, Hill et al., 2009; Martinez-Outschoorn et al., 2011). Furthermore, upon injection of lactate into mice with MDA-MB-231 xenografts, metastasis increased ten-fold (Bonuccelli et al., 2010; Martinez-Outschoorn et al., 2011). Hypoxia has also been implicated in increasing the metastatic potential of cancer cells (Hill et al., 2009; Pani et al., 2010). All of these malignant behaviors – treatment resistance, stem cell gene signatures, and increased metastasis – are correlated with tumor recurrence and poor patient prognosis. All of these behaviors have also been shown to be promoted by both hypoxia and elevated lactate. While cancer cells have long been known to produce high levels of lactate, especially in hypoxic tumor regions, cancer cells can also consume and metabolize lactate as a substrate (Kennedy et. al, 2013; Pavlides et al., 2009; Sonveaux et al., 2008). The findings in this study highlight that elevated extracellular lactate conditions can shift cancer cell metabolism towards a state normally thought to be

characteristic of hypoxia, even in the presence of sufficient oxygen.

Metabolic flexibility appears to play an important role in enabling cancer to thrive and survive in our bodies, against the harsh environmental factors encountered, including inflammation, oxidative stress, and extreme nutrient and oxygen fluctuations (Dayem et al., 2010; Pavlides, et al., 2010; Reuter et al., 2010). As a result, the ability to metabolize lactate offers potential advantages to cancer cells. To gain a better understanding of lactate uptake and metabolism, one study inhibited the main lactate transporter, MCT1, in cervical cancer cells. This induced a switch from lactate-fueled respiration to glycolysis (Sonveaux et al., 2008). In the same study, blocking MCT1 in a mouse lung cancer model as well as a colorectal cancer xenotransplant slowed tumor growth by forcing the lactate-consuming cells to switch to glucose consumption. These cells were then more sensitive to radiation treatment (Sonveaux et al., 2008). Even if the cancer cells that consume lactate are not dependent on it – though it is believed to promote treatment resistance through antioxidant effects – inhibiting lactate consumption can have downstream effects on other tumor cells, and indeed compromise the tumor itself (Hirschhaeuser et al., 2011; Kennedy and Dewhirst, 2010).

The findings of this study suggest that breast cancer cells adapt to high lactate concentrations by increasing reductive carboxylation within the TCA cycle. Reductive carboxylation is also observed to increase under hypoxia. In addition, both elevated lactate and hypoxia have been linked to treatment resistance, metastasis, and the promotion of the cancer stem cell phenotype. This suggests a potential connection between these behaviors. Normally, oxygen is required for lactate to be used as the sole

carbon source by tumors via oxidative phosphorylation in the TCA cycle (Kennedy et al., 2013); however, lactate's effect on TCA cycle activity – namely, increased reductive carboxylation of glutamine - has thus far not been reported. If elevated lactate can indeed mediate malignant behavior in cancer cells via this metabolic pathway as well as serve as a substrate, approaches to prevent lactate-induced changes should be re-evaluated, especially when targeting cancer cells residing in hypoxic niches.

^{13}C-MFA should continue to play an important role in future studies aimed at precisely determining the effects of elevated lactate on cancer cell metabolism. In order to increase resolution of the MIDs, the extracellular lactate should be entirely isotopically labeled. Additionally, low glucose and low extracellular pH should be used to promote lactate uptake. These results demonstrated that lactate plays an important role in changing cancer cell metabolism, which might contribute to the increased metastasis, treatment resistance, and patient death rates observed to be associated with elevated lactate accumulation. Additionally, the surprising link to hypoxia should be further investigated.

Moving forward, there are several details that could be refined to `improve the results of this MFA study. First, the metabolic network model contained two additional pyruvate pools (pyr.snk and pyr.mII) to manage the multiple reactions at the pyruvate node as well as to account for reactions not explicitly defined in the network (Ahn and Antoniewicz, 2013). Due to the high flux of pyruvate into the sink under the high-lactate conditions, it may be necessary to constrain or remove this pool. The additional pyruvate mitochondrial pool (pyr.mII) was included to model potential pyruvate channeling (Ahn and Antoniewicz, 2013); however, this assumption may not be supported by the cancer

MID data. Additionally, the reversibility of several reactions, could be modified to allow acetyl-CoA to re-enter the mitochondria via citrate, to account for fatty acid oxidation. Second, the lipid composition used for the breast cancer cells was for cells cultured under glucose with limited precision and only included the lipid droplets, and not the total lipid content (Abramczyk et al., 2015). Furthermore, the effects of high extracellular lactate on the lipid content of breast cancer cells was not obtained. Therefore, accurate estimates for lipid biomass for each of the cell lines under each condition is needed to resolve the intracellular fluxes. Finally, the lactate tracer used was only 50% enriched, which significantly reduced the fractional abundance of the MIDs obtained for the high-lactate cultures. In the future, using a higher enrichment for the lactate tracer would increase the fractional abundances of the MIDs, such that the MID data could be used in the MFA simulations to estimate intracellular fluxes.

5.5 Conclusion

While cancer cells have long been known to exhibit excessive glycolytic behavior resulting in the production of high levels of lactate, the role of lactate after its initial secretion has only recently come to be appreciated and has focused mainly on gene expression, metastatic potential, and correlations regarding treatment outcome and patient prognosis. In this study, the effect of high concentrations of extracellular lactate on the intracellular metabolic activity of three breast cancer cell lines was examined for the first time. Under high-lactate conditions, all three cell lines reduced glucose consumption and decreased lactate consumption. Additionally, the high-lactate condition resulted in lactate consumption and incorporation into intracellular metabolites in all three cell lines, as well as stimulation of the reverse TCA cycle via reductive carboxylation, activity that has been associated with hypoxia and correlates with several malignant behaviors. There remains much more to learn concerning lactate's role in cancer – both metabolic and otherwise – but MFA should serve as a valuable tool to decipher lactate's role in cancer metabolism, and along with inquiries from other angles, may allow us to further unravel the complex web of factors that make cancer so difficult to treat.

5.6 Acknowledgements

This research was supported by the South Carolina COBRE Center of Biomaterials for Tissue Regeneration NIH Grant# P20RR021949. Additionally, we would like to thank Dr. David Bruce and Dr. Bethany Carter of Clemson's Chemical Engineering Department for assistance with GC-MS analysis, and Mr. Scheen Thurmond of Clemson's Bioengineering Department for assistance with YSI analysis.

5.7 References

Abramczyk H, Surmacki J, Kopec M, Olejnik AK, Lubecka-Pietruszewska K, Fabianowska-Majewska K. The role of lipid droplets and adipocytes in cancer. Raman imaging of cell cultures: MCF10A, MCF7, and MDA-MB-231 compared to adipocytes in cancerous human tissue. Analyst. 2015; 140:2224–2235.

Ahn WS, Antoniewicz MR. Metabolic flux analysis of CHO cells at growth and non-growth phases using isotopic tracers and mass spectrometry. Metab Eng. 2011; 13: 598-609.

Ahn WS, Antoniewicz MR. Parallel labeling experiments with [1,2-^{13}C] glucose and [U-^{13}C] glutamine provide new insights into CHO cell metabolism. Metab Eng. 2013; 15: 34-47.

Antoniewicz MR, Kelleher JK, Stephanopoulos G. Determination of confidence intervals of metabolic fluxes estimated from stable isotope measurements. Metab Eng. 2006; 8:324-327.

Antoniewicz MR, Kelleher JK, Stephanopoulos G. Accurate assessment of amino acid mass isotopomer distributions for metabolic flux analysis. Anal Chem. 2007a; 79:7554-7559.

Antoniewicz MR, Kelleher JK, Stephanopoulos G. Elementary metabolite units (EMU): a novel framework for modeling isotopic distributions. Metab Eng. 2007b; 9:68-86.

Balliet RM, Capparelli C, Guido C, et al. Mitochondrial oxidative stress in cancer-associated fibroblasts drives lactate production, promoting breast cancer tumor growth: understanding the aging and cancer connection. Cell Cycle. 2011;10:4065-4073.

Bonarius HPJ, Hazimanikatis V, Meesters KPH, de Gooijer CD, Schmid G, Tramper J. Metabolic flux analysis of hybridoma cells in different culture media using mass balances. Biotech Bioeng. 1996; 50:299-318.

Bonuccelli G, Tsirigos A, Whitaker-Menezes D, et al. Ketones and lactate "fuel" tumor growth and metastasis: Evidence that epithelial cancer cells use oxidative mitochondrial metabolism. Cell Cycle. 2010;9:3506-3514.

Dayem AA, Choi H, Kim J, Cho S. Role of oxidative stress in stem, cancer, and cancer stem cells. Cancers. 2010;2(2):859-884.

Fernandez CA, Des Rosiers C, Previs SF, David F, Brunegraber H. Correction of 13C mass isotopomer distribution for natural isotopomer distributions for natural isotope abundance. J Mass Spectrom. 1996; 31:255-262.

Gaglio D, Metallo CM, Gameiro PA, et al. Oncogenic K-Ras decouples glucose and glutamine metabolism to support cancer cell growth. Molec Syst Biol. 2011;7:523.

Groussard C, Morel I, Chevanne M, Monnier M, Cillard J, Delamarche A. Free radical scavenging and antioxidant effects of lactate ion: an in vitro study. J App Phys. 2000;89:169-175.

Guido C, Whitaker-Menezes D, Capparelli C, et al. Metabolic reprogramming of cancer-associated fibroblasts by TGF-β drives tumor growth: Connecting TGF-β signaling with "Warburg-like" cancer metabolism and L-lactate production. Cell Cycle. 2012;11:3019 3035.

Heddleston JM, Li Z, McLendon RE, Hjelmeland AB, Rich JN. The hypoxic microenvironment maintains glioblastoma stem cells and promotes reprogramming towards a cancer stem cell phenotype. Cell Cycle. 2009;8:3274-3284.

Hill RP, Marie-Egyptienne DT, Hedley DW. Cancer stem cells, hypoxia and metastasis. Semin Radiat Oncol. 2009;19:106-111.

Hiller K, Metallo CM. Profiling metabolic networks to study cancer metabolism. Current opinion in Biotechnology. 2013;24:60-68.

Keith B, Simon MC. Hypoxia-inducible factors, stem cells, and cancer. Cell. 2007;129:465 472.

Kennedy KM, Dewhirst MW. Tumor metabolism of lactate: the influence and therapeutic potential for MCT and CD147 regulation. Future Oncology. 2010;6:127-148.

Kennedy MK, Scarbrough PM, Ribeiro A, Richardson R, Yuan H, Sonveaux P, Landon C, Chi JT, Pizzo S, Schroeder T, Dewhirst MW. Catabolism of exogenous lactate reveals it as a legitimate metabolic substrate in breast cancer. PloS ONE. 2013; 8: e75154.

Leighty RW, Antoniewicz MR. Parallel labeling experiments with [U-^{13}C] glucose validate *E. coli* metabolic network model for ^{13}C metabolic flux analysis. Metab Eng. 2012; 14:533-541.

Lu D, Mulder H, Zhao P, Burgess SC, Jensen MV, Kamzolova S, Newgard CB, Sherry AD. 13C NMR isotopomer analysis reveals a connection betwene pyruvate cycling and glucose-stimualted insulin secretion (GSIS). PNAS. 2002; 99:2708-2713.

Martinez-Outschoorn UE, Prisco M, Ertel A, et al. Ketones and lactate increase cancer cell “stemness”, driving recurrence, metastasis and poor clinical outcome in breast cancer: Achieving personalized medicine via metabolo-genomics. Cell Cycle.

2011;10:1271.

Meadows AL, Kong B, Berdichevsky M, Roy S, Rosiva R, Blanch HW, Clark DS. Metabolic and morphological differences between rapidly proliferating cancerous and normal breast epithelial cells. Biotechnol Prog. 2008; 24:334-341.

Metallo CM, Walther JL, Stephanopoulos G. Evaluation of ^{13}C isotopic tracers for metabolic flux analysis in mammalian cells. J Biotechnol. 2009; 144:167-174.

Pani G, Galeotti T, Chiarugi P. Metastasis: cancer cell's escape from oxidative stress. Cancer Metastasis Rev. 2010;29:351-378.

Pavlides S, Whitaker-Menezes D, Castello-Cros R, et al. The reverse Warburg effect: aerobic glycolysis in cancer associated fibroblasts and the tumor stroma. Cell Cycle. 2009;8:3984-4001.

Pavlides S, Tsirigos A, Vera I, et al. Loss of stromal caveolin-1 leads to oxidative stress, mimics hypoxia and drives inflammation in the tumor microenvironment, conferring the "reverse Warburg effect": A transcriptional informatics analysis with validation. Cell Cycle. 2010;9(11):2201-2219.

Quek LE, Wittmann C, Nielsen LK, Krömer JO. OpenFLUX: efficient modelling

software for 13C-based metabolic flux analysis. Microbial Cell Factories. 2009; 8:25.

Reuter S, Gupta SC, Chaturvedi MM, Aggarwal BB. Oxidative stress, inflammation, and cancer: how are they linked? Free Radical Biology and Medicine. 2010;49(11):1603-1616.

Samudio I, Fiegl M, Andreeff M. Mitochondrial uncoupling and the Warburg effect: molecular basis for the reprogramming of cancer cell metabolism. Cancer Res. 2009;69:2163-2166.

Sonveaux P, Végran F, Schroeder T, et al. Targeting lactate-fueled respiration selectively kills hypoxic tumor cells in mice. J Clin Invest. 2008;118(12):3930.

Talari ACS, Evans CA, Holen I, Coleman RE, Ur Rehman I. Raman spectroscopic analysis differentiates between breast cancer cell lines. J Raman Spectrosc. 2015; 46:421-427

Weitzel M, Nöh K, Dalman T, Niedenführ S, Stute B, Wiechert W. 13CFLUX2—high-performance software suite for ^{13}C-metabolic flux analysis. Bioinformatics. 2013;29:143-145

Wise DR, Ward PS, Shay JES, Cross JR, Gruber JJ, Sachdeva UM, Platt JM, DeMatteo RG, Simon MC, Thompson CB. Hypoxia pormotes isocitrate dehydrogenase-dependent carboxylation of α-ketoglutarate to citrate to support cell growth and viability.

Yoo H, Antoniewicz MR, Stephanopoulos G, Kelleher JK. Quantifying reductive carboxylation flux of glutamine to lipid in a brown adipocyte cell line. J Biol Chem. 2008; 283:20621-20627.

Young JD, Walther JL, Antoniewicz MR, Yoo H, Stephanopoulos G. An elementary metabolite unit (EMU) based method of isotopically nonstationary flux analysis. Biotechnol Bioeng. 2008; 99:686-699.

Zamboni N, Fendt S, Rühl M, Sauer U. 13C-based metabolic flux analysis. Nature protocols. 2009;4(6):878-892.

Zancan P, Sola-Penna M, Furtado CM, Da Silva D. Molecular Genetics and Metabolism. 2010; 100: 372-378.

CHAPTER 6: FUTURE WORK

The research contained within this dissertation employed several complementary tools to elucidate the inner workings of cells – from the expression of genes, to the display of surface phenotype markers, to the intracellular fluxes in metabolic pathways. The importance of examining cellular behavior from many independent angles cannot be understated. With respect to the metabolism of breast cancer cells, MFA was used to estimate the activity of internal metabolic pathways in response to high-lactate. While metabolite levels and intracellular labeling patterns provide information regarding the inputs, outputs, and direction of the substrates in central metabolism, examining the cellular responses using orthogonal methods would improve the results, as well as suggest possible refinements to the MFA framework, that could be used to inform and improve future studies. For instance, using DNA microarrays to examine the expression of genes that code for the enzymes involved in central carbon metabolism could provide insight with regards to control in the MFA studies. Specifically, are the genes that encode isocitrate dehydrogenase and aconitase – the enzymes that enable the reductive carboxylation of α-ketoglutarate into citrate – upregulated by elevated lactate? If not, the increased flux would be controlled at the substrate level. Histological staining could be used to visualize the lipid content or highlight the activity of the mitochondria under elevated lactate, thus confirming or rejecting the model simulation of lower lipid levels of mitochondrial pathway activity, respectively.

Furthermore, future work to decipher the specific roles that lactate plays in the progression of cancer should mimic more closely the tumor microenvironment. Specifically, tumors are known to have regions that are hypoxic. Using 3D cultures might be one method to capture different microenvironments. Another approach might be to have cultures that can allow the cells to communicate via paracrine secretions through a porous membrane, but also keep the cells separated to allow for independent harvesting of intracellular MIDs. Thus, an oxygen gradient could be established that exposes some subpopulations of cancer cells to hypoxia, while others have access to sufficient oxygen. Similar setups could also create chemogradients that expose different cancer cell subpopulations to different levels of nutrients. These more complex models of tumor compartmentalization would more accurately reflect the reality within tumors. Unlike traditional 2D models, which assume all the cells consist of a single homogeneous population, a 3D model would enable researchers to shed light on the dynamic interplay between different subsets of tumor cells, which are known to be quite heterogeneous. While the 2D culture results provide a necessary baseline, the results of 3D studies could then be compared to these 2D culture results to determine if heterogeneity plays a role or just the lactate concentration is the important factor.

Appendix A

Reactions in the metabolic network used for ^{13}C-MFA.

Table A.1 The metabolic network specified for use in 13C-MFA for the three breast cancer cell lines. The cultures grown under the control conditions only used 73 reactions for the model, while the high-lactate metabolic model contained an extra reaction, v74.

v1 Gluc.ext (abcdef) -> G6P.c (abcdef)

v2 G6P.c (abcdef) <=> F6P.c (abcdef)

v3 F6P.C (abcdef) -> FBP.C (abcdef)

v4 FBP.c (abcdef) <=>DHAP.c (cba) + GAP.c (def)

v5 DHAP.c (abc) <=> GAP.c (abc)

v6 GAP.c (abc) <=> 3PG.c (abc)

v7 3PG.c (abc)<=> PEP.c (abc)

v8 PEP.c (abc) -> Pyr.c (abc)

v9 G6P.c (abcdef) -> CO2 (a) + Ru5P.c (bcdef)

v10 Ru5P.c <=> R5P.c

v11 X5P.c (abcde) <=> EC2.c (ab) + GAP.c (cde)

v12 F6P.c (abcdef) <=> EC2.c (ab)+ E4P.c (cdef)

v13 S7P.c (abcdefg) <=> EC2.c (ab) + R5P.c (cdefg)

v14 F6P.c (abcdef) <=> EC3.c (abc) + GAP.c (def

Table A.1 The metabolic network specified for use in 13C-MFA for the three breast cancer cell lines. The cultures grown under the contol conditions only used 73 reactions for the model, while the high-lactate metabolic model contained an extra reaction, v74.

v15 S7P.c (abcdefg) <=> EC3.c (abc) + E4P.c (defg)

v16 Pyr.c (abc) <=> Lact.c (abc)

v17 Pyr.c (abc) -> Pyr.snk (abc)

v18 Pyr.c (abc) -> Pyr.m (abc)

v19 Pyr.m (abc) -> CO2 (a) + AcCoA.m (bc)

v20 AcCoA.m (ab) + OAC.m (cdef) -> Cit.m (fedbac)

v21 Cit.m(abcdef) <=> AKG.m (abcde) + CO2 (f)

v22 AKG.m (abcde) -> CO2 (a)+ Suc.m (bcde)

v23 Suc.m (abcd) <=> Fum.m (abcd)

v24 Fum.m (abcd) <=> Mal.m (abcd)

v25 Mal.m (abcd) <=> OAC.m (abcd)

v26 Mal.m (abcd)-> Pyr.mII (abc)+ CO2 (d)

v27 Pyr.mII (abc) + CO2 (d) -> OAC.m (abcd)

v28 Pyr.m (abc) <=> Pyr.mII (abc)

v29 Mal.c (abcd) -> Pyr.c (abc) + CO2 (d)

v30 Mal.m (abcd) <=> Mal.c (abcd)

v31 Mal.c (abcd) <=> OAC.c (abcd)

Table A.1 The metabolic network specificed for use in 13C-MFA for the three breast cancer cell lines. The cultures grown under the control conditions only used 73 reactions for the model, while the high-lactate metabolic model contained an extra reaction, v74.

v32 OAC.c (abcd) -> PEP.c (abc) + CO2 (d)

v33 Cit.m (abcdef) <=> Cit.c (abcdef)

v34 Cit.c (abcdef) -> AcCoA.c (ab) + OAC.c (cdef)

v35 AcCoA.c (ab) -> FA.c (ab)

v36 Gln.c (abcde) -> Glu.c (abcde)

v37 Glu.c (abcde) <=> AKG.m (abcde)

v38 Glu.c (abcde) <=> Pro.c (abcde)

v39 Asp.c (abcd) <=> OAC.c (abcd)

v40 Asp.c (abcd) -> Asn.c (abcd)

v41 Pyr.c (abc) <=> Ala.c (abc)

v42 Ser.c (abc) <=> Pyr.c (abc)

v43 Ser.c (abc) -> Gly.c (ab) + MEETHF (c)

v44 Thr.c (abcd)-> AcCoA.c (cd) + Gly.c (ab)

v45 Met.c (abcde) + CO2 (f) -> Suc.m (bcdf) + CO2 (a) + C1 (e)

v46 Val.c (abcde) + CO2 (f) -> Suc.m (dcef) + 2CO2 (a,b)

v47 Ile.c (abcdef) + CO2 (g) -> Suc.m (bcdg) + AcCoA.m (ef) + CO2 (a)

Table A.1 (continued): The metabolic network specified for use in 13C-MFA for the three breast cancer cell lines. The cultures grown under the control conditions only used 73 reactions for the model, while the high-lactate metabolic model contained an extra reaction, v74.

v48 Phe.c (abcddefghi) -> Fum.m (defg) + 2 AcCoA.m (bc, hi) + CO_2 (a)

v49 Tyr.c (abcdefghi) -> Fum.m (defg) + 2 AcCoA.m (bc, hi) + CO_2 (a)

v50 Leu.c (abcdef) + CO2 (g) -> 3 AcCoA.m (bc, de, gf) + CO_2 (a)

v51 Gln.ext (abcde) -> Gln.c (abcde)

v52 Asp.c (abcd) -> Asp.ext (abcd)

v53 Ile.ext (abcdef) -> Ile.c (abcdef)

v54 Leu.ext (abcdef) -> Leu.c (abcdef)

v55 Met.ext (abcde) -> Met.c (abcde)

v56 Phe.ext (abcdefghi) -> Phe.c (abcdefghi)

v57 Ser.ext (abc) -> Ser.c (abc)

v58 Tyr.ext (abcdefghi) -> Tyr.c (abcdefghi)

v59 Val.ext (abcde) -> Val.c (abcde)

v60 Thr.ext (abcd) -> Thr.c (abcd)

v61 Arg.ext (abcdef) -> Arg.c (abcdef)

v62 Cys.ext (abc) -> Cys.c (abc)

v63 His.ext (abcdef)-> His.c (abcdef)

Table A.1 (continued): The metabolic network specified for use in 13C-MFA for the three breast cancer cell lines. The cultures grown under the control conditions only used 73 reactions for the model, while the high-lactate metabolic model contained an extra reaction, v74.

v64 Lys.ext (abcdef) -> Lys.c (abcdef)

v65 Trp.ext (abcdefghijk) -> Trp.c (abcdefghijk)

v66 Ala.c (abc) -> Ala.ext (abc)

v67 Gly.c (ab) -> Gly.ext (ab)

v68 Pro.c (abcde) -> Pro.ext (abcde)

v69 Glu.c (abcde) -> Glu.ext (abcde)

v70 Lact.c (abc) -> Lact.ext (abc)

v71 Ru5P.c (abcde) <=> X5P.c (abcde)

0.0862 Ala + 0.0519 Arg + 0.0495 Asp + 0.0397 Asn + 0.0200 Cys + 0.0444 Glu+ 0.0532 Gln + 0.0742 Gly + 0.0197 His + 0.0446 Ile + 0.0777 Leu + 0.0785 Lys + 0.0191 Met + 0.0302 Phe + 0.0432 Pro + 0.0592 Ser + 0.0532 Thr + 0.0061 Trp + 0.025

v72 Tyr + 0.0573 Val + 0.0384 G6P + 0.0321 Ru5P -> Biomass

v73 FA.c -> Lipids

v74 Lact.tr (abc) -> Lact.c (abc)

Appendix B

Table B.1 Extracellular metabolite concentrations in the three breast cancer cell lines at 24-h and 48-h.

		MCF-10A				MCF-7				MDA-MB-231			
		CONTROL		LACTATE		CONTROL		LACTATE		CONTROL		LACTATE	
Metabolite	Fresh Media (mM)	24h (mM)	48h (mM)	24h (mM)	48h (mM)	24h (mM)	48h (mM)	24h (mM)	48h (mM)	24h (mM)	48h (mM)	24h (mM)	48h (mM)
Glucose	5	4.30	3.31	4.42	3.63	4.32	3.32	4.50	3.78	4.05	2.38	4.20	2.90
Lactate	*	1.12	2.81	10.80	11.90	1.03	2.55	20.45	21.05	1.80	4.80	21.03	22.70
Alanine	0	0.03	0.08	0.03	0.08	0.04	0.10	0.03	0.09	0.03	0.08	0.03	0.07
Aspartate	0	0.01	0.04	0.01	0.03	0.02	0.05	0.01	0.04	0.01	0.03	0.01	0.03
Glutamate	0	0.03	0.09	0.03	0.07	0.04	0.09	0.04	0.09	0.03	0.07	0.03	0.08
Glutamine	3	2.72	2.39	2.73	2.37	2.72	2.35	2.71	2.31	2.75	2.42	2.73	2.34
Glycine	0.36	0.38	0.41	0.38	0.40	0.39	0.44	0.39	0.43	0.38	0.42	0.38	0.42
Isoleucine	0.72	0.70	0.66	0.69	0.66	0.69	0.65	0.69	0.65	0.71	0.68	0.69	0.65
Leucine	0.72	0.70	0.67	0.70	0.67	0.70	0.66	0.70	0.66	0.71	0.68	0.69	0.65
Methionine	0.18	0.18	0.16	0.17	0.17	0.17	0.16	0.17	0.16	0.18	0.17	0.17	0.16
Phenylalanine	0.36	0.35	0.33	0.35	0.33	0.35	0.33	0.35	0.33	0.35	0.33	0.35	0.33
Proline	0	0.00	0.01	0.00	0.01	0.01	0.02	0.01	0.02	0.00	0.01	0.00	0.01
Serine	0.36	0.31	0.23	0.30	0.21	0.30	0.20	0.29	0.18	0.32	0.24	0.30	0.20
Threonine	0.72	0.71	0.70	0.71	0.71	0.72	0.71	0.72	0.71	0.72	0.71	0.71	0.71
Tyrosine	0.36	0.35	0.33	0.35	0.33	0.35	0.33	0.35	0.33	0.35	0.33	0.35	0.33
Valine	0.72	0.71	0.68	0.70	0.68	0.69	0.65	0.69	0.64	0.70	0.67	0.69	0.65

Appendix C

Measured and simulated MID values for

intracellular metabolites from glucose and glutamine tracers.

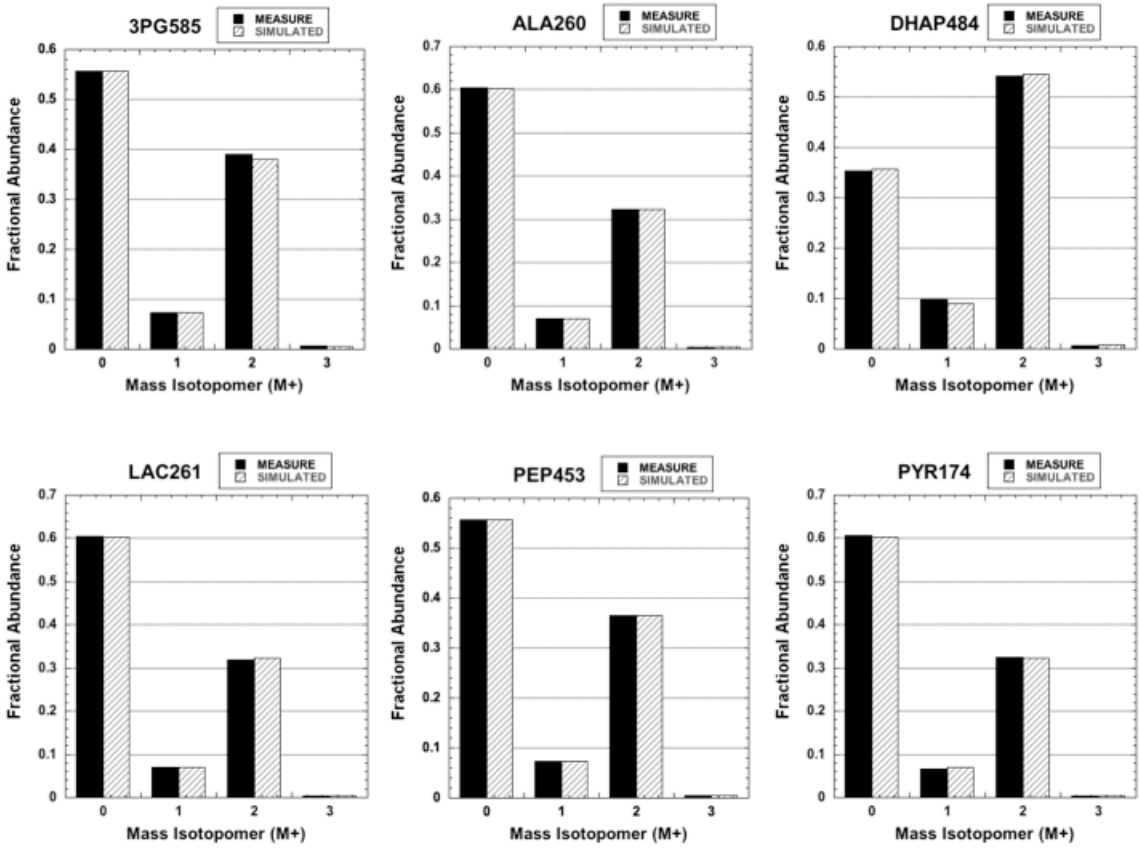

Figure C.1 MID values for intracellular metabolites from [1,2-^{13}C] glucose for MCF-10A for the control condition. All MIDs were corrected for natural isotope abundances.

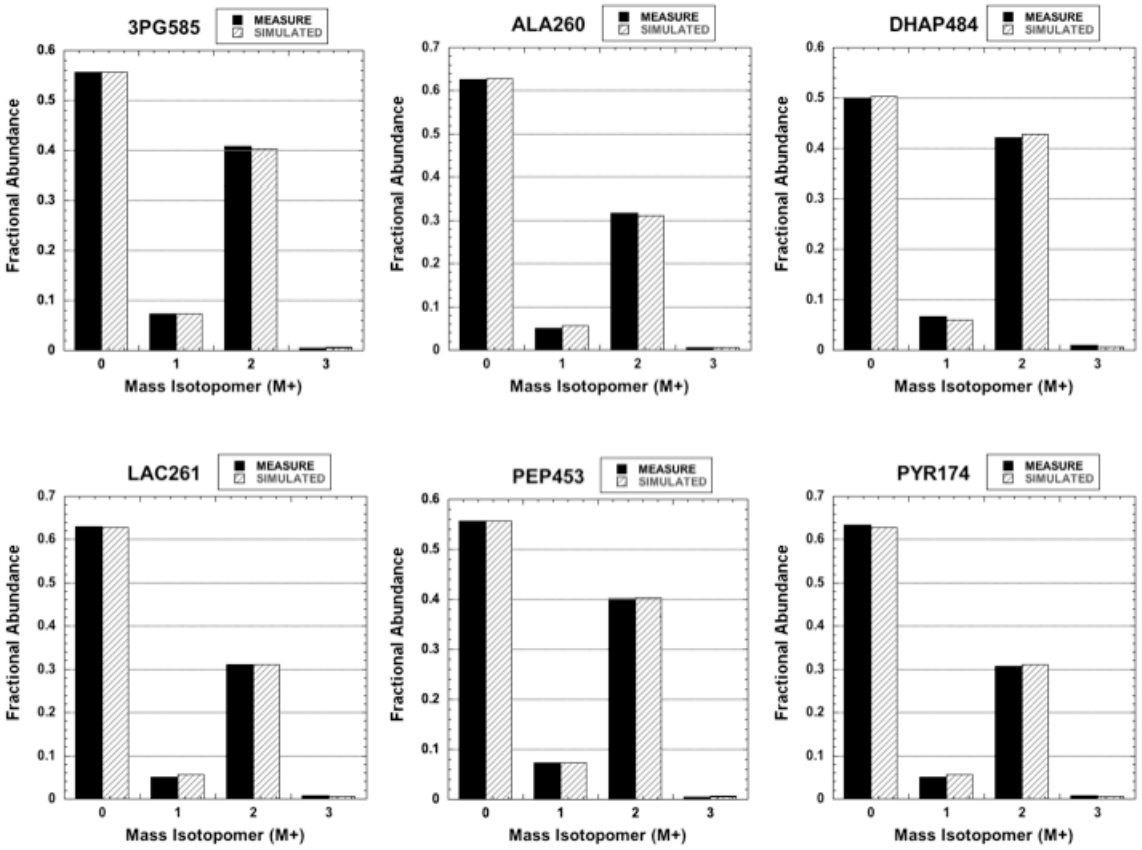

Figure C.2 MID values for intracellular metabolites from [1,2-^{13}C] glucose for MCF-10A for the high-lactate condition. All MIDs were corrected for natural isotope abundances.

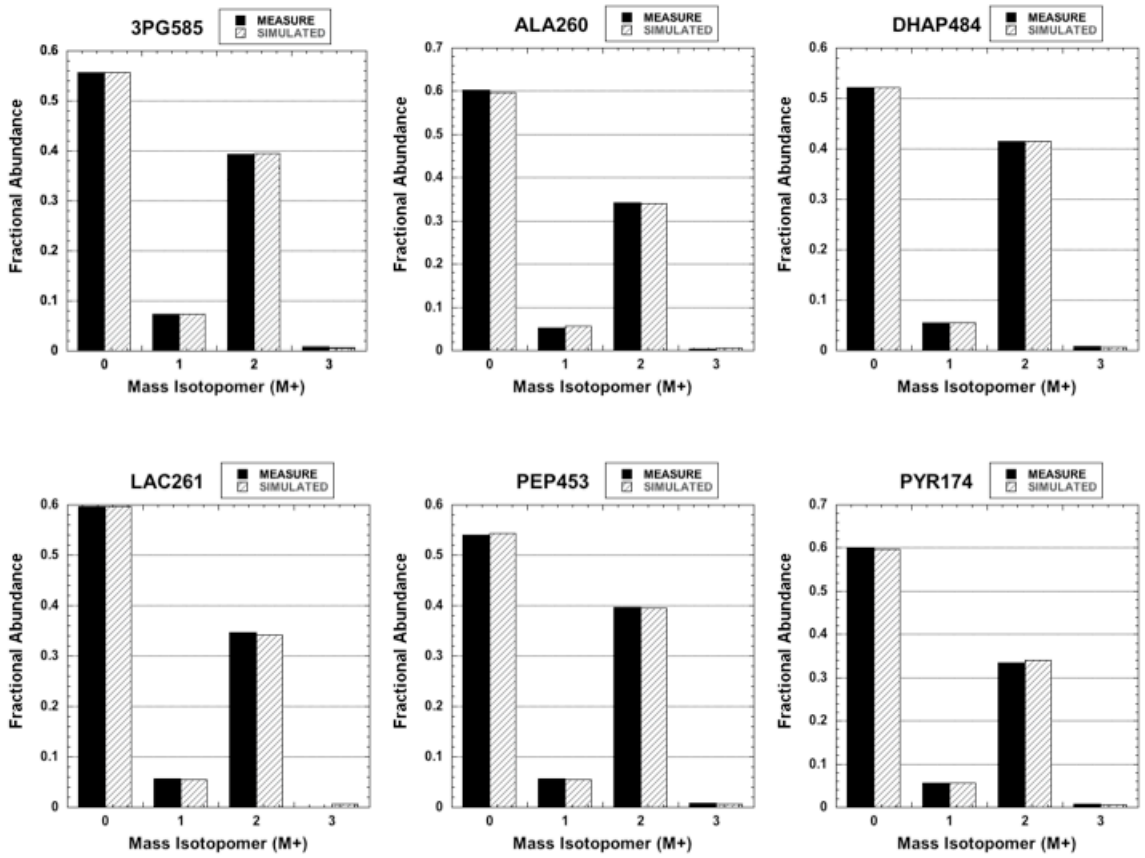

Figure C.3 MID values for intracellular metabolites from [1,2-^{13}C] glucose for MCF-7 for the control condition. All MIDs were corrected for natural isotope abundances. All MIDs were corrected for natural isotope abundances.

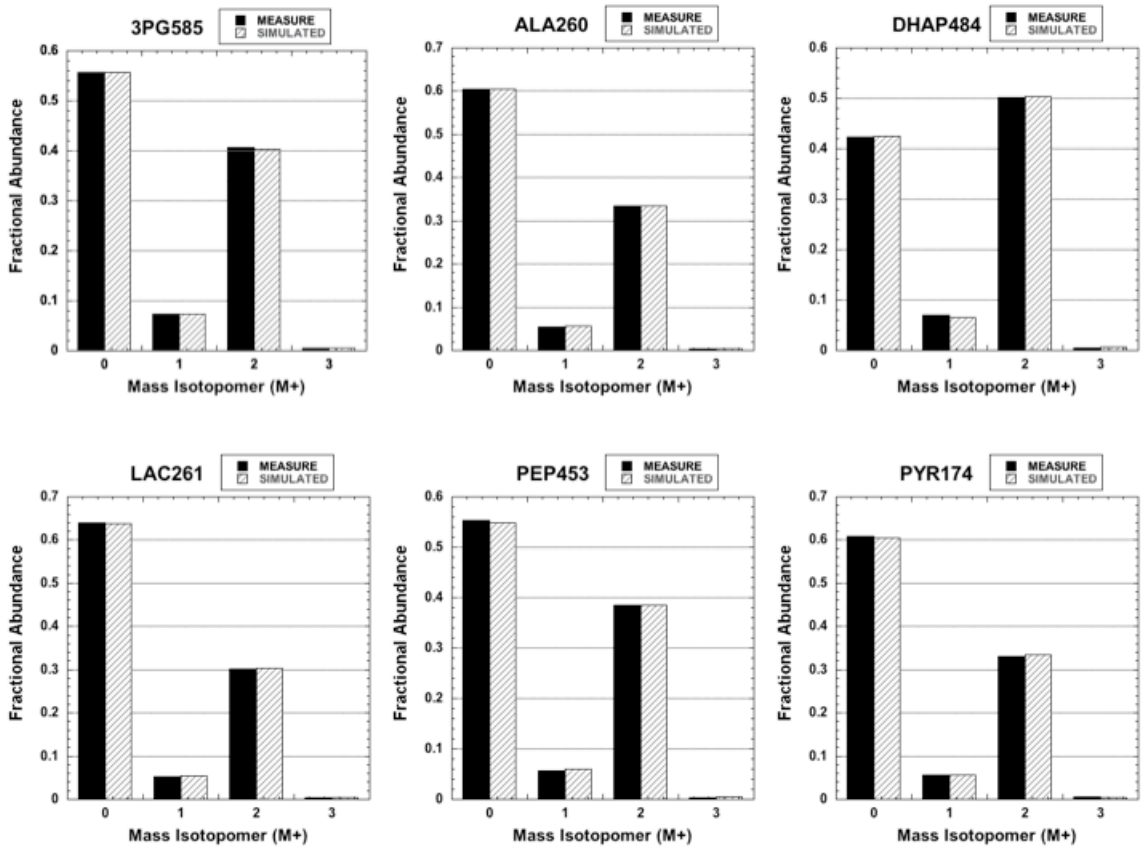

Figure C.4 MID values for intracellular metabolites from [1,2-^{13}C] glucose for MCF-7 for the high-lactate condition. All MIDs were corrected for natural isotope abundances.

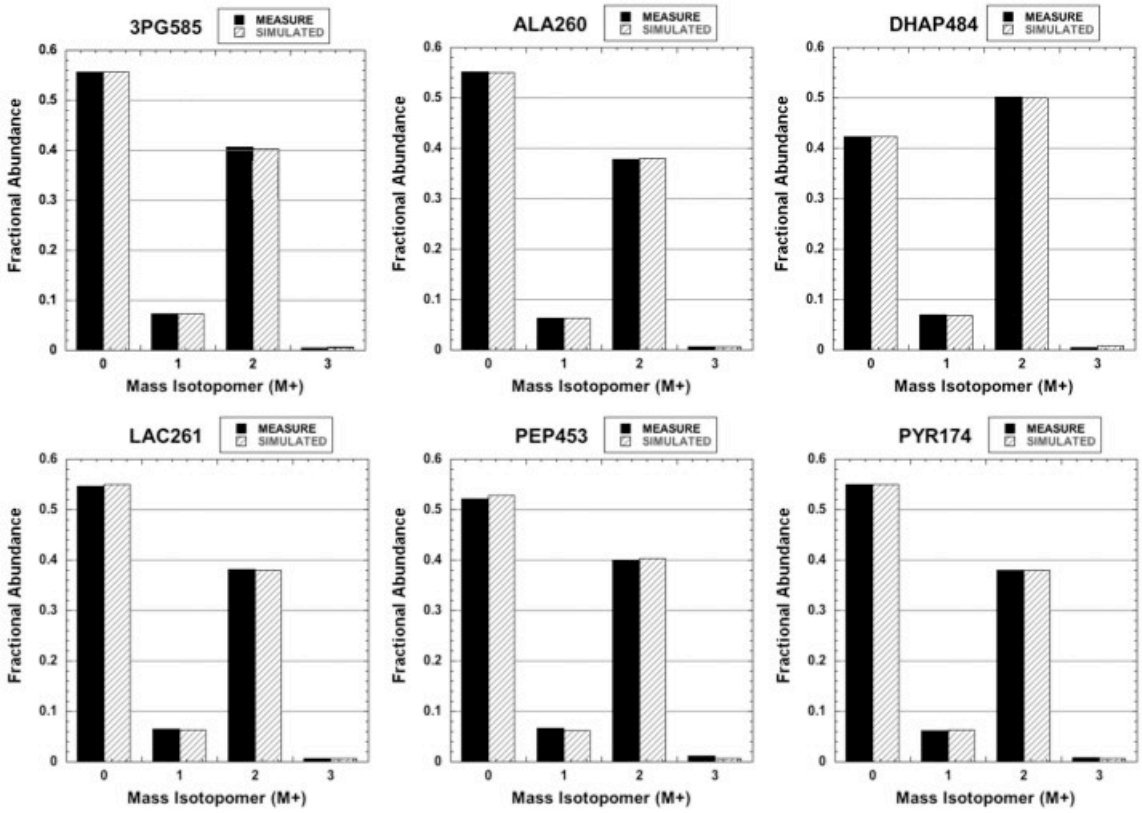

Figure C.5 MID values for intracellular metabolites from [1,2-^{13}C] glucose for MDA-MB-231 for the control condition. All MIDs were corrected for natural isotope abundances.

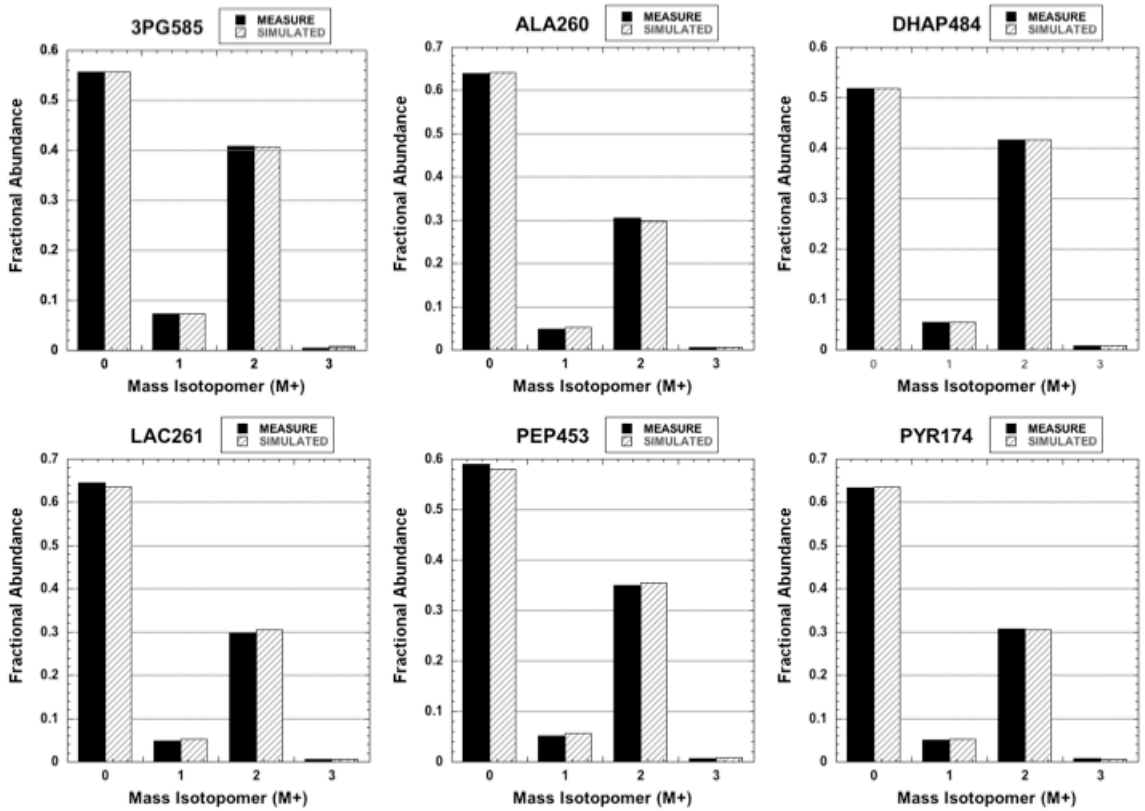

Figure C.6 MID values for intracellular metabolites from [1,2-^{13}C] glucose for MDA-MB-231 for the high-lactate condition. All MIDs were corrected for natural isotope abundances.

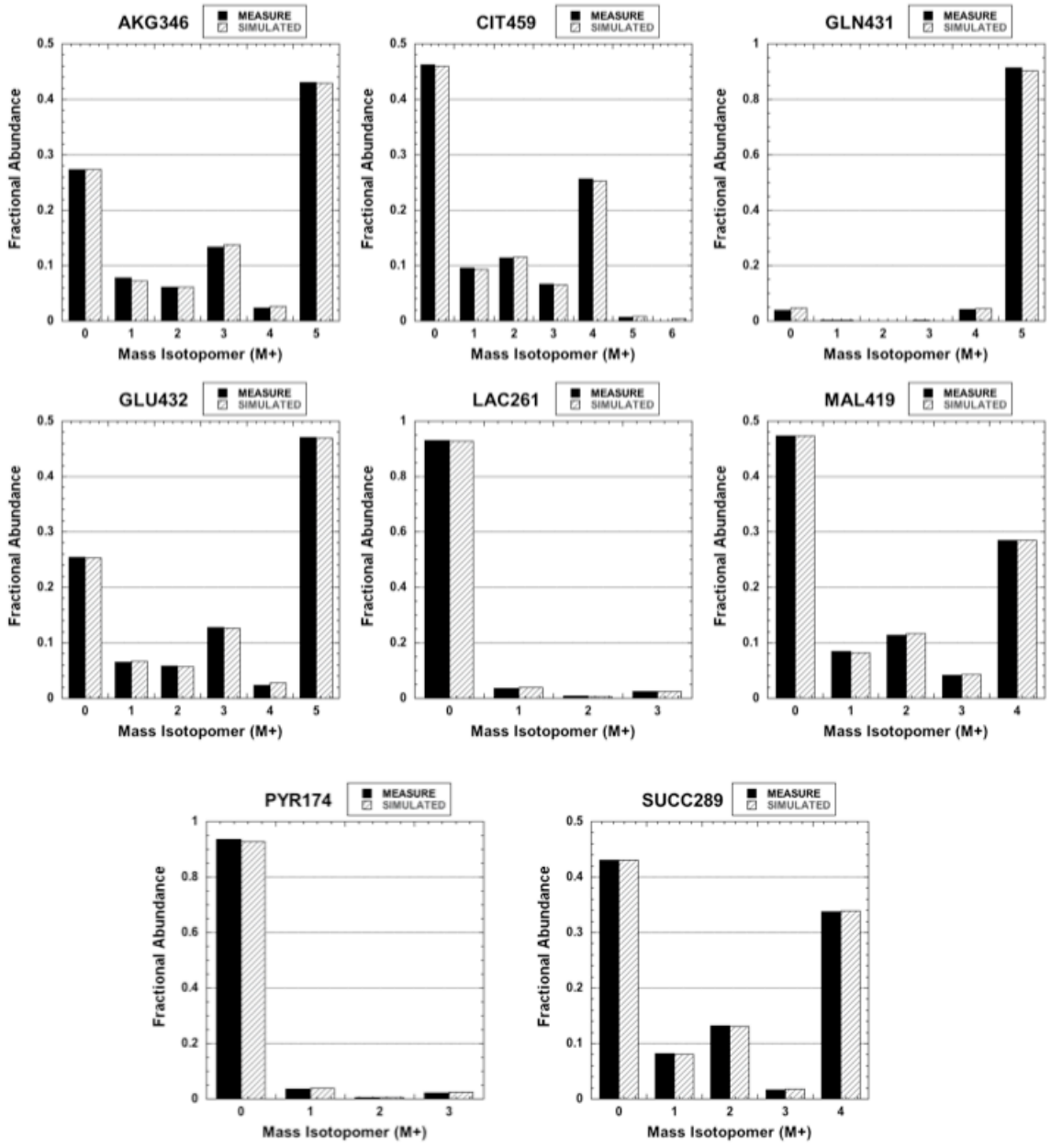

Figure C.7 MID values for intracellular metabolites from [U-^{13}C] glutamine for MCF-10A for the control condition. All MIDs were corrected for natural isotope abundances.

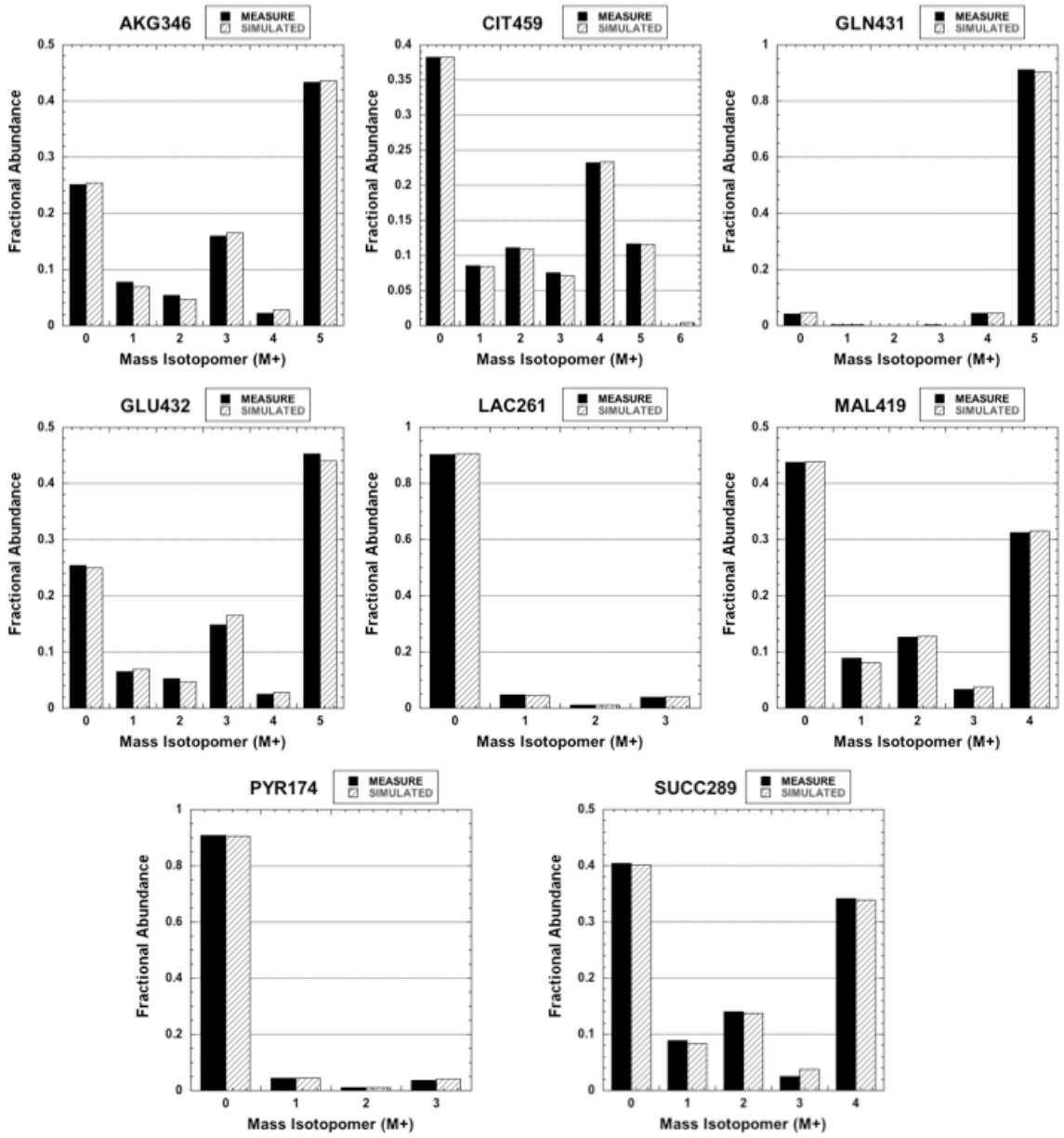

Figure C.8 MID values for intracellular metabolites from [U-^{13}C] glutamine for MCF-10A for the high-lactate condition. All MIDs were corrected for natural isotope abundances.

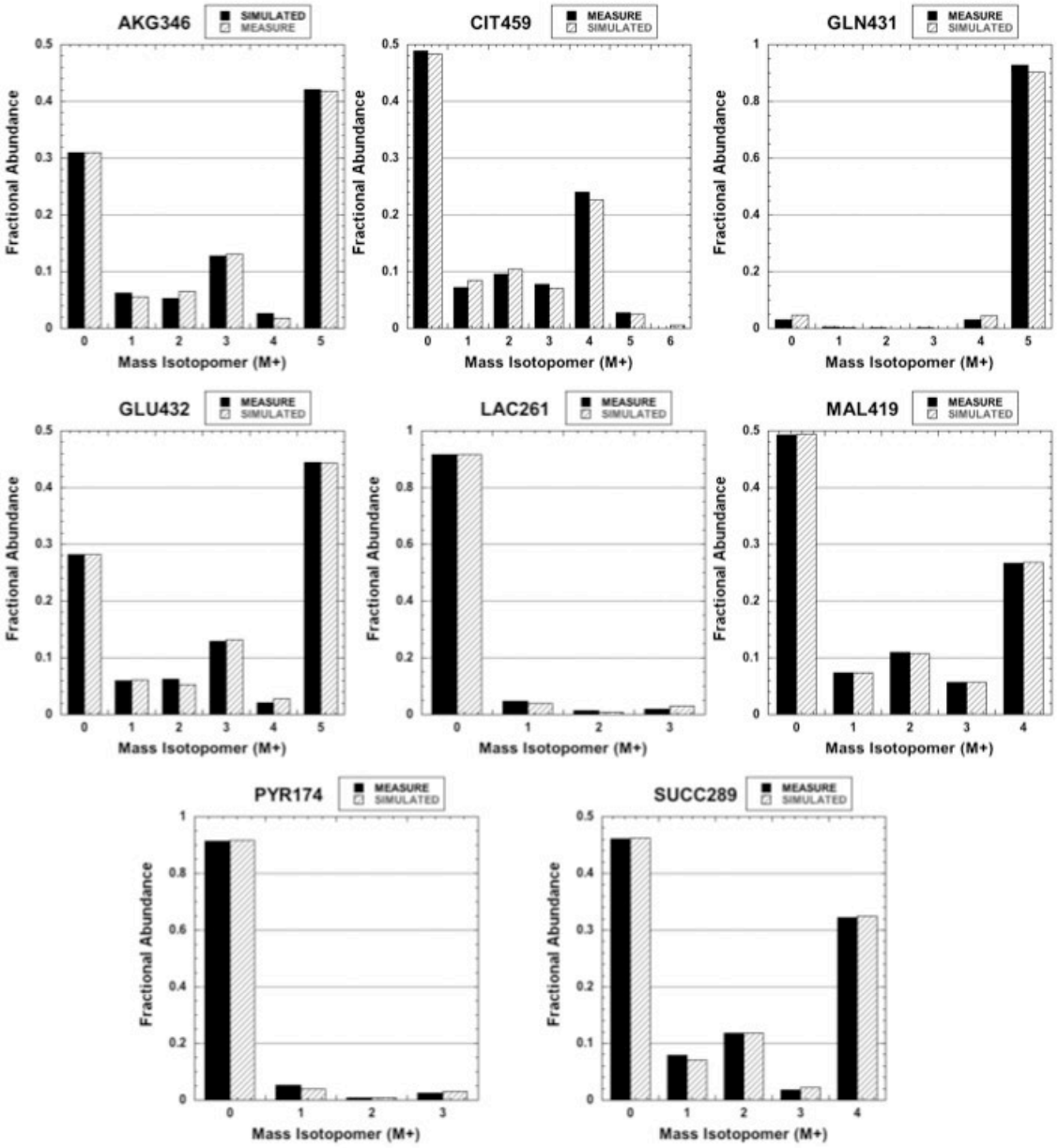

Figure C.9 MID values for intracellular metabolites from [U-^{13}C] glutamine for MCF-7 for the control condition. All MIDs were corrected for natural isotope abundances.

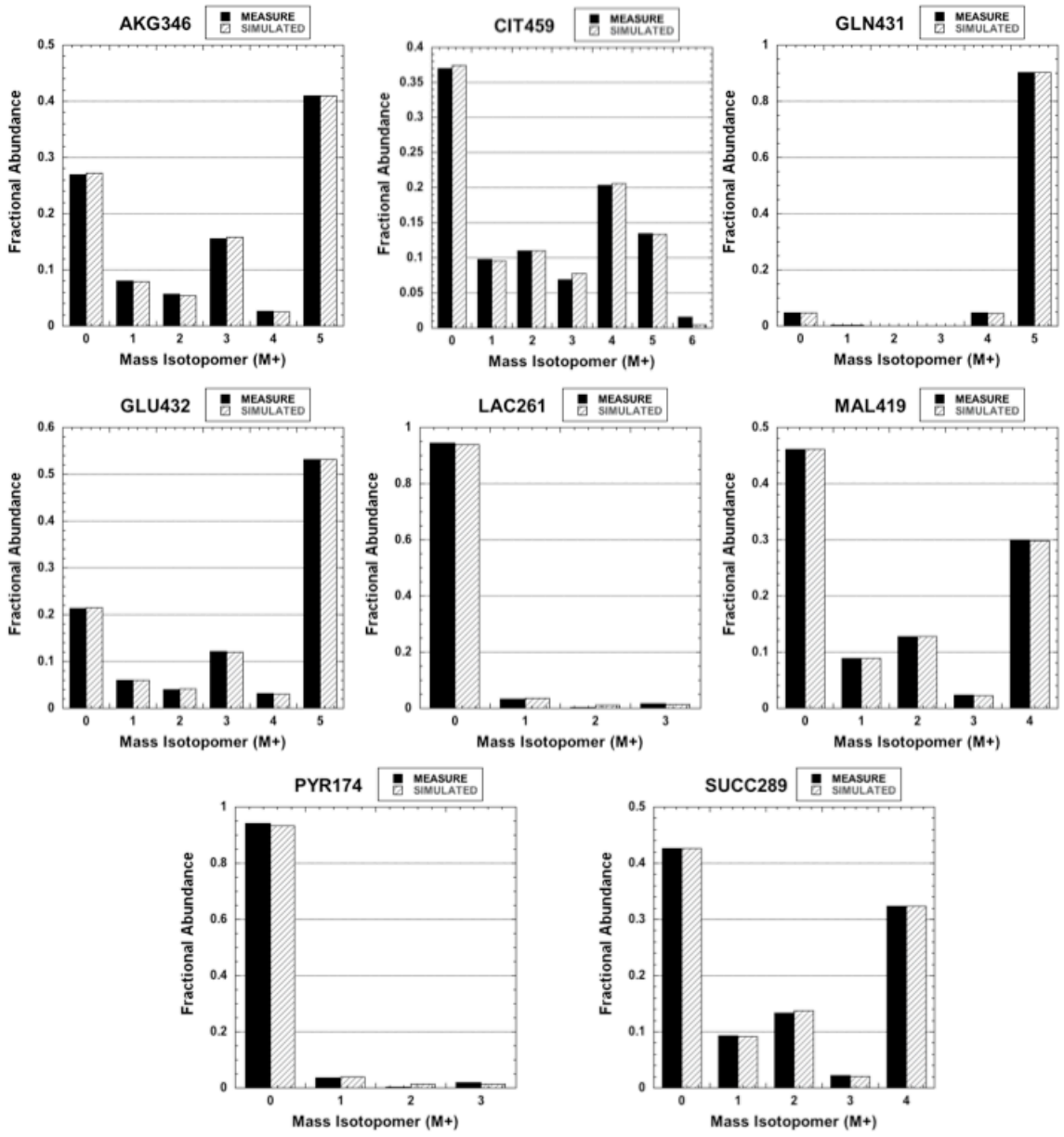

Figure C.10 MID values for intracellular metabolites from [U-^{13}C] glutamine for MCF-7 for the high-lactate condition. All MIDs were corrected for natural isotope abundances. All MIDs were corrected for natural isotope abundances.

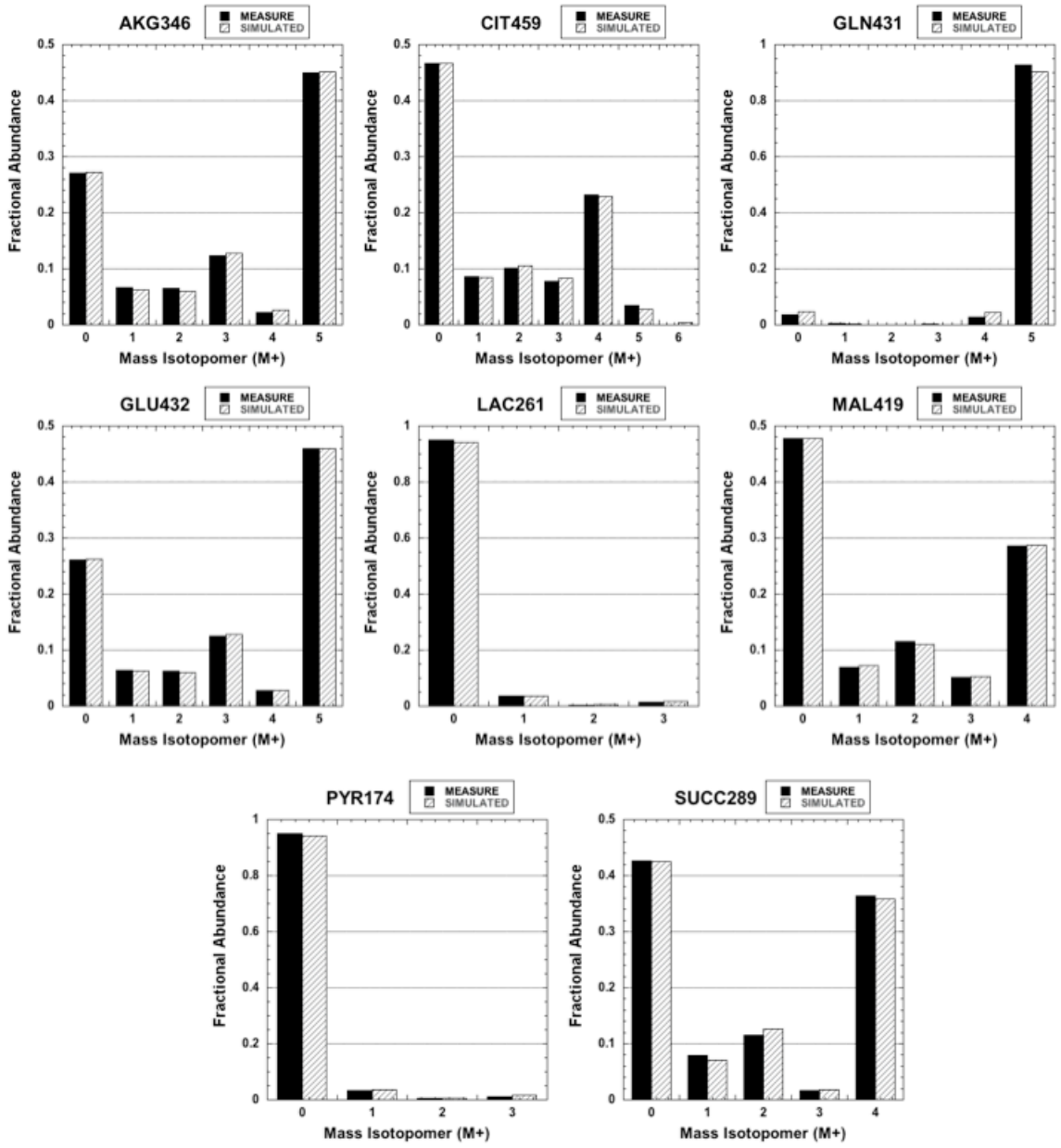

Figure C.11 MID values for intracellular metabolites from [U-^{13}C] glutamine for MDA-MB-231 for the control condition. All MIDs were corrected for natural isotope abundances.

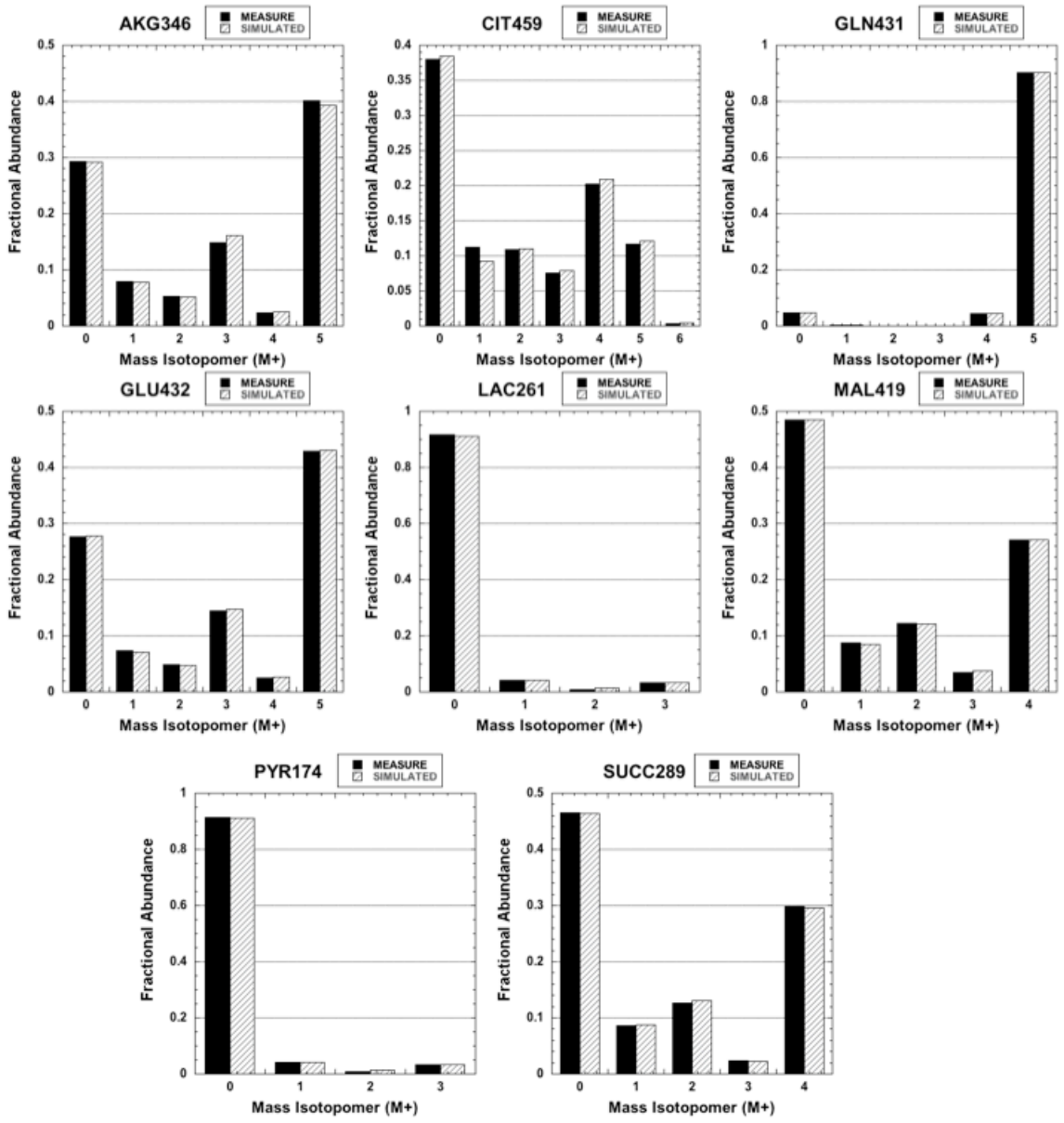

Figure C.12 MID values for intracellular metabolites from [U-^{13}C] glutamine for MDA-MB-231 for the high-lactate condition. All MIDs were corrected for natural abundances.

Appendix D

MFA results for the three breast cancer cell lines

Table D.1 MFA results for the MCF-10A cells for the control condition. Fluxes measured in nmol/10^6 cells/h.

Flux ± SD	%SD	Reaction	Confidence Interval
1. 216.087 ± 17.834	8.4 %	Gluc.ext -> G6P.c	(186.31, 255.86)
2. 137.526 ± 11.225	8.4 %	G6P.c <=> F6P.c (net)	(117.38, 161.16)
3. (>1000, >1e4) ± >1000	>100 %	G6P.c <=> F6P.c (exch)	(148.72, >10000)
4. 187.450 ± 15.761	8.6 %	F6P.c -> FBP.c	(161.20, 222.67)
5. 187.450 ± 15.761	8.6 %	FBP.c <=> DHAP.c + GAP.c (net)	(161.20, 222.67)
6. (0.0, >1e4) ± >10000	>100 %	FBP.c <=> DHAP.c + GAP.c (exch)	(0.00, >10000)
7. 187.450 ± 15.761	8.6 %	DHAP.c <=> GAP.c (net)	(161.20, 222.67)
8. 303.069 ± 29.134	9.9 %	DHAP.c <=> GAP.c (exch)	(251.94, 365.56)
9. 399.862 ± 33.612	8.5 %	GAP.c <=> 3PG.c (net)	(343.93, 475.02)
10. (0.0, >1000) ± >1000	>100 %	GAP.c <=> 3PG.c (exch)	(0.00, >10000)
11. 399.862 ± 33.612	8.5 %	3PG.c <=> PEP.c (net)	(343.93, 475.02)
12. (0.0, 3.7) ± 72.604	>100 %	3PG.c <=> PEP.c (exch)	(0.00, 283.16)
13. 417.958 ± 35.917	8.8 %	PEP.c -> Pyr.c	(357.76, 497.83)
14. 76.565 ± 8.307	11.0 %	G6P.c -> CO2 + Ru5P.c	(61.29, 93.69)
15. 24.962 ± 2.782	11.3 %	Ru5P.c <=> R5P.c (net)	(19.86, 30.72)
16. (102.2, >1e4) ± >1000	>100 %	Ru5P.c <=> R5P.c (exch)	(0.00, >10000)
17. 49.924 ± 5.565	11.3 %	X5P.c <=> EC2.c + GAP.c (net)	(39.73, 61.43)

Table D.1 (continued) MFA results for the MCF-10A cells for the control condition. Fluxes measured in nmol/10^6 cells/h.

Flux ± SD	%SD	Reaction	Confidence Interval
18. (39.4, >1e4) ± >1000	>100 %	X5P.c <=> EC2.c + GAP.c (exch)	(0.00, >10000)
19. -24.962 ± 2.782	10.8 %	F6P.c <=> EC2.c + E4P.c (net)	(-30.72, -19.86)
20. 0.000 ± 2.452	>100 %	F6P.c <=> EC2.c + E4P.c (exch)	(0.00, 9.56)
21. -24.962 ± 2.782	10.8 %	S7P.c <=> EC2.c + R5P.c (net)	(-30.72, -19.86)
22. (1.9, >1e4) ± >1000	>100 %	S7P.c <=> EC2.c + R5P.c (exch)	(0.00, >10000)
23. -24.962 ± 2.782	10.8 %	F6P.c <=> EC3.c + GAP.c (net)	(-30.72, -19.86)
24. (466.6, >1e4) ± >1000	>100 %	F6P.c <=> EC3.c + GAP.c (exch)	(0.00, >10000)
25. 24.962 ± 2.782	11.3 %	S7P.c <=> EC3.c + E4P.c (net)	(19.86, 30.72)
26. (1.8, >1e4) ± >1000	>100 %	S7P.c <=> EC3.c + E4P.c (exch)	(0.00, >10000)
27. 385.000 ± 35.901	9.6 %	Pyr.c <=> Lact.c (net)	(309.95, 449.96)
28. (0.0, >1e4) ± >1000	>100 %	Pyr.c <=> Lact.c (exch)	(0.00, >10000)
29. 18.413 ± 35.396	>100 %	Pyr.c -> Pyr.snk	(0.00, 138.04)
30. 42.283 ± 11.652	28.5 %	Pyr.c -> Pyr.m	(23.67, 69.12)
31. 42.284 ± 10.069	24.9 %	Pyr.m -> CO2 + AcCoA.m	(23.08, 62.35)
32. 66.073 ± 8.056	12.5 %	AcCoA.m + OAC.m -> Cit.m	(50.89, 82.31)
33. 40.537 ± 4.792	12.0 %	Cit.m <=> AKG.m + CO2 (net)	(32.39, 51.08)
34. 0.000 ± 0.410	>100 %	Cit.m <=> AKG.m + CO2 (exch)	(0.00, 1.60)
35. 64.128 ± 5.258	8.3 %	AKG.m -> CO2 + Suc.m	(55.36, 75.87)
36. 75.803 ± 8.363	11.2 %	Suc.m <=> Fum.m (net)	(61.08, 93.70)
37. (0.0, >1e4) ± >1000	>100 %	Suc.m <=> Fum.m (exch)	(0.00, >10000)

Table D.1 (continued) MFA results for the MCF-10A cells for the control condition. Fluxes measured in nmol/10^6 cells/h.

Flux ± SD	%SD	Reaction	Confidence Interval
38. 82.509 ± 9.134	11.2 %	Fum.m <=> Mal.m (net)	(66.38, 102.00)
39. (0.0, 7.5) ± >1000	>100 %	Fum.m <=> Mal.m (exch)	(0.00, >10000)
40. 54.364 ± 7.749	14.6 %	Mal.m <=> OAC.m (net)	(39.54, 69.76)
41. 85.624 ± 88.638	>100 %	Mal.m <=> OAC.m (exch)	(17.51, 363.20)
42. 11.710 ± 2.205	20.3 %	Mal.m -> Pyr.mII + CO2	(8.19, 16.79)
43. 11.709 ± 4.273	37.9 %	Pyr.mII + CO2 -> OAC.m	(8.55, 25.22)
44. -0.000 ± 3.316	>100 %	Pyr.m <=> Pyr.mII (net)	(-0.62, 12.31)
45. 0.000 ± 3.157	>100 %	Pyr.m <=> Pyr.mII (exch)	(0.00, 12.31)
46. 14.658 ± 8.418	59.1 %	Mal.c -> Pyr.c + CO2	(0.00, 32.83)
47. 16.435 ± 8.707	56.8 %	Mal.m <=> Mal.c (net)	(1.34, 35.29)
48. (0.0, >1e4) ± >1000	>100 %	Mal.m <=> Mal.c (exch)	(0.00, >10000)
49. 1.778 ± 10.088	>100 %	Mal.c <=> OAC.c (net)	(-18.01, 21.34)
50. (158.8, >1e4) ± >1000	>100 %	Mal.c <=> OAC.c (exch)	(0.00, >10000)
51. 18.096 ± 7.548	46.9 %	OAC.c -> PEP.c + CO2	(4.01, 33.45)
52. 25.536 ± 6.810	28.6 %	Cit.m <=> Cit.c (net)	(12.41, 38.97)
53. (0.0, >1e4) ± >10000	>100 %	Cit.m <=> Cit.c (exch)	(0.00, >10000)
54. 25.536 ± 6.810	28.6 %	Cit.c -> AcCoA.c + OAC.c	(12.41, 38.97)
55. 25.536 ± 6.810	28.6 %	AcCoA.c -> FA.c	(12.41, 38.97)
56. 44.627 ± 3.866	8.7 %	Gln.c -> Glu.c	(37.73, 52.81)
57. 23.591 ± 3.424	14.6 %	Glu.c <=> AKG.m (net)	(17.62, 30.98)

Table D.1 (continued) MFA results for the MCF-10A cells for the control condition. Fluxes measured in nmol/10^6 cells/h.

Flux ± SD	%SD	Reaction	Confidence Interval
58. 467.362 ± >100	46.3 %	Glu.c <=> AKG.m (exch)	(284.20, >1000)
59. 3.306 ± 0.663	21.4 %	Glu.c <=> Pro.c (net)	(1.98, 4.57)
60. (0.0, >1e4) ± >10000	>100 %	Glu.c <=> Pro.c (exch)	(0.00, >10000)
61. -9.218 ± 2.102	21.9 %	Asp.c <=> OAC.c (net)	(-13.24, -5.04)
62. (0.0, >1e4) ± >1000	>100 %	Asp.c <=> OAC.c (exch)	(0.00, >10000)
63. 2.100 ± 0.426	21.6 %	Asp.c -> Asn.c	(1.22, 2.88)
64. 15.356 ± 5.541	40.9 %	Pyr.c <=> Ala.c (net)	(4.50, 26.11)
65. (0.0, >1e4) ± >1000	>100 %	Pyr.c <=> Ala.c (exch)	(0.00, >10000)
66. 28.436 ± 6.271	23.9 %	Ser.c <=> Pyr.c (net)	(15.27, 39.73)
67. (660.8, >1e4) ± >1000	>100 %	Ser.c <=> Pyr.c (exch)	(30.41, >10000)
68. 9.761 ± 3.088	35.1 %	Ser.c -> Gly.c + MEETHF	(3.71, 15.75)
69. 0.000 ± 0.393	>100 %	Thr.c -> AcCoA.c + Gly.c	(0.00, 1.53)
70. 1.026 ± 0.771	>100 %	Met.c + CO2 -> Suc.m + CO2 + MEETHF	(0.00, 3.01)
71. 3.210 ± 2.331	99.6 %	Val.c + CO2 -> Suc.m + 2 CO2	(0.00, 9.09)
72. 7.439 ± 3.811	60.4 %	Ile.c + CO2 -> Suc.m + AcCoA.m + CO2	(0.00, 14.86)
73. 3.216 ± 1.802	67.8 %	Phe.c -> Fum.m + 2 AcCoA.m + CO2	(0.00, 7.03)
74. 3.490 ± 1.864	63.8 %	Tyr.c -> Fum.m + 2 AcCoA.m + CO2	(0.00, 7.27)
75. 0.980 ± 1.284	>100 %	Leu.c + CO2 -> 3 AcCoA.m + CO2	(0.00, 5.01)
76. 46.937 ± 3.977	8.5 %	Gln.ext -> Gln.c	(39.83, 55.33)
77. 4.546 ± 1.940	49.0 %	Asp.c -> Asp.ext	(0.74, 8.31)

Table D.1 (continued) MFA results for the MCF-10A cells for the control condition. Fluxes measured in nmol/10^6 cells/h.

Flux ± SD	%SD	Reaction	Confidence Interval
78. 9.801 ± 3.826	44.5 %	Ile.ext -> Ile.c	(2.19, 17.11)
79. 5.074 ± 1.514	34.1 %	Leu.ext -> Leu.c	(2.75, 8.66)
80. 2.023 ± 0.839	49.1 %	Met.ext -> Met.c	(0.70, 3.97)
81. 4.791 ± 1.850	44.2 %	Phe.ext -> Phe.c	(1.30, 8.51)
82. 41.295 ± 5.609	14.2 %	Ser.ext -> Ser.c	(29.48, 51.35)
83. 4.802 ± 1.892	45.1 %	Tyr.ext -> Tyr.c	(1.14, 8.51)
84. 6.203 ± 2.520	46.1 %	Val.ext -> Val.c	(2.12, 11.94)
85. 2.782 ± 0.644	24.6 %	Thr.ext -> Thr.c	(1.65, 4.16)
86. 2.730 ± 0.553	21.6 %	Arg.ext -> Arg.c	(1.59, 3.75)
87. 1.050 ± 0.213	21.6 %	Cys.ext -> Cys.c	(0.61, 1.44)
88. 1.050 ± 0.213	21.6 %	His.ext -> His.c	(0.61, 1.44)
89. 4.147 ± 0.841	21.6 %	Lys.ext -> Lys.c	(2.42, 5.69)
90. 0.315 ± 0.064	21.5 %	Trp.ext -> Trp.c	(0.18, 0.43)
91. 10.999 ± 5.498	59.4 %	Ala.c -> Ala.ext	(0.28, 21.72)
92. 5.876 ± 3.002	60.4 %	Gly.c -> Gly.ext	(0.07, 11.78)
93. 1.049 ± 0.497	55.9 %	Pro.c -> Pro.ext	(0.07, 2.01)
94. 14.947 ± 4.066	29.1 %	Glu.c -> Glu.ext	(6.67, 22.53)
95. 385.000 ± 35.901	9.6 %	Lact.c -> Lact.ext	(309.95, 449.96)
96. 49.924 ± 5.565	11.3 %	Ru5P.c <=> X5P.c (net)	(39.73, 61.43)
97. (39.4, >1e4) ± >1000	>100 %	Ru5P.c <=> X5P.c (exch)	(0.00, >10000) |

98. 52.499 ± 10.639	Biomass Equation (v72)	(30.59, 72.09)
99. 25.536 ± 6.810	28.6 % FA.c -> Lipids	(12.41, 38.97)

Table D.2 MFA results for the MCF-10A cells for the high-lactate condition. Fluxes measured in nmol/10^6 cells/h.

Flux ± SD	%SD	Reaction	Confidence Interval
1. 178.106 ± 14.923	8.6 %	Gluc.ext -> G6P.c	(148.54, 206.74)
2. 134.782 ± 11.032	8.4 %	G6P.c <=> F6P.c (net)	(113.09, 156.11)
3. (145.6, >1e4) ± >1000	>100 %	G6P.c <=> F6P.c (exch)	(0.00, >10000)
4. 161.499 ± 13.478	8.6 %	F6P.c -> FBP.c	(134.76, 187.32)
5. 161.499 ± 13.478	8.6 %	FBP.c <=> DHAP.c + GAP.c (net)	(134.76, 187.32)
6. (0.0, >1e4) ± >10000	>100 %	FBP.c <=> DHAP.c + GAP.c (exch)	(0.00, >10000)
7. 161.499 ± 13.478	8.6 %	DHAP.c <=> GAP.c (net)	(134.76, 187.32)
8. (>1000, >1000) ± >1000	42.6 %	DHAP.c <=> GAP.c (exch)	(>1000, >1000)
9. 336.355 ± 28.452	8.7 %	GAP.c <=> 3PG.c (net)	(279.96, 390.93)
10. (0.0, >1000) ± >1000	>100 %	GAP.c <=> 3PG.c (exch)	(0.00, >10000)
11. 336.355 ± 28.452	8.7 %	3PG.c <=> PEP.c (net)	(279.96, 390.93)
12. (0.0, >1e4) ± >10000	>100 %	3PG.c <=> PEP.c (exch)	(0.00, >10000)
13. 336.355 ± 28.452	8.7 %	PEP.c -> Pyr.c	(279.96, 390.93)
14. 41.561 ± 7.107	18.1 %	G6P.c -> CO2 + Ru5P.c	(25.28, 53.00)
15. 13.358 ± 2.383	18.9 %	Ru5P.c <=> R5P.c (net)	(7.92, 17.22)
16. (>1000, >1e4) ± >1000	>100 %	Ru5P.c <=> R5P.c (exch)	(0.00, >10000)
17. 26.717 ± 4.765	18.9 %	X5P.c <=> EC2.c + GAP.c (net)	(15.85, 34.43)
18. (>1e4, >1e4) ± >10000	>100 %	X5P.c <=> EC2.c + GAP.c (exch)	(0.00, >10000)
19. -13.358 ± 2.383	17.1 %	F6P.c <=> EC2.c + E4P.c (net)	(-17.22, -7.92)
20. 1.710 ± 3.513	>100 %	F6P.c <=> EC2.c + E4P.c (exch)	(0.00, 13.70)

Table D.2 (continued) MFA results for the MCF-10A cells for the high-lactate condition. Fluxes measured in nmol/10^6 cells/h.

Flux ± SD	%SD	Reaction	Confidence Interval
21. -13.358 ± 2.383	17.1 %	S7P.c <=> EC2.c + R5P.c (net)	(-17.22, -7.92)
22. (>1000, >1e4) ± >10000	>100 %	S7P.c <=> EC2.c + R5P.c (exch)	(0.00, >10000)
23. -13.358 ± 2.383	17.1 %	F6P.c <=> EC3.c + GAP.c (net)	(-17.22, -7.92)
24. 1.096 ± 2.898	>100 %	F6P.c <=> EC3.c + GAP.c (exch)	(0.00, 11.30)
25. 13.358 ± 2.383	18.9 %	S7P.c <=> EC3.c + E4P.c (net)	(7.92, 17.22)
26. (>1000, >1e4) ± >10000	>100 %	S7P.c <=> EC3.c + E4P.c (exch)	(0.00, >10000)
27. 259.478 ± 28.071	11.2 %	Pyr.c <=> Lact.c (net)	(204.70, 314.18)
28. (>1e4, >1e4) ± >10000	88.4 %	Pyr.c <=> Lact.c (exch)	(422.37, >10000)
29. 112.236 ± 47.312	47.5 %	Pyr.c -> Pyr.snk	(19.28, 203.79)
30. 23.143 ± 12.503	69.2 %	Pyr.c -> Pyr.m	(0.01, 48.78)
31. 19.393 ± 9.948	58.9 %	Pyr.m -> CO2 + AcCoA.m	(0.00, 38.80)
32. 61.342 ± 6.497	11.0 %	AcCoA.m + OAC.m -> Cit.m	(46.02, 71.36)
33. 47.663 ± 4.754	10.3 %	Cit.m <=> AKG.m + CO2 (net)	(37.24, 55.78)
34. 21.424 ± 2.324	11.1 %	Cit.m <=> AKG.m + CO2 (exch)	(16.66, 25.73)
35. 81.418 ± 6.179	7.7 %	AKG.m -> CO2 + Suc.m	(69.68, 93.78)
36. 96.201 ± 8.607	9.1 %	Suc.m <=> Fum.m (net)	(78.87, 112.43)
37. (0.0, >1000) ± >1000	>100 %	Suc.m <=> Fum.m (exch)	(0.00, >10000)
38. 103.768 ± 9.163	9.0 %	Fum.m <=> Mal.m (net)	(85.12, 120.85)
39. (>1000, >1e4) ± >1000	81.9 %	Fum.m <=> Mal.m (exch)	(26.33, >10000)
40. 57.591 ± 8.226	15.1 %	Mal.m <=> OAC.m (net)	(38.80, 70.89)

Table D.2 (continued) MFA results for the MCF-10A cells for the high-lactate condition. Fluxes measured in nmol/10^6 cells/h.

Flux ± SD	%SD	Reaction	Confidence Interval
41. (>1000, >1e4) ± >1000	45.7 %	Mal.m <=> OAC.m (exch)	(>1000, >10000)
42. 0.000 ± 1.531	>100 %	Mal.m -> Pyr.mII + CO2	(0.00, 5.97)
43. 3.750 ± 4.212	>100 %	Pyr.mII + CO2 -> OAC.m	(0.00, 16.43)
44. 3.750 ± 4.255	>100 %	Pyr.m <=> Pyr.mII (net)	(-0.37, 16.23)
45. (0.0, >1e4) ± >10000	>100 %	Pyr.m <=> Pyr.mII (exch)	(0.00, >10000)
46. 51.461 ± 6.902	13.9 %	Mal.c -> Pyr.c + CO2	(35.59, 62.50)
47. 46.177 ± 7.135	16.3 %	Mal.m <=> Mal.c (net)	(33.11, 60.93)
48. (>1000, >1e4) ± >1000	61.7 %	Mal.m <=> Mal.c (exch)	(>1000, >10000)
49. -5.284 ± 5.685	90.0 %	Mal.c <=> OAC.c (net)	(-13.03, 9.14)
50. (>1000, >1e4) ± >1000	83.0 %	Mal.c <=> OAC.c (exch)	(>1000, >10000)
51. -0.000 ± 2.754	>100 %	OAC.c -> PEP.c + CO2	(0.00, 10.74)
52. 13.679 ± 4.529	36.8 %	Cit.m <=> Cit.c (net)	(2.61, 20.28)
53. (0.0, >1e4) ± >10000	>100 %	Cit.m <=> Cit.c (exch)	(0.00, >10000)
54. 13.679 ± 4.529	36.8 %	Cit.c -> AcCoA.c + OAC.c	(2.61, 20.28)
55. 13.679 ± 4.568	37.1 %	AcCoA.c -> FA.c	(2.61, 20.43)
56. 51.080 ± 4.110	8.2 %	Gln.c -> Glu.c	(43.44, 59.47)
57. 33.755 ± 3.913	12.0 %	Glu.c <=> AKG.m (net)	(26.65, 41.91)
58. (272.8, >1e4) ± >1000	>100 %	Glu.c <=> AKG.m (exch)	(247.06, >10000)
59. 3.017 ± 0.703	24.8 %	Glu.c <=> Pro.c (net)	(1.60, 4.35)
60. (0.0, >1e4) ± >10000	>100 %	Glu.c <=> Pro.c (exch)	(0.00, >10000)

Table D.2 (continued) MFA results for the MCF-10A cells for the high-lactate condition. Fluxes measured in nmol/10^6 cells/h.

Flux ± SD	%SD	Reaction	Confidence Interval
61. -8.395 ± 2.196	24.5 %	Asp.c <=> OAC.c (net)	(-12.66, -4.09)
62. (0.0, >1e4) ± >1000	>100 %	Asp.c <=> OAC.c (exch)	(0.00, >10000)
63. 1.857 ± 0.469	26.6 %	Asp.c -> Asn.c	(0.88, 2.71)
64. 13.849 ± 5.087	40.8 %	Pyr.c <=> Ala.c (net)	(3.93, 23.76)
65. (0.0, >1e4) ± >10000	>100 %	Pyr.c <=> Ala.c (exch)	(0.00, >10000)
66. 20.889 ± 7.360	39.8 %	Ser.c <=> Pyr.c (net)	(6.68, 35.38)
67. (754.3, >1e4) ± >1000	>100 %	Ser.c <=> Pyr.c (exch)	(0.00, >10000)
68. 9.442 ± 3.256	37.6 %	Ser.c -> Gly.c + MEETHF	(2.78, 15.48)
68. 9.442 ± 3.256	37.6 %	Ser.c -> Gly.c + MEETHF	(2.78, 15.48)
70. 1.243 ± 0.828	89.9 %	Met.c + CO2 -> Suc.m + CO2 + MEETHF	(0.00, 3.23)
71. 4.490 ± 2.614	71.1 %	Val.c + CO2 -> Suc.m + 2 CO2	(0.00, 10.20)
72. 9.050 ± 3.724	46.6 %	Ile.c + CO2 -> Suc.m + AcCoA.m + CO2	(1.54, 16.06)
73. 3.669 ± 1.916	62.2 %	Phe.c -> Fum.m + 2 AcCoA.m + CO2	(0.00, 7.47)
74. 3.899 ± 1.948	58.6 %	Tyr.c -> Fum.m + 2 AcCoA.m + CO2	(0.09, 7.69)
75. 5.921 ± 3.048	60.1 %	Leu.c + CO2 -> 3 AcCoA.m + CO2	(0.00, 11.89)
76. 53.122 ± 4.164	8.0 %	Gln.ext -> Gln.c	(45.38, 61.62)
77. 4.263 ± 1.959	53.7 %	Asp.c -> Asp.ext	(0.42, 8.06)
78. 11.139 ± 3.748	37.3 %	Ile.ext -> Ile.c	(3.63, 18.25)
79. 9.542 ± 3.039	34.8 %	Leu.ext -> Leu.c	(3.65, 15.50)
80. 2.125 ± 0.890	49.1 %	Met.ext -> Met.c	(0.60, 4.07)

Table D.2 (continued) MFA results for the MCF-10A cells for the high-lactate condition. Fluxes measured in nmol/10^6 cells/h.

Flux ± SD	%SD	Reaction	Confidence Interval
81. 5.061 ± 1.932	43.0 %	Phe.ext -> Phe.c	(1.29, 8.82)
82. 33.070 ± 6.619	21.5 %	Ser.ext -> Ser.c	(20.33, 46.15)
83. 5.060 ± 1.941	43.2 %	Tyr.ext -> Tyr.c	(1.26, 8.82)
84. 7.136 ± 2.765	44.6 %	Val.ext -> Val.c	(2.02, 12.80)
85. 2.460 ± 0.743	31.9 %	Thr.ext -> Thr.c	(1.34, 4.24)
86. 2.414 ± 0.609	26.6 %	Arg.ext -> Arg.c	(1.15, 3.52)
87. 0.928 ± 0.234	26.6 %	Cys.ext -> Cys.c	(0.44, 1.36)
88. 0.928 ± 0.234	26.6 %	His.ext -> His.c	(0.44, 1.36)
89. 3.667 ± 0.925	26.6 %	Lys.ext -> Lys.c	(1.74, 5.35)
90. 0.279 ± 0.070	26.6 %	Trp.ext -> Trp.c	(0.13, 0.41)
91. 9.996 ± 4.998	59.4 %	Ala.c -> Ala.ext	(0.25, 19.75)
92. 6.007 ± 3.006	57.1 %	Gly.c -> Gly.ext	(0.13, 11.86)
93. 1.021 ± 0.499	55.9 %	Pro.c -> Pro.ext	(0.04, 1.99)
94. 11.847 ± 4.262	40.6 %	Glu.c -> Glu.ext	(3.30, 19.92)
95. 280.600 ± 28.088	10.3 %	Lact.c -> Lact.ext	(225.69, 335.24)
96. 21.122 ± 1.977	9.6 %	Lact.tr -> Lact.c	(17.26, 24.97)
97. 26.717 ± 4.765	18.9 %	Ru5P.c <=> X5P.c (net)	(15.85, 34.43)
98. (>1e4, >1e4) ± >10000	>100 %	Ru5P.c <=> X5P.c (exch)	(0.00, >10000)
99. 46.421 ± 11.713	Biomass Equation (v72)		(22.07, 67.76)
100. 13.679 ± 4.568	37.1 %	FA.c -> Lipids	(2.61, 20.43)

Table D.3 MFA results for the MCF-7 cells for the control condition. Fluxes measured in nmol/10^6 cells/h.

Flux ± SD	%SD	Reaction	Confidence Interval
1. 205.809 ± 18.276	9.1 %	Gluc.ext -> G6P.c	(171.39, 242.66)
2. 162.152 ± 14.524	9.2 %	G6P.c <=> F6P.c (net)	(134.74, 191.39)
3. (>1000, >1e4) ± >1000	>100 %	G6P.c <=> F6P.c (exch)	(0.00, >10000)
4. 189.819 ± 16.839	9.1 %	F6P.c -> FBP.c	(158.01, 223.68)
5. 189.819 ± 16.839	9.1 %	FBP.c <=> DHAP.c + GAP.c (net)	(158.01, 223.68)
6. (0.0, >1e4) ± >10000	>100 %	FBP.c <=> DHAP.c + GAP.c (exch)	(0.00, >10000)
7. 189.819 ± 16.839	9.1 %	DHAP.c <=> GAP.c (net)	(158.01, 223.68)
8. (>1000, >1000) ± >1000	57.6 %	DHAP.c <=> GAP.c (exch)	(>1000, >10000)
9. 393.472 ± 35.037	9.1 %	GAP.c <=> 3PG.c (net)	(327.30, 463.95)
10. (205.5, 646.5) ± >1000	>100 %	GAP.c <=> 3PG.c (exch)	(0.00, >10000)
11. 393.472 ± 35.037	9.1 %	3PG.c <=> PEP.c (net)	(327.30, 463.95)
12. (>1000, >1e4) ± >1000	>100 %	3PG.c <=> PEP.c (exch)	(236.98, >10000)
13. 410.146 ± 36.903	9.3 %	PEP.c -> Pyr.c	(340.60, 484.52)
14. 42.487 ± 7.252	17.9 %	G6P.c -> CO2 + Ru5P.c	(27.37, 55.65)
15. 13.834 ± 2.431	18.4 %	Ru5P.c <=> R5P.c (net)	(8.78, 18.26)
16. (>1000, >1e4) ± >1000	>100 %	Ru5P.c <=> R5P.c (exch)	(0.00, >10000)
17. 27.667 ± 4.861	18.4 %	X5P.c <=> EC2.c + GAP.c (net)	(17.55, 36.51)
18. (402.5, >1e4) ± >1000	>100 %	X5P.c <=> EC2.c + GAP.c (exch)	(0.00, >10000)
19. -13.834 ± 2.431	16.9 %	F6P.c <=> EC2.c + E4P.c (net)	(-18.26, -8.78)
20. 0.000 ± 2.752	>100 %	F6P.c <=> EC2.c + E4P.c (exch)	(0.00, 10.73)

Table D.3 (continued) MFA results for the MCF-7 cells for the control condition. Fluxes measured in nmol/10^6 cells/h.

Flux ± SD	%SD	Reaction	Confidence Interval
21. -13.834 ± 2.431	16.9 %	S7P.c <=> EC2.c + R5P.c (net)	(-18.26, -8.78)
22. 4.655 ± 3.330	95.3 %	S7P.c <=> EC2.c + R5P.c (exch)	(0.00, 12.99)
23. -13.834 ± 2.431	16.9 %	F6P.c <=> EC3.c + GAP.c (net)	(-18.26, -8.78)
24. (675.1, >1e4) ± >1000	>100 %	F6P.c <=> EC3.c + GAP.c (exch)	(0.00, >10000)
25. 13.834 ± 2.431	18.4 %	S7P.c <=> EC3.c + E4P.c (net)	(8.78, 18.26)
26. (>1000, >1e4) ± >1000	>100 %	S7P.c <=> EC3.c + E4P.c (exch)	(0.00, >10000)
27. 331.000 ± 33.045	10.3 %	Pyr.c <=> Lact.c (net)	(266.48, 395.35)
28. (0.0, >1e4) ± >1000	>100 %	Pyr.c <=> Lact.c (exch)	(0.00, >10000)
29. 56.896 ± 44.056	>100 %	Pyr.c -> Pyr.snk	(0.00, 171.82)
30. 60.250 ± 17.573	32.2 %	Pyr.c -> Pyr.m	(25.72, 94.25)
31. 60.250 ± 17.573	32.2 %	Pyr.m -> CO2 + AcCoA.m	(25.72, 94.25)
32. 94.227 ± 14.882	16.4 %	AcCoA.m + OAC.m -> Cit.m	(65.05, 123.10)
33. 40.127 ± 5.041	13.1 %	Cit.m <=> AKG.m + CO2 (net)	(30.55, 50.21)
34. 3.967 ± 1.659	47.6 %	Cit.m <=> AKG.m + CO2 (exch)	(1.00, 7.47)
35. 69.094 ± 6.349	9.4 %	AKG.m -> CO2 + Suc.m	(56.96, 81.72)
36. 87.333 ± 11.084	13.2 %	Suc.m <=> Fum.m (net)	(65.93, 109.16)
37. 10.895 ± 14.681	>100 %	Suc.m <=> Fum.m (exch)	(0.00, 57.26)
38. 94.976 ± 11.765	12.8 %	Fum.m <=> Mal.m (net)	(72.21, 118.09)
39. (0.0, >1e4) ± >1000	>100 %	Fum.m <=> Mal.m (exch)	(0.00, >10000)
40. 79.960 ± 15.910	21.0 %	Mal.m <=> OAC.m (net)	(48.57, 110.62)

Table D.3 (continued) MFA results for the MCF-7 cells for the control condition. Fluxes measured in nmol/10^6 cells/h.

Flux ± SD	%SD	Reaction	Confidence Interval
41. (110.4, 182.5) ± >100	>100 %	Mal.m <=> OAC.m (exch)	(1.38, >1000)
42. 14.267 ± 3.536	26.8 %	Mal.m -> Pyr.mII + CO2	(7.63, 21.42)
43. 14.267 ± 4.837	36.7 %	Pyr.mII + CO2 -> OAC.m	(7.63, 26.50)
44. 0.000 ± 2.930	>100 %	Pyr.m <=> Pyr.mII (net)	(-1.57, 9.86)
45. -0.000 ± 0.424	>100 %	Pyr.m <=> Pyr.mII (exch)	(-0.00, 1.65)
46. 28.870 ± 8.750	33.6 %	Mal.c -> Pyr.c + CO2	(12.22, 46.35)
47. 0.749 ± 17.414	>100 %	Mal.m <=> Mal.c (net)	(-32.56, 35.36)
48. (413.7, >1e4) ± >1000	>100 %	Mal.m <=> Mal.c (exch)	(0.00, >10000)
49. -28.121 ± 15.864	48.8 %	Mal.c <=> OAC.c (net)	(-59.10, 2.77)
50. (>1000, >1e4) ± >1000	>100 %	Mal.c <=> OAC.c (exch)	(>1000, >10000)
51. 16.673 ± 6.548	44.5 %	OAC.c -> PEP.c + CO2	(4.86, 30.40)
52. 54.100 ± 14.859	30.0 %	Cit.m <=> Cit.c (net)	(24.72, 82.67)
53. (0.0, >1e4) ± >10000	>100 %	Cit.m <=> Cit.c (exch)	(0.00, >10000)
54. 54.100 ± 14.859	30.0 %	Cit.c -> AcCoA.c + OAC.c	(24.72, 82.67)
55. 54.100 ± 14.859	30.0 %	AcCoA.c -> FA.c	(24.72, 82.67)
56. 46.696 ± 4.090	8.9 %	Gln.c -> Glu.c	(38.79, 54.74)
57. 28.967 ± 4.193	15.1 %	Glu.c <=> AKG.m (net)	(20.86, 37.22)
58. (>1000, >1000) ± >1000	>100 %	Glu.c <=> AKG.m (exch)	(639.25, >10000)
59. 2.352 ± 0.605	27.8 %	Glu.c <=> Pro.c (net)	(1.17, 3.53)
60. (0.0, >1e4) ± >10000	>100 %	Glu.c <=> Pro.c (exch)	(0.00, >10000)

Table D.3 (continued) MFA results for the MCF-7 cells for the control condition. Fluxes measured in nmol/10^6 cells/h.

Flux ± SD	%SD	Reaction	Confidence Interval
61. -9.306 ± 2.986	29.5 %	Asp.c <=> OAC.c (net)	(-15.13, -3.49)
62. (0.0, >1e4) ± >10000	>100 %	Asp.c <=> OAC.c (exch)	(0.00, >10000)
63. 1.232 ± 0.320	28.2 %	Asp.c -> Asn.c	(0.60, 1.85)
64. 16.557 ± 7.028	49.0 %	Pyr.c <=> Ala.c (net)	(2.85, 30.26)
65. (0.0, >1e4) ± >10000	>100 %	Pyr.c <=> Ala.c (exch)	(0.00, >10000)
66. 25.688 ± 7.937	33.9 %	Ser.c <=> Pyr.c (net)	(10.32, 41.27)
67. (>1000, >1e4) ± >1000	>100 %	Ser.c <=> Pyr.c (exch)	(17.54, >10000)
68. 11.241 ± 4.536	46.3 %	Ser.c -> Gly.c + MEETHF	(2.40, 20.09)
69. 0.000 ± 0.168	>100 %	Thr.c -> AcCoA.c + Gly.c	(0.00, 0.66)
70. 1.381 ± 0.859	80.8 %	Met.c + CO2 -> Suc.m + CO2 + MEETHF	(0.00, 3.35)
71. 6.572 ± 3.863	74.4 %	Val.c + CO2 -> Suc.m + 2 CO2	(0.00, 15.07)
72. 10.286 ± 4.894	53.8 %	Ile.c + CO2 -> Suc.m + AcCoA.m + CO2	(0.74, 19.82)
73. 3.744 ± 1.960	62.7 %	Phe.c -> Fum.m + 2 AcCoA.m + CO2	(0.00, 7.64)
74. 3.900 ± 1.997	60.9 %	Tyr.c -> Fum.m + 2 AcCoA.m + CO2	(0.00, 7.79)
75. 2.801 ± 1.748	80.1 %	Leu.c + CO2 -> 3 AcCoA.m + CO2	(0.00, 6.82)
76. 48.051 ± 4.132	8.8 %	Gln.ext -> Gln.c	(40.06, 56.17)
77. 6.564 ± 2.919	51.6 %	Asp.c -> Asp.ext	(0.88, 12.26)
78. 11.672 ± 4.866	46.6 %	Ile.ext -> Ile.c	(2.18, 21.16)
79. 5.204 ± 1.848	40.4 %	Leu.ext -> Leu.c	(1.83, 9.04)
80. 1.967 ± 0.899	54.4 %	Met.ext -> Met.c	(0.41, 3.91)

Table D.3 (continued) MFA results for the MCF-7 cells for the control condition. Fluxes measured in nmol/10^6 cells/h.

Flux ± SD	%SD	Reaction	Confidence Interval
81. 4.668 ± 1.974	49.0 %	Phe.ext -> Phe.c	(0.84, 8.55)
82. 38.747 ± 6.530	17.7 %	Ser.ext -> Ser.c	(26.10, 51.57)
83. 4.670 ± 1.989	49.4 %	Tyr.ext -> Tyr.c	(0.79, 8.55)
84. 8.328 ± 3.983	54.9 %	Val.ext -> Val.c	(1.26, 16.80)
85. 1.633 ± 0.420	27.9 %	Thr.ext -> Thr.c	(0.81, 2.45)
86. 1.602 ± 0.416	28.2 %	Arg.ext -> Arg.c	(0.78, 2.40)
87. 0.616 ± 0.160	28.2 %	Cys.ext -> Cys.c	(0.30, 0.92)
88. 0.616 ± 0.160	28.2 %	His.ext -> His.c	(0.30, 0.92)
89. 2.433 ± 0.632	28.2 %	Lys.ext -> Lys.c	(1.19, 3.65)
90. 0.185 ± 0.048	28.2 %	Trp.ext -> Trp.c	(0.09, 0.28)
91. 14.001 ± 6.998	59.4 %	Ala.c -> Ala.ext	(0.35, 27.65)
92. 8.962 ± 4.498	59.7 %	Gly.c -> Gly.ext	(0.19, 17.73)
93. 1.028 ± 0.499	57.7 %	Pro.c -> Pro.ext	(0.05, 2.00)
94. 13.744 ± 4.607	37.5 %	Glu.c -> Glu.ext	(4.77, 22.74)
95. 331.000 ± 33.045	10.3 %	Lact.c -> Lact.ext	(266.48, 395.35)
96. 27.667 ± 4.861	18.4 %	Ru5P.c <=> X5P.c (net)	(17.55, 36.51)
97. (402.5, >1e4) ± >1000	>100 %	Ru5P.c <=> X5P.c (exch)	(0.00, >10000)
98. 30.802 ± 8.006	Biomass equation (v72)		(15.02, 46.24)
99. 54.100 ± 14.859	30.0 %	FA.c -> Lipids	(24.72, 82.67)

Table D.4 MFA results for the MCF-7 cells for the high-lactate condition. Fluxes measured in nmol/10^6 cells/h.

Flux ± SD	%SD	Reaction	Confidence Interval
1. 169.893 ± 15.016	9.1 %	Gluc.ext -> G6P.c	(139.99, 198.55)
2. 128.736 ± 12.726	10.2 %	G6P.c <=> F6P.c (net)	(104.37, 154.00)
3. (543.3, >1e4) ± >1000	>100 %	G6P.c <=> F6P.c (exch)	(0.00, >10000)
4. 154.467 ± 13.998	9.4 %	F6P.c -> FBP.c	(126.57, 181.16)
5. 154.467 ± 13.998	9.4 %	FBP.c <=> DHAP.c + GAP.c (net)	(126.57, 181.16)
6. (0.0, >1e4) ± >10000	>100 %	FBP.c <=> DHAP.c + GAP.c (exch)	(0.00, >10000)
7. 154.467 ± 13.998	9.4 %	DHAP.c <=> GAP.c (net)	(126.57, 181.16)
8. 547.530 ± 75.292	14.3 %	DHAP.c <=> GAP.c (exch)	(424.97, 718.61)
9. 321.800 ± 29.029	9.3 %	GAP.c <=> 3PG.c (net)	(263.96, 377.18)
10. (0.0, >1000) ± >1000	>100 %	GAP.c <=> 3PG.c (exch)	(0.00, >10000)
11. 321.800 ± 29.029	9.3 %	3PG.c <=> PEP.c (net)	(263.96, 377.18)
12. (1.8, 64.2) ± >100	>100 %	3PG.c <=> PEP.c (exch)	(0.00, 744.14)
13. 340.597 ± 31.547	9.5 %	PEP.c -> Pyr.c	(278.00, 401.03)
14. 39.767 ± 6.463	16.7 %	G6P.c -> CO2 + Ru5P.c	(25.04, 50.25)
15. 12.866 ± 2.141	17.1 %	Ru5P.c <=> R5P.c (net)	(8.00, 16.35)
16. (361.1, >1e4) ± >1000	>100 %	Ru5P.c <=> R5P.c (exch)	(0.00, >10000)
17. 25.731 ± 4.282	17.1 %	X5P.c <=> EC2.c + GAP.c (net)	(15.99, 32.69)
18. (54.9, >1e4) ± >1000	>100 %	X5P.c <=> EC2.c + GAP.c (exch)	(0.00, >10000)
19. -12.866 ± 2.141	15.9 %	F6P.c <=> EC2.c + E4P.c (net)	(-16.35, -8.00)
20. 0.000 ± 2.052	>100 %	F6P.c <=> EC2.c + E4P.c (exch)	(0.00, 8.00)

Table D.4 (continued) MFA results for the MCF-7 cells for the high-lactate condition. Fluxes measured in nmol/10^6 cells/h.

Flux ± SD	%SD	Reaction	Confidence Interval
21. -12.866 ± 2.141	15.9 %	S7P.c <=> EC2.c + R5P.c (net)	(-16.35, -8.00)
22. (285.1, >1e4) ± >1000	>100 %	S7P.c <=> EC2.c + R5P.c (exch)	(0.00, >10000)
23. -12.866 ± 2.141	15.9 %	F6P.c <=> EC3.c + GAP.c (net)	(-16.35, -8.00)
24. (0.0, >1e4) ± >1000	>100 %	F6P.c <=> EC3.c + GAP.c (exch)	(0.00, >10000)
25. 12.866 ± 2.141	17.1 %	S7P.c <=> EC3.c + E4P.c (net)	(8.00, 16.35)
26. (283.5, >1e4) ± >1000	>100 %	S7P.c <=> EC3.c + E4P.c (exch)	(0.00, >10000)
27. 133.279 ± 19.894	15.7 %	Pyr.c <=> Lact.c (net)	(91.83, 169.42)
28. 279.857 ± >100	67.1 %	Pyr.c <=> Lact.c (exch)	(64.65, 729.62)
29. 167.594 ± 40.602	24.8 %	Pyr.c -> Pyr.snk	(92.44, 250.79)
30. 39.915 ± 13.667	38.8 %	Pyr.c -> Pyr.m	(13.31, 66.61)
31. 39.915 ± 12.927	36.7 %	Pyr.m -> CO2 + AcCoA.m	(13.31, 63.73)
32. 65.995 ± 8.067	12.6 %	AcCoA.m + OAC.m -> Cit.m	(48.02, 79.48)
33. 34.845 ± 4.598	13.7 %	Cit.m <=> AKG.m + CO2 (net)	(25.28, 43.21)
34. 29.833 ± 3.822	13.3 %	Cit.m <=> AKG.m + CO2 (exch)	(21.85, 36.76)
35. 53.962 ± 5.337	10.3 %	AKG.m -> CO2 + Suc.m	(42.98, 63.79)
36. 66.222 ± 7.798	12.1 %	Suc.m <=> Fum.m (net)	(49.14, 79.55)
37. (58.5, >1e4) ± >1000	>100 %	Suc.m <=> Fum.m (exch)	(0.00, >10000)
38. 70.945 ± 7.927	11.4 %	Fum.m <=> Mal.m (net)	(53.79, 84.70)
39. (26.3, >1000) ± >1000	>100 %	Fum.m <=> Mal.m (exch)	(0.00, >10000)
40. 61.376 ± 7.827	12.9 %	Mal.m <=> OAC.m (net)	(44.79, 75.31)

Table D.4 (continued) MFA results for the MCF-7 cells for the high-lactate condition. Fluxes measured in nmol/10^6 cells/h.

Flux ± SD	%SD	Reaction	Confidence Interval
41. (16.9, 37.2) ± >1000	>100 %	Mal.m <=> OAC.m (exch)	(0.00, >10000)
42. 4.618 ± 1.799	39.9 %	Mal.m -> Pyr.mII + CO2	(0.98, 7.99)
43. 4.618 ± 3.027	72.6 %	Pyr.mII + CO2 -> OAC.m	(0.81, 12.61)
44. 0.000 ± 2.500	>100 %	Pyr.m <=> Pyr.mII (net)	(-1.17, 8.58)
45. 0.000 ± 0.300	>100 %	Pyr.m <=> Pyr.mII (exch)	(0.00, 1.17)
46. 4.951 ± 4.072	>100 %	Mal.c -> Pyr.c + CO2	(0.00, 15.88)
47. 4.951 ± 7.500	>100 %	Mal.m <=> Mal.c (net)	(-5.06, 24.19)
48. (0.0, >1e4) ± >1000	>100 %	Mal.m <=> Mal.c (exch)	(0.00, >10000)
49. -0.000 ± 9.823	>100 %	Mal.c <=> OAC.c (net)	(-14.02, 24.29)
50. (0.0, 1.0) ± >1000	>100 %	Mal.c <=> OAC.c (exch)	(0.00, >10000)
51. 18.797 ± 5.457	31.8 %	OAC.c -> PEP.c + CO2	(8.66, 29.94)
52. 31.150 ± 8.164	27.6 %	Cit.m <=> Cit.c (net)	(12.02, 43.86)
53. (0.0, >1e4) ± >10000	>100 %	Cit.m <=> Cit.c (exch)	(0.00, >10000)
54. 31.150 ± 8.164	27.6 %	Cit.c -> AcCoA.c + OAC.c	(12.02, 43.86)
55. 31.150 ± 7.203	24.3 %	AcCoA.c -> FA.c	(15.55, 43.64)
56. 43.820 ± 3.913	9.1 %	Gln.c -> Glu.c	(36.04, 51.30)
57. 19.117 ± 3.432	18.4 %	Glu.c <=> AKG.m (net)	(12.23, 25.61)
58. 134.232 ± 18.456	14.3 %	Glu.c <=> AKG.m (exch)	(101.63, 173.61)
59. 3.803 ± 1.030	29.3 %	Glu.c <=> Pro.c (net)	(1.81, 5.83)
60. (0.0, >1e4) ± >10000	>100 %	Glu.c <=> Pro.c (exch)	(0.00, >10000)

Table D.4 (continued) MFA results for the MCF-7 cells for the high-lactate condition. Fluxes measured in nmol/10^6 cells/h.

Flux ± SD	%SD	Reaction	Confidence Interval
61. -12.353 ± 2.846	21.8 %	Asp.c <=> OAC.c (net)	(-17.97, -6.87)
62. (0.0, >1e4) ± >10000	>100 %	Asp.c <=> OAC.c (exch)	(0.00, >10000)
63. 1.463 ± 0.240	16.5 %	Asp.c -> Asn.c	(1.11, 2.04)
64. 13.999 ± 5.510	44.9 %	Pyr.c <=> Ala.c (net)	(3.24, 24.73)
65. (0.0, >1e4) ± >10000	>100 %	Pyr.c <=> Ala.c (exch)	(0.00, >10000)
66. 9.239 ± 10.787	>100 %	Ser.c <=> Pyr.c (net)	(-11.46, 30.61)
67. (389.9, >1e4) ± >1000	>100 %	Ser.c <=> Pyr.c (exch)	(0.00, >10000)
68. 11.653 ± 4.513	44.0 %	Ser.c -> Gly.c + MEETHF	(2.85, 20.45)
69. 0.000 ± 0.124	>100 %	Thr.c -> AcCoA.c + Gly.c	(0.00, 0.48)
70. 1.221 ± 0.811	79.5 %	Met.c + CO2 -> Suc.m + CO2 + MEETHF	(0.00, 3.16)
71. 5.697 ± 3.255	61.6 %	Val.c + CO2 -> Suc.m + 2 CO2	(0.00, 12.70)
72. 5.342 ± 3.108	62.7 %	Ile.c + CO2 -> Suc.m + AcCoA.m + CO2	(0.00, 12.12)
73. 2.201 ± 1.602	83.9 %	Phe.c -> Fum.m + 2 AcCoA.m + CO2	(0.00, 6.25)
74. 2.522 ± 1.645	74.2 %	Tyr.c -> Fum.m + 2 AcCoA.m + CO2	(0.00, 6.42)
75. 3.764 ± 2.626	95.3 %	Leu.c + CO2 -> 3 AcCoA.m + CO2	(0.00, 10.24)
76. 45.429 ± 3.936	8.8 %	Gln.ext -> Gln.c	(37.61, 52.96)
77. 9.099 ± 2.815	33.7 %	Asp.c -> Asp.ext	(3.70, 14.68)
78. 6.988 ± 3.171	48.0 %	Ile.ext -> Ile.c	(1.48, 13.85)
79. 6.616 ± 2.707	48.5 %	Leu.ext -> Leu.c	(2.42, 12.98) |
80. 1.916 ± 0.830	48.6 %	Met.ext -> Met.c	(0.60, 3.84)

Table D.4 (continued) MFA results for the MCF-7 cells for the high-lactate condition. Fluxes measured in nmol/10^6 cells/h.

Flux ± SD	%SD	Reaction	Confidence Interval
81. 3.298 ± 1.639	54.6 %	Phe.ext -> Phe.c	(0.94, 7.33)
82. 23.050 ± 9.789	47.6 %	Ser.ext -> Ser.c	(4.37, 42.55)
83. 3.436 ± 1.672	53.4 %	Tyr.ext -> Tyr.c	(0.80, 7.32)
84. 7.782 ± 3.329	45.2 %	Val.ext -> Val.c	(1.90, 14.88)
85. 1.938 ± 0.339	18.5 %	Thr.ext -> Thr.c	(1.14, 2.46)
86. 1.902 ± 0.311	16.5 %	Arg.ext -> Arg.c	(1.44, 2.66)
87. 0.731 ± 0.120	16.5 %	Cys.ext -> Cys.c	(0.55, 1.02)
88. 0.731 ± 0.120	16.5 %	His.ext -> His.c	(0.55, 1.02)
89. 2.889 ± 0.473	16.5 %	Lys.ext -> Lys.c	(2.19, 4.04)
90. 0.219 ± 0.036	16.5 %	Trp.ext -> Trp.c	(0.17, 0.31)
91. 10.963 ± 5.498	59.4 %	Ala.c -> Ala.ext	(0.28, 21.72)
92. 8.947 ± 4.497	59.4 %	Gly.c -> Gly.ext	(0.22, 17.76)
93. 2.231 ± 0.988	50.5 %	Pro.c -> Pro.ext	(0.33, 4.19)
94. 18.962 ± 4.446	24.9 %	Glu.c -> Glu.ext	(10.43, 27.77)
95. 175.999 ± 17.520	10.3 %	Lact.c -> Lact.ext	(141.51, 209.84)
96. 42.719 ± 12.711	31.1 %	Lact.tr -> Lact.c	(23.23, 72.81)
97. 25.731 ± 4.282	17.1 %	Ru5P.c <=> X5P.c (net)	(15.99, 32.69)
98. (54.9, >1e4) ± >1000	>100 %	Ru5P.c <=> X5P.c (exch)	(0.00, >10000)
99. 36.571 ± 5.988	16.5 %	Biomass equation (v72)	(27.73, 51.09)
100. 31.150 ± 7.203	24.3 %	FA.c -> Lipids	(15.55, 43.64)

Table D.5 MFA results for the MDA-MB-231 cells for the control condition. Fluxes measured in nmol/10^6 cells/h.

Flux ± SD	%SD	Reaction	Confidence Interval
1. 367.744 ± 29.665	8.3 %	Gluc.ext -> G6P.c	(314.56, 430.25)
2. 286.820 ± 25.084	9.0 %	G6P.c <=> F6P.c (net)	(241.50, 339.33)
3. (0.0, >1000) ± >1000	>100 %	G6P.c <=> F6P.c (exch)	(0.00, >10000)
4. 339.152 ± 26.946	8.2 %	F6P.c -> FBP.c	(291.03, 396.12)
5. 339.152 ± 26.946	8.2 %	FBP.c <=> DHAP.c + GAP.c (net)	(291.03, 396.12)
6. (0.0, >1e4) ± >10000	>100 %	FBP.c <=> DHAP.c + GAP.c (exch)	(0.00, >10000)
7. 339.152 ± 26.946	8.2 %	DHAP.c <=> GAP.c (net)	(291.03, 396.12)
8. 1224.863 ± >100	12.4 %	DHAP.c <=> GAP.c (exch)	(982.48, >1000)
9. 704.470 ± 56.310	8.2 %	GAP.c <=> 3PG.c (net)	(603.67, 823.28)
10. (0.0, >1000) ± >1000	>100 %	GAP.c <=> 3PG.c (exch)	(0.00, >10000)
11. 704.470 ± 56.310	8.2 %	3PG.c <=> PEP.c (net)	(603.67, 823.28)
12. (697.2, >1e4) ± >1000	>100 %	3PG.c <=> PEP.c (exch)	(0.00, >10000)
13. 709.705 ± 57.900	8.4 %	PEP.c -> Pyr.c	(606.71, 832.52)
14. 79.607 ± 13.946	18.7 %	G6P.c -> CO2 + Ru5P.c	(53.92, 108.31)
15. 26.166 ± 4.647	19.0 %	Ru5P.c <=> R5P.c (net)	(17.61, 35.74)
16. (0.0, >1e4) ± >10000	>100 %	Ru5P.c <=> R5P.c (exch)	(0.00, >10000)
17. 52.332 ± 9.293	19.0 %	X5P.c <=> EC2.c + GAP.c (net)	(35.23, 71.47)
18. (0.0, >1e4) ± >1000	>100 %	X5P.c <=> EC2.c + GAP.c (exch)	(0.00, >10000)
19. -26.166 ± 4.647	16.6 %	F6P.c <=> EC2.c + E4P.c (net)	(-35.74, -17.61)
20. 6.289 ± 6.347	>100 %	F6P.c <=> EC2.c + E4P.c (exch)	(0.00, 24.75)

21. -26.166 ± 4.647	16.6 %	S7P.c <=> EC2.c + R5P.c (net)	(-35.74, -17.61)
22. (0.0, >1e4) ± >1000	>100 %	S7P.c <=> EC2.c + R5P.c (exch)	(0.00, >10000)
23. -26.166 ± 4.647	16.6 %	F6P.c <=> EC3.c + GAP.c (net)	(-35.74, -17.61)
24. (0.0, >1e4) ± >1000	>100 %	F6P.c <=> EC3.c + GAP.c (exch)	(0.00, >10000)
25. 26.166 ± 4.647	19.0 %	S7P.c <=> EC3.c + E4P.c (net)	(17.61, 35.74)
26. (0.0, >1e4) ± >10000	>100 %	S7P.c <=> EC3.c + E4P.c (exch)	(0.00, >10000)
27. 615.000 ± 55.905	9.4 %	Pyr.c <=> Lact.c (net)	(495.11, 713.15)
28. (0.0, >1e4) ± >1000	>100 %	Pyr.c <=> Lact.c (exch)	(0.00, >10000)
29. (0.0, 43.7) ± 51.914	>100 %	Pyr.c -> Pyr.snk	(0.00, 202.46)
30. 101.038 ± 30.524	36.2 %	Pyr.c -> Pyr.m	(49.49, 168.53)
31. 93.498 ± 27.433	33.9 %	Pyr.m -> CO2 + AcCoA.m	(46.40, 153.39)
32. 113.406 ± 26.704	26.5 %	AcCoA.m + OAC.m -> Cit.m	(66.91, 171.05)
33. 34.300 ± 4.465	14.1 %	Cit.m <=> AKG.m + CO2 (net)	(23.20, 40.61)
34. 5.606 ± 1.624	31.2 %	Cit.m <=> AKG.m + CO2 (exch)	(2.69, 9.02)
35. 52.635 ± 5.817	11.5 %	AKG.m -> CO2 + Suc.m	(40.25, 62.94)
36. 62.617 ± 8.055	13.4 %	Suc.m <=> Fum.m (net)	(45.41, 76.83)
37. (0.0, >1e4) ± >1000	>100 %	Suc.m <=> Fum.m (exch)	(0.00, >10000)
38. 68.821 ± 8.852	13.4 %	Fum.m <=> Mal.m (net)	(50.17, 84.70)
39. (0.0, 6.2) ± >1000	>100 %	Fum.m <=> Mal.m (exch)	(0.00, >10000)
40. 91.078 ± 23.928	29.2 %	Mal.m <=> OAC.m (net)	(50.09, 143.41)
41. 22.999 ± 42.782	>100 %	Mal.m <=> OAC.m (exch)	(0.00, 166.85)
42. 14.787 ± 2.568	17.5 %	Mal.m -> Pyr.mII + CO2	(10.22, 20.24)
43. 22.328 ± 6.977	38.8 %	Pyr.mII + CO2 -> OAC.m	(10.13, 37.35)
44. 7.540 ± 5.901	>100 %	Pyr.m <=> Pyr.mII (net)	(-1.13, 21.89)

Table D.5 (Continued) MFA results for the MDA-MB-231 cells for the control condition. Fluxes measured in nmol/10^6 cells/h.

Flux ± SD	%SD	Reaction	Confidence Interval
45. 0.000 ± 0.663	>100 %	Pyr.m <=> Pyr.mII (exch)	(0.00, 2.59)
46. 33.742 ± 12.740	44.3 %	Mal.c -> Pyr.c + CO2	(3.90, 53.58)
47. (-45.6, -33.8) ± 20.667	45.4 %	Mal.m <=> Mal.c (net)	(-85.00, -4.40)
48. (0.0, 2.0) ± >1000	>100 %	Mal.m <=> Mal.c (exch)	(0.00, >10000)
49. (-82.5, -59.3) ± 26.084	31.6 %	Mal.c <=> OAC.c (net)	(-128.92, -27.20)
50. (0.0, >1e4) ± >1000	>100 %	Mal.c <=> OAC.c (exch)	(0.00, >10000)
51. 5.235 ± 9.700	>100 %	OAC.c -> PEP.c + CO2	(0.00, 37.83)
52. 79.106 ± 24.083	35.0 %	Cit.m <=> Cit.c (net)	(39.36, 133.28)
53. (0.0, >1e4) ± >10000	>100 %	Cit.m <=> Cit.c (exch)	(0.00, >10000)
54. 79.106 ± 24.083	35.0 %	Cit.c -> AcCoA.c + OAC.c	(39.36, 133.28)
55. 79.106 ± 24.145	35.1 %	AcCoA.c -> FA.c	(39.12, 133.28)
56. 39.828 ± 4.040	10.5 %	Gln.c -> Glu.c	(32.54, 48.29)
57. 18.335 ± 4.199	24.7 %	Glu.c <=> AKG.m (net)	(10.90, 27.27)
58. (>1000, >1e4) ± >1000	>100 %	Glu.c <=> AKG.m (exch)	(612.11, >10000)
59. 2.561 ± 0.610	25.7 %	Glu.c <=> Pro.c (net)	(1.37, 3.75)
60. (0.0, >1e4) ± >10000	>100 %	Glu.c <=> Pro.c (exch)	(0.00, >10000)
61. -3.085 ± 0.939	28.3 %	Asp.c <=> OAC.c (net)	(-5.32, -1.66)
62. (0.0, >1e4) ± >10000	>100 %	Asp.c <=> OAC.c (exch)	(0.00, >10000)
63. 1.386 ± 0.329	25.4 %	Asp.c -> Asn.c	(0.74, 2.03)
64. 13.877 ± 5.540	45.7 %	Pyr.c <=> Ala.c (net)	(3.08, 24.68)

Table D.5 (Continued) MFA results for the MDA-MB-231 cells for the control condition. Fluxes measured in nmol/10^6 cells/h.

Flux ± SD	%SD	Reaction	Confidence Interval
65. (0.0, >1e4) ± >10000	>100 %	Pyr.c <=> Ala.c (exch)	(0.00, >10000)
66. 5.253 ± 8.372	>100 %	Ser.c <=> Pyr.c (net)	(-10.67, 21.98)
67. (812.9, >1e4) ± >1000	>100 %	Ser.c <=> Pyr.c (exch)	(812.88, >10000)
68. 10.561 ± 4.047	43.6 %	Ser.c -> Gly.c + MEETHF	(2.67, 18.45)
69. 0.000 ± 0.138	>100 %	Thr.c -> AcCoA.c + Gly.c	(0.00, 0.54)
70. 1.350 ± 0.852	82.8 %	Met.c + CO2 -> Suc.m + CO2 + MEETHF	(0.00, 3.32)
71. 5.124 ± 3.073	76.6 %	Val.c + CO2 -> Suc.m + 2 CO2	(0.00, 11.98)
72. 3.509 ± 2.160	79.6 %	Ile.c + CO2 -> Suc.m + AcCoA.m + CO2	(0.00, 8.42)
73. 3.015 ± 1.782	74.8 %	Phe.c -> Fum.m + 2 AcCoA.m + CO2	(0.00, 6.95)
74. 3.189 ± 1.825	71.4 %	Tyr.c -> Fum.m + 2 AcCoA.m + CO2	(0.00, 7.12)
75. 1.331 ± 1.389	>100 %	Leu.c + CO2 -> 3 AcCoA.m + CO2	(0.00, 5.42)
76. 41.353 ± 4.074	10.2 %	Gln.ext -> Gln.c	(33.99, 49.88)
77. 0.000 ± 0.497	>100 %	Asp.c -> Asp.ext	(0.00, 1.94)
78. 5.068 ± 2.255	52.7 %	Ile.ext -> Ile.c	(1.14, 9.93)
79. 4.034 ± 1.598	47.0 %	Leu.ext -> Leu.c	(1.70, 7.94)
80. 2.008 ± 0.895	52.9 %	Met.ext -> Met.c	(0.47, 3.96)
81. 4.055 ± 1.841	53.8 %	Phe.ext -> Phe.c	(0.78, 7.96)
82. 17.858 ± 7.209	44.9 %	Ser.ext -> Ser.c	(4.24, 32.36)
83. 4.055 ± 1.869	54.6 %	Tyr.ext -> Tyr.c	(0.67, 7.96)
84. 7.099 ± 3.194	53.2 %	Val.ext -> Val.c	(1.46, 13.92)

Table D.5 (Continued) MFA results for the MDA-MB-231 cells for the control condition. Fluxes measured in nmol/10^6 cells/h.

Flux ± SD	%SD	Reaction	Confidence Interval
85. 1.837 ± 0.435	25.4 %	Thr.ext -> Thr.c	(0.99, 2.68)
86. 1.802 ± 0.427	25.4 %	Arg.ext -> Arg.c	(0.97, 2.63)
87. 0.693 ± 0.164	25.4 %	Cys.ext -> Cys.c	(0.37, 1.01)
88. 0.693 ± 0.164	25.4 %	His.ext -> His.c	(0.37, 1.01)
89. 2.738 ± 0.649	25.4 %	Lys.ext -> Lys.c	(1.47, 4.00)
90. 0.208 ± 0.049	25.4 %	Trp.ext -> Trp.c	(0.11, 0.30)
91. 11.000 ± 5.498	59.4 %	Ala.c -> Ala.ext	(0.28, 21.72)
92. 7.996 ± 3.999	59.4 %	Gly.c -> Gly.ext	(0.20, 15.79)
93. 1.071 ± 0.500	54.7 %	Pro.c -> Pro.ext	(0.10, 2.05)
94. 17.095 ± 4.297	27.1 %	Glu.c -> Glu.ext	(8.80, 25.56)
95. 615.000 ± 55.905	9.4 %	Lact.c -> Lact.ext	(495.11, 713.15)
96. 52.332 ± 9.293	19.0 %	Ru5P.c <=> X5P.c (net)	(35.23, 71.47)
97. (0.0, >1e4) ± >1000	>100 %	Ru5P.c <=> X5P.c (exch)	(0.00, >10000)
98. 34.660 ± 8.216	25.4 %	Biomass equation (v72)	(18.60, 50.64)
99. 79.106 ± 24.145	35.1 %	FA.c -> Lipids	(39.12, 133.28)

Table D.6 MFA results for the MDA-MB-231 cells for the high-lactate condition. Fluxes measured in nmol/10^6 cells/h.

Flux ± SD	%SD	Reaction	Confidence Interval
1. 223.612 ± 18.929	8.7 %	Gluc.ext -> G6P.c	(184.77, 258.60)
2. 174.917 ± 14.716	8.6 %	G6P.c <=> F6P.c (net)	(144.40, 201.79)
3. (>1000, >1e4) ± >1000	>100 %	G6P.c <=> F6P.c (exch)	(57.35, >10000)
4. 206.134 ± 17.295	8.6 %	F6P.c -> FBP.c	(170.13, 237.58)
5. 206.134 ± 17.295	8.6 %	FBP.c <=> DHAP.c + GAP.c (net)	(170.13, 237.58)
6. (0.0, >1e4) ± >10000	>100 %	FBP.c <=> DHAP.c + GAP.c (exch)	(0.00, >10000)
7. 206.134 ± 17.295	8.6 %	DHAP.c <=> GAP.c (net)	(170.13, 237.58)
8. (>1000, >1000) ± >1000	34.6 %	DHAP.c <=> GAP.c (exch)	(>1000, >10000)
9. 427.878 ± 36.033	8.7 %	GAP.c <=> 3PG.c (net)	(352.92, 493.45)
10. (728.7, >1000) ± >1000	>100 %	GAP.c <=> 3PG.c (exch)	(0.00, >10000)
11. 427.878 ± 36.033	8.7 %	3PG.c <=> PEP.c (net)	(352.92, 493.45)
12. 0.000 ± 18.112	>100 %	3PG.c <=> PEP.c (exch)	(0.00, 70.64)
13. 492.882 ± 40.788	8.5 %	PEP.c -> Pyr.c	(407.35, 566.43)
14. 47.681 ± 6.178	13.5 %	G6P.c -> CO2 + Ru5P.c	(36.14, 60.24)
15. 15.609 ± 2.040	13.6 %	Ru5P.c <=> R5P.c (net)	(11.67, 19.62)
16. (>1000, >1e4) ± >1000	84.2 %	Ru5P.c <=> R5P.c (exch)	(>1000, >10000)
17. 31.218 ± 4.080	13.6 %	X5P.c <=> EC2.c + GAP.c (net)	(23.34, 39.25)
18. (0.0, >1e4) ± >1000	>100 %	X5P.c <=> EC2.c + GAP.c (exch)	(0.00, >10000)
19. -15.609 ± 2.040	12.9 %	F6P.c <=> EC2.c + E4P.c (net)	(-19.62, -11.67)
20. 0.000 ± 2.420	>100 %	F6P.c <=> EC2.c + E4P.c (exch)	(0.00, 9.44)

Table D.6 (Continued) MFA results for the MDA-MB-231 cells for the high-lactate condition. Fluxes measured in nmol/10^6 cells/h.

Flux ± SD	%SD	Reaction	Confidence Interval
21. -15.609 ± 2.040	12.9 %	S7P.c <=> EC2.c + R5P.c (net)	(-19.62, -11.67)
22. (>1000, >1e4) ± >1000	>100 %	S7P.c <=> EC2.c + R5P.c (exch)	(>1000, >10000)
23. -15.609 ± 2.040	12.9 %	F6P.c <=> EC3.c + GAP.c (net)	(-19.62, -11.67)
24. (>1000, >1e4) ± >1000	>100 %	F6P.c <=> EC3.c + GAP.c (exch)	(0.00, >10000)
25. 15.609 ± 2.040	13.6 %	S7P.c <=> EC3.c + E4P.c (net)	(11.67, 19.62)
26. 5.821 ± 4.101	73.3 %	S7P.c <=> EC3.c + E4P.c (exch)	(0.00, 15.99)
27. 319.887 ± 39.362	12.9 %	Pyr.c <=> Lact.c (net)	(240.49, 394.00)
28. (>1000, >1000) ± >1000	>100 %	Pyr.c <=> Lact.c (exch)	(610.82, >10000)
29. 151.385 ± 60.019	43.9 %	Pyr.c -> Pyr.snk	(27.75, 261.82)
30. 29.456 ± 14.042	53.5 %	Pyr.c -> Pyr.m	(7.07, 61.83)
31. 29.456 ± 13.983	53.3 %	Pyr.m -> CO2 + AcCoA.m	(7.07, 61.60)
32. 83.441 ± 11.740	14.8 %	AcCoA.m + OAC.m -> Cit.m	(64.67, 110.46)
33. 52.152 ± 5.596	11.1 %	Cit.m <=> AKG.m + CO2 (net)	(41.31, 63.13)
34. 33.556 ± 4.761	14.8 %	Cit.m <=> AKG.m + CO2 (exch)	(25.71, 44.28)
35. 91.381 ± 7.623	8.5 %	AKG.m -> CO2 + Suc.m	(76.83, 106.56)
36. 114.345 ± 9.941	8.9 %	Suc.m <=> Fum.m (net)	(95.10, 133.87)
37. (23.6, 57.9) ± >100	>100 %	Suc.m <=> Fum.m (exch)	(0.00, 715.93)
38. 123.152 ± 9.921	8.2 %	Fum.m <=> Mal.m (net)	(103.82, 142.51)
39. (>1000, >1e4) ± >1000	>100 %	Fum.m <=> Mal.m (exch)	(85.61, >10000)
40. 83.441 ± 12.509	15.8 %	Mal.m <=> OAC.m (net)	(61.67, 110.46)

Table D.6 (Continued) MFA results for the MDA-MB-231 cells for the high-lactate condition. Fluxes measured in nmol/10^6 cells/h.

Flux ± SD	%SD	Reaction	Confidence Interval
41. (0.0, >1e4) ± >10000	>100 %	Mal.m <=> OAC.m (exch)	(0.00, >10000)
42. -0.000 ± 0.191	>100 %	Mal.m -> Pyr.mII + CO2	(-0.00, 0.74)
43. 0.000 ± 2.704	>100 %	Pyr.mII + CO2 -> OAC.m	(0.00, 10.55)
44. 0.000 ± 2.895	>100 %	Pyr.m <=> Pyr.mII (net)	(-0.74, 10.55)
45. (0.0, >1e4) ± >10000	>100 %	Pyr.m <=> Pyr.mII (exch)	(0.00, >10000)
46. 0.000 ± 1.840	>100 %	Mal.c -> Pyr.c + CO2	(0.00, 7.18) |
47. 39.711 ± 13.998	39.1 %	Mal.m <=> Mal.c (net)	(8.59, 63.18)
48. (>1000, >1e4) ± >1000	>100 %	Mal.m <=> Mal.c (exch)	(>1000, >10000)
49. 39.711 ± 13.941	39.0 %	Mal.c <=> OAC.c (net)	(8.59, 62.96)
50. (70.3, 209.5) ± >1000	>100 %	Mal.c <=> OAC.c (exch)	(23.17, >10000)
51. 65.004 ± 6.011	9.5 %	OAC.c -> PEP.c + CO2	(52.77, 76.21)
52. 31.289 ± 12.826	48.0 %	Cit.m <=> Cit.c (net)	(12.83, 62.85)
53. (0.0, >1e4) ± >10000	>100 %	Cit.m <=> Cit.c (exch)	(0.00, >10000)
54. 31.289 ± 12.826	48.0 %	Cit.c -> AcCoA.c + OAC.c	(12.83, 62.85)
55. 31.289 ± 12.826	48.0 %	AcCoA.c -> FA.c	(12.83, 62.85)
56. 50.097 ± 3.745	7.6 %	Gln.c -> Glu.c	(42.81, 57.42)
57. 39.229 ± 4.026	10.6 %	Glu.c <=> AKG.m (net)	(31.14, 46.84)
58. 567.474 ± >100	40.0 %	Glu.c <=> AKG.m (exch)	(354.06, >1000)
59. 2.121 ± 0.553	26.6 %	Glu.c <=> Pro.c (net)	(1.14, 3.30)
60. (0.0, >1e4) ± >10000	>100 %	Glu.c <=> Pro.c (exch)	(0.00, >10000)

Table D.6 (Continued) MFA results for the MDA-MB-231 cells for the high-lactate condition. Fluxes measured in nmol/10^6 cells/h.

Flux ± SD	%SD	Reaction	Confidence Interval
61. -5.996 ± 1.874	28.2 %	Asp.c <=> OAC.c (net)	(-10.04, -2.74)
62. (0.0, >1e4) ± >10000	>100 %	Asp.c <=> OAC.c (exch)	(0.00, >10000)
63. 1.068 ± 0.326	31.3 %	Asp.c -> Asn.c	(0.42, 1.69)
64. 11.218 ± 4.241	39.9 %	Pyr.c <=> Ala.c (net)	(3.54, 20.08)
65. (0.0, >1e4) ± >10000	>100 %	Pyr.c <=> Ala.c (exch)	(0.00, >10000)
66. 19.064 ± 9.322	58.7 %	Ser.c <=> Pyr.c (net)	(-0.68, 35.68)
67. (436.5, >1e4) ± >1000	>100 %	Ser.c <=> Pyr.c (exch)	(0.00, >10000)
68. 9.949 ± 3.650	38.0 %	Ser.c -> Gly.c + MEETHF	(3.59, 17.83)
69. 0.000 ± 0.236	>100 %	Thr.c -> AcCoA.c + Gly.c	(0.00, 0.92)
70. 1.598 ± 0.848	66.1 %	Met.c + CO2 -> Suc.m + CO2 + MEETHF	(0.00, 3.31)
71. 9.616 ± 3.754	43.2 %	Val.c + CO2 -> Suc.m + 2 CO2	(2.11, 16.75)
72. 11.749 ± 3.662	34.5 %	Ile.c + CO2 -> Suc.m + AcCoA.m + CO2	(4.51, 18.79)
73. 4.337 ± 1.862	49.8 %	Phe.c -> Fum.m + 2 AcCoA.m + CO2	(0.62, 7.88)
74. 4.470 ± 1.883	48.6 %	Tyr.c -> Fum.m + 2 AcCoA.m + CO2	(0.75, 8.10)
75. 8.207 ± 2.872	39.4 %	Leu.c + CO2 -> 3 AcCoA.m + CO2	(2.25, 13.45)
76. 51.271 ± 3.641	7.2 %	Gln.ext -> Gln.c	(44.40, 58.61)
77. 3.620 ± 1.894	63.2 %	Asp.c -> Asp.ext	(0.00, 7.39)
78. 12.950 ± 3.502	28.0 %	Ile.ext -> Ile.c	(6.41, 20.06)
79. 10.289 ± 2.996	31.9 %	Leu.ext -> Leu.c	(4.62, 16.31)
80. 2.106 ± 0.931	51.9 %	Met.ext -> Met.c	(0.41, 4.04)

Table D.6 (Continued) MFA results for the MDA-MB-231 cells for the high-lactate condition. Fluxes measured in nmol/10^6 cells/h.

Flux ± SD	%SD	Reaction	Confidence Interval
81. 5.138 ± 1.860	41.0 %	Phe.ext -> Phe.c	(1.61, 8.87)
82. 30.589 ± 9.170	33.1 %	Ser.ext -> Ser.c	(12.63, 48.40)
83. 5.138 ± 1.860	41.0 %	Tyr.ext -> Tyr.c	(1.61, 8.87)
84. 11.138 ± 3.636	34.2 %	Val.ext -> Val.c	(4.15, 18.33)
85. 1.415 ± 0.383	29.7 %	Thr.ext -> Thr.c	(0.58, 2.07)
86. 1.388 ± 0.424	31.3 %	Arg.ext -> Arg.c	(0.55, 2.20)
87. 0.534 ± 0.163	31.3 %	Cys.ext -> Cys.c	(0.21, 0.85)
88. 0.534 ± 0.163	31.3 %	His.ext -> His.c	(0.21, 0.85)
89. 2.109 ± 0.645	31.3 %	Lys.ext -> Lys.c	(0.83, 3.34)
90. 0.160 ± 0.049	31.2 %	Trp.ext -> Trp.c	(0.06, 0.25)
91. 9.002 ± 4.499	59.4 %	Ala.c -> Ala.ext	(0.23, 17.77)
92. 7.974 ± 3.999	59.6 %	Gly.c -> Gly.ext	(0.18, 15.77)
93. 0.973 ± 0.499	61.2 %	Pro.c -> Pro.ext	(0.00, 1.95)
95. 380.000 ± 37.990	10.4 %	Lact.c -> Lact.ext	(303.17, 451.33)
96. 60.113 ± 11.222	19.9 %	Lact.tr -> Lact.c	(37.97, 81.74)
97. 31.218 ± 4.080	13.6 %	Ru5P.c <=> X5P.c (net)	(23.34, 39.25)
98. (0.0, >1e4) ± >10000	>100 %	Ru5P.c <=> X5P.c (exch)	(0.00, >10000)
99. 26.695 ± 8.159	31.3 %	Biomass equation (v72)	(10.49, 42.31)
100. 31.289 ± 12.826	48.0 %	FA.c -> Lipids	(12.83, 62.85)